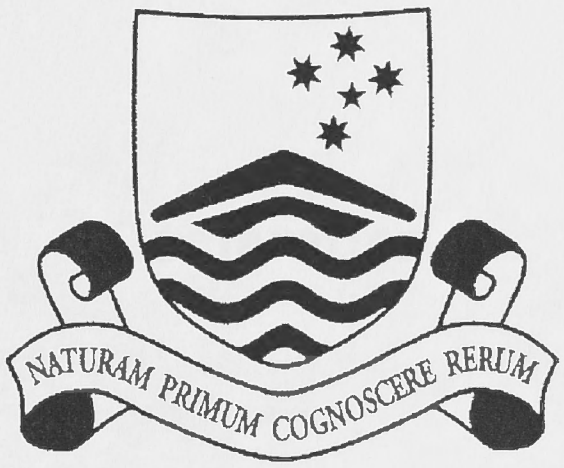

THE AUSTRALIAN NATIONAL UNIVERSITY

Studies of the Oxygen-Evolving Complex of Photosystem II.

a Thesis submitted for the degree of
Doctor of Philosophy

by **Karin Ann-Sofie Åhrling**

Department of Chemistry
Faculty of Science
Australian National University

October 1996

Declaration

Except where otherwise acknowledged, the work in this thesis is my own.

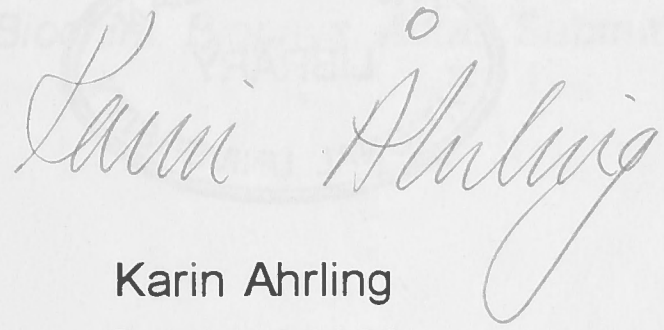

Karin Ahrling
October, 1996

Publications

Smith, P. J., Åhrling, K. A. and Pace, R. J. 1993. Nature of the S_2 state electron paramagnetic resonance signals from the oxygen evolving complex of photosystem II: Q-band and oriented X-band studies. *J. Chem. Soc. Faraday Trans.* 89:2863-2868.

Åhrling, K. A. and Pace, R. J. 1995. Simulation of the S_2 state multiline electron paramagnetic resonance signal of photosystem II: A multifrequency approach. *Biophys. J.* 68:2081-2090.

Åhrling, K.A. and Pace, R.J., 1995. Theoretical and experimental studies of the orientation dependence of the S_2 multiline signal of photosystem II. *In*: Photosynthesis: From light to biosphere. P. Mathis. ed. Kluwer Academic Publishers, Dordrecht. II:309-312.

Åhrling, K. A. and Pace, R. J. 1996. Simulation of the two forms of the g=4.1 signals of photosystem II. *Biochim. Biophys. Acta.* Submitted.

Acknowledgements

A sincere thank you to my supervisor, Dr Ron Pace, for his support and encouragement over the years. My thanks also go to the advisors on my committee, Dr Tom Wydrzynski and Prof. Jan Andersson, who have always been available for discussion and help.

Dr Richard Bramley of the Research School of Chemistry has willingly contributed much time in discussion with me and the use of his Q-band spectrometer.

The Supercomputer Facility at ANU has provided access to the vector processor, together with excellent programmer support.

The Plant Science Centre at ANU awarded me a top-up scholarship for which I am very grateful.

I had great support from Marilyn Olliff and Laurence Maher while they were in the Department, and not to forget Paul Smith, Christof Klughammer, Reza Razeghifard and Damien Kuzek from this group.

Finally, my most sincere thanks to my husband, Brian Polden, without whose support I would not have been able to undertake this study, and also to our children Thomas and Joseph, who, for the first time in their lives will now have a mother who is not studying.

Synopsis

The oxygen evolving centre (OEC) of photosystem II (PSII) catalyses the oxidation of water to molecular oxygen. The OEC contains four Mn ions in an as yet undetermined geometry. Water molecules are known to be associated with the Mn cluster. A photon of light causes the oxidation of the PSII reaction centre chlorophyll *a* molecule (P680). The reaction centre is subsequently reduced by an electron from the OEC. The total energy necessary to split water is accumulated in a four-step process, each electron removed resulting in an intermediate oxidation state of the OEC, the so called S-states, labelled S_0- S_4. Molecular oxygen is released after the fourth electron is removed, in the S_4 state. In the dark, the OEC relaxes to the S_1 state. Continuous illumination of PSII particles in the S_1 state at 200K generates the S_2 state without further advancement.

The S_2 state is paramagnetic and gives rise to two characteristic EPR signals, a Mn hyperfine structured signal (the multiline) centred at g=2 and a broad, unresolved signal centred at g=4 (the g=4.1) signal. Temperature dependence studies of these EPR signals are consistent with the multiline signal arising from an *S*=1/2 ground state. Smith and Pace (1995) have shown that there are two separate g=4.1 signals. One is the first excited (*S*=3/2) state of the multiline signal, observed by 200K illumination of PSII samples to which alcohol has not been added. Addition of alcohol (3-5%) suppresses this g=4.1 signal. The other signal appears after illumination at 130K of samples cryoprotected with 30% ethylene glycol. It is thought to stem from a pair of bridged Mn of the same oxidation state (III/III or IV/IV) coupled to a radical, to give a net *S*=3/2 state. Temperature dependence studies have shown this signal to be a ground state.

The study reported here involves the simulation of the EPR signals arising from the S_2 state, to investigate whether the data is consistent with the four Mn being organised as two magnetically isolated μ-oxo-bridged dimers.

The multiline signal has been simulated at Q-, X- and S-band frequencies. The model used for the simulation assumes that the signal arises from an essentially magnetically isolated Mn^{III}-Mn^{IV} dimer, with a ground state electronic spin S_T =1/2. The spectra are generated from exact numerical solution of a general spin Hamiltonian containing anisotropic hyperfine and quadrupolar interactions at both Mn nuclei. The features that distinguish the multiline from the EPR spectra of model manganese dimer complexes are

plausibly explained assuming an unusual ligand geometry at both Mn nuclei, giving rise to normally forbidden transitions from quadrupole interactions as well as hyperfine anisotropy. The fitted parameters indicate that the hyperfine and quadrupole interactions arise from Mn ions in low symmetry environments, corresponding approximately to the removal of one ligand from an octahedral geometry in both cases. For a quadrupole interaction of the magnitude indicated here to be present, the Mn^{III} ion must be 5-coordinate and the Mn^{IV} 5-coordinate or possibly have a sixth, weakly bound ligand. The hyperfine parameters indicate a quasi-axial anisotropy at Mn^{III} consistent with Jahn-Teller distortion as expected for a d^4 ion and corresponds to the unpaired spin being in the ligand deficient, z-direction of the molecular reference axes. The fitted parameters for Mn^{IV} are very unusual, showing a high degree of anisotropy not expected in a d^3 ion. The anisotropy could be qualitatively accounted for by a histidine ligand providing π-backbonding into the metal d_{xy} orbital, together with a weakly bound or absent ligand in the x-direction.

The two forms of the g=4.1 signals have been simulated at Q-and X-band. The spin Hamiltonian employed calculated the zero field splitting (ZFS) and Zeeman interaction exactly and includes the hyperfine and quadrupolar interactions as perturbations on the main transitions. The simulations confirm that the g=4.1 signals arise from two separate spin centres, with two distinct sets of ZFS parameters. The excited spin state arises from the system with a large ZFS (4.8 cm^{-1}) and the ground state form from a centre with a significantly smaller ZFS (1.1 cm^{-1}). Both spin centres are quasi-axial (E/D 0.02). A justification of the magnitude of the interactions in terms of the intrinsic ZFS for Mn^{III} and Mn^{IV} is provided together with an estimate of the coupling coefficients for the excited spin state.

EPR studies of one dimensionally oriented PSII particles were performed. For the multiline signal these showed an orientation dependence of a degree not previously reported. The orientation dependence was consistent with the principal axes oriented approximately equidistant from the membrane plane normal. This was confirmed by simulations of the signals. The z-axis showed an orientation of 36° off the membrane plane and the x- and y-axis were oriented 45° off the membrane plane. The simulations also showed that the g-tensor is not coincident with the hyperfine and quadrupole tensors, but oriented with the z-axis ~10° closer to the membrane plane.

The orientation studies of the excited state form of the g=4.1 signal showed an orientation of the ZFS tensor with the z-axis nearly co-incident with the hyperfine tensors. Using the orientation of the Mn-Mn vector based on EXAFS studies of ammonia treated oriented PSII samples (Dau, *et al,* 1995) an orientation of the Mn-dimer giving rise to the multiline and excited state g=4.1 signal was predicted. The x- and y-axis of the ZFS tensors are oriented with the μ-oxo bridges, whereas the hyperfine tensors are offset by ~30°.

Two other aspects of this study collaborate the thesis that the Mn are organised as two magnetically isolated Mn-dimers. The first is the observation (Fiege, *et al,* 1995) and simulation of a modified multiline signal arising from a Ca depleted PSII sample, with less than four Mn per reaction centre. The simulation parameters indicate a system with similar geometry as that giving rise to the normal multiline signal. The second is the preliminary results reported here, that plants may be able to use another metal (Ru in this study) in one of the Mn-dimer sites. EPR spectroscopy of PSII material prepared from a system grown in a Mn-depleted media, with Ru ions present, show both a Mn multiline signal as well as a Ru signal that is consistent with a Ru dimer in an oxidation state differing by one (such as III/IV or II/III)

Contents

FIGURES:

TABLES:

Commonly Used Symbols and Abbreviations

Symbols:

ß = Bohr magneton

β_n = nuclear (proton) Bohr magneton 5.050824×10^{-27} JT^{-1}.

c = speed of light

g= g-value, for a free electron 2.0023

g_n= nuclear g-value for Mn.

h = Planck's constant

μ_o = permitivity of free space

Abbreviations:

chl = chlorophyll

DCMU = 3,4-Dichlorophenyl-1,1-dimethylurea

DMSO = Dimethyl sulphoxide

EPR = Electron paramagnetic resonance

EXAFS = Extended X-ray absorption fine structure spectroscopy

ICP = Inductively coupled plasma spectroscopy

MO = molecular orbital

NMR = Nuclear magnetic resonance

OEC = oxygen-evolving complex (of PSII)

PpBQ = phenyl-para-benzoquinone

PSII = photosystem II

Q_A = primary quinone electron acceptor of PSII

Tris = (tris[Hydroxymethyl]aminomethane) $C_4H_{11}NO_3$

XANES = X-ray absorption near edge structure spectroscopy

Y_Z= Tyrosine 161 on D1 protein of PSII

ZFS = Zero-field splitting

1: INTRODUCTION

Photosystem II and the Oxygen Evolving Complex

The process of photosynthesis can be described as the capture of solar energy and its conversion into biomass. Photosynthesis occurs not only in green plants but also in lower eukaryotic organisms (for example algae) and in prokaryotic organisms (for example cyanobacteria). Photosynthetic organisms rely on different hydrogen donors to reduce carbon dioxide according to the general equation:

$$2H_2X + CO_2 \xrightarrow{h\nu} CH_2O + H_2O + 2X.$$

The donor can be, for instance, hydrogen sulfide or water. Water is very stable and difficult to oxidise, but is abundant on earth, does not affect pH and will not readily react with and, therefore, modify protein residues. Oxygen producing photosynthetic plants and organisms use water as the hydrogen donor for the reduction of carbon dioxide, yielding glucose, with molecular oxygen as a bi-product:

$$6H_2O + 6CO_2 \xrightarrow{h\nu} (CH_2O)_6 + 6O_2.$$

Photosynthesis in green plants is a complex series of reactions which takes place in two stages, the light and the dark reactions. During the light reactions the pigment molecules (for example, chlorophylls and carotenoids) absorb light energy and, through a sequence of photochemical reactions, convert it to the two energy-rich products, ATP and NADPH. In the dark reactions these two products are used to reduce carbon dioxide to form glucose. The production of oxygen from water takes place during the light reactions.

The light-dependent reactions occur in the thylakoid membrane system of the chloroplast. The thylakoid membranes are organised into stacked regions, called grana, and into extended, unstacked regions, called the stroma lamellae. The surrounding fluid, the stroma, harbours the enzymes required for the dark reactions.

The energy required to drive the electron transport for the reduction of $NADP^+$ is provided by two photons of light absorbed by the pigment molecules in the light harvesting complexes of photosystem I and II. One photon of light is absorbed by the reaction centre, P680, of photosystem II (PSII) and it becomes excited, resulting in its oxidation. P680 is a special pair of chlorophyll *a* molecules (Seibert, 1995) and is so called as its maximum

absorption of light is at this wavelength. The electron, released by P680 is first accepted by a nearby pheophytin molecule. Charge stabilisation is achieved by the rapid oxidation of the reduced pheophytin by an iron quinone complex (Q_A) on the opposite side of the membrane, together with the rapid reduction of $P680^+$ by a tyrosine residue called Y_Z. The electron continues along a path of increasingly more positive potential. It receives another boost of light energy in photosystem I (PSI), through the PSI reaction centre P700. The oxidised PSI reaction centre receives electrons from plastocyanin and reduces a low potential iron-sulphur protein in the stroma. Protons, as well as electrons, are transported through the membrane during the overall process, thereby creating a proton gradient which drives the ATP synthetase. Cytochrome b_6f is also situated in the thylakoid membrane and believed to be involved in proton pumping and cyclic electron transport (Chitnis, 1996).

PSII is a protein complex, situated in the appressed regions (grana) of the thylakoid membrane system and it spans the thylakoid membrane. The core complex of PSII is dimeric in structure. The two constituent polypeptides, the D_1 and D_2 proteins, are each about 32 kDa in size and consist of five membrane spanning helices and a sixth smaller helix on the lumenal side of the thylakoid membrane. Held between the two polypeptides are the redox components involved in the electron transport. The D_1 and D_2 are capped by three other proteins, a 33 kDa, a 23 kDa and a 17 kDa (Hansson and Wydrzynski, 1990). Surrounding the D_1 and D_2 polypeptides are accessory extrinsic proteins and chlorophyll light harvesting complexes (Hansson and Wydrzynski, 1990). The oxygen evolving complex (OEC) catalyses the oxidation of water to molecular oxygen. It contains a complex of four Mn ions bound at least in part to the D_1 polypeptide, near P680 (Svensson, *et al.*, 1990). Water molecules are thought to be associated with this Mn cluster (Hansson, *et al.*, 1986).

The exact location of the Mn cluster is unknown, since a protein containing functional Mn has not yet been isolated, and hence no crystal structure is available. The structural information available to date comes mostly from comparison with the crystal structure of the purple bacteria reaction centre, based on the homology between the D_1 and D_2 proteins and the L and M subunits of the bacterial reaction centre complex (Deisenhofer, *et al.*, 1985). Svensson *et al* (1990) have proposed a three-dimensional structure of the D_1/D_2 unit based on the structure of *Rhodopseudomonas viridis.*

Mutation studies using cyanobacteria have aided in the identification of essential cofactors and possible ligands to the Mn ions. These have largely been found on the D_1 protein. Debus *et al* (Debus, 1988; Debus, *et al.* 1988) identified Tyr-161 (Y_z) as the immediate electron donor to P680. On the lumenal side of the membrane there are 13 aspartate and glutamate residues and six histidine residues. These residues are the most likely candidates as ligands to the Mn ions and have been studied by site directed mutagenesis (Diner, *et al.*, 1991; Diner, *et al.*, 1990; Nixon and Diner, 1992; Nixon and Diner, 1994). The amino acids that, when mutated, show an effect on oxygen evolution or assembly of the Mn-complex are clustered in two regions. One region is situated near the small α-helix on the lumen side, near Tyr-161. The amino acids affected here are Asp-170, His-190 and possibly also Glu-189. Ala-170 affects the binding of the first Mn ion in the so called high affinity site. The other region is near the C-terminus end of the D_1 polypeptide. Here His-332, Glu-333, Asp-342, as well as the carboxy terminus itself on Ala-344, all affect the protein's ability to oxidise water. His-337 may also play some role. However, the mutants in the second region all allow Mn to bind to the high affinity site and Y_z to be oxidised. Glu-69 on the D_2 protein is the only residue shown to have a drastic effect on water oxidation. See also Chapter 2 - Model.

After a photon of light has caused the oxidation of the PSII reaction centre chlorophyll *a* special pair (P680), the reaction centre is quickly reduced via the Y_z by an electron from the OEC. The total energy necessary to split water is accumulated in a four step process, each electron removed resulting in a quasi-stable intermediate oxidation state of the OEC, the so called S-states, labelled S_0 - S_4 (Kok, *et al.*, 1970). Molecular oxygen is released after the fourth electron is removed, in the S_4 state, and the cycle repeats. Four protons are released during the cycle, but the stoichiometry for each step is not clear (Debus, 1992).

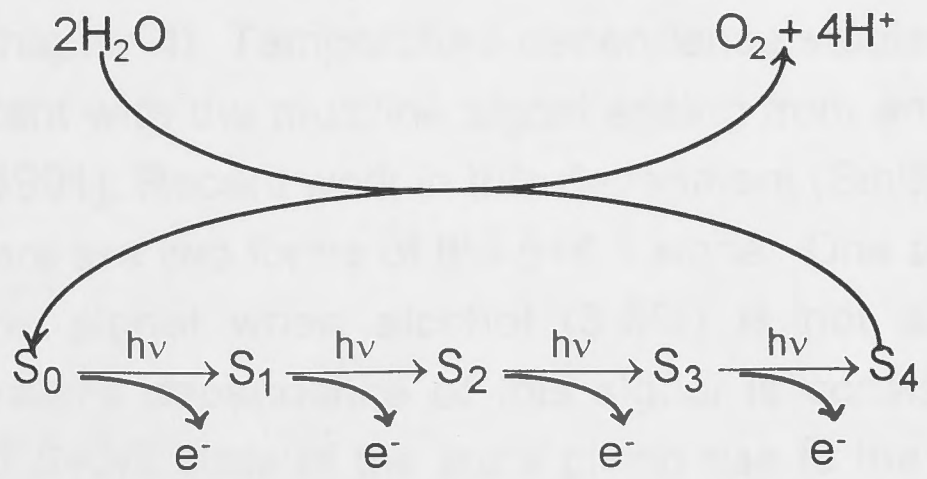

Figure 1.1 The Kok cycle.

The rate of S-state transitions can be measured unambiguously using the re-reduction rates of Y_Z^+. At physiological conditions the life times of each the S-states are: $S_0 \rightarrow S_1$, $t_{1/2}$=40-60μs; $S_1 \rightarrow S_2$, $t_{1/2}$=85μs; $S_2 \rightarrow S_3$, $t_{1/2}$=140μs; $S_3 \rightarrow (S_4) \rightarrow S_0$, $t_{1/2}$=750μs. The kinetics of the $S_4 \rightarrow S_0$ transition could not be resolved. However, by comparing the $S_3 \rightarrow S_4$ kinetics, measured as above, with oxygen release kinetics, using a time resolved ESR oximetry technique, under the same experimental conditions used for measurement of Y_Z^+ re-reduction rates, an upper limit of 70μs for the $S_4 \rightarrow S_0$ transition $t_{1/2}$ may be obtained (Razeghifard, *et al,* 1996).

Dismukes and Siderer (1981) first observed a Mn EPR multiline signal in spinach chloroplasts by subjecting them to a series of laser flashes at room temperature followed by rapid freezing to ~130K. The signal appeared after the first flash, decreased on subsequent flashes to reappear again on the fifth flash. They postulated that the signal arose from a Mn-cluster in a net III/IV (dimer) or perhaps III/III/III/IV (tetramer) oxidation state, with antiferromagnetic coupling giving a net S =1/2 state and hence the characteristic 16 line spectrum as seen in dimeric Mn synthetic complexes. They identified the multiline with the S_2 state in Kok's model. This signal was also generated by Hansson and Andreasson (1982) in broken chloroplasts by freezing the preparation under continuous illumination. Subsequently it was confirmed that the OEC relaxes to the S_1 state in the dark, with $t_{1/2}$ ~ 30 s, such that about 75% of the OEC are in the S_1 and the remaining 25% in the S_0 state. Continuous illumination of PSII particles in the S_1 state at 200K generates the S_2 state without further advancement.

The S_2 state is paramagnetic and gives rise to two characteristic EPR signals, a Mn hyperfine structured signal (the multiline), centred at g=2, and a broad, unresolved signal centred around g=4 (the 4.1 signal). The g=4 signal was first observed by Casey and Sauer, and Zimmerman and Rutherford in 1984 (see Chapter 4). Temperature dependence studies of these EPR signals are consistent with the multiline signal arising from an S=1/2 ground state (Pace, *et al.*, 1991). Recent work in this department (Smith and Pace, 1996) indicates that there are two forms of the g=4.1 signal. One arises in the presence of the multiline signal when alcohol (3-5%) is not added to the buffer. The temperature dependence of this signal is consistent with it being the first excited S=3/2 state of the state giving rise to the multiline signal. The other arises from 130K illumination of PSII particles in the presence of 30% ethylene glycol as cryoprotectant. It has been shown to stem from an S=3/2 ground state. An estimate of the antiferromagnetic exchange coupling (J) of

the multiline signal in the presence of alcohol (~4% to the PSII sample buffer) gives $|J|>10$ cm^{-1} (Pace, *et al.*, 1991). In the presence of alcohol the excited state g=4.1 signal does not appear, suggesting that in this case the energy gap to the g=4.1 signal state increases, resulting in this state being unpopulated at normal observation temperatures (Smith and Pace, 1996). Britt *et al* (1992) have confirmed that the multiline signal arises from a ground spin state and this conclusion is now accepted. For a general overview see reviews by Debus (1992) and Hansson and Wydrzynski (1990).

The work by Smith and Pace (1996) suggests that the four Mn ions are organised as two magnetically isolated, antiferromagnetically coupled pairs. Under appropriate conditions (in the presence of alcohol), one pair is EPR silent and the other gives a net S=1/2 ground state (Smith and Pace, 1996). For the Mn^{III}-Mn^{IV} pair to be magnetically isolated it needs to be physically isolated (but presumably within electron transfer distance, ~10Å) or weakly coupled to a pair with net zero spin.

Based on comparisons with model compounds (Dismukes and Siderer, 1981) and X-ray K-shell absorption studies (Goodin, *et al.*, 1984), the OEC is thought to consist of a pair of di-μ-oxo bridged Mn dimers organised in an as yet undetermined geometry. It is generally accepted that in the S_2 state, one pair of Mn ions differ in oxidation state by one (eg Mn^{III}-Mn^{IV}) and are antiferromagnetically coupled, yielding a net spin of 1/2. The other pair is assumed to be Mn^{III}-Mn^{III} or Mn^{IV}-Mn^{IV}, yielding a net spin of 0. Suitably weak interactions between the two pairs yield a system with spin 1/2 ground state (Liang, *et al.*, 1994).

Compared to model Mn dimers, the multiline signal from the OEC shows more complex, superhyperfine structure. This resolved superhyperfine structure cannot be attributed to ligand hyperfine interactions with protons or nitrogen from the protein matrix, nor with chloride that may be associated with oxygen evolution (DeRose, *et al.*, 1991; Yachandra, *et al.*, 1986b; Andreasson, 1989; Haddy, *et al.*, 1989). Individual ligand hyperfine interactions of protons, nitrogen, or chloride with the metal cluster are narrower than the observed linewidth and are not usually resolved. Combined ligand hyperfine interactions, however, may contribute to the greater linewidth seen in the multiline signal, and in signals from metal clusters in proteins generally, compared with model compounds (Brudvig, 1989).

EXAFS studies (MacLachlan, *et al.*, 1992; George, *et al.*, 1989; DeRose, *et al.*, 1994; Penner-Hahn, *et al.*, 1990) identify two Mn-metal interactions, one at

2.7Å, one at 3.3-3.7Å. The data indicate that the PSII Mn ions each have one Mn neighbour at a distance of 2.7 Å. There is general agreement that the scatterer at 3.3-3.7 Å results from one Mn-metal interaction (~0.5 neighbour/Mn). Depending on analysis, this could represent Mn-Mn or Mn-Ca and could also include interactions from carbon, oxygen and nitrogen. On the basis of the above arguments, Klein *et al* (Yachandra, *et al.*, 1993) favour a model of a pair of di–μ–oxo bridged dimers, linked by one μ–carboxylato bridge between one Mn ion of each pair. However, the EXAFS data are also consistent with two non-interacting pairs of Mn dimers, with a Ca^{2+} ion associated with one of them. The data is not consistent with a trimeric cluster and a single isolated Mn ion within the OEC. EXAFS indicates that the Mn ions may be coordinatively unsaturated and the data can be modelled by a fit of two oxygen atoms (or nitrogen) at 1.91 Å and two at 2.13 Å (Penner-Hahn, *et al.*, 1990) or 1.8 Å and ~2.0 Å (DeRose, *et al.*, 1994; MacLachlan, *et al.*, 1992).

A signal from the S_1 state has been observed by parallel polarisation EPR studies (Dexheimer and Klein, 1992; Dexheimer, *et al.*, 1990). This species is thought to arise from the first excited S=1 state of an S=0 ground state, of a homodimer (Mn^{III}-Mn^{III} or Mn^{IV}-Mn^{IV}). The study shows that the species that gives rise to the S_1 state signal converts only to the multiline signal in the S_2 state. The authors conclude that the two S_2 state signals (multiline and 4.1) originate from magnetically distinct centres within the OEC and therefore imply a model of non-interacting dimers. This is in conflict with EXAFS interpretations from the same group (above) which implies a tetranuclear complex.

Although the body of data regarding the structure of the OEC is now quite extensive there is still much unknown. For instance, where are the Mn ions situated in PSII, what protein residues ligate the Mn, does the OEC consist of two magnetically isolated heterodimers, what are the geometries of such dimers, what would be the function of the two separate dimers? The EPR signals themselves are complex and by simulation of these signals I hope to contribute to the understanding of the interactions that give rise to them and hence the structure of the OEC.

Chemistry Relevant to the OEC

Manganese

Mangania is the Greek word for magic. Mn metal makes up 0.085% of the earths crust, only iron is a more abundant transition metal. Mn can take oxidation states from Mn^0 (d^7) to Mn^{VII} (d^0), with Mn^{II} (d^5) being the most common. Mn^{III} and Mn^{IV} are of most interest to photosynthesis. These two exist mainly in the high spin state, which means that Mn^{III}, a d^4 ion, has the t_{2g} orbitals occupied together with one of the e_g orbitals. The degeneracy of the e_g orbitals is normally lost by a spontaneous lowering of symmetry called the Jahn Teller effect. This works to lower the energy of the occupied e_g orbital while raising the other, thereby removing degeneracy. The distortion takes the form of an elongation along one of the octahedral axes. This is not generally the case for Mn^{IV} which has its d^3 electrons in the t_{2g} orbitals, which when uniformly occupied give rise to spherical symmetry. (Cotton and Wilkinson, 1966). Mn^{III} and Mn^{IV} are both strong Lewis acids and prefer hard Lewis bases as electron donors, which can be hydroxide or oxide ligands, carboxylates, alkoxides, phenoxides. In a protein this is equivalent to side chains in aspartate, glutamate or tyrosine residues. Nitrogen donors such as imidazole (histidine) can also function as ligands (Larson and Pecoraro, 1992) and will involve themselves in π-bonding made possible through the low-lying acceptor orbitals on the ligands (Huheey, *et al.*, 1993). In most environments Mn^{III} can act both as an oxidant and a reductant. This is because of its high spin d^4 configuration, where the loss of one electron would yield the stable t_{2g} configuration and the gain of an electron yields a half-filled shell. Mn^{IV}, on the other hand, remains strongly oxidising under most conditions (Larson and Pecoraro, 1992).

Magnetic properties of Manganese

Manganese multinuclear centres interact magnetically in a complex fashion. The magnitude of the magnetic interaction is reported as J or $2J$ in units of cm^{-1}. A negative value of J indicates antiferromagnetic coupling. Typically in biologically relevant complexes J ranges from -1 to -400 cm^{-1} (Larson and Pecoraro, 1992). In Mn-dimers with oxygen bridging between the Mn ions, antiferromagnetic coupling is often seen. Antiferromagnetic coupling means that the electron spins of the two ions align themselves so as to reduce the magnetic susceptibility of the dimer. It arises through spin pairing of the high spin *d*-electrons on the Mn ions through the *p*-electrons on the oxygen bridges (Cotton and Wilkinson, 1966). The magnitude of the interaction depends on the degree of overlap and the type of ligand. Small changes in bridging angle

and changes in bond length can lead to differences in magnetic exchange (Baldwin, *et al.*, 1994).

Water oxidation

The water-oxidation process: $2H_20 \rightarrow O_2 + 4H^+ + 4e^-$ as a concerted, one-step process has a redox potential, E^o, of +0.82V (vs NHE) at pH7. The reduction of $P680^+$ has a potential of ~1.1 V (Jursinic and Govindjee, 1977; Klimov, *et al.*, 1979). The Y_z residue, which is oxidised by $P680^+$, must therefore have a potential <1.1 V and the Mn must be able to oxidise the water, keeping the potential for each oxidation step >0.82 V and < ~ 1.0 V.

Table 1.1: Redox potentials at pH 7.0 and 25°C for the oxidation of water.
Potential in V vs NHE for 1e, 2e, 3e, and 4e oxidation represented by → for each electron.
Source (Yamaguchi and Sawyer, 1985).

Species	H_2O		$\cdot OH$		H_2O_2		$O_2^{-\cdot}$		O_2
Pot. V	+2.20V	→	+0.50V	→	+0.89V	→	-0.16V	→	
Pot. V	+1.35V	→		→	+0.36V	→		→	
Pot. V	+1.20V	→		→		→	-0.16V	→	
Pot. V	+0.86V	→		→		→		→	

Table 1.1, derived from the work of Yamaguchi and Sawyer (1985), indicate that only a concerted pathway keeps the potential of water oxidation within the appropriate limit. Yamaguchi and Sawyer suggest that in order to cope with the above requirement, at least two Mn will need to be involved.

Baldwin *et al* (1993,1994) have studied the effect of protonation of oxo bridges in synthetic Mn dimer $[Mn^{IV}(salpn)(\mu\text{-}O)]_2$. Each protonation step causes an increase in the Mn-Mn distance of 0.1Å and a concomitant dramatic decrease in the antiferromagnetic coupling between the Mn^{IV} ions. Furthermore, it was found that the oxidising potential increased substantially upon protonation. It is possible that this mechanism is utilised by PSII to ensure that the Mn-cluster is poised in a state with the appropriate potential. If the Mn-dimer lost a proton at the time of early oxidations, the Mn-dimer could remain stably non-reactive in the earlier S-states. A protonation with an oxidation at the Mn would convert the dimer into an extremely oxidising centre. Yamaguchi and Sawyer found that a single Mn ion had sufficiently positive potential for a one-electron oxidation and the OEC must contain at least two Mn ions that can act together to oxidise two molecules of H_2O, one bound to each Mn ion. One way to achieve the concerted four electron oxidation is to take one electron from each Mn ion in the dimer and a further two electrons from ligands, before a rapid oxidation of water takes place and the OEC is reduced. This would ensure a system poised at the right potential.

Electron Paramagnetic Resonance - Basic Theory

The EPR experiment

An atom or molecule which contains unpaired electrons has non-zero angular momentum and therefore possesses a magnetic moment. There are two kinds of angular momentum. An electron possesses intrinsic angular momentum, denoted with the symbol **S**. In the classical picture the intrinsic angular momentum can be described as the electrons possessing spin. Molecular systems or single atoms with one or more electrons may also possess orbital angular momentum arising out of the movement of the electron (S) in an orbit, denoted with the symbol **L**.

Associated with the total angular momentum is a magnetic moment,

$$\mu_e = -\beta(\mathbf{L} + g_e\mathbf{S})$$

where: g_e = g-value of the free electron

β = Bohr magneton

L,S dimensionless multiples of the basic quantum of angular momentum, $\hbar$

$\hbar$ = Planck's constant/2π

In a magnetic field the magnetic moment vector μ_e acquires energy depending on how it aligns itself in the magnetic field. The energy associated with this interaction is

$$E = -\mu \cdot \mathbf{H_o} = -\mu_z \cdot H_o$$

where: $\mathbf{H_o}$ is the applied static magnetic field and the z-axis is taken to be along the direction of the applied field H_o.

Quantum mechanically only certain values of μ_z are allowed, producing discrete energy states. If an oscillating magnetic field is applied, transitions are induced between the energy levels, previously degenerate, but now separated in energy by the static magnetic field. A single electron has two allowed orientations, corresponding to $S_z = \pm 1/2$, where +1/2 is the high energy state. The magnetic moment associated with a nucleus is much smaller, for ^{1}H the ratio is $g\beta/g_n\beta_n \sim 658$, which means that such magnetic moments contribute only in second order, as hyperfine structure, for instance. The resonance condition gives $\Delta E = g\beta H$, where the field H is the local magnetic field and includes contributions from hyperfine and other fields (see below)(Bersohn and Baird, 1966) and ΔE is the energy of the exciting electromagnetic quantum.

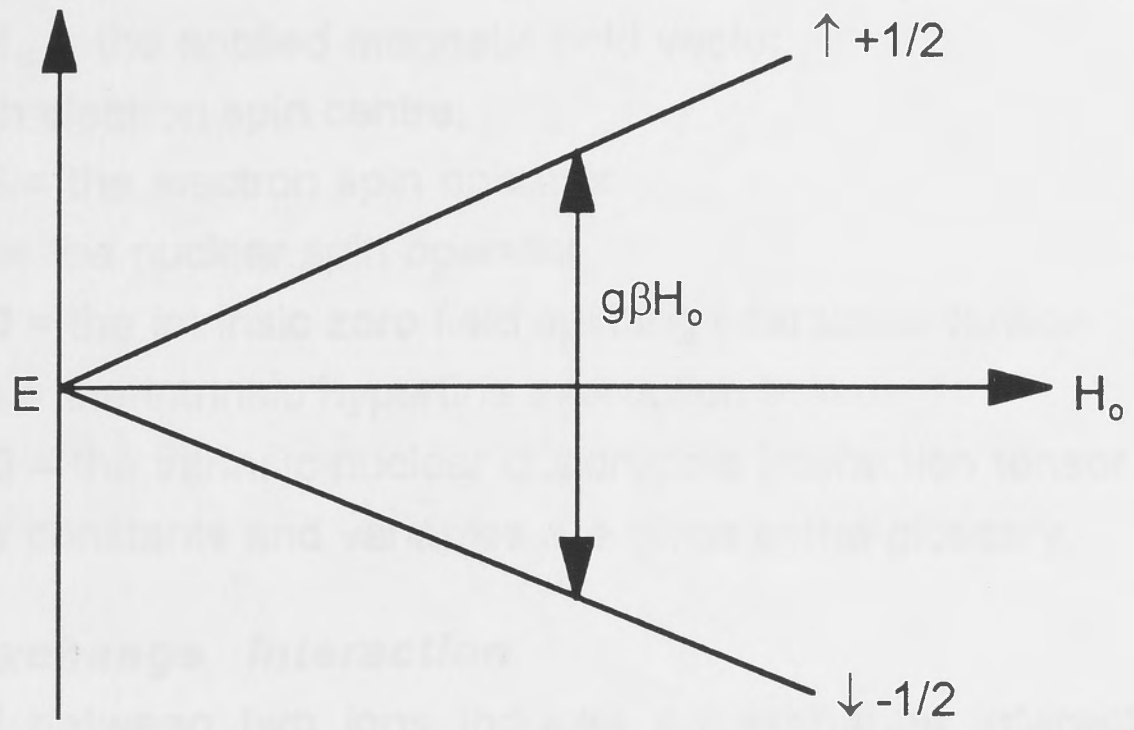

Figure 1.2 The variation of energy levels with increasing magnetic field.
Resonance occurs when the energy gap equals the microwave quantum $h\upsilon = g\beta H_o$.

In practice the static magnetic field is not kept constant, instead microwaves whose quanta have energy appropriate for the resonance condition, $h\upsilon = g\beta H$, are applied. This radiation is kept at constant frequency, υ, and the magnetic field scanned for transitions. The EPR experiment can be conducted at several distinct frequencies, the most common are:

S-band ~ 4 GHz
X-band ~ 9 GHz
P-band ~ 15 GHz
Q-band ~ 35 GHz

The spin Hamiltonian

The total Hamiltonian to describe the energy interactions includes electronic, ligand field and spin-orbit contributions. The ground manifold of a paramagnetic ion frequently consists of a group of electronic levels well separated from the next levels. The interactions in the ground manifold can be determined by defining an 'effective spin' S and with the condition that the interactions between the spin states in the full Hamiltonian are proportional to the interactions of the effective spin, the magnetic interactions in the ground manifold can be described by a spin Hamiltonian involving just the effective spins (Abragam and Bleaney, 1986). The ground spin states form the basis vectors for calculating the spin interactions.

The general spin Hamiltonian to describe interactions involving two electron spin centres, of the type relevant in this study is:

$$\mathcal{H} = -2J\mathbf{S_1}\cdot\mathbf{S_2} + \sum_{i=1}^{2}[\beta\mathbf{H_o}\cdot\boldsymbol{g}\cdot\mathbf{S_i} + \mathbf{S_i}\cdot\boldsymbol{D_i}\cdot\mathbf{S_i} + \mathbf{S_i}\cdot\boldsymbol{a_i}\cdot\mathbf{I_i} - g_n\beta_n\mathbf{H_o}\cdot\mathbf{I_i} + \mathbf{I_i}\cdot\boldsymbol{P_i}\cdot\mathbf{I_i}]$$

where: J = the isotropic exchange interaction between spin centres

$\mathbf{H_o}$ = the applied magnetic field vector

For each electron spin centre:

$\mathbf{S}$ = the electron spin operator

$\mathbf{I}$ = the nuclear spin operator

$\boldsymbol{D}$ = the intrinsic zero field splitting interaction tensor

$\boldsymbol{a}$ = the intrinsic hyperfine interaction tensor

$\boldsymbol{Q}$ = the intrinsic nuclear quadrupole interaction tensor

All other constants and variables are given in the glossary.

The exchange interaction

A bond between two ions induces an exchange interaction, that is, the valence electrons from each ion pair up to obey the Pauli principle. The stronger the bond, the larger is the energy gap between the state with anti-parallel spins and the state with parallel spins. The weaker the bond the smaller is the gap until the two energy levels are degenerate (no bond). Two ions that couple have an exchange interaction characterised by a number of total spin states $|S_1\text{-}S_2| \leq S_T \leq S_1+S_2$ (Bencini and Gatteschi, 1990). The system is antiferromagnetic when $|S_1\text{-}S_2|$ denotes the ground state. The exchange interaction occurs most commonly when spin pairing of the paramagnetic ions is brought about by an intervening, often diamagnetic, atom (see Magnetic properties of Manganese, above). In the strong coupling regime the exchange interaction is much greater than the other interaction terms in the Hamiltonian, such that there is no mixing of the energy states in each exchange interaction manifold, to a good approximation ($D/J<<1$, where D is the single ion zero-field splitting parameter). In such a case the Zeeman and other terms can be described as a perturbation on the exchange interaction. The above Hamiltonian can then be simplified considerably. The interaction terms in the uncoupled Hamiltonian above are now scaled by projection operators. The projection operator for a dimer becomes:

$$\alpha_1 = \frac{\mathbf{S_1}\cdot\mathbf{S_2}}{\mathbf{S_T}^2} = \frac{S_T(S_T+1)+S_1(S_1+1)-S_2(S_2+1)}{2S_T(S_T+1)} \qquad 1.1$$

with a similar calculation for α_2 (Sands and Dunham, 1975).

Here $\mathbf{S_T}= \mathbf{S_1}+\mathbf{S_2}$ and the Hamiltonian is simplified to:

$$\mathcal{H}=\beta\mathbf{H_o}\cdot\boldsymbol{g}\cdot\mathbf{S_T} + \mathbf{S_T}\cdot\boldsymbol{D}\cdot\mathbf{S_T} + \sum_{i=1}^{2}[\mathbf{S_T}\cdot\boldsymbol{A}_i\cdot\mathbf{I_i} - g_n\beta_n\mathbf{H_o}\cdot\mathbf{I_i} + \mathbf{I_i}\cdot\boldsymbol{P_i}\cdot\mathbf{I_i}]$$

where $\boldsymbol{A}_i = \alpha_i \boldsymbol{a}_i$ and $\boldsymbol{D}$ is the net zero field splitting for the dimer. The projection operator for $\mathbf{S_T}\cdot\boldsymbol{D}\cdot\mathbf{S_T}$ is more complex to evaluate and is discussed in Chapter 4.

The Mn nucleus has I= 5/2 and m_I = {+5/1,+3/2,+1/2,-1/2,-3/2,-5/2}. The electron spin value for the multiline is S_T= 1/2, with m_s = {-1/2,+1/2}. A system with S_T=3/2 has m_s = {-3/2,-1/2,+1/2,+3/2}. The product spin functions of these states, $|m_{I1},m_{I2},m_s\rangle$, are taken as the basis functions to solve the above spin Hamiltonian for a particular system.

For a system with three interacting nuclei, the vector coupling scheme is more complex. If, however, the coupling between the nuclei is such that J_{12} =J_{13} = J then the system simplifies considerably (McCusker, *et al.*, 1992). The Hamiltonian for such an interaction becomes:

$$\mathcal{H}= -2J(\mathbf{S_1}\cdot\mathbf{S_2} + \mathbf{S_1}\cdot\mathbf{S_3}) - 2J_{23}\,\mathbf{S_2}\cdot\mathbf{S_3}$$

If the total spin is defined as $\mathbf{S_T} = \mathbf{S_1} + \mathbf{S_A}$ and $\mathbf{S_A} = \mathbf{S_2} + \mathbf{S_3}$, the Hamiltonian becomes:

$$\mathcal{H}= -J(\mathbf{S_T}^2 - \mathbf{S_A}^2) - J_{23}\mathbf{S_A}^2.$$

The projection operators can then be calculated by first calculating the projection operator for $\mathbf{S_A}$ and then projecting this value on to the total spin, $\mathbf{S_T}$. This method is used for the ground state g=4.1 signal in Chapter 4, where a symmetric three spin coupling model is assumed with S_1= 1/2. This corresponds to a radical which bridges two Mn ions of equal oxidation state.

The Zeeman interaction

The energy of the magnetic dipole $\mu_e = -\beta(\mathbf{L} + g_e\mathbf{S})$ in a magnetic field is given by $\mathcal{H}= \beta\,(\mathbf{L} + g\mathbf{S})\cdot\mathbf{H_o}$. The Hamiltonian is more often expressed as $\mathcal{H}= g\beta\mathbf{S}\cdot\mathbf{H_o}$ where g is no longer the g-value of the free electron but has been modified to accommodate the effect of spin-orbit coupling, which induces some excited state orbital angular momentum even into a single unpaired spin in an orbital singlet (L=0) ground state. If a system with S>1/2 possesses orbital angular momentum, it is often expressed in the Zeeman term as an effective g-value, now differing substantially from g=2, and an 'effective' S= 1/2 state. For example the effective g-value for an axially symmetric S=3/2 system, where the orbital angular momentum interacts in the xy-plane, has $g_\perp \sim 4$ and $g_{||} \sim 2$ (Carrington and McLachlan, 1967). The || and $\perp$ symbols refer to orientations parallel and perpendicular to the molecular symmetry (z) axis.

The nuclear Zeeman interaction

The nuclear Zeeman interaction describes the interaction of the nuclear magnetic moment with the static field. It takes the form

$$\mathcal{H}= \sum_i g_n\beta_n\mathbf{H_o}\cdot\mathbf{I_i}$$

For the two Mn nuclei considered here we have :

$$\mathcal{H}= g_n\beta_n\mathbf{H_o}\cdot(\mathbf{I_1} + \mathbf{I_2})$$

Often this interaction is small and falls within the linewidth of the individual transitions within the powder pattern spectrum and can therefore be ignored. However the field at Q-band is large and the nuclear Zeeman interaction may contribute to the observed EPR spectra. β_n is the nuclear Bohr magneton. The nuclear g-value is calculated using the NMR frequency for ^{55}Mn (14.798 MHz at 1.4092T; 24.667 MHz at 2.3490 T; Source Dean, 1985), which give the nuclear g-value for ^{55}Mn =1.376. The maximum value of this interaction (with both nuclei I = 5/2) takes the value of ~7 Gauss at X-band and ~ 25 Gauss at Q-band. The nuclear Zeeman has therefore been included in the Hamiltonian.

Hyperfine interaction

The hyperfine interaction has two contributions, the contact interaction term and the dipolar interaction term.

Contact interaction

The interaction between the magnetic moments of the electrons and nuclei is called the contact, or Fermi, interaction. It is isotropic in nature and represent the energy of the nuclear moment in the magnetic field produced at the nucleus by the electrons. The interaction takes the form:

$$\mathcal{H}=a_{iso}\,\mathbf{I}\cdot\mathbf{S} = a_{iso}(I_xS_x + I_yS_y + I_zS_z).$$

The coupling constant is given by

$$a_{iso} = (8\pi/3)\, g\beta g_n\beta_n\, |\psi(0)|^2$$

where $|\psi(0)|^2$ is the squared amplitude of the electronic wave function at the nucleus. For this term to be non-zero, the electron has to have a non-zero probability density at the nucleus - in other words, the wave function has to have some *s*-orbital character, as all other atomic orbitals have nodes at the nucleus (Carrington and McLachlan, 1967).

Dipolar interaction

The magnetic moments of the electron and nucleus couple according to classical dipolar coupling:

$$E = \frac{\mu_e \cdot \mu_n}{r^3} - \frac{3(\mu_e \cdot \mathbf{r})(\mu_n \cdot \mathbf{r})}{r^5}$$

μ = the magnetic moment vector (for electron and nucleus respectively)

r = the vector between the two moments with cartesian components x,y,z

r = the distance between the two moments.

Whenever the electron cloud has spherical symmetry, this interaction averages to zero. It is therefore a measure of the anisotropy of the orbital carrying unpaired spin density within a molecule.

Substituting $\mu_e = -g\beta\mathbf{S}$ $\mu_n = -g_n\beta_n\mathbf{I}$ the Hamiltonian becomes:

$$\mathcal{H} = -g\beta g_n\beta_n\left\{\frac{\mathbf{I}\cdot\mathbf{S}}{r^3} - \frac{3(\mathbf{I}\cdot\mathbf{r})(\mathbf{S}\cdot\mathbf{r})}{r^5}\right\}$$ and the principal values of the interaction become

$$a_{xx} = -g\beta g_n\beta_n\left\langle\frac{r^2 - 3x^2}{r^5}\right\rangle$$ averaged over the whole distribution of the unpaired spin. The terms for a_{yy} and a_{zz} are similar (Carrington and McLachlan, 1967). From this expression the magnitude and orientation of the anisotropic dipolar interaction can be estimated. See Chapter 2.

The Hamiltonian for this interaction is: $\mathcal{H} = \mathbf{S}\cdot\boldsymbol{a}_{aniso}\cdot\mathbf{I}$ and $\boldsymbol{a}_{aniso}$ is now a tensor interaction.

The total spin Hamiltonian for the hyperfine interaction is:

$$\mathcal{H} = a_{iso}\mathbf{I}\cdot\mathbf{S} + \mathbf{S}\cdot\boldsymbol{a}_{aniso}\cdot\mathbf{I} = \mathbf{S}\cdot\boldsymbol{a}\cdot\mathbf{I}.$$

The zero-field splitting term

The zero-field splitting (ZFS) parameter removes the degeneracy of spin wave functions even without the influence of an applied magnetic field. In transition metal ion complexes the ZFS term is largely due to spin-orbit coupling rather than electron dipole-dipole interaction as seen in organic molecules (triplet states). This interaction is only present in systems with $S>1/2$. For an $S=3/2$ system with axial symmetry, the energy levels are split into two (Kramer's) doublets at zero field separated by $2D$. The interaction is discussed more fully in Chapter 4.

Quadrupole interaction

Quadrupole effects arise out of the interactions of a non-spherical nucleus ($I>1/2$) with a non-spherical electric field gradient set up around that nucleus, due to the charges from either other nuclei or electrons that surround the nucleus. The potential gradient at the nucleus in question, due to an electric charge, e, located at a position $\mathbf{r}(x,y,z)$ from the origin (nucleus), is given by

$$V_{zz} = \frac{\partial^2 V}{\partial z^2} = e\frac{(3z^2 - r^2)}{r^5}$$ or $V_{zz} = eq$, with similar terms for V_{xx} and V_{yy}

The field gradient, q, is often reported in atomic units. The Hamiltonian takes the form:

$$\mathcal{H}=Q'[3(I_z^2- I(I+1))+\eta(I_x^2-I_y^2)]$$

$$Q' = \frac{e^2qQ}{4I(2I-1)} = \text{measured interaction}$$

eq = field gradient at nucleus

$|e|Q$ = quadrupole moment for the nucleus

$\eta = V_{xx}-V_{yy}/V_{zz}$, the asymmetry parameter

Transition probabilities

The paramagnetic ion interacts not only with the steady applied field, H_o, but also with an oscillating (time-varying) field H_1 arising from the microwave field used to induce resonance. This oscillating field for the standard EPR experiment is polarised and perpendicular to H_o. The interaction Hamiltonian $\mathcal{H}'$ is then

$$\mathcal{H}' = \beta\, \mathbf{H_1} \cdot \mathbf{g} \cdot \mathbf{S} \sin \omega t.$$

For a simple S=1/2 system the induced transition rate between 'spin up' and 'spin down' states is given by

$$I = \frac{\pi^2\beta^2}{h} g(v) \left| \langle \psi_\uparrow | \mathbf{H_1} \cdot \mathbf{g} \cdot \mathbf{S} | \psi_\downarrow \rangle \right|^2 \qquad 1.2$$

where $|\psi_\uparrow\rangle$ and $|\psi_\downarrow\rangle$ are the eigenfunctions of the spin Hamiltonian $\mathcal{H}_0$ for the energy levels $E_\uparrow$ and $E_\downarrow$. g(v) is the line shape function, see below. The H_1 field is perpendicular to the static field H_O and the matrix element required to calculate the transition probability therefore involved components in the x or y direction

$$\mathcal{H}_{\uparrow\downarrow} = \langle \psi_\uparrow | H_1 \cdot g_\perp \cdot S_x | \psi_\downarrow \rangle.$$

As we are really only interested in relative intensities, the intensity term simplifies to

$$I = \left| \langle \psi_\uparrow | g_\perp \cdot S_x | \psi_\downarrow \rangle \right|^2.$$

For an isotropic system the transition probability is simply 1.

For an S=3/2 system, the matrix element is

$$\mathcal{H}_{\uparrow\downarrow} = H_1 \left\langle \psi_\uparrow \left| g_{xy}S_x + g_{yy}S_y + g_{zy}S_z \right| \psi_\downarrow \right\rangle \qquad 1.3$$

In this situation the g-value becomes important as the anisotropy in g is large: $g_\perp$ ~4 and $g_{||}$ ~ 2. See below and Chapter 4.

Forbidden transitions

The normal selection rule for EPR transitions is $\Delta m_s = \pm 1$ and $\Delta m_i = 0$. This is true if there is no mixing of electron and nuclear eigenstates. When there is mixing, which arises from off-diagonal terms in the Hamiltonian matrix (corresponding to anisotropic hyperfine interactions), transitions with $\Delta m_i = \pm 1$ become partially allowed. The intensity for such 'forbidden transitions' is small and of order $A^2/(g\beta H_0)^2$, which, for a Mn ion at X-band, is ~10^{-2} (Orton, 1968). The magnitude of the forbidden transitions increase when quadrupolar coupling is introduced, as nuclear state mixing is now much more pronounced. The quadrupolar coupling induces transitions within the same nuclear spin manifold. When the magnitude of the quadrupole interaction is substantial (say 10% of hyperfine interaction), the $\Delta m_i = \pm 1$ transition intensity is an order of magnitude larger than for $\Delta m_i = \pm 1$ transitions resulting out of hyperfine coupling. Quadrupolar coupling also gives rise to $\Delta m_i = \pm 2$ transitions, but these are again of small intensity. The net effect, when quadrupolar coupling is of sufficient magnitude, is that a great many transitions are induced.

Spin state populations

The oscillating H_1 field gives rise to transitions from an upper to lower energy state due to emission of microwaves, as well as transitions from a lower to an upper arising from absorption. If the populations are equal, emission is equal to absorption and no observable signal will result. For there to be net absorption, the lower energy state has to be more populated than the upper.

At thermal equilibrium the population of the upper and lower states obey the Boltzmann distribution function:

$$N^-/N^+ = \exp(\Delta E/kT)$$

Where: N^+ = population of upper state

N^- = population of lower state

For an EPR experiment with H_o= 0.32 T the following table gives the population ratio:

Table 1.2: Variation of spin populations with temperature.

Temperature	N^-/N^+
295K	1.0015
77K	1.007
5K	1.09

The EPR experiment relies on this small population difference.

Linewidth

The absorption of energy giving rise to a particular transition does not, in practice occur at a unique value of the static magnetic field. The net result is that the absorption lines are broadened. Several factors influence line broadening, they can be homogenous or inhomogenous. Homogenous broadening arises out of the finite life time of the higher energy state involved in the transition. These can relax via spin-lattice relaxation (the interaction of the ion with the surrounding lattice, called T_1 processes) or spin-spin relaxation (dipole-dipole interaction of similar ions, called T_2 processes). Inhomogenous broadening is comprised of an envelope of homogenously broadened lines (Orton, 1968). Factors that influence inhomogenous broadening are, for instance, poorly resolved hyperfine structure (particularly in the g=4 signals) and the so-called g-strain, which results from a statistical spread of g-values in a frozen glass. The linewidth we see in a powder pattern spectrum results from randomly oriented molecules, fixed in position in the frozen glass rather than experiencing rotational averaging due to tumbling.

There are two commonly used lineshape functions:

Lorentzian $$A(H) = \frac{A_o}{1 + a^2(H_o - H)^2}$$

and Gaussian $$A(H) = A_o \exp[-b^2(H_o - H)^2]$$

where A_o = the amplitude at H_o , a and b are constants and $A(H)$ is the amplitude at a particular field H. The Lorentzian curve is sharper than the Gaussian near the centre, but has considerably greater amplitude in the wings. Usually the true line shape lies somewhere between the two functions (Orton, 1968).

Because a powder pattern spectrum typically has inhomogenous line broadening, resulting from a statistical spread of broadened lines, the Gaussian lineshape was chosen. The actual form of the Gaussian used in the analysis is:

$$A = \exp\left[-(b^2/lw^2)\right]$$

where b is stepped through the total width of the envelope ($-b_{max}/2$ ... $+b_{max}/2$) and lw is the half width when A~0.77 (b/lw=1/2). For the simulation programs lw is varied to fit the spectrum in question and b_{max} is set for a particular simulation program. For instance, the total envelope width for the g=4

programs is about 150 Gauss (for each line in the powder pattern spectrum) and 75 Gauss for the multiline spectra.

Powder pattern spectra

The Hamiltonian given above is expressed in the laboratory frame, that is, in the axis system in which the experiment is made. Each molecule in a frozen sample has its own molecular (principal) axes orientation with respect to the laboratory frame. The EPR spectra of PSII preparations are mostly powder pattern spectra; that is, they arise from molecules frozen in random orientations in the sample. To simulate such a spectrum, one must calculate individual spectra at a number of random orientations of the molecule and add them up to form the powder pattern spectrum.

If the principal axes systems for all tensors are assumed to be coincident, as a first approximation, the field H_0 makes polar angles θ,ϕ with the molecular frame. Any diagonal (molecular frame) matrix, $\mathbf{B'}$, can be transformed into the laboratory frame matrix $\mathbf{B}$ by a unitary transformation of the form $\mathbf{B}=\mathbf{R}\cdot\mathbf{B'}\cdot\mathbf{R^t}$, where $\mathbf{R}$ is the matrix of direction cosines (Rose, 1957).

$$\mathbf{R}(\phi,\theta) = \begin{bmatrix} \cos\phi\cos\theta & -\sin\phi & \cos\phi\sin\theta \\ \sin\phi\cos\theta & \cos\phi & \sin\phi\sin\theta \\ -\sin\theta & 0 & \cos\theta \end{bmatrix}$$

The molecular frame interaction tensor is diagonal. In a system where the g-value does not vary much it is sufficient to rotate over the two angles ϕ,θ. However to calculate transition probabilities for a system where the g-anisotropy is substantial a third rotation may be required. This third rotation, over angle γ, describes the orientation of the H_1 field relative to the molecular frame. See Chapter 4.

It is important to sample each orientation with the same probability. This is described fully in Chapter 2.

2: SIMULATION OF THE S_2 STATE MULTILINE EPR SIGNAL OF PHOTOSYSTEM II - A MULTIFREQUENCY APPROACH.

Introduction

Comparison of the multiline signal with X-band EPR spectra of dimeric model compounds reveals that the multiline signal is more complex: it exhibits detailed internal 'superhyperfine' structure and more than the 16 peaks generally observed in model compounds. Of particular note are the peaks of low, variable intensity beyond the commonly recognised width of ~1800 Gauss (>18-20 peaks). The multiline Q-band spectrum shows the same number of peaks (Smith, *et al*, 1993) but less of the superhyperfine structure, reflecting both linewidth effects and the increasing dominance of the Zeeman interaction at high microwave frequency. At lower frequencies, such as S-band, the hyperfine interactions are relatively more important. The multiline spectrum at S-band is particularly complex, exhibiting ~50 lines.

Haddy *et al* (1994) have studied the EPR spectra of Mn^{III}-Mn^{IV} catalase at three frequencies (S-band, X-band and P-band). Like model compounds, the catalase spectrum shows 16 peaks at X-band. The S-band spectrum (~20 peaks) does not exhibit the same complexity as the S-band of the PSII multiline signal. In fact, it is remarkably similar to the spectra at both X- and P-band. The additional complexity of the PSII S-band multiline signal however, cannot be explained simply by a linewidth effect, nor can it be adequately explained in terms of hyperfine anisotropy alone.

The above factors have led to the belief that all four Mn ions give rise to the multiline pattern, with each Mn ion contributing substantially different effective hyperfine interactions to the total net spin=1/2 system. Simulations based on the above assumption have appeared (Bonvoisin, *et al.*, 1992; Kusunoki, 1992; Zheng and Dismukes, 1992; Zheng and Dismukes, 1996). The simulations, with the exception of those by Kusunoki, have been performed at X-band only, and no attempt has yet been made to address the superhyperfine structure or additional peaks. Even though oriented spectra at X-band (Rutherford, 1985) and S-band (Haddy, *et al.*, 1989) have shown that substantial hyperfine anisotropy exists in the centre giving rise to the multiline signal, the simulations have been confined to isotropic (Bonvoisin *et al*, Kusunoki) or axial hyperfine parameters (Zheng and Dismukes).

Synthetic complexes of multimeric Mn have been prepared which attempt to model aspects of the structural organisation and EPR properties of the OEC (for example: Bashkin, *et al.*, 1987; Kessissoglou, *et al.*, 1989; Sarneski, *et al.*, 1990). Although all three model compounds have EPR signals that exhibit a ground S=1/2 state signal with multiple lines, the only spectrum that resembles the OEC multiline signal (Kessissoglou, *et al.*, 1989) stems from a Mn^{III}-Mn^{II}-Mn^{III} trimer, whereas EXAFS and XANES studies indicate an average oxidation state greater than III for Mn in the S_2 state of the OEC (Goodin, *et al.*, 1984; Yachandra, *et al.*, 1987; Penner-Hahn, *et al.*, 1990).

Zheng, *et al* (1994) have studied the factors that influence the number of resolved lines in the EPR spectra of Mn dimers. They found that the number of lines in the EPR spectrum of a Mn dimer differing in oxidation state by one and antiferromagnetically coupled, depends on the strength of the exchange interaction, which in turn directs the influence of the zero field splitting interaction on the spectrum. In particular, the number of lines can differ from 16 depending on the strength of these interactions.

The results summarised above indicate that the multiline signal in the S_2 state of PSII could arise from a magnetically isolated Mn^{III}-Mn^{IV} dimer. Here I explore circumstances under which such a dimer might give rise to the detailed multiline EPR spectrum observed in PSII. The large number of peaks resolved in the S-band multiline spectrum require that normally forbidden transitions have become substantially allowed. The most likely mechanism that could give rise to these normally forbidden transitions, is one in which the two Mn centres in the protein have sufficiently low ligand symmetry so that Mn nuclear quadrupolar effects contribute significantly to the hyperfine interaction. Under such circumstances perturbation theory is inadequate to treat the spin Hamiltonian and the problem must be solved numerically. The results reported here attempt to explain not only the general features of the multiline signal, but also its superhyperfine structure. Simulations were performed, at three frequencies; S-band , X-band and Q-band, for which good experimental data are currently available. A brief discussion of possible ligand geometries for the dimer, consistent with the fitted parameter set is also given.

Materials and methods

Experimental

PSII membrane fragments (PSII samples) were prepared from greenhouse-grown spinach as previously described (Pace, *et al.*, 1991) (Appendix 1). The

samples showed an activity of 500-600 μmol O_2 per mg chl h^{-1}. The PSII samples were suspended at about 15 mg chl ml^{-1} in a buffer containing 20 mM MES (pH 6.0 KOH), 10 mM $MgCl_2$, 15 mM NaCl and 400 mM sucrose. 4% ethanol and 1 mM EDTA were added prior to illumination. The samples were allowed to adapt in the dark at room temperature for 10 minutes prior to illumination. For X-band measurements the samples were illuminated with green light for 4 min at 200K, with subsequent storage at 77K. The light intensity was 140 W m^{-2}. The X-band spectra have been reported (Smith, *et al.*, 1993). Samples for Q-band spectra were prepared similarly but illuminated for 3 minutes at 220K.

EPR measurements were performed on a Varian V-4502 spectrometer equipped with an Oxford ESR9 helium-flow cryostat as described previously (Pace, *et al.*, 1991). Q-band measurements were performed on the same spectrometer using a home-built He flow cylindrical Q-band cavity, adapted from a Varian design (V4566) (Bramley, unpublished). This was totally contained within an Oxford Instrument flow cryostat.

Theory and calculations

The magnetic exchange interaction Hamiltonian is taken to be $-2JS_1 \cdot S_2$, where J is the exchange interaction parameter between the two Mn centres (Abragam and Bleaney, 1986). From the temperature dependence of the signal intensity in the presence of ethanol, it is inferred that the multiline signal arises from a well isolated ground state (gap to the nearest state >30 cm^{-1}, Pace, *et al.*, 1991). The magnitude of the exchange interaction places the dimer in the strong coupling regime ($D/J \ll 1$, where D is a single ion zero-field splitting parameter), so that the exchange interaction spin states can be taken as the zeroth order states. For an antiferromagnetically coupled pair the total spin will take the following values: $S = \{1/2, 3/2 \ldots 7/2\}$, where $S=1/2$ is the ground state for a dimer with a total spin 7/2 (Mn^{III}-Mn^{IV}).

The effective spin Hamiltonian for the system in a particular total spin state may be written as

$$\mathcal{H} = \mathbf{S}\cdot\boldsymbol{D}\cdot\mathbf{S} + \beta\mathbf{H_o}\cdot\boldsymbol{g}\cdot\mathbf{S} - \sum_{\text{nuclei}}(g_n\beta_n\mathbf{H_o}\cdot\mathbf{I_i} + \mathbf{I_i}\cdot\boldsymbol{A_i}\mathbf{S} + \mathbf{I_i}\cdot\boldsymbol{Q_i}\cdot\mathbf{I_i})$$

The fine structure interaction ($\mathbf{S}\cdot\boldsymbol{D}\cdot\mathbf{S}$) does not contribute to the splitting for an $S=1/2$ state. Considering only Mn hyperfine interactions, the simplified Hamiltonian takes this form:

$$\mathcal{H} = \beta \mathbf{H_o} \cdot \boldsymbol{g} \cdot \mathbf{S} - g_n \beta_n \mathbf{H_o} \cdot \mathbf{I_1} - g_n \beta_n \mathbf{H_o} \cdot \mathbf{I_2} + \mathbf{I_1} \cdot \boldsymbol{A_1} \cdot \mathbf{S} + \mathbf{I_1} \cdot \boldsymbol{Q_1} \cdot \mathbf{I_1} + \mathbf{I_2} \cdot \boldsymbol{A_2} \cdot \mathbf{S} + \mathbf{I_2} \cdot \boldsymbol{Q_2} \cdot \mathbf{I_2}$$

The parameters have been described in Chapter 1. The subscripts 1 and 2 refer to the Mn^{III} and Mn^{IV}, respectively.

$\boldsymbol{A_1}$ and $\boldsymbol{A_2}$ are the effective nuclear hyperfine interaction tensors including the spin projection factors for each individual ion spin. In the strong coupling limit, this gives $\boldsymbol{A_{1\text{effective}}}$ (Mn^{III}) = $2\boldsymbol{a_1}$ and $\boldsymbol{A_{2\text{effective}}}$ (Mn^{IV}) = $-\boldsymbol{a_2}$ (equation 1.1), where $\boldsymbol{a_1}$ and $\boldsymbol{a_2}$ are the true ion parameters. Any contribution of the zero-field splitting term of the individual Mn ions (Zheng, *et al.*, 1994) to the hyperfine interaction is included in the effective hyperfine parameter $\boldsymbol{A}$.

$\boldsymbol{Q_1}$ and $\boldsymbol{Q_2}$ are the quadrupole interaction tensors and $\mathbf{I_1}$, $\mathbf{I_2}$ are the nuclear spin vectors (I=5/2).

Expanding the Hamiltonian in the laboratory frame

The applied magnetic field is taken to be along the laboratory z-axis. The $\boldsymbol{g}$ and $\boldsymbol{A}$ interactions can be separated into an isotropic, scalar component and the anisotropic tensor elements.

<u>The Zeeman terms:</u>

$$\beta \mathbf{H_o} \cdot \boldsymbol{g} \cdot \mathbf{S} = g_{iso} \beta \, \mathbf{H_o} \cdot \mathbf{S} + \beta \, \mathbf{H_o} \cdot \boldsymbol{g_{aniso}} \cdot \mathbf{S}$$

The field is taken to be along the z-axis, therefore H_x, H_y=0 and the isotropic term becomes $g_{iso}\beta H_z S_z$

$$\beta \cdot \mathbf{H_o} \cdot \boldsymbol{g_{aniso}} \cdot \mathbf{S} = [0,0,H_z] \begin{bmatrix} g_{xx} & g_{xy} & g_{xz} \\ g_{yx} & g_{yy} & g_{yz} \\ g_{zx} & g_{zy} & g_{zz} \end{bmatrix} \begin{bmatrix} S_x \\ S_y \\ S_z \end{bmatrix} = H_z[g_{zx}S_x + g_{zy}S_y + g_{zz}S_z]$$

The nuclear Zeeman terms for each Mn are $g_n \beta_n H_z I_z$ where g_n and β_n are the nuclear g-value for Mn and nuclear Bohr magneton respectively. I= 5/2 for ^{55}Mn.

<u>The hyperfine terms:</u>

$$\mathbf{S} \cdot \boldsymbol{A} \cdot \mathbf{I}^{\,*} = A_{iso} \mathbf{S} \cdot \mathbf{I} + \mathbf{S} \cdot \boldsymbol{A_{aniso}} \cdot \mathbf{I}$$

$$A_{iso} \times [S_x, S_y, S_z] \begin{bmatrix} I_x \\ I_y \\ I_z \end{bmatrix} = A_{iso}[S_x I_y + S_y I_y + S_z I_z]$$

---

* $\mathbf{S} \cdot \boldsymbol{A} \cdot \mathbf{I}$ refers to $\mathbf{S} \cdot \boldsymbol{A_1} \cdot \mathbf{I_1}$ or $\mathbf{S} \cdot \boldsymbol{A_2} \cdot \mathbf{I_2}$

$$\mathbf{S}\cdot\boldsymbol{A}_{aniso}\cdot\mathbf{I} = [S_x, S_y, S_z]\begin{bmatrix} A_{xx} & A_{xy} & A_{xz} \\ A_{yx} & A_{yy} & A_{yz} \\ A_{zx} & A_{zy} & A_{zz} \end{bmatrix}\begin{bmatrix} I_x \\ I_y \\ I_z \end{bmatrix} =$$

$$S_x[A_{xx}I_x + A_{xy}I_y + A_{xz}I_z] + S_y[A_{yx}I_x + A_{yy}I_y + A_{yz}I_z] + S_z[A_{zx}I_x + A_{zy}I_y + A_{zz}I_z]$$

The quadrupole terms:

$$\mathbf{I}\cdot\mathbf{Q}\cdot\mathbf{I}^{\dagger} = Q_{xx}I_x^2 + Q_{yy}I_y^2 + Q_{zz}I_z^2 + Q_{xy}(I_xI_y + I_yI_x) + Q_{xz}(I_xI_z + I_zI_x) + Q_{yz}(I_yI_z + I_zI_y)$$

The complete Hamiltonian in the laboratory frame:

$$\begin{aligned}\mathcal{H} = {} & g_{iso}\beta H_z S_z + \beta H_z[1/2\, g_{zx}(S_+ + S_-) - 1/2\, ig_{yz}(S_+ - S_-) + g_{zz}S_z] + g_n\beta_n H_z I_{1z} \\ & + A_{1iso}S_zI_z + 1/2\, A_{1iso}[S_+I_{1-} + S_-I_{1+}] + 1/4\,(A_{1xx}-A_{1yy})[S_-I_{1-}+S_+I_{1+}] + \\ & 1/4\,(A_{1xx} + A_{1yy})[S_-I_{1+} + S_+I_{1-}] - 1/2\, iA_{1xy}[S_+I_{1+} - S_-I_{1-}] + \\ & 1/2A_{1xz}[S_+ + S_-]I_{1z} - 1/2\, iA_{1yz}[S_+ - S_-]I_{1z} + 1/2A_{1xz}S_z[I_{1+} + I_{1-}] - \\ & 1/2\, iA_{1yz}S_z[I_{1+} - I_{1-}] + A_{1zz}S_zI_{1z} + 1/2Q_{1zz}[3I_{1z}^2 - I_1^2] + \\ & 1/4\,(Q_{1xx} - Q_{1yy})[I_{1+}^2 + I_{1-}^2] - 1/2\, iQ_{1xy}[I_{1+}^2 - I_{1-}^2] + \\ & 1/2\, Q_{1xz}[I_{1+}I_{1z} + I_{1z}I_{1+} + I_{1-}I_{1z} + I_{1z}I_{1-}] - \\ & 1/2\, iQ_{1yz}[I_{1+}I_{1z} + I_{1z}I_{1+} - I_{1-}I_{1z} - I_{1z}I_{1-}]\end{aligned}$$

plus similar terms for interactions at the other manganese.

Where: $\boldsymbol{A_1}$ represents the hyperfine interaction

$\boldsymbol{Q_1}$ represents the quadrupole interaction at Mn^{III}

I_1 is the nuclear spin for Mn (5/2)

S is the net electron spin (1/2).

Using shift operators: $S_x = 1/2(S_+ + S_-)$,

$S_y = i/2(S_+ - S_-)$ and similarly for I_{1x}, I_{1y} and I_{2x}, I_{2y}.

The Hamiltonian is expressed in field space so that all terms are divided by $g_{iso}\beta$ and hence the parameters are expressed in Gauss.

The principal axes systems for all tensors are assumed to be coincident, as a first approximation. Introducing non-coincident tensors would add many more variables and make the already extensive calculations prohibitive. In this system, where the tensors are assumed to be coincident, the field H_o makes polar angles θ,ϕ with the molecular (principal axes) frame, as described in Chapter 1. The interaction terms in the laboratory frame become:

$$A_{1xx} = \cos^2\phi\cos^2\theta X_{1a} + \sin^2\phi\cos^2\theta Y_{1a} - \sin^2\theta\,(X_{1a}+Y_{1a})$$
$$A_{1yy} = \sin^2\phi X_{1a} + \cos^2\phi Y_{1a}$$
$$A_{1zz} = \cos^2\phi\sin^2\theta X_{1a} + \sin^2\phi\sin^2\theta_1 Y_{1a} - \cos^2\theta\,(X_{1a}+Y_{1a})$$

---

† $\mathbf{I}\cdot\mathbf{Q}\cdot\mathbf{I}$ refers to $\mathbf{I_1}\cdot\boldsymbol{Q_1}.\mathbf{I_1}$ or $\mathbf{I_2}\cdot\boldsymbol{Q_2}\cdot\mathbf{I_2}$

$A_{1xz} = A_{1zx} = \sin\theta \cos\theta (\cos^2\phi X_{1a} + \sin^2\phi Y_{1a} + X_{1a} + Y_{1a})$
$A_{1yz} = A_{1zy} = \sin\phi \cos\phi \sin\theta (Y_{1a} - X_{1a})$
$A_{1xy} = A_{1yx} = \cos\phi \sin\phi \cos\theta (Y_{1a} - X_{1a})$

X_{1a} and Y_{1a} are the diagonal components of the traceless, molecular frame, tensor $\boldsymbol{A'}$ and $Z_{1a} = -(X_{1a} + Y_{1a})$ due to the traceless nature of $\boldsymbol{A'}$. The terms for the other tensor, which are all traceless as defined, are derived similarly. The product spin functions $|m_{i1}, m_{i2}, m_s\rangle$ are taken as the basis functions for the Hamiltonian matrix ($m_{i1}, m_{i2} = +5/2, \cdots\cdots -5/2; m_s = -1/2, +1/2$). The Hamiltonian matrix, $\langle m_s m_{i2}, m_{i1} | \mathcal{H} | m_{i1}, m_{i2}, m_s \rangle$, generated in this way is 72x72 in size. g_{iso} is the isotropic component of the g-tensor (1/3 the trace).

The matrix is diagonalised using a standard routine (NAG FO2AXF, The Numerical Algorithms Group Ltd, Oxford, UK) and the energy levels derived directly from the eigenvalues. In the field range of the resulting X- and Q-band spectra, the energy levels vary linearly with the field to a good approximation and hence the field position where the transition occurs can be found by simple extrapolation, see Figure 2.1. The linear relationship breaks down at lower frequencies. At S-band this is overcome by dividing the field range into six sections, over each of which the field-energy relation again can be considered linear. The number of sections required was determined by increasing the number until no variation in the spectrum was seen. There was no significant variation between six and nine sections.

The experimental multiline spectra are powder pattern spectra. Therefore, a number of random angles θ, ϕ as described above, that will suitably sample the random orientations of the molecule to the laboratory frame, have to be generated. For a system in which all tensor axes are co-incident, it is sufficient to generate these angles over one octant of the unit sphere. The method chosen was to divide the surface of the octant into 'tiles' of equal solid angle. To avoid biasing one edge of the octant an adjustment was made so that the average discrepancy in tiling was even along both meridians. A tile subtending an angle of 4.5° along an edge results in 284 single crystal orientations added together to contribute to the powder pattern, which has been found to be more than adequate to reduce any 'sampling noise' on the simulation. A Gaussian envelope was centred on each individual transition, with the width parameter as the only lineshape variable. No m_I-dependence or orientation dependence was included. See Figure 2.2.

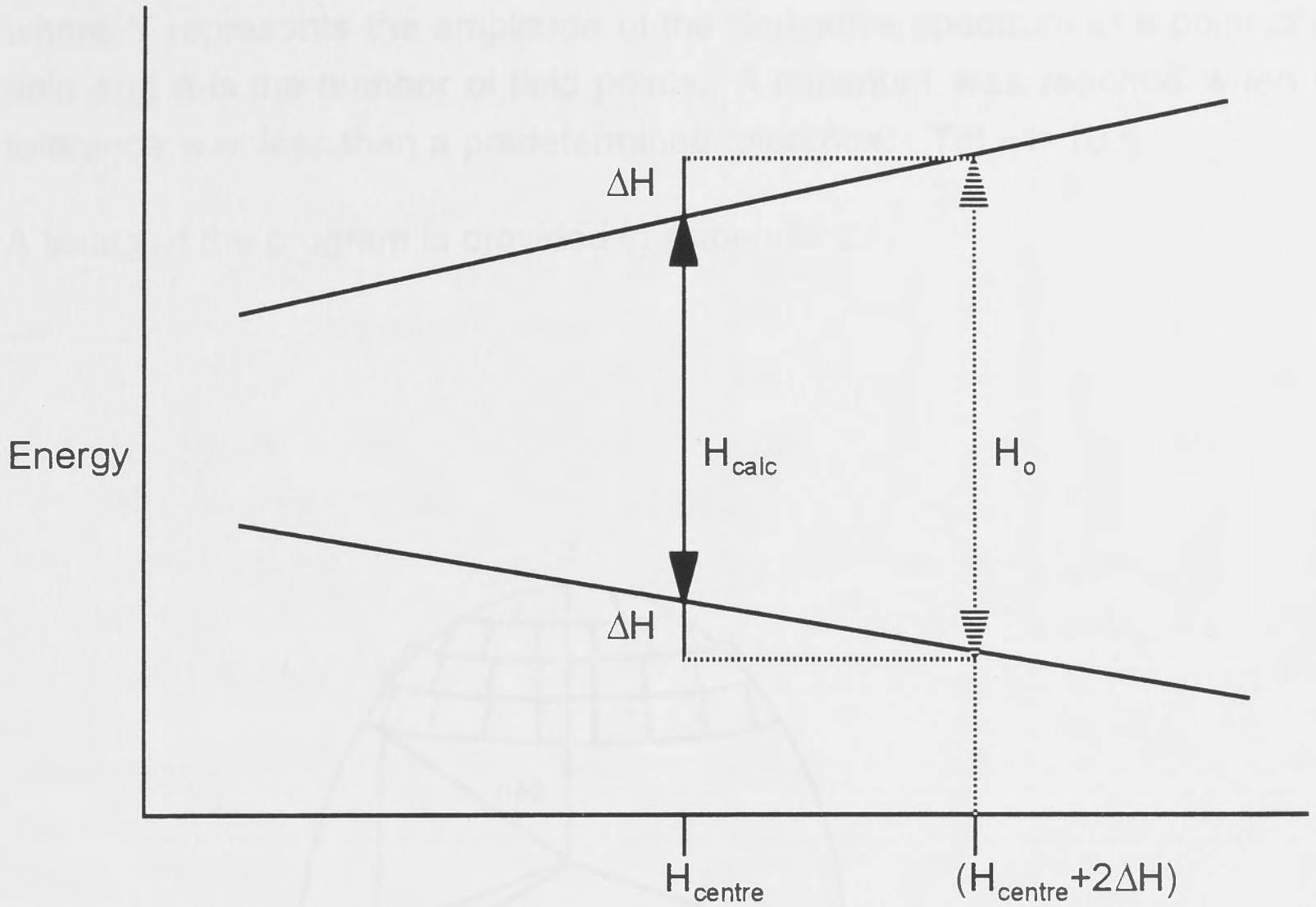

Figure 2.1.
Field positions corresponding to particular transitions between pairs of states are calculated from the difference in eigenvalues of those states, H_{calc} (in field units). In the diagram, $2\Delta H = H_O - H_{calc}$, where H_0 is the microwave quantum for the spectrum (in field units). Then the transition occurs at $H_{obs} = H_{centre} + 2\Delta H = H_O + H_{centre} - H_{calc}$, where H_{centre} is the centre field (calculated point) for the spectral region to be simulated.

The EPR transition probability (I) is proportional to $|\langle m_{\uparrow}|\beta \mathbf{H_1}\cdot\boldsymbol{g}\cdot\mathbf{S}|m_{\downarrow}\rangle|^2$, where H_1 is the amplitude of the applied microwave field magnetic vector and $\langle m_{\uparrow}|$, $\langle m_{\downarrow}|$ are the states between which the transition occurs. For a conventional system with the applied field H_o along the z-direction and small g anisotropy (estimated at ±0.5%, (Smith, *et al.*, 1993)), the simplified expression is obtained:

$$I = \text{Const}|\langle m_{\uparrow}|S_x + S_y|m_{\downarrow}\rangle|^2 \qquad 2.1$$

When the system has $S = 1/2$ it is sufficient to calculate $I = \text{Const}|\langle m_{\uparrow}|S_+|m_{\downarrow}\rangle|^2$, where S_+ is the raising operator. The derivative of the absorption spectrum was computed numerically for comparison with the experimental data.

Minimisation of the fit was carried out using a simplex routine (AMOEBA, (Press, *et al.*, 1986)). This routine minimised

$$X^2 = \sum_{i=1}^{n}\left(Y_i^{sim} - Y_i^{exp}\right)^2, \qquad Tol = 2\times\left|X^2_{high} - X^2_{low}\right| \Big/ \left(\left|X^2_{high}\right| - \left|X^2_{low}\right|\right)$$

where Y represents the amplitude of the derivative spectrum at a point of the field and n is the number of field points. A minimum was reached when the tolerance was less than a predetermined tolerance, Tol $=1\times10^{-4}$.

A listing of the program is provided in Appendix 2.

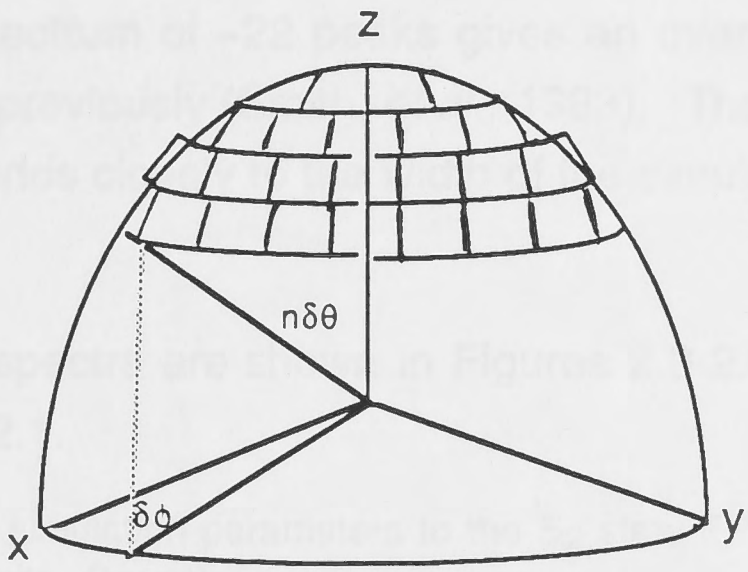

Figure 2.2. Generation of random angles in one octant of the unit sphere for calculation of powder pattern spectra.
Length of arc for an angle δθ is r sinδθ. Length of arc for angle δϕ is δϕ sinδθ. For each step n of δθ and approximate square on the surface of the unit sphere is described by δθ.δϕsin nδθ. Number of tiles (Nt) going from x-axis to y-axis is given by Nt=π/(2*δϕ). The offset required to balance the tiles across the octant OFS= (π/2- δϕ*Nt)/2. The angle δϕ,for each step of δθ is then given by: OFS +nδϕ as n is varied from 1 to Nt. A tile subtending an angle of 4.5° along an edge results in 284 spectra added together to contribute to the powder pattern.

Results and discussion

Experimental spectra

The Q-band spectrum (Figure 2.3a & b) was acquired as the illuminated-minus-dark spectrum of the downfield (a) and the upfield (b) portions of the multiline signal, acquired on separate 1000 Gauss scans. The spectrum is the average of 15 sets of scans. The break in the spectrum results from the removal of a superimposed radical signal at g=2. The X-band spectrum (Figure 2.4a & b) seen here has been reported previously (Smith, *et al.*, 1993). The S-band spectrum (Figure 2.5a & b) is reproduced with permission (Haddy, *et al.*, 1989).

In addition to the main X-band spectrum, spectra of the edges of the multiline signal were carefully acquired to ascertain the width of the spectra. Other workers (Bonvoisin, *et al.*, 1992) have indicated peaks below 2400 Gauss and above 4100 Gauss, additional to those 18-20 peaks commonly observed. When simulating the superhyperfine structure, these additional peaks of varying low intensity become important. Variable frequency studies at X-band (Pace and Smith unpubl.) have shown that peaks additional to the ~22 peaks attributed to the multiline signal have an apparent g-value quite different to that of the multiline signal. These peaks have therefore not been included. The X-band spectrum of ~22 peaks gives an overall width differing from that reported by us previously (Smith, *et al.*, 1993). The spectral edge, as we now see it, corresponds closely to the width of the simulation, see Figure 2.4a & b.

Simulations

The simulated spectra are shown in Figures 2.3-2.5 and the parameters used listed in Table 2.1.

Table 2.1. Fitted simulation parameters to the S_2 state EPR multiline signal of PSII at Q-, X- and S-band (units Gauss):

Parameter*	Q-band	X-band	S-band
a1iso‡	-75.6	-75.9	-75.7
a2iso‡	-91.4	-92.0	-91.1
a1x	-93.0	-94.6	-95.4
a1y	-108.3	-107.2	-105.4
a1z	-25.4	-25.9	-26.3
q1x	8.6	8.5	8.8
q1y	10.4	10.1	9.6
q1z	-19.0	-18.6	-18.4
a2x	-96.0	-96.7	-94.4
a2y	-127.1	-128.5	-130.0
a2z	-51.1	-50.9	-49.0
q2x	-15.1	-15.8	-16.5
q2y	8.7	8.5	8.9
q2z	6.4	7.3	7.6
gx	1.97486	1.97032	1.97012
gy	1.96670	1.96925	1.96972
gz	2.00751	2.00774	2.01116
linewidth	18	16	8

* True single ion parameters assuming a coupled Mn^{III}-Mn^{IV} dimer with A_1 effective (Mn^{III}) = $2a_1$ and A_2 effective (Mn^{IV}) = $-a_2$ (Sands and Dunham, 1975)

‡ $a1_{iso} = (a1x+a1y+a1z)/3$.

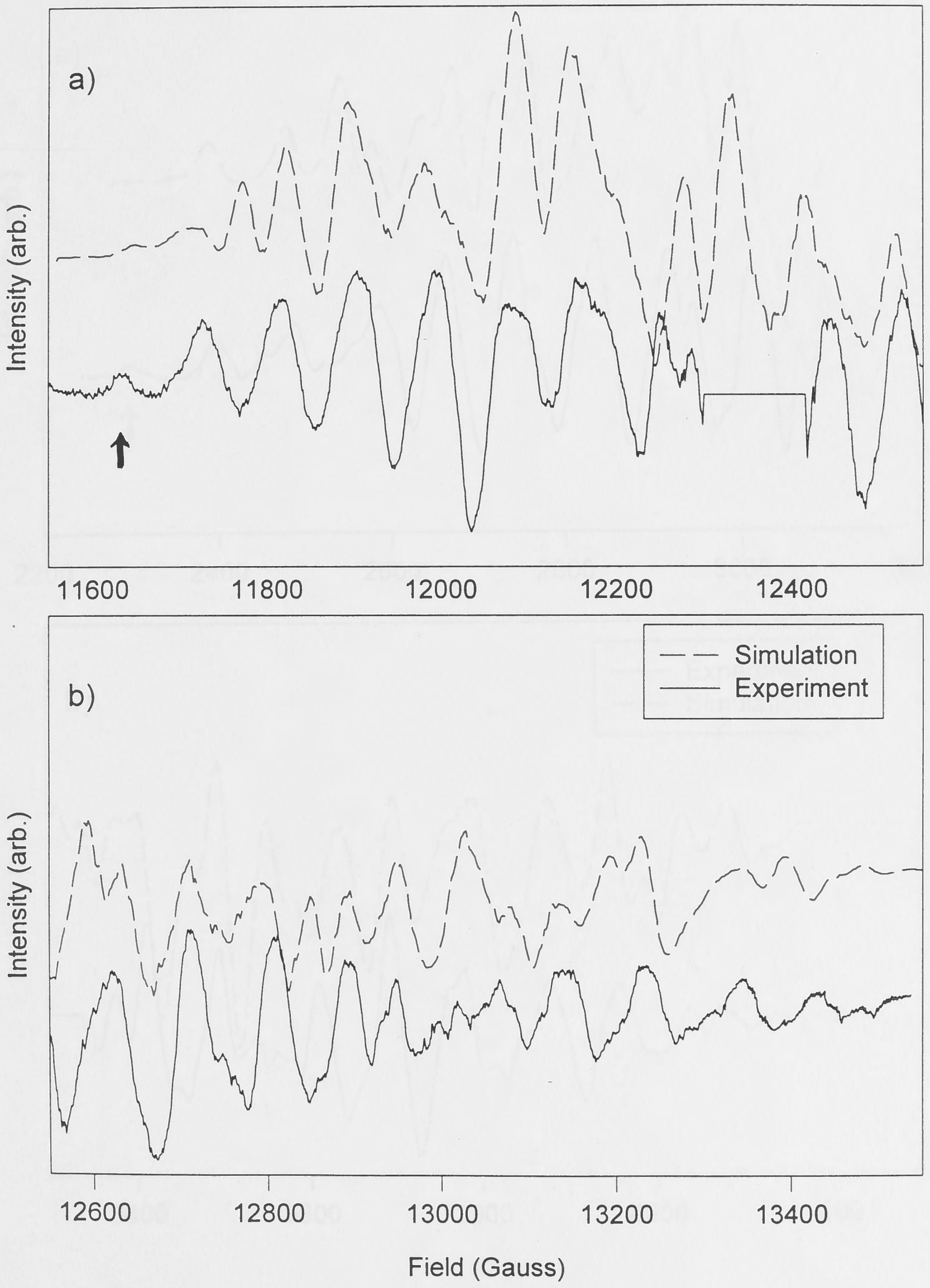

Figure 2.3. Q-band experimental difference spectrum and best fit simulation. Spectrometer conditions: Frequency 34.64 GHz, 5 Gauss modulation amplitude, 30 mW microwave power, 100 kHz modulation frequency, temperature 8K. Spectra are the averages of 15 scans and the downfield (a) and upfield (b) regions were acquired on separate 1000 Gauss scans. The parameters used in the simulation are listed in Table 2.1.

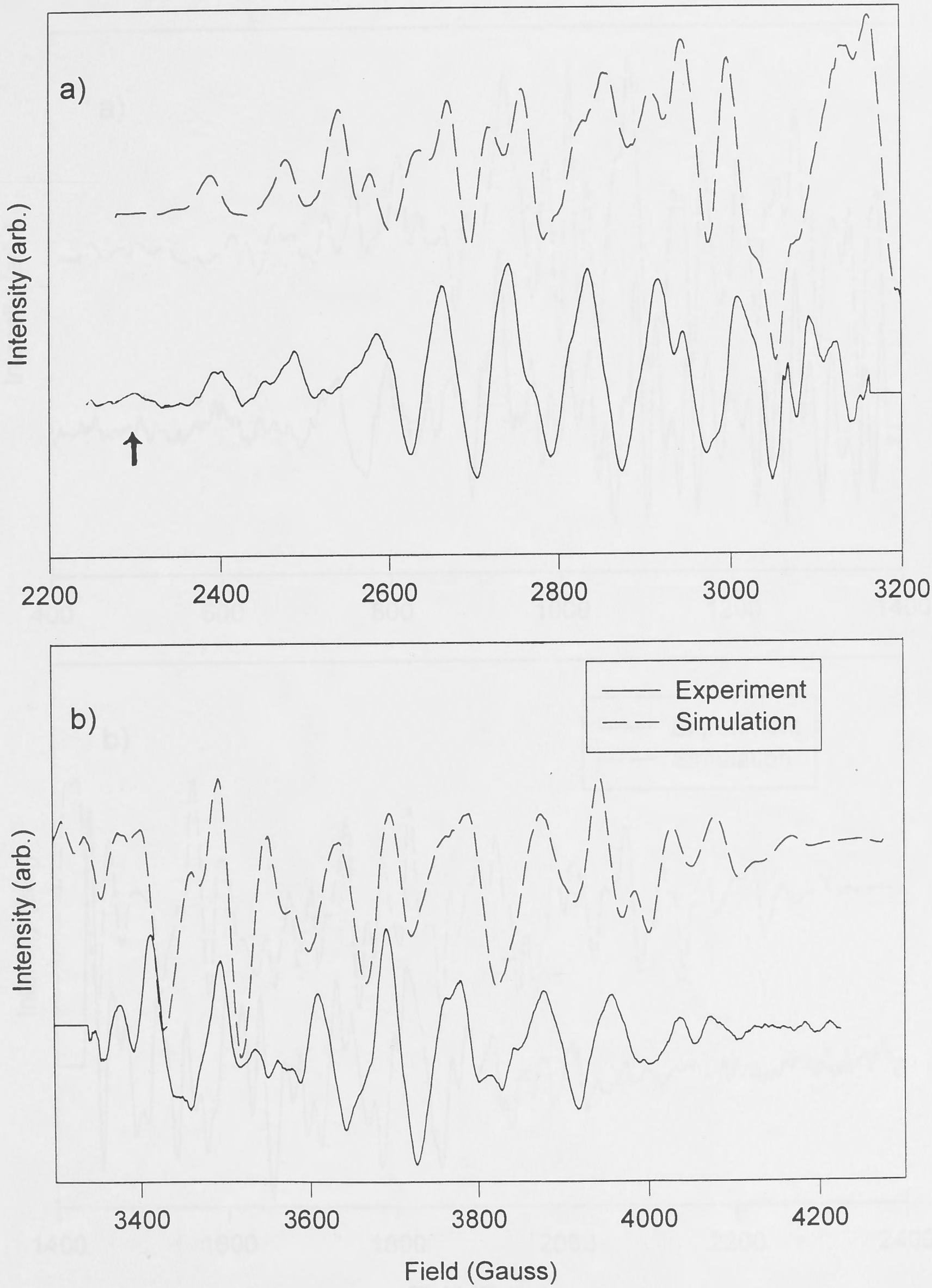

Figure 2.4. X-band experimental difference spectrum as seen in (Smith, *et al.*, 1993) together with simulated spectrum.
Spectrometer conditions: Frequency 9.04 GHz, 20 Gauss modulation amplitude, 30 mW microwave power, 100 kHz modulation frequency, temperature 8K. Spectra are averages of five scans and the downfield (a) and upfield (b) regions were acquired on separate 1000 Gauss scans. The parameters used in the simulation are listed in Table 2.1.

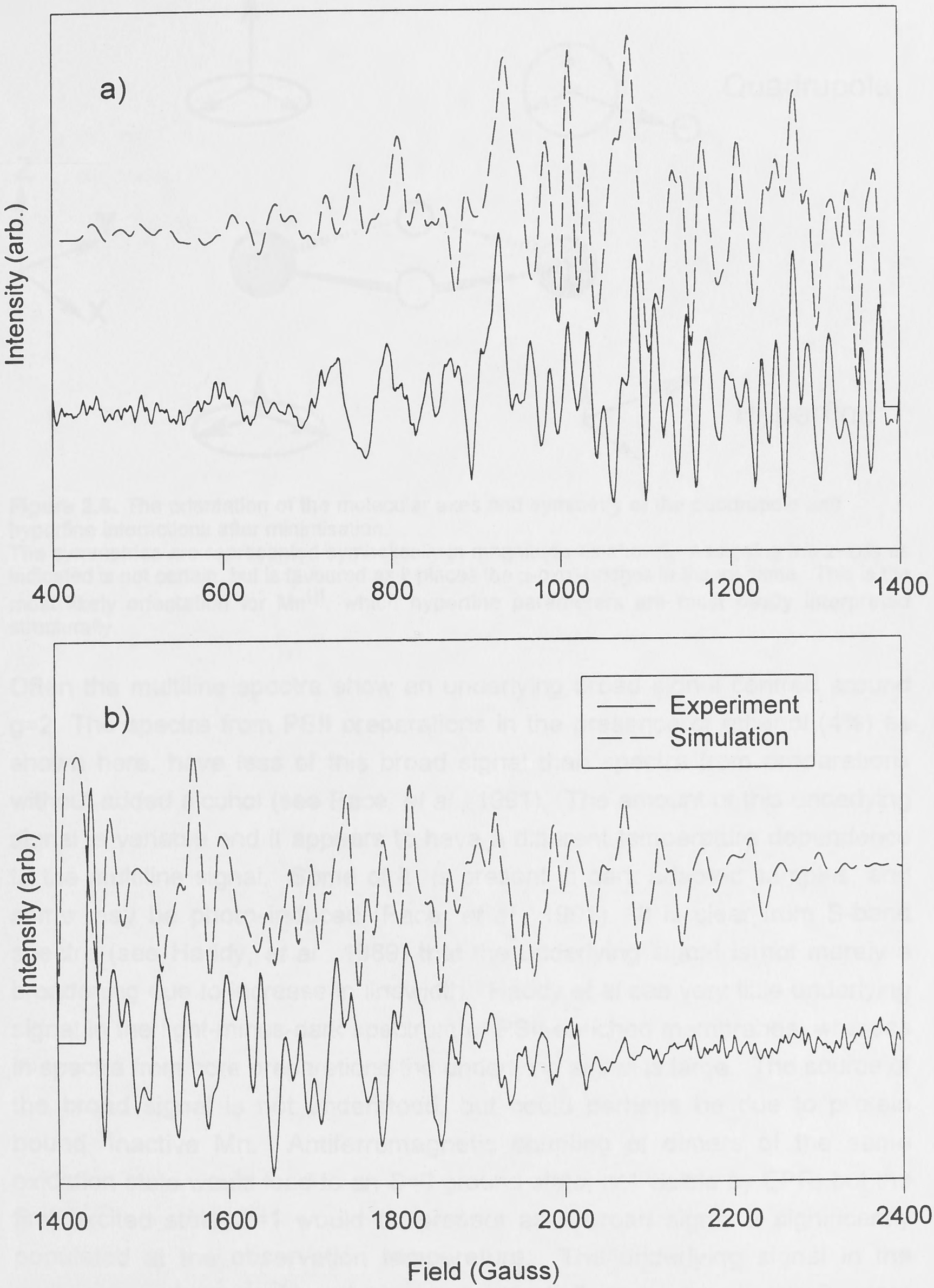

Figure 2.5. S-band experimental difference spectrum as reported in (Haddy, *et al.*, 1989) together with simulated spectrum.
(Reproduced with kind permission of the authors.) Frequency 3.91 GHz. 2% ethanol and 100 mM DCMU added. The parameters used in the simulation are listed in Table 2.1.

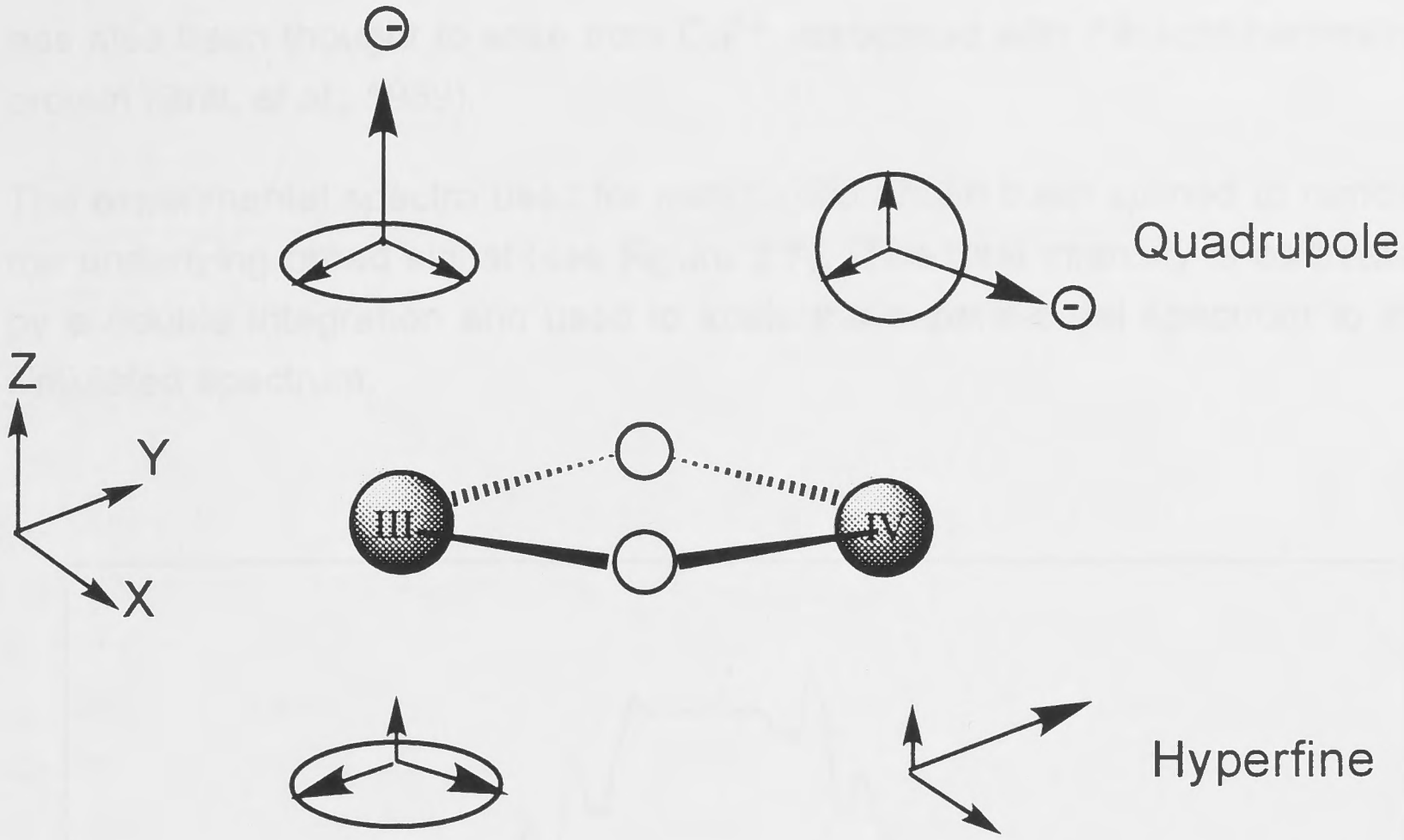

Figure 2.6. The orientation of the molecular axes and symmetry of the quadrupole and hyperfine interactions after minimisation.
The symmetries are represented symbolically in magnitude as shown. Assigning the z-axis as indicated is not certain, but is favoured as it places the μ-oxo -bridges in the xy-plane. This is the most likely orientation for Mn^{III}, which hyperfine parameters are most easily interpreted structurally.

Often the multiline spectra show an underlying broad signal centred around g=2. The spectra from PSII preparations in the presence of ethanol (4%) as shown here, have less of this broad signal than spectra from preparations without added alcohol (see Pace, *et al.*, 1991). The amount of this underlying signal is variable and it appears to have a different temperature dependence to the multiline signal. Some of it is present in dark adapted samples, and some may be photo-induced (Pace, *et al.*, 1991). It is clear from S-band spectra (see Haddy, *et al.*, 1989) that the underlying signal is not merely a broadening due to increase in linewidth. Haddy *et al* see very little underlying signal in the light-minus-dark spectrum of PSII-enriched membranes, whereas in spectra from core preparations the underlying signal is large. The source of the broad signal is not understood, but could perhaps be due to protein bound, inactive Mn. Antiferromagnetic coupling of dimers of the same oxidation state would lead to an $S=0$ ground state, not visible by EPR, but the first excited state $S=1$ would be present as a broad signal if significantly populated at the observation temperature. The underlying signal in the multiline spectrum could perhaps be due partially to centres in the S_1 state after illumination. Samples without alcohol, which are inferred to have a smaller antiferromagnetic coupling (at least in the S_2 state) (Pace, *et al.*, 1991) show more underlying signal, which supports this argument. The broad signal

has also been thought to arise from Cu^{2+} associated with the light-harvesting protein (Britt, *et al.*, 1989).

The experimental spectra used for minimisation have been splined to remove the underlying broad signal (see Figure 2.7). The total intensity is calculated by a double integration and used to scale the experimental spectrum to the simulated spectrum.

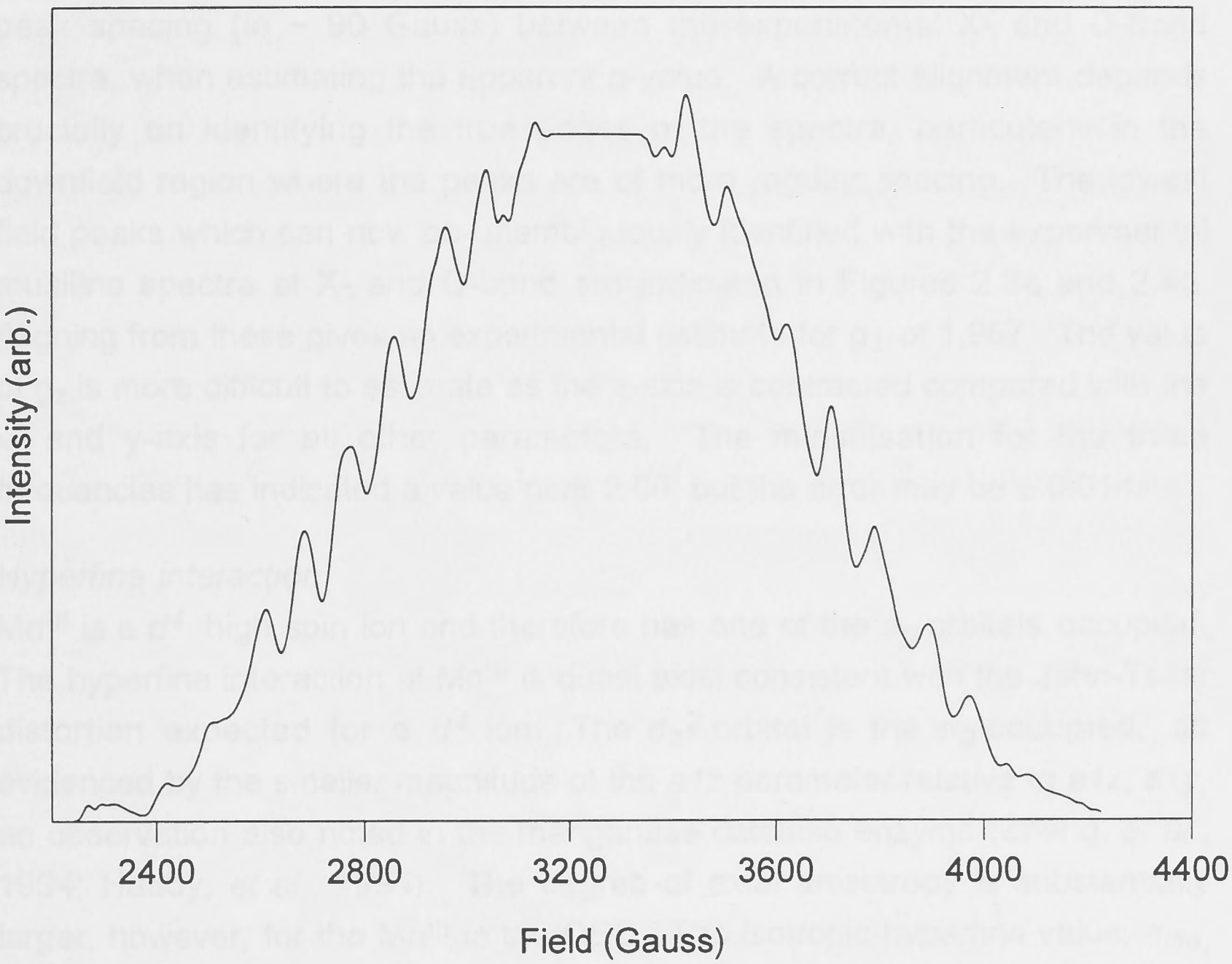

Figure 2.7. The integrated experimental X-band spectrum after splining to remove the underlying broad signal. The centre section has been removed as it contains a component from a tyrosine radical.

To simulate the spectra, the general procedure has been to start with a minimum number of parameters, incorporating additional interactions as required. Once an overall general fit has been achieved, by single calculations, the simplex routine was linked to the program. Initially only the major parameters were allowed to vary, gradually adding all parameters to vary in the minimisation. The parameters were then swapped between X- and Q-band minimisations. In this fashion an overall fit was achieved. The S-band spectrum is much more complex and minimisation was only attempted at S-

band when a good fit had been achieved at both X- and Q-band. After a global fit was achieved, the simulations were allowed to minimise independently at each frequency. The parameters reported are those reached after the individual minimisation.

g-value

The values for g_X and g_Y (~1.971 from Q-band) are lower than our earlier estimate of $g_\perp$~1.984 (Smith, *et al.*, 1993) and that found by Hansson *et al.* (1987) of g=1.982±0.002. This difference is due to an alignment error of one peak spacing (ie ~ 90 Gauss) between the experimental X- and Q-band spectra, when estimating the apparent g-value. A correct alignment depends crucially on identifying the true edges of the spectra, particularly in the downfield region where the peaks are of more regular spacing. The lowest field peaks which can now be unambiguously identified with the experimental multiline spectra at X- and Q-band are indicated in Figures 2.3a and 2.4a. Aligning from these gives an experimental estimate for $g_\perp$ of 1.967. The value of g_z is more difficult to estimate as the z-axis is contracted compared with the x- and y-axis for all other parameters. The minimisation for the three frequencies has indicated a value near 2.00, but the error may be ± 0.014.

Hyperfine interaction

Mn^{III} is a d^4 high spin ion and therefore has one of the e_g orbitals occupied. The hyperfine interaction at Mn^{III} is quasi axial consistent with the Jahn-Teller distortion expected for a d^4 ion. The $d_z{}^2$ orbital is the e_g occupied, as evidenced by the smaller magnitude of the *a1z* parameter relative to *a1x*, *a1y*, an observation also noted in the manganese catalase enzyme (Zheng, *et al.*, 1994; Haddy, *et al.*, 1994). The degree of axial anisotropy is substantially larger, however, for the Mn^{III} in the OEC. The isotropic hyperfine value, a_{iso}, for Mn^{III} of -75.7 Gauss is within the expected range (Al'tshuler and Kozyrev, 1974). The symmetry of the hyperfine interaction is consistent with that of the quadrupole interaction, together indicating that the highest energy orbital, $d_x{}^2$-$_y{}^2$, is vacant of unpaired spin density and the $d_z{}^2$ orbital has only one ligand aligned with it.

The anisotropic hyperfine interaction at Mn^{IV} of the OEC is unprecedented. However, the hyperfine interactions of the Mn dimer must be unusual to give rise the >20 line spectra, with superhyperfine structure that sets the multiline signal apart from other systems such as the manganese catalase and model compounds. A d^3 ion in a near octahedral environment is expected to have its three electrons in the spherically symmetric set of d_{xy}, d_{xz}, d_{yz} orbitals. The

interaction parameters here indicate a substantial rhombic anisotropy not expected for a d^3 ion in a near octahedral environment. The unpaired electron spin density resides mainly along the z-direction, with the y-direction most depleted of spin. This can be interpreted in terms of a substantially covalent π-bonding interaction between the metal ion and the ligands in a low symmetry environment. The antibonding molecular orbitals arising from the three metal t_{2g} orbitals and ligand p orbitals will have different amounts of metal orbital character along the x-, y- and z-directions. Because of the $\langle r^{-3} \rangle$ dependence of the dipolar hyperfine interaction (Abragam and Bleaney, 1986), only the metal d orbital character of the resulting molecular orbitals (MOs) contributes significantly to the hyperfine anisotropy. The results suggest that the d_{xy} orbital is depleted of unpaired spin relative to d_{xz} and d_{yz}, which is indicative of a ligand with a substantially different interaction to the other ligands. One such possibility is a histidine ligand. It would provide σ-bonding into a vacant e_g orbital and π-backbonding into the d_{xy} orbital of the metal.

Referring to the anisotropic hyperfine tensor components of Mn^{IV} as A_{xx} etc, it is seen that $A_{yy} \sim -A_{zz}$ and $A_{xx} \sim 0$. If the total fractional components of d_{yz}, d_{xz} and d_{xy} in the MOs, carrying unpaired spin density on Mn^{IV} are a,b and c respectively, then one has:

	d_{yz}	d_{xz}	d_{xy}	
$A_{xx}/\kappa =$	$-2a$	$+ b$	$+ c$	~ 0
$A_{yy}/\kappa =$	$+ a$	$-2b$	$+ c$	~ -1.5
$A_{zz}/\kappa =$	$+ a$	$+ b$	$- 2c$	$\sim +1.5$

Where κ is evaluated as follows:

For each electron in a pure metal $3d$, t_{2g} orbital, the nuclear hyperfine dipole-dipole interaction tensor is given by:

$$A_{||} = -g_e g_n \beta \beta_n \langle r^{-3} \rangle 2/7\mathbf{S} = -2\kappa$$

$$A_{\perp} = \kappa$$

where **S** is the total electron spin of the ion (Abragam and Bleaney, 1986), chapter 7) The $_{||}$ direction is normal to the plane of the orbital lobes, ie is the z-direction for d_{xy} etc. Assuming $\langle r^{-3} \rangle \sim 5.3$ au^{-3} for Mn^{IV} (Abragam and Bleaney, 1986),chapter 7) κ is ~ 25 Gauss.

Evaluation of a,b and c gives $b - c \sim 1$ and $a = 1/2\ (b+c)$

This calculation is only crude, in that is assumes orbital independent free ion values for $\langle r^{-3} \rangle$ among other things, but indicates that $b>a>c$ and that c is relatively small.

That b is largest, indicating that the greatest proportion of unpaired spin from d electrons resides in the d_{xz} orbital, is consistent with the x-axis being ligand deficient (see also quadrupole interaction, below) or has a ligand which is distant or weakly bound. The fact that c is the smallest would mean that the putative histidine ligand along the y-axis is oriented with the p-orbital of the π-system parallel to the xy-plane (see Figure 2.9). Two less strongly π-bonding ligands would be located along the z-axis.

The a_{iso} of -91.5 Gauss for Mn^{IV} is larger than expected. Factors which may contribute are:

1. Hyperfine constants for a Mn^{IV} ion in a low co-ordination environment can be very large. Ferrante *et al* (1977) recorded the spectra for molecular MnO_2 ($D_{\infty h}$ symmetry) in an argon matrix and found that $A_{||}$ was 125 Gauss and $A_{\perp}$ 260 Gauss. This arises from significant unpaired spin density in the metal 4*s* orbital. The large hyperfine values obtained here may merely be a reflection of an incomplete co-ordination environment for Mn^{IV} in the protein.

2. The effect of the individual ion crystal field (D) parameters in the strong coupling regime ($D/J<<1$) (Zheng, *et al.*, 1994) on the effective hyperfine parameters in a Mn^{III}-Mn^{IV} dimer, is relatively greater for the Mn^{IV} than for the Mn^{III}. For example, taking $J \sim -50$ cm^{-1}, which is large enough to ensure an isolated ground state, together with typical D values for Mn^{III} of ~-4 cm^{-1} and for Mn^{IV} of ~-1cm^{-1} (Al'tshuler and Kozyrev, 1974), results in effective hyperfine parameters of $A_1 \sim 2.2a_1$ and $A_2 \sim -1.2a_2$ (Mn^{III} and Mn^{IV} respectively). These in turn give isolated ion values of $a_{1iso} \sim -69$ Gauss and $a_{2iso} \sim -75$ Gauss. Such values are totally 'conventional' (Al'tshuler and Kozyrev, 1974) and caution against using simple arguments based on the multiline pattern width to exclude dimer models. Notwithstanding this however, the quadrupole interaction indicates an unusual ligand geometry, so that the large a_{iso} is more likely, in my view, to result from a distorted ligand environment, which is further supported by the low (rhombic) symmetry of the hyperfine parameters. Of course some combination of the above effects could be operating.

Quadrupole interaction

The quadrupole interaction depends on the product of the nuclear quadrupole moment and the non-spherically symmetric component of the electric field gradient at the nucleus. The Mn nucleus is a good potential candidate for a large quadrupole interaction as the nuclear quadrupole moment of ^{55}Mn is 0.4 to 0.6 barns, about 10 times larger in magnitude than that of ^{35}Cl (-0.04 to - 0.08) which is routinely studied by quadrupole spectroscopy. The quadrupole interaction is not often seen by EPR in synthetic Mn complexes, because the Mn ligand environment is relatively symmetric, giving an electric field gradient at the nucleus of the central cation which is nearly spherical. However, the ~50 lines seen in the S_2 state S-band spectrum, compared with the ~20 in the manganese catalase enzyme (Haddy, *et al.*, 1994) is an indication that the environment for the OEC may be highly strained leading to large nuclear quadrupolar effects. For a quadrupole interaction of the magnitude seen here, the ligand distribution must be highly non-symmetric, that is, at least one ligand must be weakly bound (ionic or distant) or not be present at all.

Table 2.2 lists quadrupole interactions studied in a number of transition metal elements. The table shows that the quadrupole interaction in a system with similar ligands varies with coordination. A five-coordinate system has a quadrupole interaction about three times that of a six-coordinate system if the five-coordinate system approximates a square pyramidal geometry. Tc^{II} and Mn^{II} shown in the table both have d^5 electron low spin configuration and are six coordinate (Baldas, *et al.*, 1984a; Fortman and Hayes, 1965). The field gradient at Mn^{II} is more than twice that at Tc^{II}, a reflection of the $\langle r^{-3} \rangle$ dependence (r being the distance between the charge and the nucleus). Tc has its outer electrons in 4*d* orbitals, rather than the 3*d* orbitals of Mn. The field gradients shown for V^{IV} reflect a range of rigidly square pyramidal complexes (Stewart and Porte, 1972). The quadrupole interaction seen in the multiline therefore is well within the expected range for a nearly square planar, five-coordinate system and could only been seen if the geometry of the molecule is severely distorted from octahedral. High spin six-coordinate complexes with inequivalent ligands do not have enough anisotropy to give rise to the magnitude of interaction seen here. There is no evidence of forbidden transitions in their EPR spectra.

Table 2.2 Estimate of field gradient (expressed as q in a.u.) at nucleus from the measured quadrupole interaction Q':

Metal ion	Coordin.	No. of *d* electrons	Nuclear spin	Q_n^* 10^{-24} cm^2	Quad. Int. Q' 10^{-4} cm^{-1}	Field grad. $\|eq\|$ (a.u.)
Tc^{III}† (Baldas, *et al* 1984a)	6	5 low spin	9/2	0.34	2	0.268
Tc^{VI} (Baldas, *et al* 1984b)	5	1	9/2	0.34	3-5	~ 0.670
Re^{VI} (Lack, Gibson, 1978)	6	1	5/2	2.3	16	0.088
Re^{VI} (Lack, Gibson, 1978)	5	1	5/2	2.3	47	0.258
V^{IV} (Belford, 1972)	6	1	7/2	-0.052	-0.032	0.016
V^{IV} (Belford, 1972)	5	1	7/2	-0.052	-0.1	0.051
V^{IV} (Stewart, Porte, 1972)	5	1	7/2	-0.052	1-3	0.510-1.532
Mn^{III}† (Fortman, Hayes, 1965)	6	5 low spin	5/2	0.4	21	0.754
$Mn^{III,IV}$#	6	4,3	5/2	0.4	~1	0.03
$Mn^{III,IV}$⊕	5	4,3	5/2	0.4	25	0.79

*Source (Landolt-Börnstein, 1988)

†$\{Tc(NO)(CNS)_5\}^{2-}$ and $\{Mn(CN)_5NO\}^{2-}$ (Baldas, *et al.*, 1984a),(Fortman and Hayes, 1965)

#Mn Catalase enzyme(Haddy, *et al.*, 1994). Estimate of Q'.

⊕Mn^{III} and Mn^{IV} quadrupole interaction as predicted by the simulation of the multiline.

In addition, because the magnitude of the quadrupole interaction has an $\langle r^{-3} \rangle$ dependency (Slichter, 1990) where r is the distance between the electron charge and the nucleus, the charge density must be close the central cation to contribute significantly to the interaction, ie the ligands must be backbonding into vacant metal orbitals.

The quadrupole interaction at Mn^{III} is quasi-axial. Previously we fitted the multiline spectrum with negative quadrupole ($Q_\perp$) parameters which gives an interpretation that the bonding is covalent (Åhrling and Pace, 1995). From the simulations of the multiline from one dimensionally oriented particles it was found that the g-tensor is not coincident with the hyperfine and quadrupole tensors (see Chapter 3). This fact led me to increase the emphasis on the S-band simulations as the g-tensor has the least effect at this frequency. The improved fit at S-band resulted in quadrupole parameters of opposite sign to those previously obtained, with some (slight) compensating alteration of the hyperfine parameters. The quadrupole interaction now has the same symmetry as the hyperfine interaction and the parameters fitted to the spectra at three frequencies and listed in Table 2.1, have a positive $Q_\perp$ value, indicating that the electric field gradient is dominated by Mn *d*- orbital charge distribution. As the d_{xy}, d_{xz}, d_{yz} orbitals, for a high spin d^4 ion are spherically symmetric and therefore do not contribute to the net field gradient at the nucleus, only the *d*-electron in the d_z^2 orbital does. As the quadrupole interaction has a dependency on $\langle r^{-3} \rangle$, it makes more sense that it should be dominated by the *d*-orbital charge distribution.

The interaction at Mn^{IV} is also quasi-axial but in this case about the x-axis, indicating that the net charge density is along the x-axis. The interaction is similar in magnitude to the quadrupole term for Mn^{III}. Previous simulations have shown that the two quadrupole tensors must have the same sign about their symmetry axes, so that Mn^{IV} now has the net charge density along the x-axis, see Figure 2.6.

An estimate of the squared *d*-orbital contributions in the MOs, similar to that carried out for the hyperfine interaction, can be also be carried out for the quadrupole interaction.

Here $P_{zz} = 2\kappa$ and P_{zz} is evaluated by $P_{||} = 3/2\ P_{zz} = \dfrac{3|e|Q_n}{4I(2I-1)}eq$

(Abragam and Bleaney, 1986). *P* designates the theoretical quadrupole interaction, to differentiate it from the empirical quadrupole interaction given by the multiline simulation (Q).

I= nuclear spin 5/2

e = electronic charge

Q_n = nuclear quadrupole moment as in Table 2.2

The field gradient at the nucleus, eq, is given by (Semin, *et al.*, 1975)

$$eq = \frac{\partial^2 V}{\partial z^2} = -e\frac{2l}{2l+3}\left\langle r^{-3}\right\rangle$$

Here $l = 2$ (for a d orbital, with $m_l = \pm 2$) and $\langle r^{-3}\rangle$ is defined as above. This gives a value for κ of 2.5 Gauss for Mn^{IV}. The contributions to the measured Q_{xx}, Q_{yy} and Q_{zz} of fractional components of d_{xy}, d_{xz}, d_{yz} in the MOs can then be calculated:

	d_{yz}	d_{xz}	d_{xy}	
$Q_{xx}/\kappa =$	$+2a$	$-b$	$-c$	~ -6.4
$Q_{yy}/\kappa =$	$-a$	$+2b$	$-c$	~+3.6
$Q_{zz}/\kappa =$	$-a$	$-b$	$+2c$	~+ 2.8

and $a \sim 3$, $b \sim c \sim 6$. This implies that the contribution to the quadrupole interaction is equal in the d_{xz} and d_{xy} orbitals and the contribution on the d_{yz} orbital is only half of the other two. That the apparent electron population numbers are large is a reflection of the fact that in this system 4p-orbital contributions and contributions from back-bonding into vacant e_g orbital are substantial. To see this, a similar calculation for the Mn^{III} was carried out. In the Mn^{III} ion, the unpaired electron contribution to the quadrupole comes only from the d_z^2 orbital (see above). For a d_z^2 orbital $P_{zz} = -2\kappa$ (ie of opposite sign to the other orbitals) and the value of κ ~2.3 Gauss ($\langle r^{-3}\rangle$ for Mn^{III} ~ 4.8 au (Abragam and Bleaney, 1986)). This gives an estimate for P_{zz} of ~ -5 Gauss. However, the measured value is ~-18 Gauss. The increase in the quadrupole interaction can only arise from an increase in the field gradient at the nucleus of the ion in question. In an octahedral complex, the ligand may backbond into vacant 4p orbitals without adding a substantial contribution to the field gradient. If, however, the complex is coordinatively unsaturated and high valent, the contribution from *charge* density in the p-orbitals is no longer spherically symmetric, and a substantial net interaction could result. This arises because the field gradient contribution from a 4p orbital is at least four times that of a 3d-orbital (Semin, *et al.*, 1975). The same effect must be taking place on the Mn^{IV} ion and in this case the x-direction, based on the magnitude of the interaction, must be ligand deficient.

Taking the two calculations of quadrupole and hyperfine interactions to the fractional contributions of d - orbitals of Mn^{IV} in the MOs:

Fractional Contribution	Quadrupole Estimate	Hypefine Estimate
a (d_{yz})	0.5	0.5
b (d_{xz})	1.0	1.0
c (d_{xy})	1.0	0.0

For the hyperfine interaction *b* - c =1 implies that *c* is small. It has been set to 0.0 here. The contributions from the quadrupole interaction have been scaled. We can see from the above that the interactions are consistent with *no* unpaired spin in the d_{xy} orbital, but there is still substantial *d*-electron density in that orbital. This implies that one ligand electron backbonds into that orbital. This is an interaction not normally seen in metal complexes where the *d*-orbitals generally have higher energy than the ligand orbitals. However, as the Mn ion becomes more positively charged its orbitals may be lowered in energy, allowing ligand electrons to backbond. *Ab initio* calculations of dioxygen complexes of Mn-porphyrins show that such an effect is possible (Dedieu, *et al.*, 1979). Significantly, in these systems the ligand geometry is five coordinate square pyramidal, as assumed here. The d_{xz} orbital points directly at the x-axis as defined by the quadrupole and hyperfine interactions. The contribution is entirely consistent with the x-direction being ligand deficient, making that orbital favoured for the largest contribution of the unpaired spin. A small amount of unpaired spin must also reside the d_{yz} orbital

The above interpretation, in terms of the Mn dimer being coordinatively unsaturated and possessing low symmetry, is tempting since relatively few likely ligands to Mn in the proteins of PSII have been identified. To date, all candidates are on the D1 peptide of the PSII reaction centre core. Diner *et al*, using site directed mutagenesis, have identified Asp-170, His-190, Tyr-161 (Y_z), possibly also Glu-189; His-332, Glu-333, Asp-342, Ala-344 (carboxy terminal residue) on the D1 protein (His-337 may also play some role) (Diner, *et al.*, 1991; Nixon and Diner, 1992) as important for the assembly of the Mn cluster. Therefore there are three, maybe four, possible protein supplied ligands at present for each Mn dimer, one presumably a histidine. As the complex accumulates charge during the oxidation cycle, further stabilisation of the charge via interaction with π–orbitals would be favourable.

Linewidth

A change in linewidth was observed with the increase in frequency, indicating that g-strain broadening is important. This is expected due to the slightly larger g-anisotropy seen in PSII compared to model compounds and the manganese catalase, together with the significantly larger hyperfine anisotropy (Haddy, *et al.*, 1994; Zheng, *et al.*, 1994). It is interesting to note that the increase in linewidth is linear between S- and X-band, but the linearity breaks down at Q-band, where the linewidth is approximately the same as at

X-band. This could be due to a contribution of relaxation effects which are inversely dependent on the applied frequency (the $\omega\tau>1$ regime).

Although the simulations are, in my judgement, convincing, they are not yet of the quality achieved for simpler dimer systems which require hyperfine only interactions. Of course the multiline pattern is far more complex than any such dimer spectra and the substantial involvement of partially allowed transitions means that both field positions and intensities must be accurately reproduced. This is particularly challenging at S-band. It is likely that some of the discrepancies observed in the simulations may be indications of non-coincidence of the principal axes directions of the five tensors associated with the two Mn ions. As noted above, this is most evident along the z-axis, where the greatest parameter variation with frequency is observed. The four hyperfine tensors are probably reasonably well aligned but the g-tensor alignment is different from the rest (see Chapter 3).

Britt *et al* (Randall, *et al.*, 1995) have studied the S_2 state of PSII with ENDOR. They find that the only model that can explain the ENDOR and EPR data is a tetranuclear model. The argument is based on the fact that, using our EPR simulation parameters, they cannot get a reasonable fit to their data. A tetranuclear model, however, gives a more reasonable fit and a reasonable ENDOR simulation of a synthetic Mn-dimer complex gives too narrow an EPR spectrum. The pulsed ENDOR experiment operates on the total absorption signal, not the derivative signal as in conventional EPR. Other spin centres which may contribute to the broad underlying signal often seen on the multiline, must then contribute in a significant manner to the total absorption signal. Figure 2.8 shows the absorption signal reproduced from Britt *et al* (Randall, *et al.*, 1995) together with the absorption signal, observed in this laboratory, from PSII samples containing 5% ethanol, which is the same regime as used by Britt *et al*. This latter signal does not contain any apparent contribution other spin centres, as is evidenced by the derivative multiline signal also shown. It is clear from Figure 2.8 that the absorption signal from Randall, *et al.*, 1995 contains additional contributions. In particular, the shape near g=2, where the ENDOR experiment was performed, is sharper than that of the multiline absorption signal in our hands. Our experience is that underlying signals of this type are suppressed, in varying amounts, by the addition of alcohol (Pace, *et al.*, 1991; Åhrling and Pace, 1995). The spectrum with no contribution from underlying signals, shown in Figure 2.8, was incubated with 5% ethanol on ice for several hours. However, if the underlying signal is present, it may contribute to the ENDOR experiment on

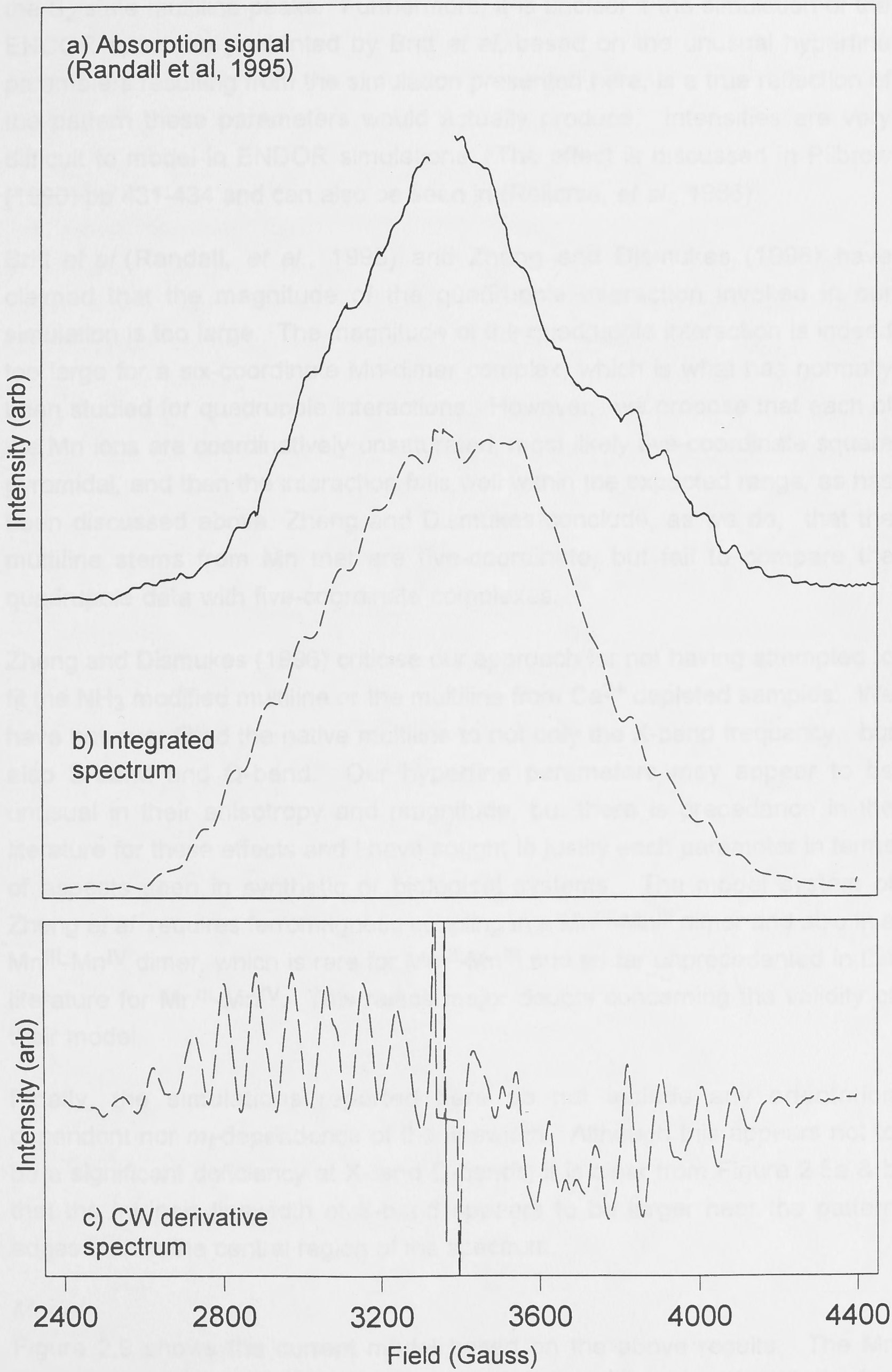

Figure 2.8 Absorption signal (Randall, *et al.*, 1995)(a) compared with integrated multiline signal (b).
(a) and (b) have been taken in presence of 5% ethanol and are aligned at g=2.00. (b) contains no contribution from underlying broad signals, as is evidenced by the derivative spectrum (c).

the S_2 state multiline peaks. Furthermore, it is unclear if the simulation of the ENDOR spectrum presented by Britt *et al*, based on the unusual hyperfine parameters resulting from the simulation presented here, is a true reflection of the pattern these parameters would actually produce. Intensities are very difficult to model in ENDOR simulations. The effect is discussed in Pilbrow (1990) pp 431-434 and can also be seen in (Reijerse, *et al*., 1986).

Britt *et al* (Randall, *et al*., 1995) and Zheng and Dismukes (1996) have claimed that the magnitude of the quadrupole interaction invoked in our simulation is too large. The magnitude of the quadrupole interaction is indeed too large for a six-coordinate Mn-dimer complex, which is what has normally been studied for quadrupole interactions. However, we propose that each of the Mn ions are coordinatively unsaturated, most likely five-coordinate square pyramidal, and then the interaction falls well within the expected range, as has been discussed above. Zheng and Dismukes conclude, as we do, that the multiline stems from Mn that are five-coordinate, but fail to compare the quadrupole data with five-coordinate complexes.

Zheng and Dismukes (1996) criticise our approach for not having attempted to fit the NH_3 modified multiline or the multiline from Ca^{2+} depleted samples. We have however fitted the native multiline to not only the X-band frequency, but also S-band and Q-band. Our hyperfine parameters may appear to be unusual in their anisotropy and magnitude, but there is precedence in the literature for these effects and I have sought to justify each parameter in terms of aspects seen in synthetic or biological systems. The model system of Zheng *et al* requires ferromagnetic coupling in a Mn^{III}-Mn^{III} dimer and also in a Mn^{III}-Mn^{IV} dimer, which is rare for Mn^{III}-Mn^{III} and so far unprecedented in the literature for Mn^{III}-Mn^{IV}. This raises major doubts concerning the validity of their model.

Finally, the simulations reported here do not include any orientation dependent nor m_I-dependence of the linewidth. Although this appears not to be a significant deficiency at X- and Q-bands, it is clear from Figure 2.5a & b that the intrinsic linewidth at S-band appears to be larger near the pattern edges than in the central region of the spectrum.

Model

Figure 2.9 shows the current model based on the above results. The Mn dimer is assumed to be di-μ-oxo, μ-carboxylato bridged to comply with the few ligands known. Model compounds of this configuration have been shown to have Mn-Mn distances of ~2.7Å (Christou, 1989). The histidine is pictured as

liganded to Mn^{IV} because of the unusual quadrupole interaction and rhombic hyperfine interaction seen at Mn^{IV}. The orientation of the histidine ring plane relative to the cluster is determined by the arguments above. Histidine is an electron-donating ligand and π-bonding would stabilise oxidation of Mn^{III} to Mn^{IV} in the S_1- S_2 transition. The other ligands are carboxylic acids and presumably substrate water, but both Mn are only 5 co-ordinate, with the ligand deficient axes determined by the quadrupole terms. Based on model compounds, the axial carboxylic acid oxygen ligands would have longer bonds to Mn (~2.1Å) than the di–μ-oxo ligands (~1.8Å)(Bashkin, *et al.*, 1987). The histidine with its strong π-interaction would presumably have a shorter bond. A bond length of ~1.9Å is reported for an imidazole ligand to Mn (Bashkin, *et al.*, 1987). These are consistent with the average bond lengths indicated by EXAFS.

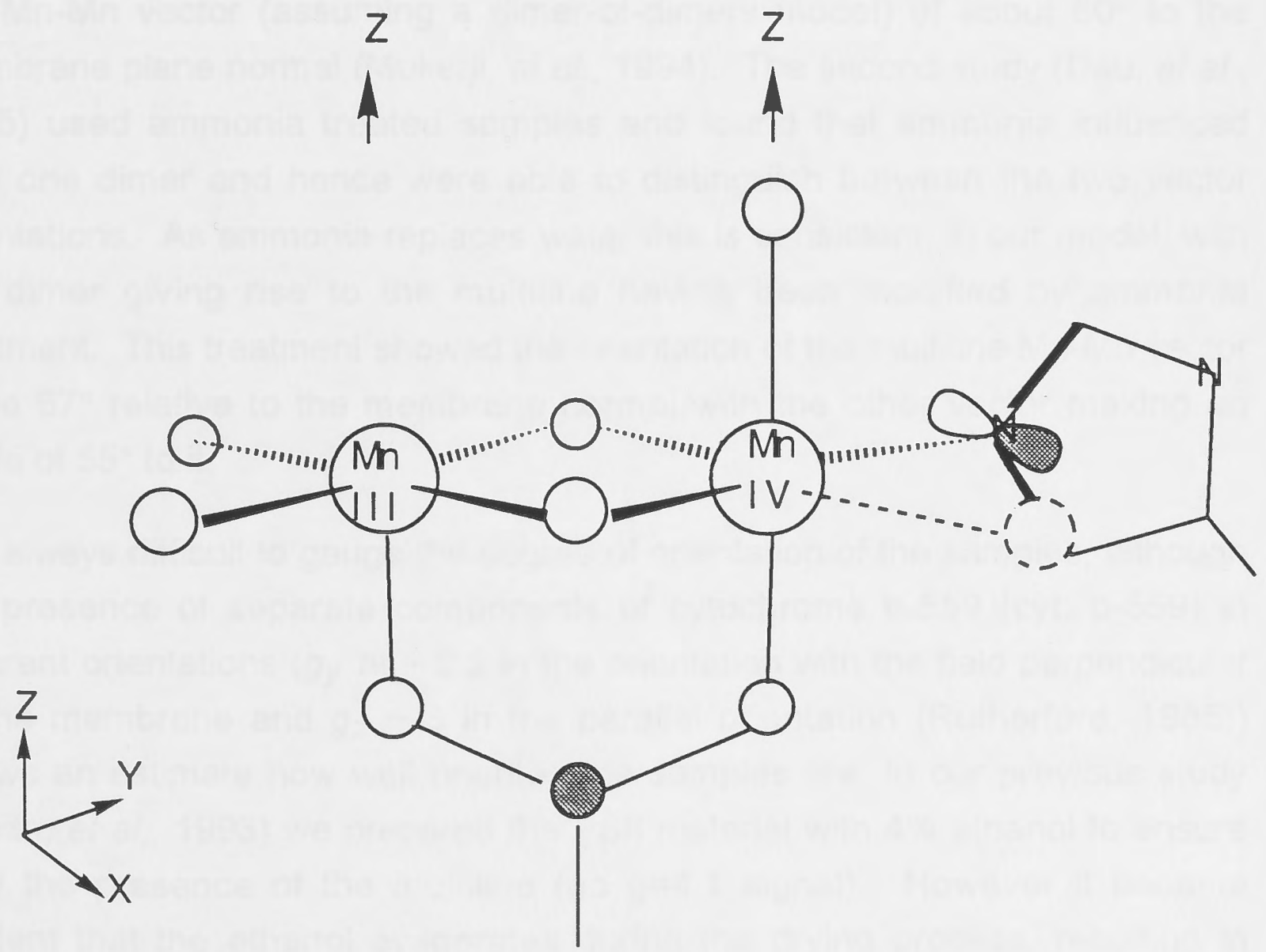

Figure 2.9: The Model
My interpretation of the parameter set given by the simulation for the Mn-dimer responsible for the multiline signal. The Mn-dimer is di-μ-oxo, μ-carboxylato bridged. The histidine is liganded to the Mn^{IV}. The dotted circle indicates a distant or very weakly bound ligand. Mn^{III} is 5-coordinate.

3: STUDIES OF THE S2 STATE MULTILINE SIGNAL OF PHOTOSYSTEM II IN ONE DIMENSIONALLY ORIENTED SAMPLES

Introduction

In the absence of a crystal structure of good resolution with the Mn cluster intact, one way to obtain information about the orientation of the Mn cluster in the membrane plane is to study one dimensionally ordered PSII samples. The first attempt at studies of oriented systems were performed by Hansson *et al* (1984), where chloroplasts were frozen under illumination in the magnetic field. Studies of PSII samples oriented on mylar have been performed by several groups (Rutherford, 1985; Haddy, *et al.*, 1989; Kim, *et al.*, 1992; Smith, *et al.*, 1993; Vänngård, *et al.*, 1992). EXAFS studies of one dimensionally ordered samples have also been reported (Dau, *et al.*, 1995; Mukerji, *et al.*, 1994). The EXAFS studies initially arrived at an approximate orientation of the Mn-Mn vector (assuming a dimer-of-dimers model) of about 60° to the membrane plane normal (Mukerji, *et al.*, 1994). The second study (Dau, *et al.*, 1995) used ammonia treated samples and found that ammonia influenced only one dimer and hence were able to distinguish between the two vector orientations. As ammonia replaces water this is consistent, in our model, with the dimer giving rise to the multiline having been modified by ammonia treatment. This treatment showed the orientation of the multiline Mn-Mn vector to be 67° relative to the membrane normal with the other vector making an angle of 55° to it.

It is always difficult to gauge the degree of orientation of the samples, although the presence of separate components of cytochrome b-559 (cyt. b-559) in different orientations (g_y at ~ 2.2 in the orientation with the field perpendicular to the membrane and g_z ~ 3 in the parallel orientation (Rutherford, 1985)) allows an estimate how well oriented the samples are. In our previous study (Smith, *et al.*, 1993) we prepared the PSII material with 4% ethanol to ensure only the presence of the multiline (no g=4.1 signal). However it became evident that the ethanol evaporates during the drying process, resulting in spectra of the non-alcohol form of the multiline, which has a nearby first excited S=3/2 state, the g=4.1 signal. By choosing a mono-alcohol with a lower vapour pressure, this problem was overcome. Reported here are studies of the multiline of one dimensionally ordered PSII samples together with simulations of their orientation dependence. Successful simulation of these spectra should allow us to predict an orientation of the Mn-dimer in the membrane plane.

Method

Experimental procedure

PSII samples were prepared from freshly picked spinach according to the method described previously (Appendix 1). The PSII samples showed an activity of ~300μmol O_2 per mg chl h^{-1} and were used immediately for oriented samples.

Preparation of Oriented Samples

The method is derived from that of Rutherford (1985). All work was carried out at 4° C, in a glove box, under nitrogen atmosphere and dim green light. To the freshly prepared PSII samples in a buffer containing 20 mM MES, 10 mM $MgCl_2$, 15 mM NaCl, 400 mM Sucrose were added 4% Propanol, 50 mM DCMU. The concentration of the sample was about 12 mg Chl mL^{-1} as determined by the method of Porra (1989). Three coats of the material were painted onto mylar strips, allowing 30 minutes of drying between coats. The strips were dried overnight under N_2 atmosphere at 90% relative humidity with propanol present. The relative humidity was provided by a saturated solution of $ZnSO_4$. Filter paper strips were draped into the $ZnSO_4$ solution and the propanol to ensure saturation. The following day the strips (~12) were packed in a N_2-flushed quartz capillary tube, with two to three unpainted strips as spacers. The tubes were flushed with N_2 again, sealed and allowed to dark-adapt at room temperature for 10 minutes or kept on ice until needed. The samples were illuminated for 3 min at 195K using yellow light, intensity ~600 W m^{-2}. Samples were cooled to 77K prior to loading them into the EPR cavity.

X-band (9.425 GHz) EPR spectroscopy was performed using a Bruker ESP300E. Three orientations of the mylar strips to the applied field (reported as the angle between the normal to the membrane plane and the applied magnetic field) were taken.

Theory

The spin Hamiltonian and the simulation program used for the multiline from one dimensionally ordered samples are the same as those employed in the multliline powder pattern simulations, with the following variations:

To simulate the spectra of one dimensionally ordered samples two rotations are performed: One rotates the principal axes (assumed coincident) of the molecule into the membrane plane (α and β) and the other rotates the membrane plane axes system to the laboratory frame (θ and ϕ). The expected

statistical variation of the alignment of the samples relative to the mylar plane, has been incorporated using a Gaussian distribution with a variance of 15°. Only two parameters are varied during the fitting procedure. They are the two angles that define the orientation of the principal axes in the membrane plane. β defines the Euler angle between the principal z-axis and the membrane plane normal. α defines the Euler angle between the principal y-axis and the membrane plane. All other parameters were those for the powder pattern spectra (Table 3.1). A listing of the program is provided in Appendix 3.

Because the variation in g-value is small for each orientation ($\Delta g \sim 0.03$), the transition probabilities were calculated in the same manner as for the powder pattern spectrum.

Results

The parameter set used in the simulations are the same as used in the unoriented powder pattern multiline simulations (Chapter 2) and shown in Table 3.1.

Table 3.1. Single ion parameters for multiline simulation a1,q1(MnIII), a2,q2(MnIV). Units: Gauss

Param	*a1*	*q1*	*a2*	*q2*	*g*	*lw*
x	-94.6	8.5	-96.7	-15.8	1.970	16
y	-107.2	10.1	-128.5	8.5	1.969	16
z	-25.9	-18.6	-50.9	7.3	2.008	16

The addition of 4% propanol to the sample resulted in the alcohol form of the multiline as evidenced by the lack of 4.1 signal. There is no significant difference between the multiline signal of conventional PSII preparations with 4% ethanol or 4% propanol added. The signal with propanol added may however be somewhat better resolved, see Figure 3.1.

The experimental oriented spectra are shown in Figure 3.2 a & b. The spectra were well oriented as could be seen by the presence of g_y component of cyt. b-559 in the parallel orientation (g~2.22) and g_z in the perpendicular (g~2.97). Contributions from Q_A^- at g=1.9 and g=1.82 were also apparent in the 45° and 90° orientations. The careful flushing of the EPR tubes with N_2 prior to sealing them ensured that no oxygen signals were present in these spectra, as is commonly seen (Berthomieu and Boussac, 1995). To match the spectra with the simulated multiline of oriented samples, underlying signals such as cyt. b-559, contributions from Q_A^- have been removed by subtracting a cubic

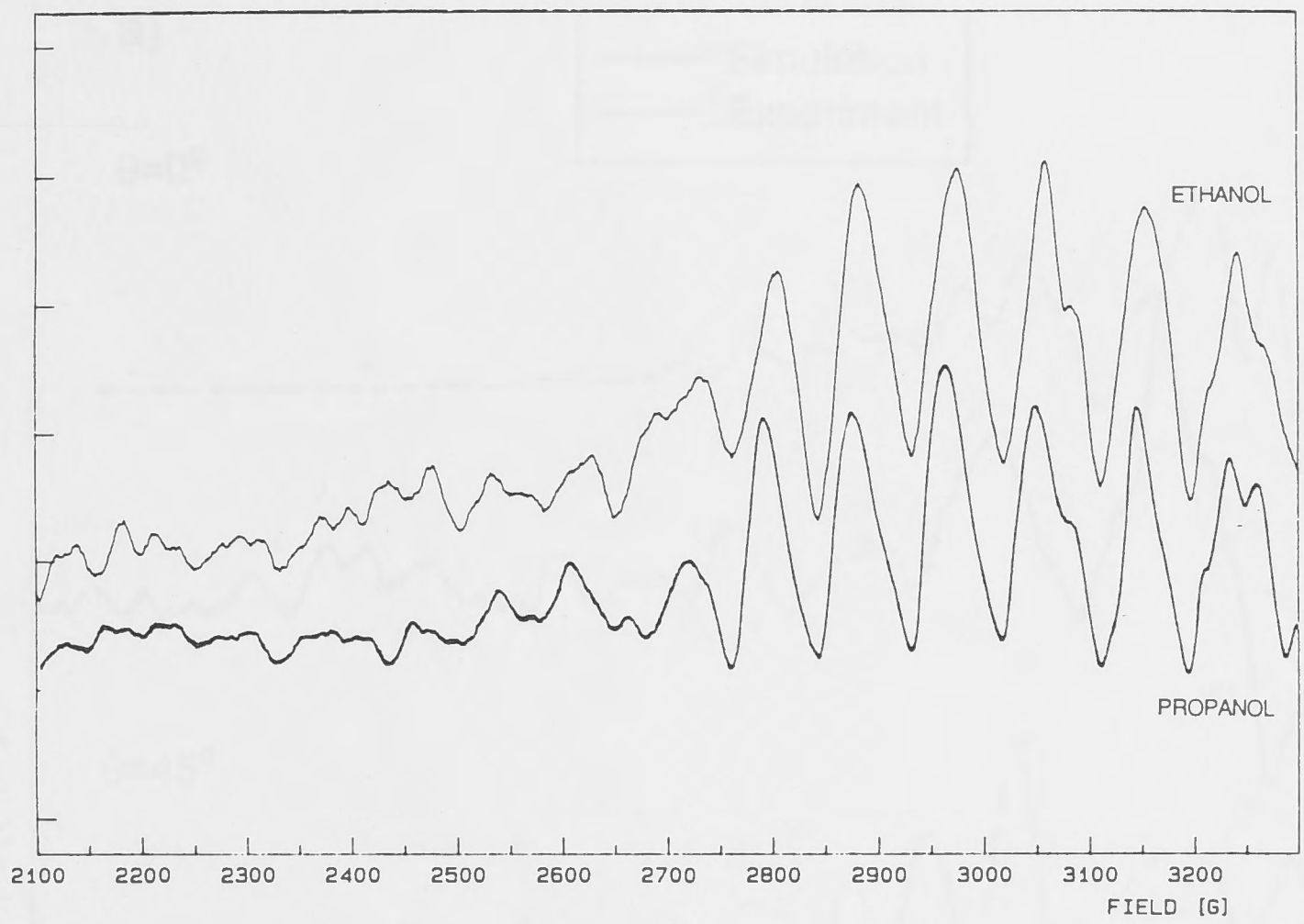

Figure 3.1: Multiline spectrum of sample with 4% propanol added compared with multiline of sample with 4% ethanol added.

spline base line. Figure 3.2 shows the spectra after the baseline have been subtracted. These spectra show a greater degree of orientation dependence than any previously reported at X-band. However, orientation dependence of a higher degree than previously reported has been seen by others (Rutherford, pers com.) The spectrum is most intense in the downfield region of the 0° orientation. Furthermore, the spectrum at 45° appears to be almost a complete powder pattern spectrum, whereas the spectra at the other two orientations are diminished at the edges. For this to appear, the tensor axes must be oriented in the membrane plane such that each of the principal axes are approximately equidistant from the perpendicular and therefore sampled in the 45° orientation. To be equidistant requires α=45° and β ~54°.

Initial simulations of the spectra confirm the above results. However, even though the spectral pattern is of good fit for α=45° and β ~54°, the calculated g-value at 0° is less than the experimental. This is a clear indication that the g-tensor is not coincident with the hyperfine and quadrupole tensors. By allowing the g-tensor to vary separately to the hyperfine tensors, an improved

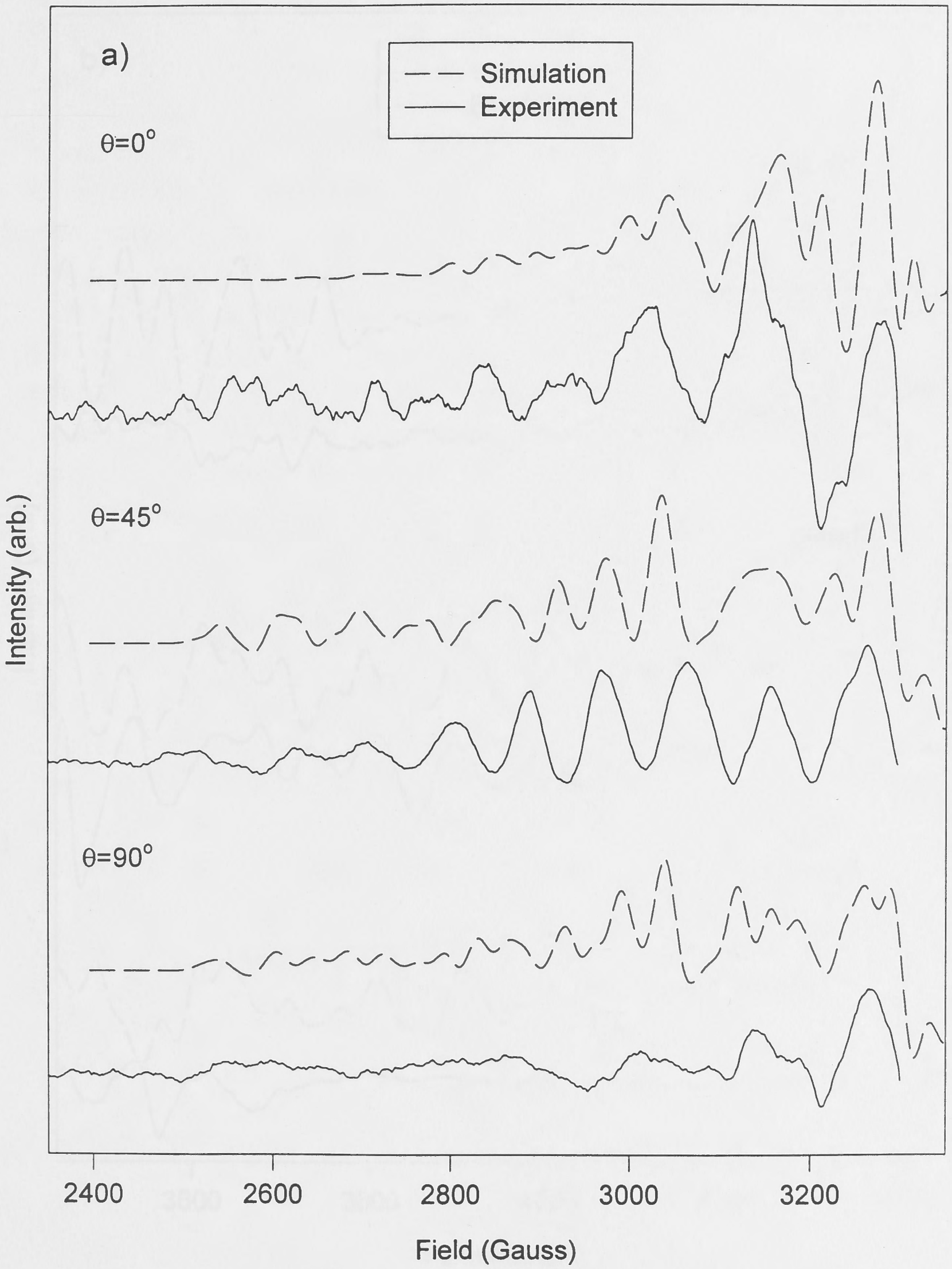

Figure 3.2. Experimental oriented multiline spectra together with best fit simulated spectra. The orientation of the applied field to the membrane normal is indicated by θ for each spectrum. Spectrometer conditions: Frequency 9.42 GHz; modulation amplitude 20 Gauss; microwave power 6.32 mW; modulation frequency 100 kHz; temperature 7K. Spectra (illuminated-dark) are the averages of 8 scans and downfield **(a)** and upfield **(b)** were acquired on separate 1000 Gauss scans. Parameters used for the simulations are given in Table 3.1.

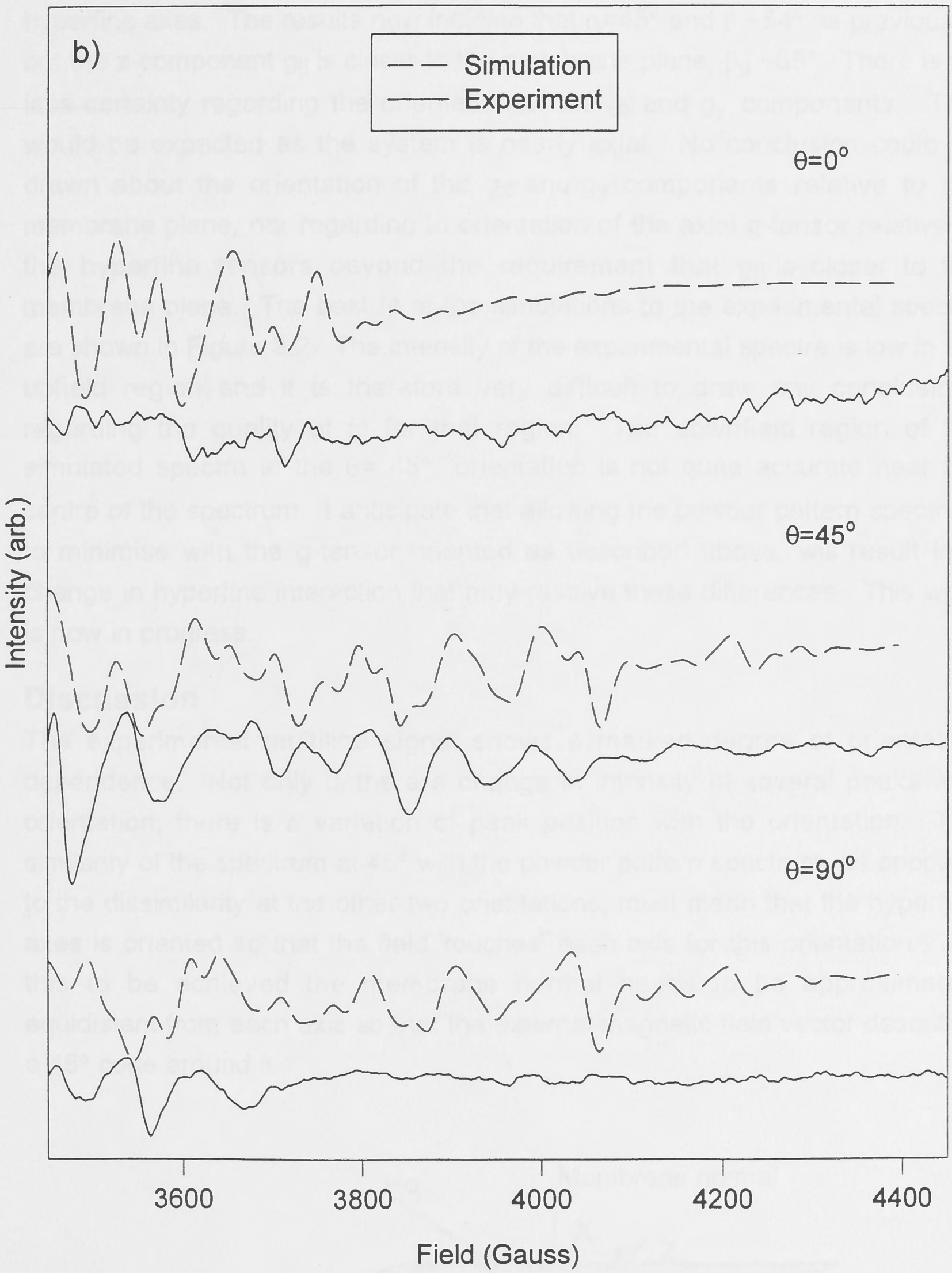

Figure 3.2b. Upfield region of experimental oriented multiline spectra together with simulated best fit. See figure caption on previous page.

fit was obtained. The g-tensor was rotated separately into the membrane frame using three Euler angles (Rose, 1957), two of these α_g and β_g rotate the g-tensor into the membrane frame, the third γ_g rotates the axes relative to the hyperfine axes. The results now indicate that α=45° and β ~54° as previously, but the z-component $g_{||}$ is closer to the membrane plane, β_g ~65°. There is far less certainty regarding the orientation of the g_x and g_y components. This would be expected as the system is nearly axial. No conclusion could be drawn about the orientation of the g_x and g_y components relative to the membrane plane, nor regarding to orientation of the axial g-tensor relative to the hyperfine tensors beyond the requirement that $g_{||}$ is closer to the membrane plane. The best fit of the simulations to the experimental spectra are shown in Figure 3.2. The intensity of the experimental spectra is low in the upfield region and it is therefore very difficult to draw any conclusions regarding the quality of fit for that region. The downfield region of the simulated spectra in the θ= 45° orientation is not quite accurate near the centre of the spectrum. I anticipate that allowing the powder pattern spectrum to minimise with the g-tensor oriented as described above, will result in a change in hyperfine interaction that may resolve these differences. This work is now in progress.

Discussion

The experimental multiline signal shows a marked degree of orientation dependence. Not only is there a change in intensity of several peaks with orientation, there is a variation of peak position with the orientation. The similarity of the spectrum at 45° with the powder pattern spectrum, as opposed to the dissimilarity at the other two orientations, must mean that the hyperfine axes is oriented so that the field 'touches' each axis for this orientation. For this to be achieved the membrane normal needs to be approximately equidistant from each axis so that the external magnetic field vector describes a 45° cone around it.

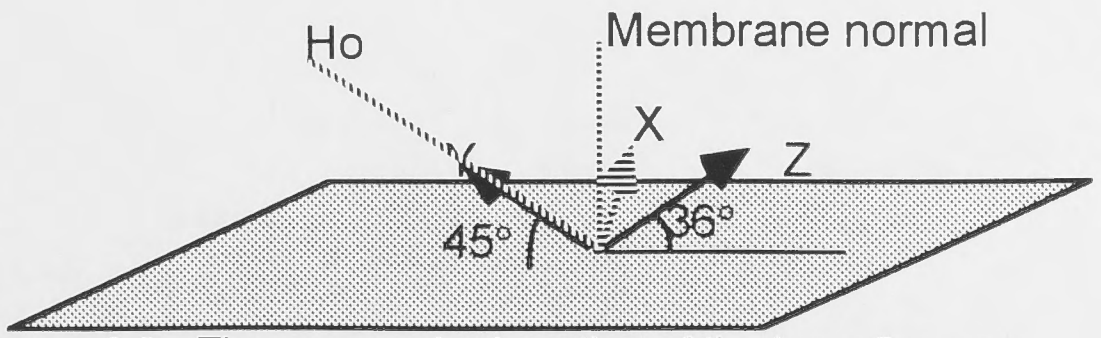

Figure 3.3. The proposed orientation of the hyperfine axes in the membrane plane.

The spectra at 0° and 90° are very different to what has previously been seen for oriented samples. The peaks in the central region are broad and relatively intense, but the peaks at the edges appear to be smeared out, indicating that the peaks shift relative to each other, so that the intensity is reduced. The upfield region (g<2) has, overall, less intensity than the downfield region. This effect has been seen in all published upfield regions of the oriented samples (Smith, *et al.*, 1993; Kim, *et al.*, 1992). It is interesting to note, however, that this effect is reversed in the oriented spectra of ammonia treated PSII samples (Kim, *et al.*, 1992). Small variations in hyperfine interactions have this effect in simulations of the multiline signal, that is, the peaks appear in the same position, but their relative intensities in a derivative pattern have changed. It is of course very likely that there are small changes in the hyperfine interaction caused by the binding of ammonia at a water site on the Mn dimer.

Simulations of the spectra of oriented samples confirm the orientation of the hyperfine axes in the membrane plane with the z-axis ~36° off the membrane plane and the x- and y-axes around 45° off the membrane plane. These simulations also unambiguously identify that the orientation of the g-tensor is not coincident with the orientation of the hyperfine tensors. Its orientation is with the g_z axis 25° off the membrane plane.

The difficulty in fitting the Q-band powder pattern spectrum is probably a reflection of the non-coincidence of these tensors, especially since the Q-band spectrum is the most sensitive to changes in the g-tensor.

4: SIMULATION OF THE TWO FORMS OF THE 4.1 SIGNAL

Introduction

The so called g=4.1 signal is a 350 Gauss wide signal now thought to arise from an *S*=3/2 state. It was first seen by Casey and Sauer in 1984 and also by Zimmerman and Rutherford (1984). One proposal suggested that this *S*=3/2 centre could result from a near axial Mn^{IV} (Hansson, *et al.*, 1987). The appearance of 16 Mn hyperfine lines with a spacing of approximately 36 Gauss on an oriented 4.1 signal after the PSII preparation had been treated with ammonia (Kim, *et al.*, 1990; Kim, *et al.*, 1992), gives a clear indication however, that the signal's origin is multinuclear. There has been some debate as to how the signal appears: it has been considered a ground *S*=3/2 state (Hansson, *et al.*, 1987) and also shown to be a first excited *S*=3/2 state of the ground *S*=1/2 multiline state (Smith, *et al.*, 1993). A recent paper (Smith and Pace, 1996) shows that there are two forms of the 4.1 signal. One is generated by illumination at 130K with the PSII preparation in a buffer containing 30% ethylene glycol, and shown by temperature dependence studies to be a ground state. It is proposed to arise from a bridged dimer of Mn^{III}, with a net *S*=1 state, coupled to a radical, such that the total interaction is *S*=3/2. The other form of the 4.1 signal is confirmed by temperature dependence studies to be the first excited *S*=3/2 state of the *S*=1/2 ground state multiline signal, thought to arise from a Mn^{III}-Mn^{IV} di-μ-oxo bridged dimer. This signal is generated by illumination at 200K. The presence of small mono-alcohols suppresses this signal (Smith, *et al.*, 1993), something already noted by Zimmermann and Rutherford (1986). The ground state form of the signal, however, requires the presence of ethylene glycol (30% v:v in final buffer), or glycerol (50% v:v), which is the regime in which Casey and Sauer (1984) first saw the signal.

Haddy *et al* (1992) have simulated the g=4 signal at S-, X- and P-band. By their analysis, the spin centre giving rise to the signal must be *S*=5/2, in order to explain the features at P-band. Astashkin *et al* (1994) also concluded, from a pulsed EPR study, that the g=4 signal arises from an *S*=5/2 state. However, Kusunoki *et al* (1992) has suggested that inhomogeneous distributions of Mn tetramers in PSII samples give rise to the *S*=1/2 ground state and *S*=3/2 ground state respectively. Furthermore, the arguments offered by Astashkin *et al* for an *S*=5/2 state have been seriously challenged (Smith and Pace, 1996).

Simulations of the two forms reported here, confirm the results from Smith and Pace (1996) that the signals arise from two separate spin 3/2 centres which are distinguished by the zero-field splitting (ZFS) parameters for the system. Simulation of one dimensionally oriented samples allow the orientation of the ZFS tensor axes in the membrane plane of one of the spin centres to be determined, with the assumption that the membrane plane is parallel (within a statistical spread) to the mylar film it is supported on.

Method

Theory

The spin Hamiltonian for an S=3/2 system has the form

$$\mathcal{H} = \beta \cdot \mathbf{H_o} \cdot \boldsymbol{g} \cdot \mathbf{S} + \mathbf{S} \cdot \boldsymbol{D} \cdot \mathbf{S} + \Sigma_i (\mathbf{S} \cdot \boldsymbol{A_i} \cdot \mathbf{I_i} + \mathbf{I_i} \cdot \mathbf{Q_i} \cdot \mathbf{I_i}) . \qquad 4.1$$

D is the ZFS tensor (Chapter 1), which splits the electron energy levels into two Kramer's doublets at zero field (see Figure 4.1). The hyperfine interactions (the bracketed expression) are calculated for each atom involved, as a perturbation on the main transitions. Often the zero field component of the Hamiltonian, $\mathcal{H}_D$, is expressed in the form:

$$\mathcal{H}_D = D\,(S_z^2 - 1/3 S^2) + E\,(S_x^2 + S_y^2)$$

where: D = axial ZFS parameter= 3/2 D_{zz}

E = asymmetry parameter given by $(D_{xx} - D_{yy})/2$.

I have chosen to use the traceless cartesian tensor form, ie $D_{zz} = -(D_{xx} + D_{yy})$, but will give the resultant parameters in the most commonly used forms of D and E. For an axial system E/D is small, whereas for a pure rhombic system, E/D=0.3.

The ZFS interaction now becomes:

$$\mathbf{S} \cdot \boldsymbol{D} \cdot \mathbf{S} = D_{xx}S_x^2 + D_{yy}S_y^2 + D_{zz}S_z^2 + D_{xy}(S_xS_y + S_yS_x) + D_{xz}(S_xS_z + S_zS_x) + D_{yz}(S_yS_z + S_zS_y)$$

The zero-field splitting removes the degeneracy of wave functions with $S > 1/2$, even without the presence of a magnetic field - hence its name. In transition metal complexes the ZFS is due mainly to spin-orbit coupling rather than spin-spin magnetic dipole interaction, as seen in organic molecules (triplet states).

The spin states (m_S) for the system are {-3/2,-1/2,1/2,3/2}. There are three possible $\Delta m_S=\pm 1$ transitions for this system, however, as can be seen in Figure 4.1, only the transition |-1/2> to |1/2> and |1/2> to |3/2> will occur for positive values of D in the range 0.3-5 cm^{-1}, at fields generated at X- and Q-band. If $D > h\upsilon$ only the |-1/2> to |1/2> is visible. However $\Delta m_S=\pm 2$ transitions are also weakly allowed. These are included by the matrix diagonalisation method used here. The magnitude of the zero-field splitting parameter for an ion depends on the separation to the next excited state in the *d* orbital manifold through spin-orbit coupling. Mn^{IV} has a t_{2g}^3 ground state electron configuration and the promotion of one electron to the nearest excited state involves the e_g orbitals, which, for Mn^{IV} are remote. As a result the intrinsic zero-field splitting for Mn^{IV} is, as a rule, small (< 1 cm^{-1})(McGarvey, 1966). Mn^{III} on the other hand has already one electron in an e_g orbital, and the gap to it has been reduced through Jahn-Teller effects. The result is a substantial ZFS parameter for Mn^{III} (~1-4 cm^{-1}) (Kennedy and Murray, 1985).

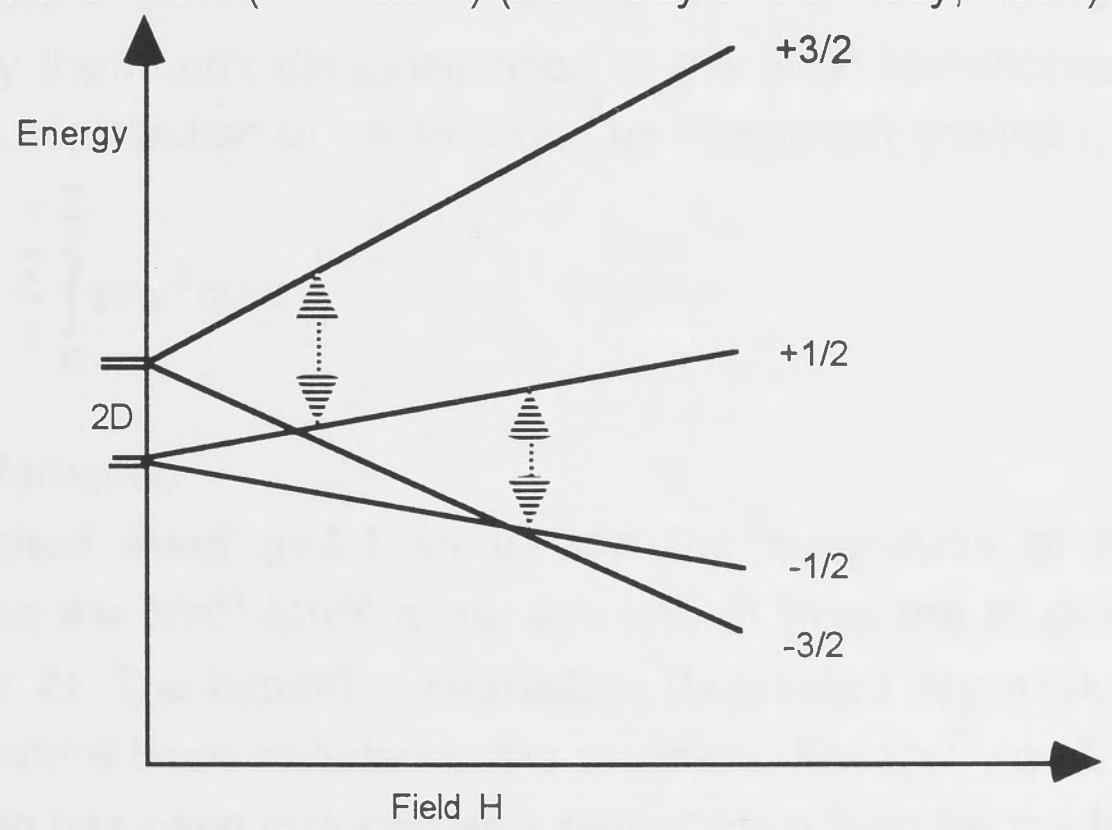

Figure 4.1. Zero-field splitting and Zeeman splitting for an *S*=3/2 state with axial symmetry.

Simulations of powder pattern 4.1 signals

The simulation program for the two forms of the 4.1 signal draws from the structure of the multiline program. A listing of the program is provided in Appendix 4.

Field positions

The energy levels for this system do not vary linearly with the field, and each field position where resonance occurs must be calculated exactly. This is done by calculating the energy difference (ΔE) between states at a particular field value and then again at another 100 Gauss further upfield (ΔE_{100}). To detect if a transition has occurred on this interval, the microwave field quantum ($h\upsilon/g\beta$) is subtracted from ΔE and also from ΔE_{100}. A transition has occurred

if there is a change in sign between the two difference values. If a transition has occurred, the field is searched at one Gauss intervals until the exact position for the transition is found.

Transition probabilities

For a system such as this with a large variation in effective g-values ($g_{\perp}$~4, $g_{||}$~2) the transition probabilities cannot be calculated simply by $[<m_{\uparrow}|S_{+}|m_{\downarrow}>]^2$ (equation 2.1). We have to consider the full effect of the g-anisotropy and include averaging over the third Euler angle (γ), which accounts for the position of the H_1 field relative to the molecular axes. The transition probabilities are therefore calculated from equation 1.2:

$$I \propto [<m_{\uparrow}|\mathbf{H_1 \cdot g \cdot S}|m_{\downarrow}>]^2 =$$
$$+H_1^2[<m_{\uparrow}|\cos\gamma(g_{xx}S_x+g_{xy}S_y+g_{xz}S_z)+\sin\gamma(g_{yx}S_x+g_{yy}S_y+g_{yz}S_z)|m_{\downarrow}>]^2$$

Here $m_{\uparrow}$ and $m_{\downarrow}$ stand for the spin up and spin down eigenvectors as generated by the matrix diagonalisation of the main Hamiltonian expression. The average contribution of γ is included by integration around γ, for example:

$$\text{Ave} = \frac{2}{\pi}\int_0^{\frac{\pi}{2}} \sin\gamma^2 d\gamma = \frac{1}{2}$$

Hyperfine interaction

For the excited state g=4.1 simulation the magnitude of the hyperfine interactions in the Mn^{III}-Mn^{IV} dimer are known from the multiline simulation (see Chapter 2). The hyperfine interaction (bracketed expression in equation 4.1) has therefore been included in the program. For Mn^{III}, as it is quasi axial, the interaction has been included as a perturbation term for the hyperfine only. For Mn^{IV}, because of the unique interactions seen (as discussed previously) the energy terms due to the hyperfine and quadrupole interactions are calculated by the diagonalisation of two 6x6 matrices. These energy terms together with the Mn^{III} perturbation terms modify the main transitions.

For the ground state 4.1 simulation, the program includes only the hyperfine interactions of the two Mn^{III}, as simple perturbations to the main transitions. It does not include the hyperfine interaction for the radical, as it is assumed to be small. This third spin centre does however affect the projection operators calculated for the hyperfine interactions.

Hyperfine coupling coefficients are calculated from projection operators according to the method indicated earlier (Chapter 2). For an isolated pair of

Mn^{III}-MnIV with a net S=3/2 state, they are 4/5 for Mn^{III} and 1/5 for Mn^{IV}. However, when $D/J \sim 1$ this relationship breaks down (Zheng, *et al.*, 1994). The strong coupling projection operators do not give an accurate description of the coupling coefficients and the effect of the large zero-field splitting for Mn^{III} has to be considered. For a ground state, the net effect is that the coefficients approach each other (Zheng, *et al.*, 1994). I have not attempted to calculate the coefficients for an excited state, but rather allowed the coefficients to vary.

In the case of the ground state form in the strong coupling limit, with three interacting spin centres, the net projection operator is 1/3 for each, calculated as described in Chapter 1.

Simulation of one dimensionally ordered samples

To simulate the spectra of one dimensionally ordered samples two rotations are performed: one describes the orientation of the ZFS axes relative to the mylar sheet normal (α, rotation about z-axis, β, rotation about y-axis), the other the orientation of the membrane plane normal relative to the applied magnetic field (ϕ, rotation about z-axis, θ, rotation about y-axis)(Rose, 1957). A Gaussian distribution of the angle, between the thylakoid membrane normal and the mylar sheet was included, with variance of about 15°.

Transition probabilities

The oscillating H_1 field which induces transitions between the energy levels is always perpendicular to H_o. For the spectra of one dimensionally oriented samples this means that the H_1 field is always in the mylar membrane plane for the TE_{102} cavity geometry used here. The axis that remains in the membrane plane for each orientation of the membrane normal to the H_o direction, is the laboratory y-axis. The transition probabilities are therefore calculated based on equation 1.3:

$$I \propto H_1^2 \left| \left\langle m_{\uparrow} \left| g_{xy} S_x + g_{yy} S_y + g_{zy} S_z \right| m_{\downarrow} \right\rangle \right|^2$$

For the transition probabilities then, the rotation of α and β as above describes the orientation of the molecule in the membrane, ϕ describes the orientation of the membrane y-axis relative to the H_1 field and θ describes the orientation of the mylar plane normal to the incident H_o field.

Experimental:

The experimental EPR work for the unoriented, powder pattern simulations were undertaken by Smith and published previously (Smith and Pace, 1996).

The PSII preparations were either a modification of that of Bricker (1985) (Pace, *et al.*, 1991) or that of Berthold *et al* (1981) as modified by Beck *et al* (1985).

X-band studies were performed on a Bruker ESP300E spectrometer with an Oxford Instruments ESR9 liquid helium cryostat. Q-band studies were performed on a Varian V-4502 spectrometer.

Excited state g=4.1 signal

The preparations stored with sucrose (400mM) as cryoprotectant showed the excited state 4.1 signal. The signal was seen after illumination with green light (intensity ~300 W m^{-2}) for 3 minutes at 200K. The multiline signal was also present.

Ground state g=4.1 signal

The preparation stored with 30% v:v ethylene glycol showed the low temperature 4.1 signal form. Illumination with yellow light (intensity ~600 W m^{-2}) for 6 minutes at 130K allows only this 4.1 signal to be seen.

One dimensionally ordered samples

The PSII material for these samples were prepared by the modified Bricker method (Pace, *et al.*, 1991) and used fresh for painting onto mylar sheets according to the method described in Chapter 3. In these samples 4% ethanol was added to the sample prior to painting, rather than propanol. It was clear however that the ethanol evaporated during the drying process as the high temperature form of the 4.1 signal was present. The X-band studies were performed on the Varian V-4502 spectrometer. Spectrometer conditions are given in the figure caption (Figure 4.3). These spectra have been published previously (Smith, *et al.*, 1993).

Results

The experimental spectra at X- and Q-band together with the simulations for each of the two forms of the g=4.1 signal are shown in Figure 4.2a & b. The simulation parameters for the same are listed in Table 4.1.

The excited state form of the X-band spectrum appears broader in the downfield region of the spectrum than does the simulation. This broadening has been explained as the appearance of the next excited state (Smith and Pace, 1996), near g=6 and is probably apparent as a separate peak in the corresponding Q-band spectrum. The fit at Q-band is not exact, however the parameters used to fit the spectrum is the only set, using this Hamiltonian, that

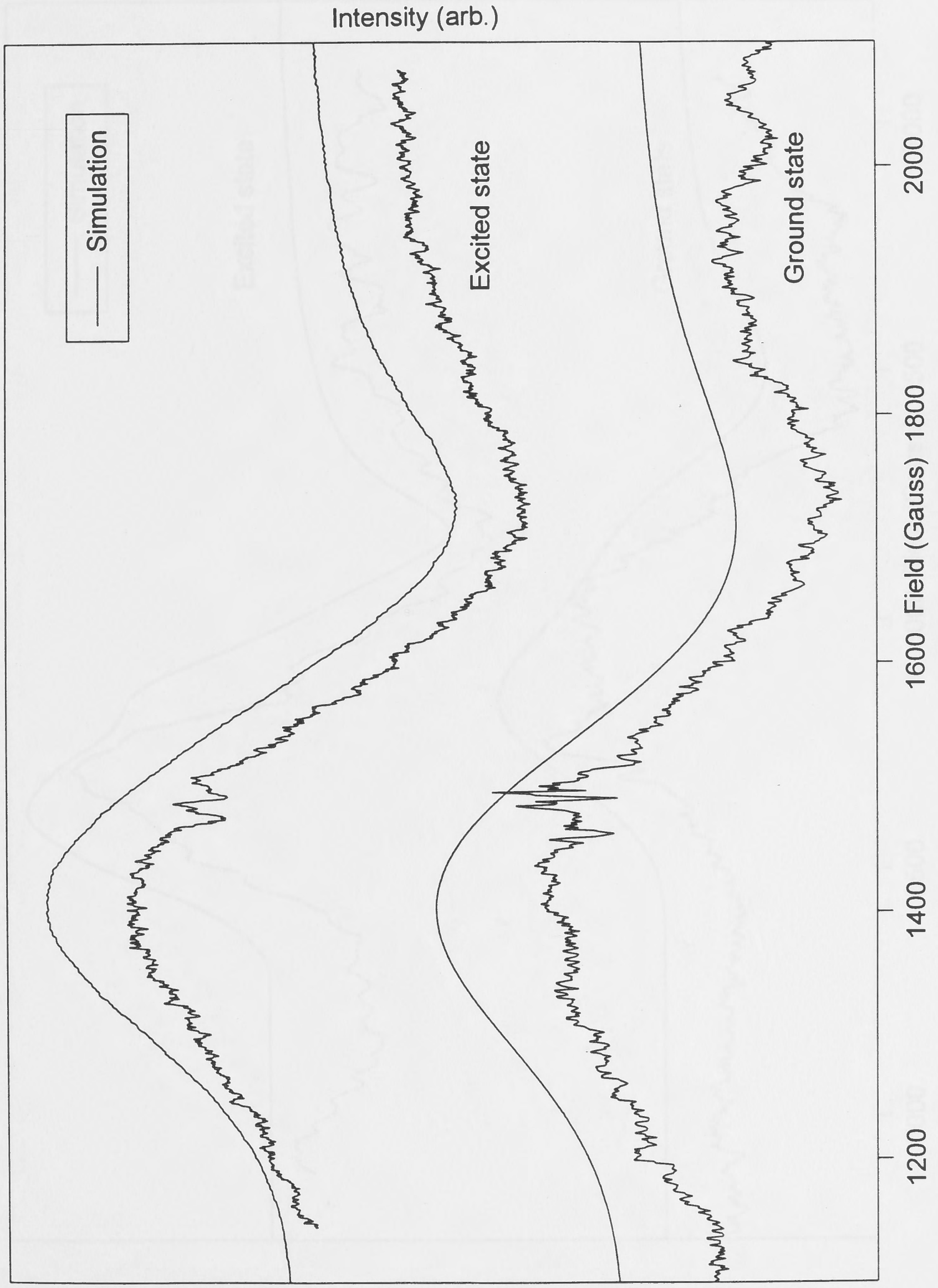

Figure 4.2a Experimental X-band EPR g=4.1 signal from ground state and excited state (illuminated-annealed) together with simulations.
Spectrometer conditions: Frequency: 9.42 GHz; microwave power 6.3 mW; modulation frequency 100 KHz, modulation amplitude 14 Gauss; temperature 9K.

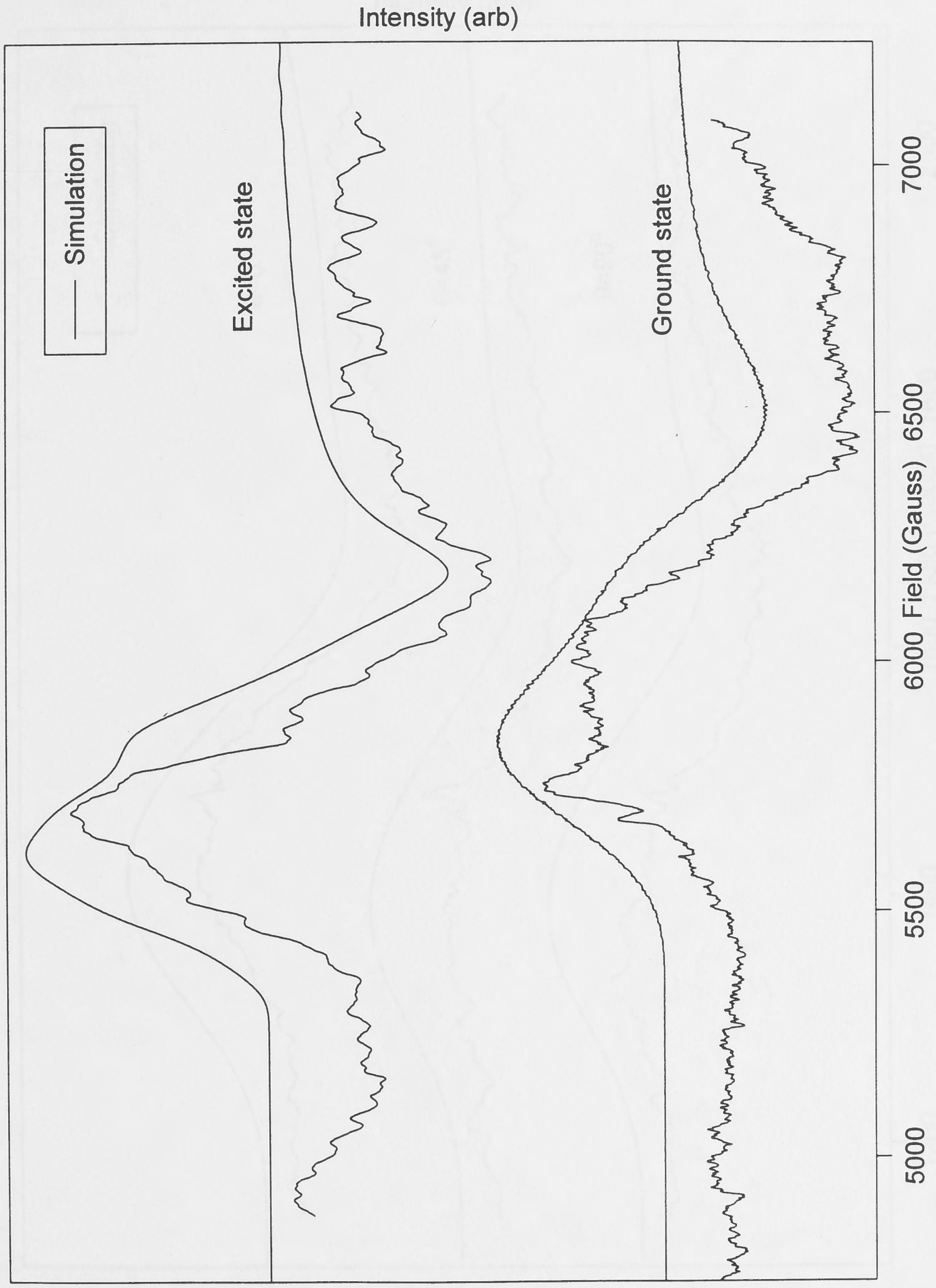

Figure 4.2b Experimental Q-band EPR g=4.1 signal from ground state and excited state (illuminated-annealed) together with simulations.
Spectrometer conditions: Frequency 34.7 GHz, microwave power 100 mW; modulation frequency 100 KHz; modulation amplitude 11 Gauss; temperature 9K.

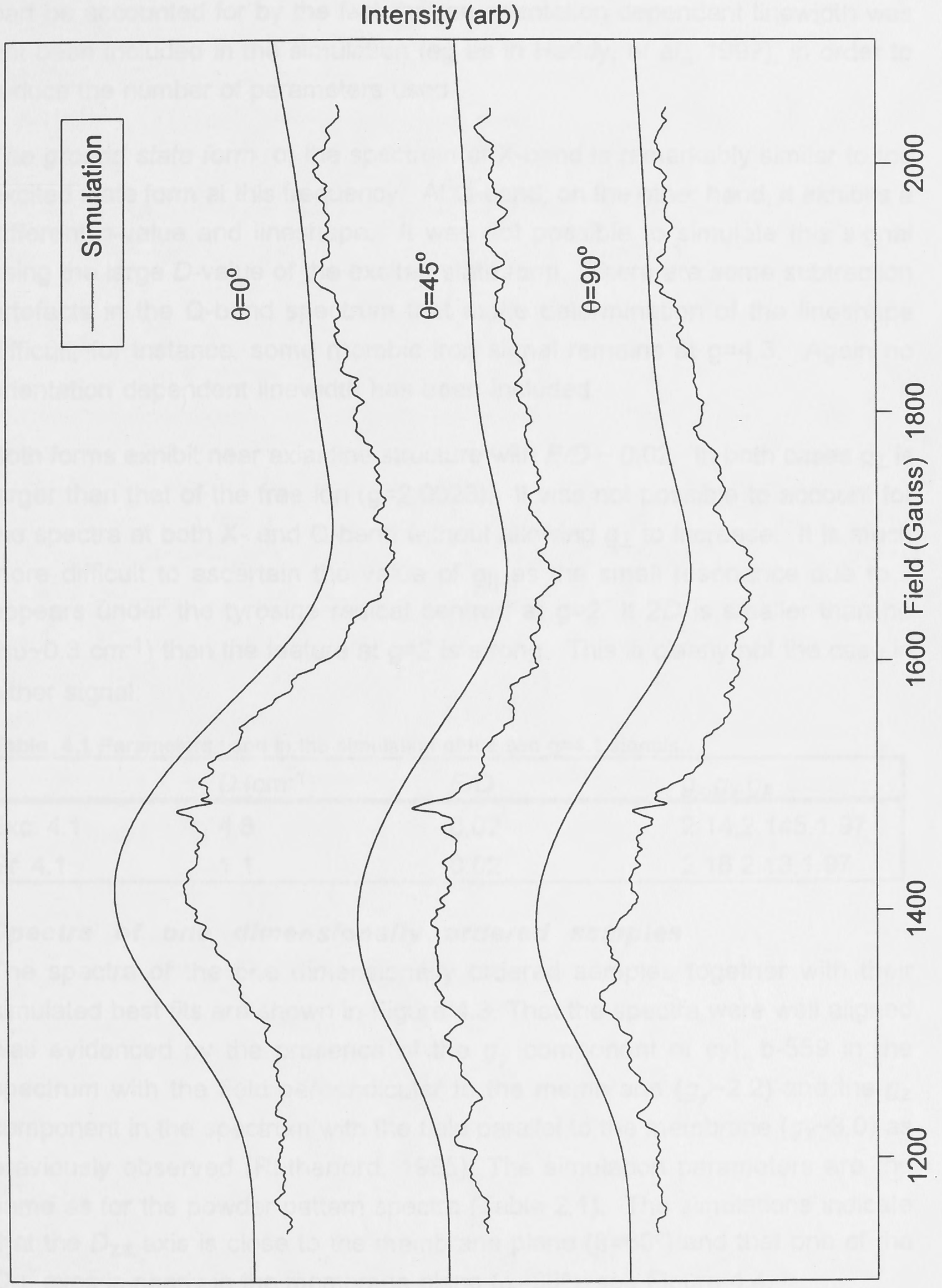

Figure 4.3 X-band experimental and simulated spectra of the first excited state g=4.1 signal in one dimensionally ordered samples.
Spectrometer conditions: Frequency 8.975 GHz; microwave power 30 mW; modulation amplitude 20 Gauss; temperature 8K; scans 5.Simulation parameters as for the powder pattern spectrum, Table 4.1. The angle indicated (θ) is the angle between the membrane plane normal and the applied field.

will fit the spectrum reasonably at both frequencies. The discrepancies may in part be accounted for by the fact that an orientation dependent linewidth was not been included in the simulation (eg as in Haddy, *et al.*, 1992), in order to reduce the number of parameters used.

The ground state form of the spectrum at X-band is remarkably similar to the excited state form at this frequency. At Q-band, on the other hand, it exhibits a different g-value and lineshape. It was not possible to simulate this signal using the large *D*-value of the excited state form. There are some subtraction artefacts in the Q-band spectrum that make determination of the lineshape difficult, for instance, some rhombic iron signal remains at g=4.3. Again no orientation dependent linewidth has been included.

Both forms exhibit near axial fine structure with $E/D \sim 0.02$. In both cases $g_\perp$ is larger than that of the free ion (g=2.0023). It was not possible to account for the spectra at both X- and Q-band without allowing $g_\perp$ to increase. It is much more difficult to ascertain the value of $g_{||}$ as the small resonance due to it appears under the tyrosine radical centred at g=2. If $2D$ is smaller than $h\upsilon$ ($h\upsilon \sim 0.3$ cm^{-1}) then the feature at g=2 is strong. This is clearly not the case in either signal.

Table 4.1 Parameters used in the simulation of the two g=4.1 signals.

	D (cm^{-1})	E/D	g_x, g_y, g_z
Exc. 4.1	4.8	0.02	2.14,2.145,1.97
Gr 4.1	1.1	0.02	2.18,2.13,1.97

Spectra of one dimensionally ordered samples

The spectra of the one dimensionally ordered samples together with their simulated best fits are shown in Figure 4.3. That the spectra were well aligned was evidenced by the presence of the g_y component of cyt. b-559 in the spectrum with the field perpendicular to the membrane ($g_y \sim 2.2$) and the g_z component in the spectrum with the field parallel to the membrane ($g_z \sim 3.0$) as previously observed (Rutherford, 1985). The simulation parameters are the same as for the powder pattern spectra (Table 2.1). The simulations indicate that the D_{zz} axis is close to the membrane plane ($\beta=60°$) and that one of the $D\perp$ axes is nearly in the membrane plane ($\alpha=80°$), see Figure 4.4.

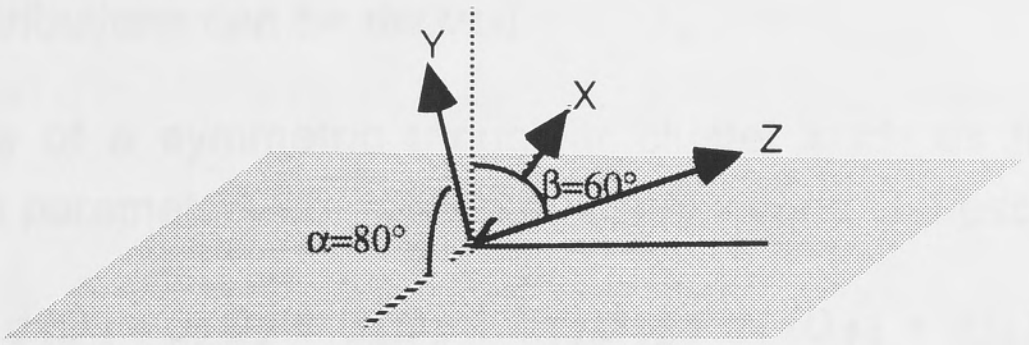

Figure 4.4. The orientation of the *D* tensor in the membrane plane.

Discussion

Estimate of contributions of intrinsic zero-field splitting values to total D

The ground state g=4.1 signal

There is evidence that the ground state giving rise to the g=4.1 signal has an *S*=1/2 first excited state (Paul Smith, PhD Thesis, 1996). For a coupled pair of Mn^{III} to give rise to a spin system with a ground state *S*=3/2 and a first excited state *S*=1/2, they must be coupled to another spin 1/2 centre, presumably, in the case of PSII, a radical. A pair of Mn^{III} coupled to a radical can give rise to such a signal provided the couplings between each Mn and the radical are ferromagnetic and the same (that is $J_{13} = J_{23}$, see Figure 4.5) and the coupling between the Mn^{III} must be antiferromagnetic and suitably strong, giving a net $S_{12} = 1$.

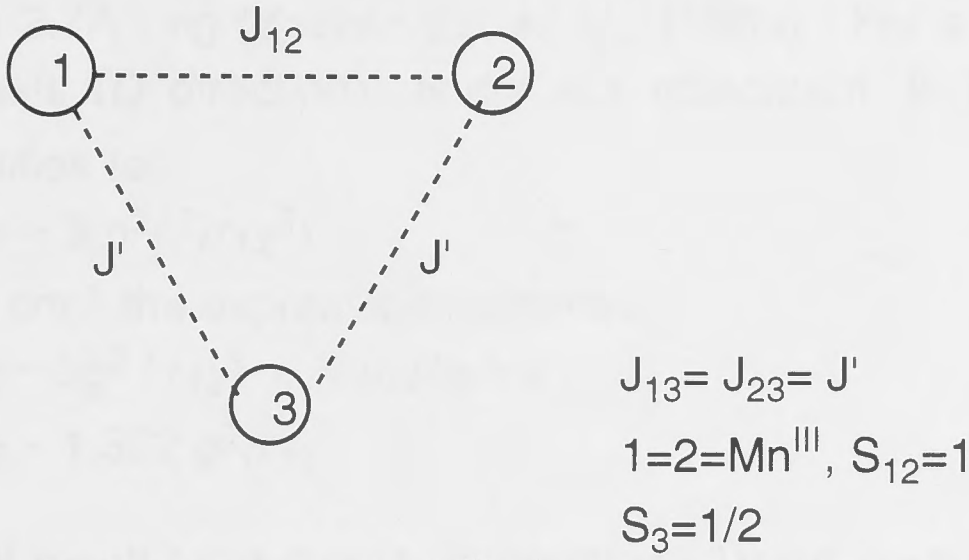

Figure 4.5 The coupling scheme for two Mn^{III} (1 and 2 above) coupled to an atom with *S*=1/2.

The required relationship between the exchange couplings for such a system can be calculated (de Paula, *et al.*, 1986). For the system to adopt an *S*=3/2 ground state the requirement is $2|J_{12}|<J_{1,23}<4|J_{12}|$ (Paul Smith, PhD Thesis, 1996). For a coupling to the radical , estimated at about 70 cm^{-1}, the coupling between the Mn^{III} could be ~160 cm^{-1}(Smith and Pace, manuscript in preparation). This estimate places the interaction between the manganese in

the strong coupling regime ($|D/J|<<1$). For such a system an expression for the contributions of the individual zero-field splitting parameters together with dipolar contributions can be derived.

In the case of a symmetric trinuclear cluster such as this one, the spin Hamiltonian parameters are related by (Bencini and Gatteschi, 1990):

$$\boldsymbol{D_T} = d_1\boldsymbol{D_1} + d_2\boldsymbol{D_2} + d_3\boldsymbol{D_3} + d_{12}\boldsymbol{D_{12}} + d_{13}\boldsymbol{D_{13}} + d_{23}\boldsymbol{D_{23}}.$$

where: $\boldsymbol{D_{12}}$ etc are cross term (dipolar) contributions between centres.

The contribution from the radical (d_3) can be neglected as the intrinsic D vanishes for such a system.

The coupling coefficients can be calculated by expressions given by Bencini and Gatteschi and are $d_1 = d_2 = -7/10$ and $d_{12} = 13/15$ for the spin states assumed here. The magnitude of the dipolar coupling, D_{12}, in the Mn^{III}-Mn^{III} dimer can be estimated using a simple dipole-dipole approximation (Slichter, 1990):

$$D_{12} \sim 3/2(-g^2\beta^2(1-3\cos^2\theta)/r_{12}^3)$$

where θ = The angle between the dipolar interaction and the Mn-Mn vector.

r_{12} = distance in Å between the two Mn.

The distance between the two Mn in a dimer interaction has been estimated by EXAFS to be 2.7Å , eg (Yachandra, *et al.*, 1986a). For a situation where the symmetry axis (D direction) and r are coincident, θ is zero and the expression simplifies to:

$$D_{12} \sim 3(g^2\beta^2/r_{12}^3)$$

To obtain D_{12} in cm^{-1} the expression becomes

$$D_{12} \sim 3g^2 / r_{12}^3 \times \beta^2 \mu_o/4\pi\, h\, c$$

$$D_{12} \sim 1.302\, g^2/r_{12}^3$$

This is a general result for a dipolar interaction. Using r_{12} = 2.7Å and g=2.1 (g_{iso} from simulations), $D_{12} = 0.3cm^{-1}$. The D_{13} and D_{23} terms are expected to be smaller still as the magnetic moment of an $S=1/2$ state is small. Thus the largest contribution to D_T will come from the intrinsic zero-field parameters of Mn^{III}.

For $D_T = 1.1\ cm^{-1}$ that requires a very small zero-field parameter for each Mn^{III}, $\sim 0.6\ cm^{-1}$. Whereas intrinsic zero-field parameters for Mn^{III} are in the range $1 - 4\ cm^{-1}$, lower values have been reported (Vincent, *et al.*, 1993) These

compounds with low *D* values all exhibit tetragonal distortion, which, as a rule, leads to lowered *D* values. On the other hand, it cannot be excluded that the Mn dimer has a IV-IV oxidation state. Mn^{IV} has an intrinsic zero field splitting of <1 cm^{-1} (McGarvey, 1966). The coupling parameters are the same for Mn^{IV}-Mn^{IV} as for Mn^{III}-Mn^{III}, so that the D_T= 1.1 cm^{-1} could well be accounted for by such a system. However, in the system above, ***D*** is a net tensor interaction. If the two individual Mn^{III} tensors were non-coincident, the contributions from the two tensors could cancel each other, thereby bringing about the small value of D_T seen here. At present we cannot distinguish between these possibilities.

Excited state g=4.1 signal

Smith and Pace have estimated the magnitude of the coupling constant for the multiline/excited state dimer to be J~ 2 cm^{-1} (Smith and Pace, 1996). With an energy gap to the S=1/2 ground state of 3J and to the next excited S=5/2 state of 5J, this dimer is in the weakly coupled regime (D/J~1). For such a system it is more complex to estimate the coefficients of the intrinsic single ion ZFS parameters. However, again the dipolar coupling will be small and the major contributions would have to come from the intrinsic zero-field parameters themselves. The zero-field parameter for Mn^{IV} is also generally small, and therefore the major contribution must come from Mn^{III}. Values as large as 4 cm^{-1} have been reported for Mn^{III} in Schiff base complexes (Kennedy and Murray, 1985). Allowing some contribution from Mn^{IV} and the dipolar interaction, a value of 4.8 cm^{-1} would not be unrealistic.

It would be speculation to attempt to interpret the effects that would lead to a difference in ZFS for the two 4.1 signals. Some justification of the magnitude of the ZFS of the ground state form which is in the strong coupling regime, can be made in terms of the intrinsic ZFS for each ion, with the conclusion that the data is consistent with a lowering of symmetry relative to cubic symmetry, at that site. No such analysis is possible with the excited state form in the weak coupling regime.

Comparison with previous work

Excited state g=4.1 signal

The excited state 4.1 signal can be modelled as an S=3/2 state at both Q- and X-band. The rather large value of D (4.8 cm^{-1}) and E/D of 0.02 agree with estimates given in our earlier paper (Smith, *et al.*, 1993).

Haddy *et al* (1992) have simulated the 4.1 signal at S-, X-, and P-band. Their interpretation is that the signal arises from a rhombic, S=5/2 multimeric centre,

with D=0.43 cm^{-1} and E/D=0.25. The P-band spectrum reveals a greater anisotropy than can be seen in our Q-band spectrum. In fact, the anisotropy would indicate that the turning points are well separated at Q-band and would therefore explain why an earlier study from the same group failed to detect any obvious g=4.1 signal at Q-band (Haddy, *et al.*, 1992)(see Figure 4.6). The preparation protocol indicates that the 4.1 signal from Haddy *et al* should be the excited state signal, and simulations indicate that it is not a mixture of the ground and excited state forms identified by Smith and Pace. This fact is also born out by the spectra of one dimensionally ordered samples (Haddy, *et al.*, 1992).

Two sets of parameters that will simulate this 4.1 signal as an S=3/2 state at three frequencies are given in Table 4.2. Both these sets of parameters give signal components that are well separated at Q-band and hence difficult to observe against the background, especially since g-strain broadening effects increase with frequency. The magnitude of D places this signal in a similar high zero-field splitting region as 'our' excited state signal. The difference between the two may be no more than a slight decrease in axial symmetry (E/D ~ 0.07 rather than 0.02). Second order effects that would influence the magnitude of the coupling coefficients in an excited state dimer include the magnitude of J. Protonation/deprotonation, particularly of bridging ligands, is known to alter J. (Hagen, *et al.*, 1989). Distortion from cubic symmetry reduces the magnitude of D (Carrington and McLachlan, 1967). Both these effects could contribute to the differences seen, and may be brought about by subtle variations in preparation protocols.

One dimensionally ordered samples

The orientation dependence of the signal shape for the excited state form of the 4.1 signal is similar to that previously observed at X-band (Rutherford, 1985). Haddy *et al* (1992) have shown the orientation dependence of this signal at P-band, where the components, parallel and perpendicular to the field, are separated by about 380 Gauss. It is similar again to the X-band spectra seen by us, in that the perpendicular orientation exhibits a greater intensity. The signal seen with parallel orientation at P-band appears to be a turning point, with the intensity mostly above the base line. The P-band spectrum can be reasonably well simulated, using the parameters in Table 4.2, by an orientation of the fine structure tensor corresponding to α=70°, and β=75° (compared with α=80° and β=60° for our oriented samples) see Figure 4.7. For β>70° the shape of the two dimensional powder pattern spectrum in the parallel orientation changes. The intensity in the g=2 region becomes

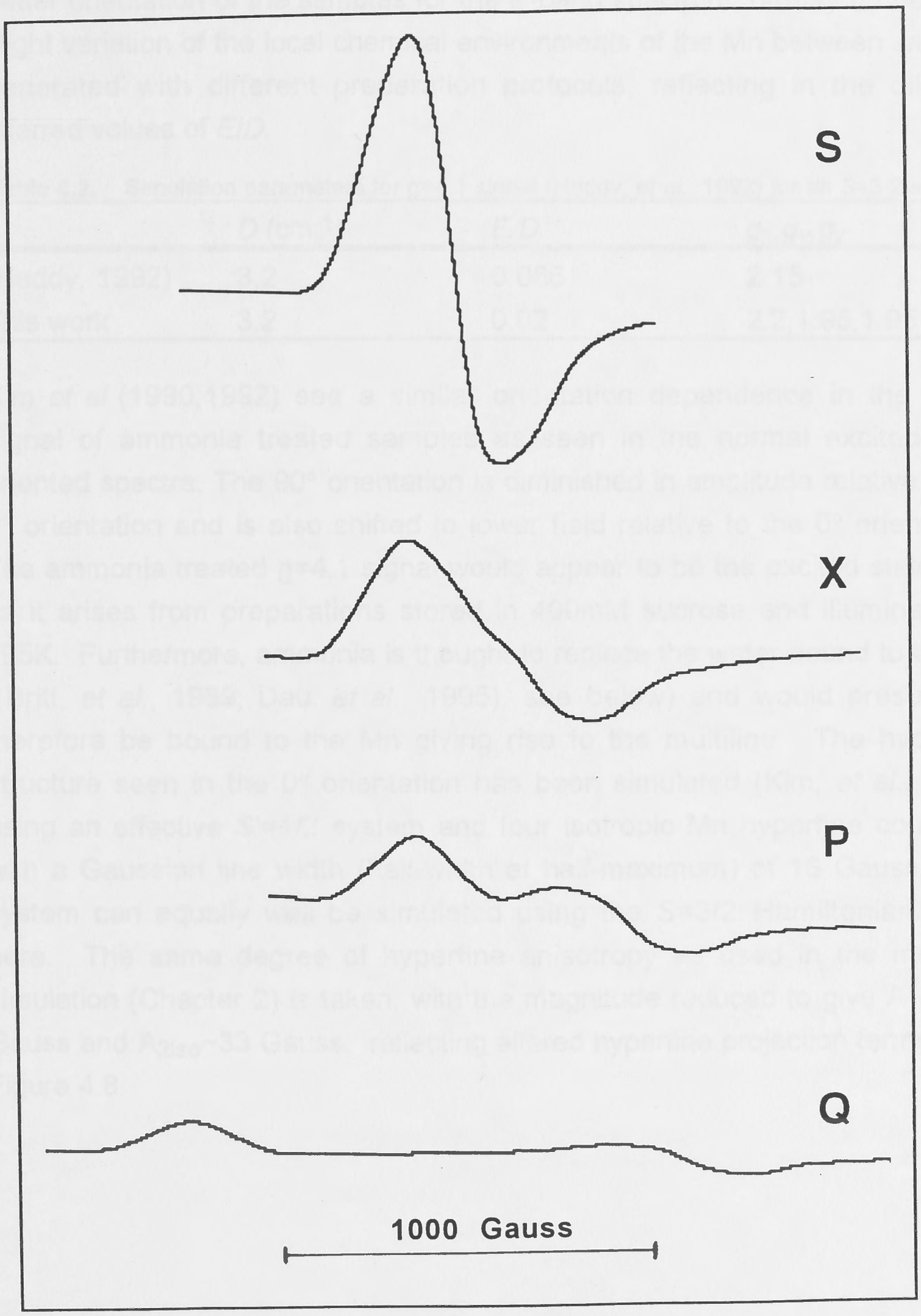

Figure 4.6 Simulation of g=4.1 signal from Haddy *et al* (1992) assuming S=3/2 state. Parameters are given in Table 4.2. The larger E/D value spreads the peaks as the frequency is increased such that the spectrum at Q-band is greatly broadened. The Q-band experimental spectrum may therefore be difficult to see.

significant and there is very little contribution below the base line in the g=4 region. The two oriented studies show a similar orientation of the ***D***-tensor with regard to the membrane plane. The small difference seen may reflect a better orientation of the samples for the P-band spectrum, or may be due to a slight variation of the local chemical environments of the Mn between samples generated with different preparation protocols, reflecting in the different inferred values of *E/D*.

Table 4.2. Simulation parameters for g=4.1 signal (Haddy, *et al.*, 1992) for an *S*=3/2 system.

	D (cm^{-1})	E/D	g_x, g_y, g_z
(Haddy, 1992)	3.2	0.066	2.15
This work	3.2	0.02	2.2,1.95,1.95

Kim *et al* (1990,1992) see a similar orientation dependence in the g=4.1 signal of ammonia treated samples as seen in the normal excited state oriented spectra. The 90° orientation is diminished in amplitude relative to the 0° orientation and is also shifted to lower field relative to the 0° orientation. The ammonia treated g=4.1 signal would appear to be the excited state form as it arises from preparations stored in 400mM sucrose and illuminated at 195K. Furthermore, ammonia is thought to replace the water bound to the Mn ((Britt, *et al.*, 1989; Dau, *et al.*, 1995), see below) and would presumably therefore be bound to the Mn giving rise to the multiline. The hyperfine structure seen in the 0° orientation has been simulated (Kim, *et al.*, 1992) using an effective *S'*=1/2 system and four isotropic Mn hyperfine constants with a Gaussian line width (half-width at half-maximum) of 16 Gauss. The system can equally well be simulated using the *S*=3/2 Hamiltonian given here. The same degree of hyperfine anisotropy as used in the multiline simulation (Chapter 2) is taken, with the magnitude reduced to give A_{1iso}~35 Gauss and A_{2iso}~33 Gauss, reflecting altered hyperfine projection terms, see Figure 4.8.

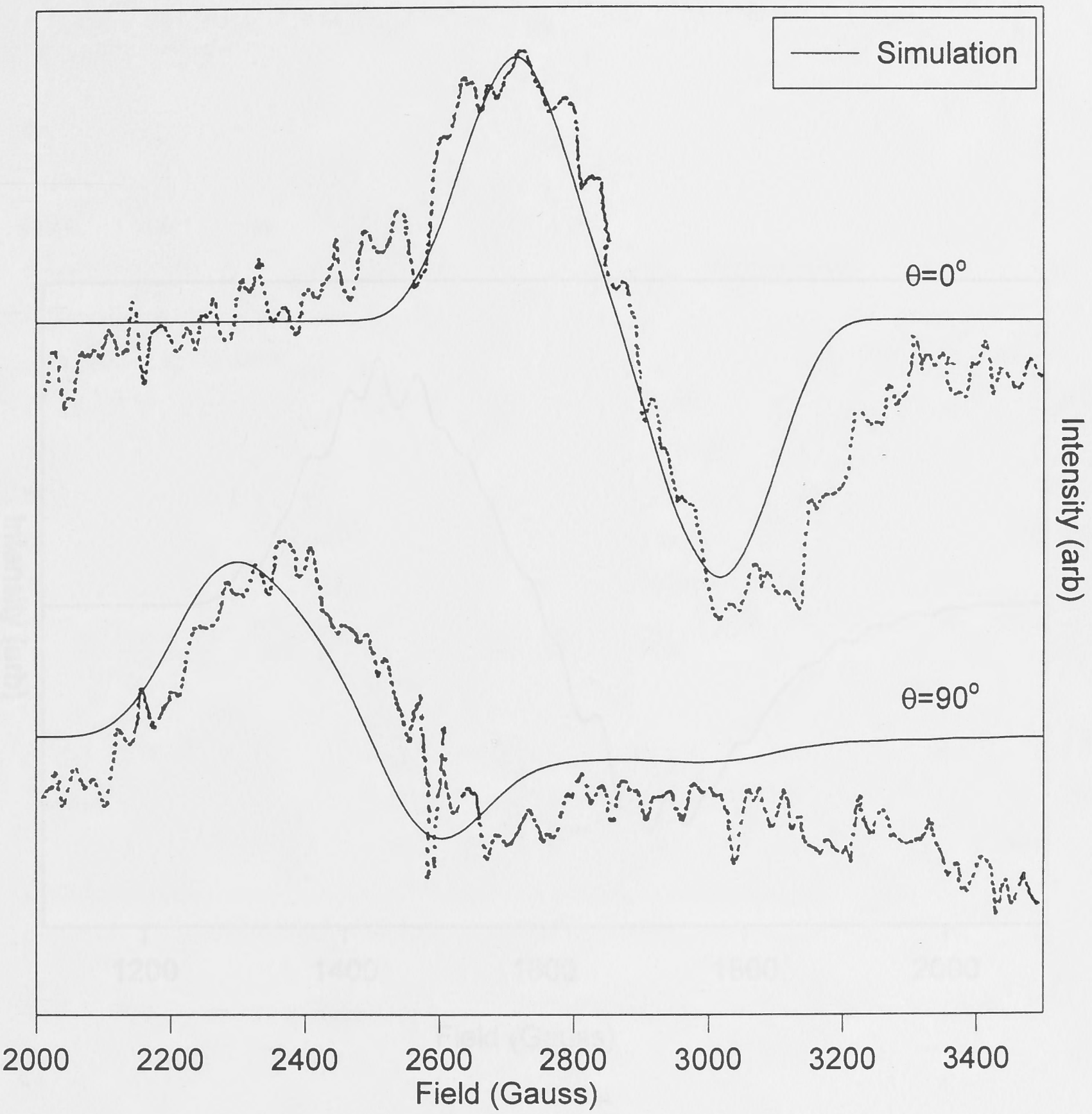

Figure 4.7 Simulation of P-band spectrum of one dimensionally ordered samples. Parameters are given in table 4.2. Experimental P-band spectrum (Haddy, *et al.*, 1992) reproduced with kind permission of the author.

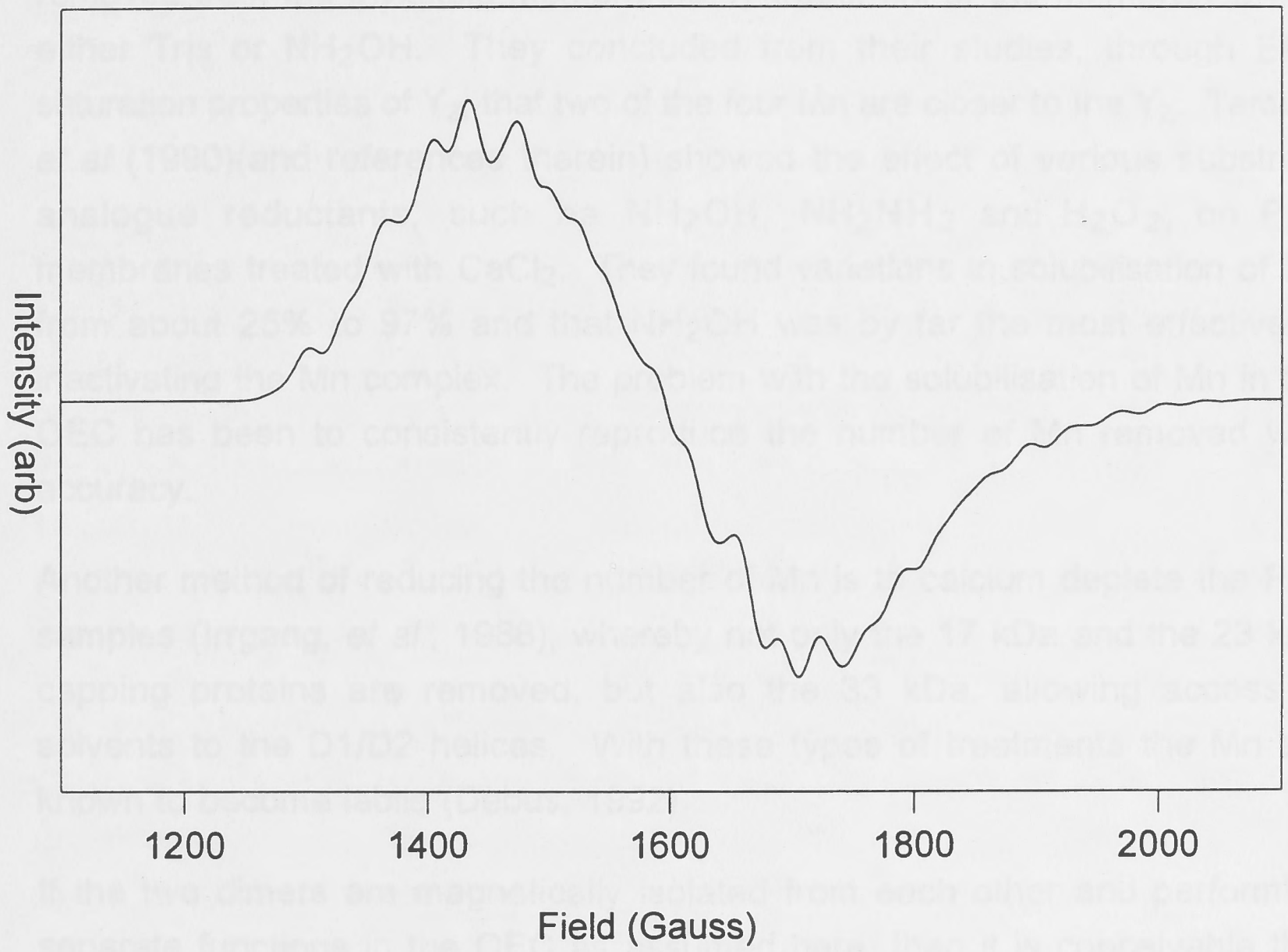

Figure 4.8 Simulation of the θ= 0° orientation showing hyperfine structure, as it appears in the ammonia influenced g=4.1 signal.
The simulations use anisotropic hyperfine parameters corresponding to A_{iso} ~35 Gauss and $A2_{iso}$ of ~33 Gauss. See text.

The main contribution to the effective *D* and *E* parameters comes from Mn^{III} (see above). The zero-field tensor is assumed to be coincident with the Zeeman, hyperfine and quadrupole tensors for this system. As for the hyperfine and quadrupole parameters, the zero-field parameters are quasi-axial, as expected for a high spin d^4 ion. The zero-field tensor as modelled here, and the hyperfine tensors have nearly coincident z-axis (Figure 2.9, Figure 3.3), see Chapter 7.

5: SIMULATION OF A MODIFIED MULTILINE EPR SIGNAL FROM A PREPARATION CONTAINING LESS THAN FOUR MANGANESE

Introduction

The concept of heterogeneity in the OEC has interested researchers for a long time. Yocum *et al* (1981) showed that approximately half of the Mn could be removed from the thylakoid membranes by treatment of the membranes with either Tris or NH_2OH. They concluded from their studies, through EPR saturation properties of Y_z, that two of the four Mn are closer to the Y_z. Tamura *et al* (1990)(and references therein) showed the effect of various substrate analogue reductants, such as NH_2OH, NH_2NH_2 and H_2O_2, on PSII membranes treated with $CaCl_2$. They found variations in solubilisation of Mn from about 25% to 97% and that NH_2OH was by far the most effective in inactivating the Mn complex. The problem with the solubilisation of Mn in the OEC has been to consistently reproduce the number of Mn removed with accuracy.

Another method of reducing the number of Mn is to calcium deplete the PSII samples (Irrgang, *et al.*, 1988), whereby not only the 17 kDa and the 23 kDa capping proteins are removed, but also the 33 kDa, allowing access of solvents to the D1/D2 helices. With these types of treatments the Mn are known to become labile (Debus, 1992)

If the two dimers are magnetically isolated from each other and performing separate functions in the OEC as assumed here, then it is conceivable that signals similar to those arising from the intact system will arise from systems containing only two Mn.

Simulations have been performed on a modified multiline signal from a preparation where the extrinsic proteins have been removed, thereby releasing some of the Mn (Fiege, *et al.*, 1995).

Method

Calcium depleted PSII samples

The PSII samples were prepared by K.-D. Irrgang and EPR spectroscopy undertaken by R. Fiege, Max-Volmer-Institute für Biophysikalische und Physikalische Chemie, Technische Universität, Berlin (Fiege, *et al.*, 1995)

PSII samples were isolated according to the BBY procedure (Bertrand, *et al.*, 1991) modified as described in Völker, *et al.* (1985). The 33 kDa protein was stepwise extracted by salt washing as in Irrgang, *et al.* (1988) and concentrated via Centripep centrifugation (Amicon). The salt treated sample with all extrinsic proteins removed showed only 10% of the oxygen evolution activity of the control (~400 μmol O_2 mg^{-1} chl h^{-1}), but showed a significant increase of peroxide production from 5 (control) to 40 μmol H_2O_2 mg^{-1} chl h^{-1}.

Illumination for these samples was performed at 200K.

The simulation used was the powder pattern simulation described in Chapter 2, and Appendix 2.

Results

For simulation of the multiline signal of the $CaCl_2$ treated samples, the underlying broad signal was removed using a cubic spline. The amount of multiline signal was quantified by comparing the doubly integrated signal for the treated samples and a control by the method described in Chapter 2. The scaling found the intensity of the modified multiline to be 0.9 of the normal multiline signal. The $CaCl_2$ washed PSII samples did not show any signal in the g=4 region.

The modified multiline signal from $CaCl_2$ treated samples together with the multiline signal from the normal S_2 state at X-band is shown in Figure 5.1. We found that when comparing the spectra from which the underlying signals had been subtracted, there was very little difference in peak separation. The resolution of the edges of the modified multliline signal is such that it is difficult to ascertain the number of peaks, but it appears to be the same for both. In the region g>2 there is quite a bit of variation, particularly in the region where Q_A^- may contribute, near g=1.9-1.8. The modified multiline signal appears to have no contributions from Q_A^-. Indeed, the core preparation used for the modified multiline signal, with the extrinsic proteins (17 kDa, 23 kDa, 33 kDa) removed, show impairment of the Q_A function (Irrgang, *et al.*, 1988) and therefore has PpBQ added as electron acceptor.

Figure 5.2a & b shows the modified multiline signal together with the best fit simulation of the same. The parameters of the best fit modified multiline parameters together with the best fit normal multiline simulation are shown in Table 5.1.

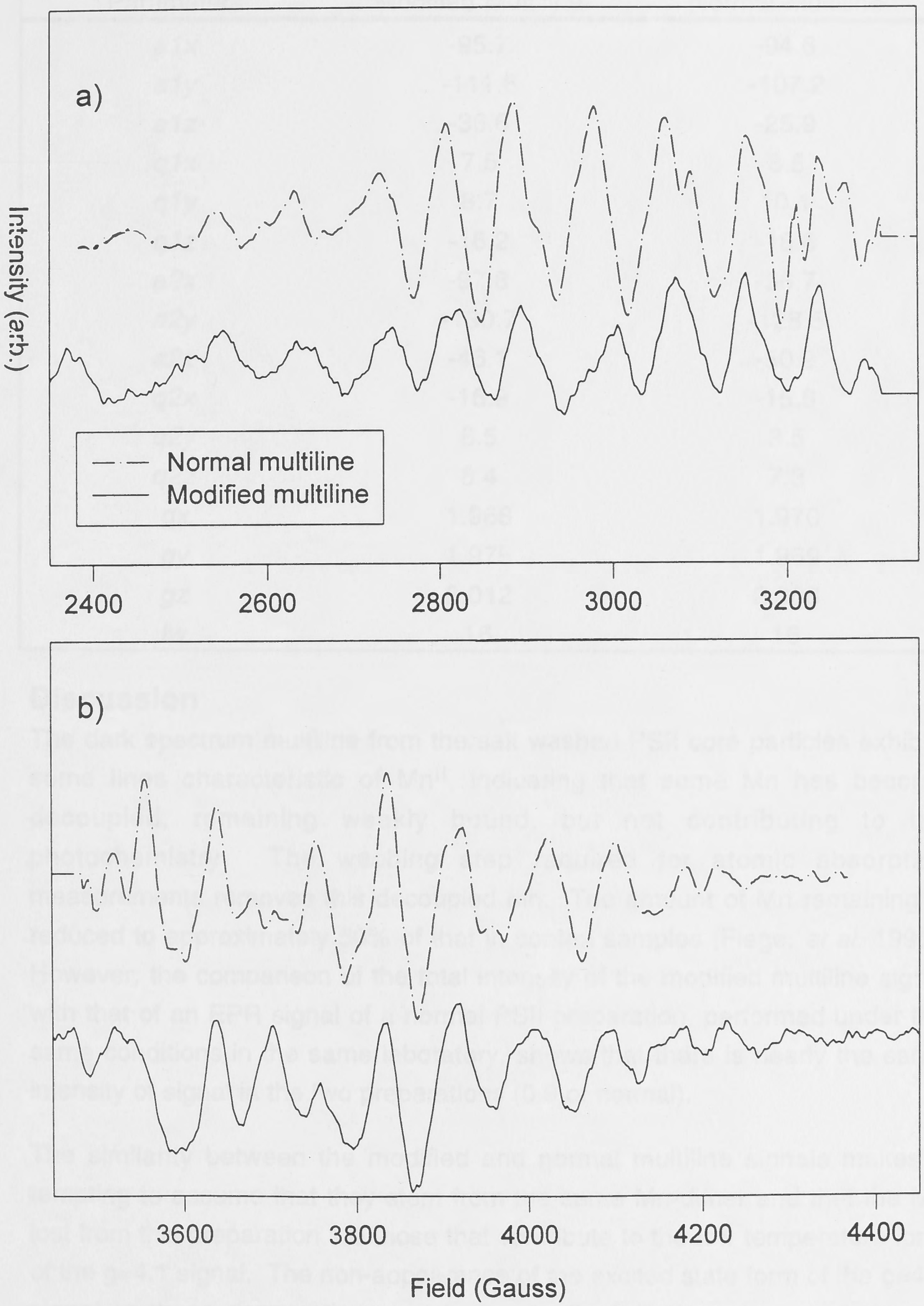

Figure 5.1 The modified multiline spectrum compared with the normal PSII multiline spectrum downfield (a) and upfield (b). The normal multiline has been shifted to the modified multiline frequency (9.44 GHz). The broad feature at the downfield edge of the spectrum of the modified multiline may be a subtraction artefact.

Table 5.1. Best fit simulation parameters for the modified multiline together with those for the normal multiline (units Gauss)

Parameters	Modified Multiline	Normal Multiline
a1x	-95.7	-94.6
a1y	-111.6	-107.2
a1z	-36.6	-25.9
q1x	7.5	8.5
q1y	8.7	10.1
q1z	-16.2	-18.6
a2x	-97.8	-96.7
a2y	-130.7	-128.5
a2z	-46.1	-50.9
q2x	-16.9	-15.8
q2y	8.5	8.5
q2z	8.4	7.3
gx	1.968	1.970
gy	1.975	1.969
gz	2.012	2.008
lw	16	16

Discussion

The dark spectrum multiline from the salt washed PSII core particles exhibits some lines characteristic of Mn^{II}, indicating that some Mn has become decoupled, remaining weakly bound, but not contributing to the photochemistry. The washing step required for atomic absorption measurements removes this decoupled Mn. The amount of Mn remaining is reduced to approximately 50% of that in control samples (Fiege, *et al*, 1995). However, the comparison of the total intensity of the modified multiline signal with that of an EPR signal of a normal PSII preparation, performed under the same conditions in the same laboratory, shows that there is nearly the same intensity of signal in the two preparations (0.9 of normal).

The similarity between the modified and normal multiline signals makes it tempting to assume that they stem from the same Mn-dimer and that the Mn lost from this preparation are those that contribute to the low temperature form of the g=4.1 signal. The non-appearance of the excited state form of the g=4.1 signal in these preparation may be a result of an increase in exchange coupling, similar to the small change seen with addition of a mono-alcohol (Pace, *et al.*, 1991). For instance, a decrease in the Mn-O bond length will

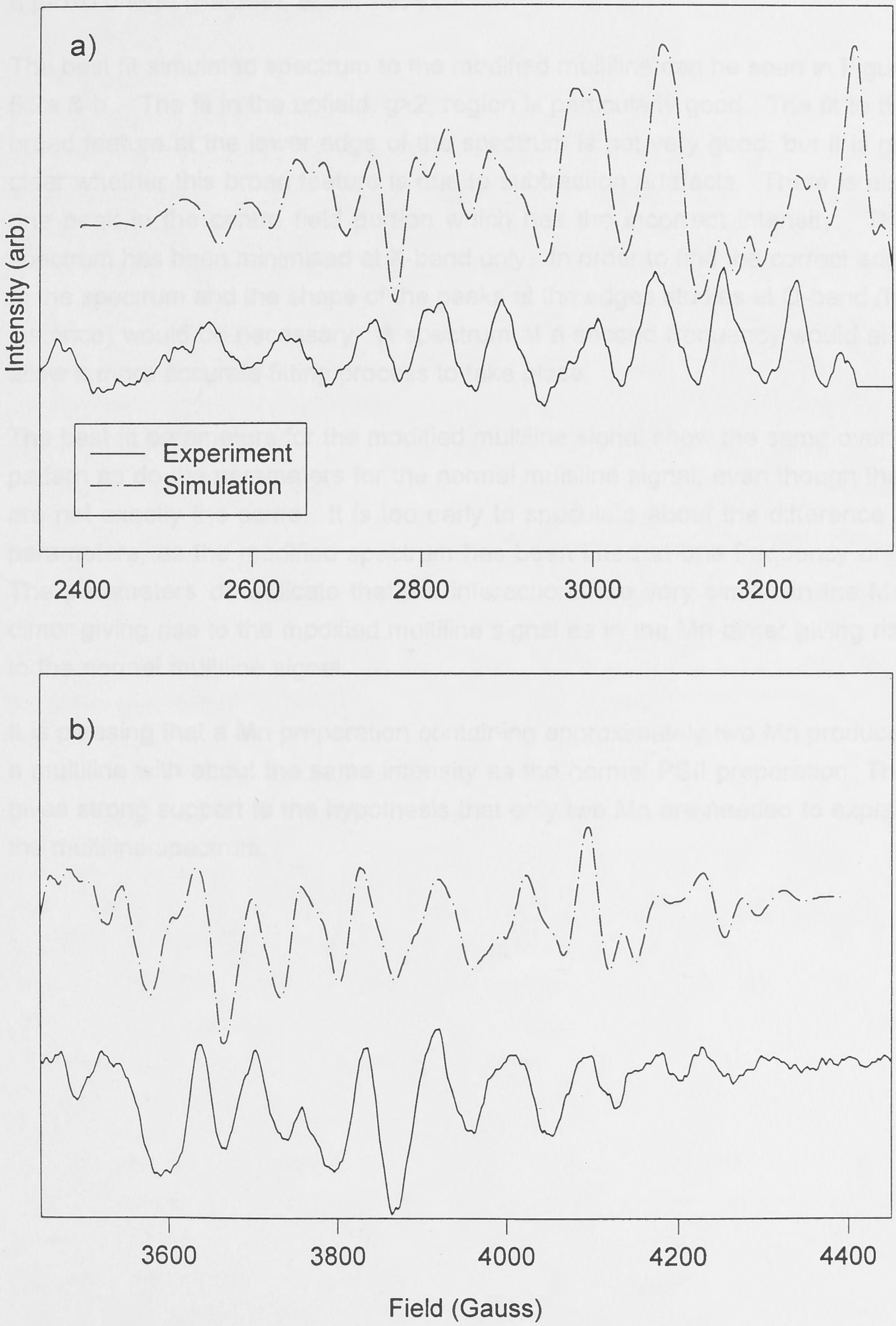

Figure 5.2 Best fit simulation of the modified experimental spectrum, compared with the experimental spectrum; a) downfield, b) upfield. Parameters used are listed in Table 5.1. Frequency 9.44 GHz; microwave power 10 mW; modulation amplitude 20 Gauss.

increase $|J|$, such a small decrease can be brought about by deprotonation of a μ-oxo bridge (Baldwin, *et al.*, 1994).

The best fit simulated spectrum to the modified multiline can be seen in Figure 5.2a & b . The fit in the upfield, g>2, region is particularly good. The fit to the broad feature at the lower edge of the spectrum is not very good, but it is not clear whether this broad feature is due to subtraction artefacts. There is also one peak in the centre field portion which has the incorrect intensity. This spectrum has been minimised at X-band only. In order to find the correct edge of the spectrum and the shape of the peaks at the edges studies at Q-band (for instance) would be necessary. A spectrum at a second frequency would also allow a more accurate fitting process to take place.

The best fit parameters for the modified multiline signal show the same overall pattern as do the parameters for the normal multiline signal, even though they are not exactly the same. It is too early to speculate about the difference in parameters, as the modified spectrum has been fitted at one frequency only. The parameters *do* indicate that the interactions are very similar in the Mn-dimer giving rise to the modified multiline signal as in the Mn-dimer giving rise to the normal multiline signal.

It is pleasing that a Mn preparation containing approximately two Mn produces a multiline with about the same intensity as the normal PSII preparation. This gives strong support to the hypothesis that only two Mn are needed to explain the multiline spectrum.

6: GROWTH EXPERIMENTS/METAL REPLACEMENT

Introduction

This work grew out of a need to test the quadrupole parameters resulting from the multliline simulations, as these are rather larger than indicated by other researchers (Randall, et al., 1995; Zheng and Dismukes, 1996). There is no stable isotope for Mn except ^{55}Mn, so the option of growing the plants in the presence of a different isotope was not open to me.

T. Wydrzynski brought to my notice the literature available on Ruthenium (Ru) and the fact that Ru dimers oxidise water (Comte, et al., 1989; Doppelt and Meyer, 1987). The idea of metal replacement using $RuCl_3.3H_20$ was raised. I decided to first try to grow spinach plants in a medium depleted of Mn ions but with Ru ions present instead.

Ruthenium belongs to group VIII, called the platinum metals. Ruthenium exists in all oxidation states from 0 to VIII, with Ru^{III} a $4d^5$ ion. All known complexes of Ru^{III} are of low-spin t_{2g}^5, with one unpaired electron (Cotton and Wilkinson, 1966). The ionic radius of Ru^{IV} is the same as Mn^{III} (0.63Å vs 0.62Å) (Dean, 1985). It is therefore of a suitable size to fit into the Mn site in the protein.

All of the characteristics indicated above make Ru a suitable candidate for metal replacement.

There are several isotopes of Ru. Two possess nuclear spin ^{99}Ru (I=5/2) with 12.63% natural abundance and ^{101}Ru (I=5/2) with 17.02% natural abundance (Dean, 1985). If Ru ions are taken up by the plant it is likely that the spectrum from a dimer species is going to be greatly simplified. Any hyperfine interaction seen is going to be present at low intensity.

Method

Spinach seeds were planted in vermiculite to germinate. When seedlings were large enough to plant out, they were grown hydroponically in a growth chamber, using a water culture solution for spinach (Appendix 5). Trace elements were prepared with $RuCl_3.3H_2O$ replacing $MnCl_2.4H_2O$. Water purified using a Milli-Q Plus® (Millipore) ultra pure water system, was used for solutions and for watering. A control was grown simultaneously with neither Mn^{II} nor Ru^{III} ions present in nutrient solution.

Results

After a period of five weeks the Mn-deficient plants were dying but the plants grown in the presence of Ru^{III} ions were still in good condition, see Figure 6.1.

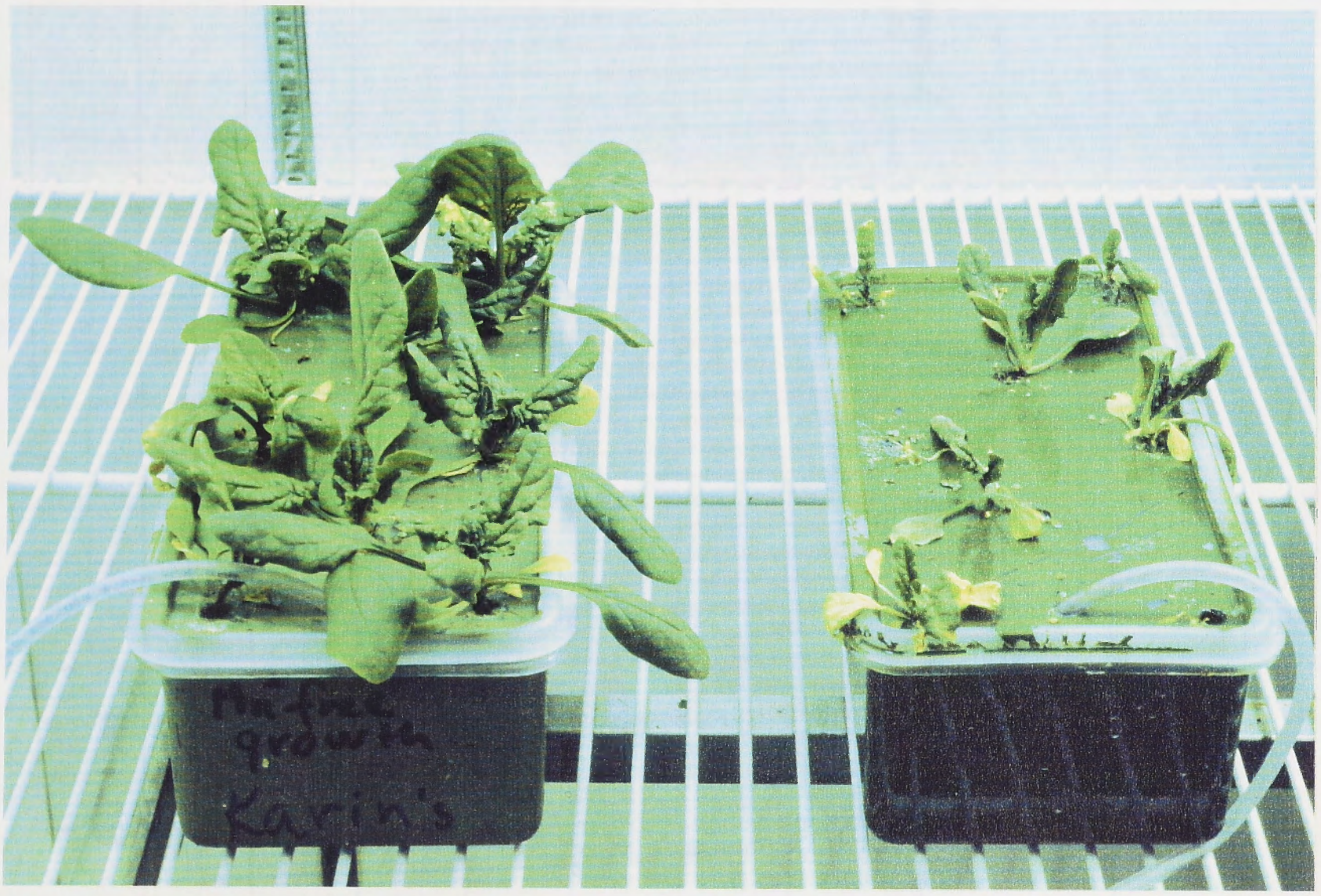

Figure 6.1 Plants grown in the presence of $RuCl_3$ only (left) and plants grown without addition of $MnCl_2$ and $RuCl_3$ (right) after 4 weeks growth.

Whole leaf measurements

Fluorescence measurements were made on a whole leaf, compared with a normal leaf of the same age (Christof Klughammer), see Figure 6.2. The fluorescence yield, according to the method described in Schreiber, et al., 1986, was measured after dark adaption, giving the F_0 value, corresponding to a system with an open acceptor side, in other words, Q_A is oxidised. After a saturation pulse, assumed to close all PSII centres, there is an increase of the fluorescence yield to the maximum possible value (F_m). The ratio $(F_m-F_0)/F_m$ (or F_v/F_m) is related to the quantum yield for PSII chemistry (Schreiber, et al., 1995). For the Ru-PSII leaf F_v/F_m was 0.82 compared with 0.81 for the normal leaf. Healthy leaves have a F_v/F_m in the range 0.80-0.87. The values of quantum yield using fluorescence measurements correlates closely to values obtained by a variety of other methods (Schreiber, et al., 1995).

Flash-induced 0_2 oscillation patterns were measured (Johannes Messinger) in a leaf segment with the epidermis removed, using a modified Joliot-type electrode (Messinger and Renger, 1990). The leaf grown in the presence of

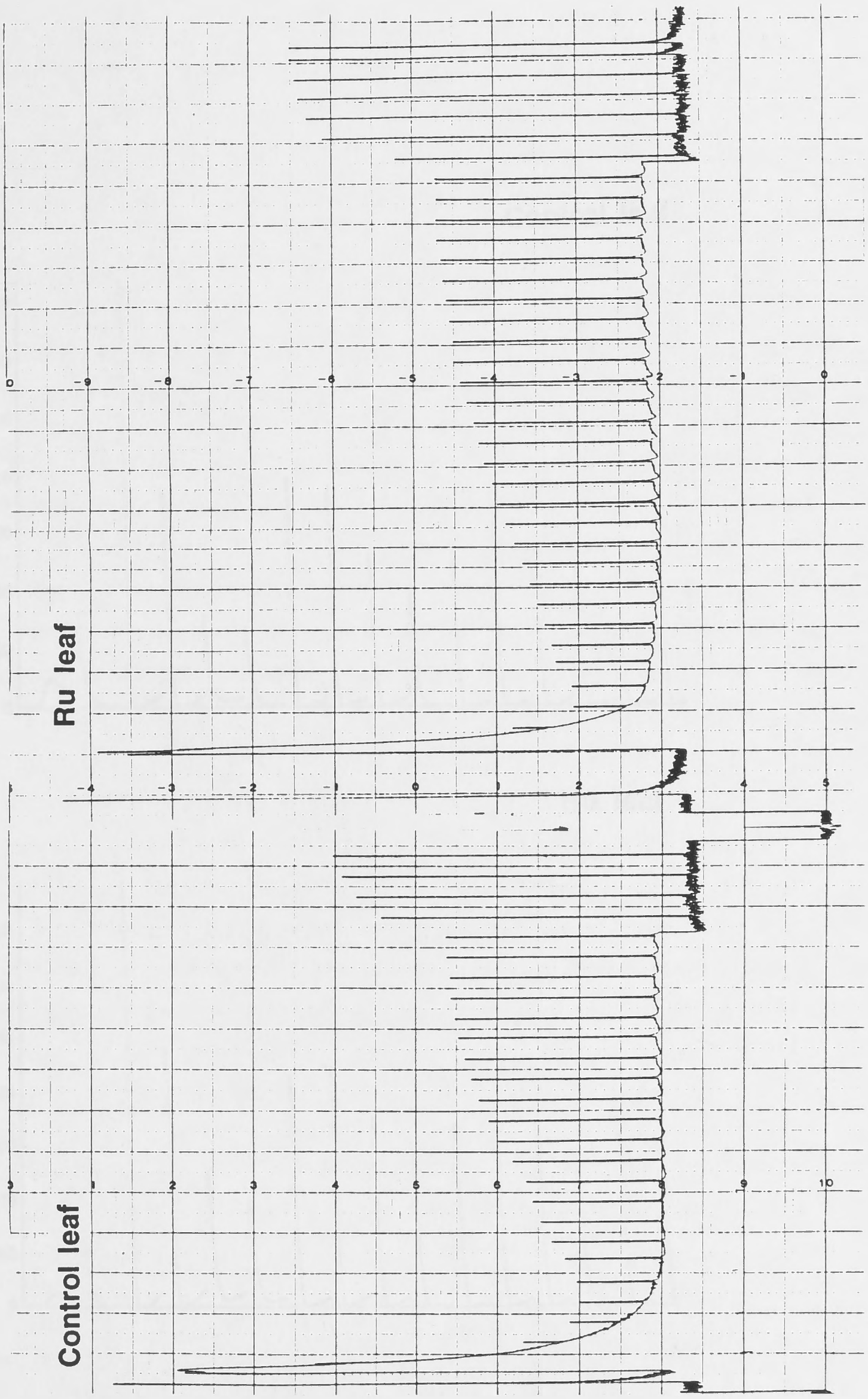

Figure 6.2 Fluorescence measurements on leaf grown on $RuCl_3$ compared with normal leaf. Control (left) and Ru-leaf (right) show similar activity, with F_v/F_m 0.81 and 0.82 respectively.

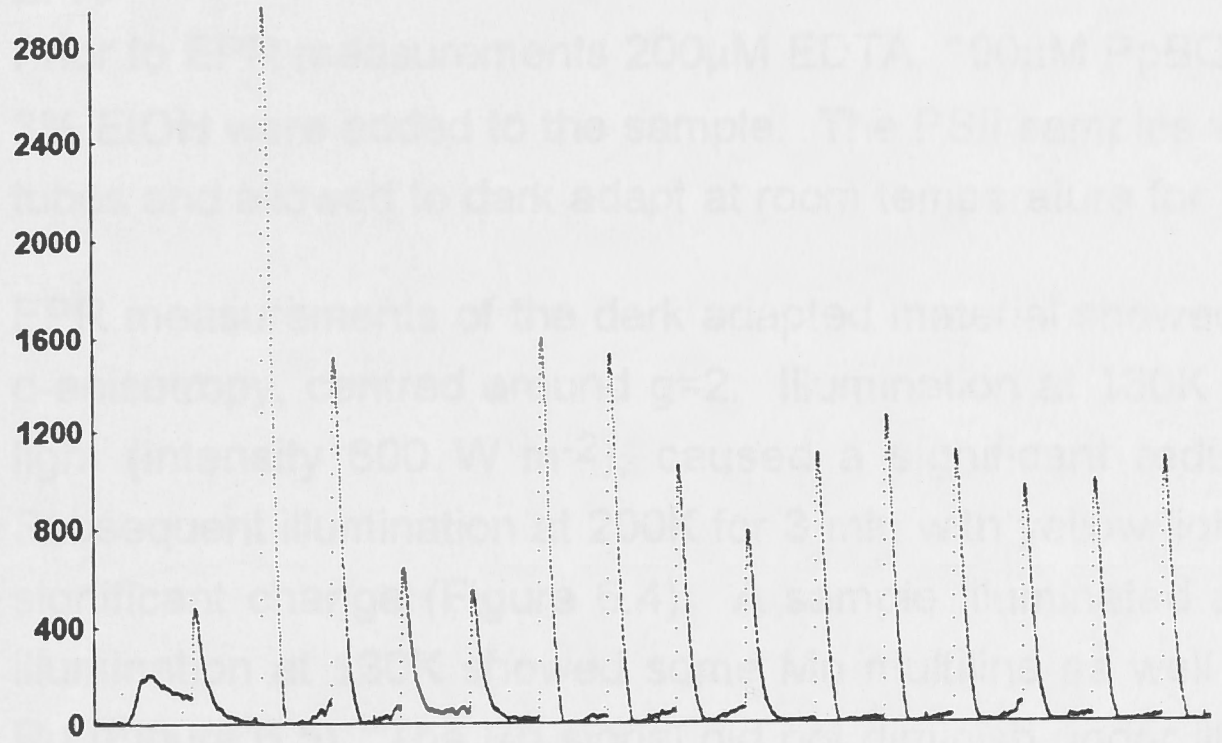

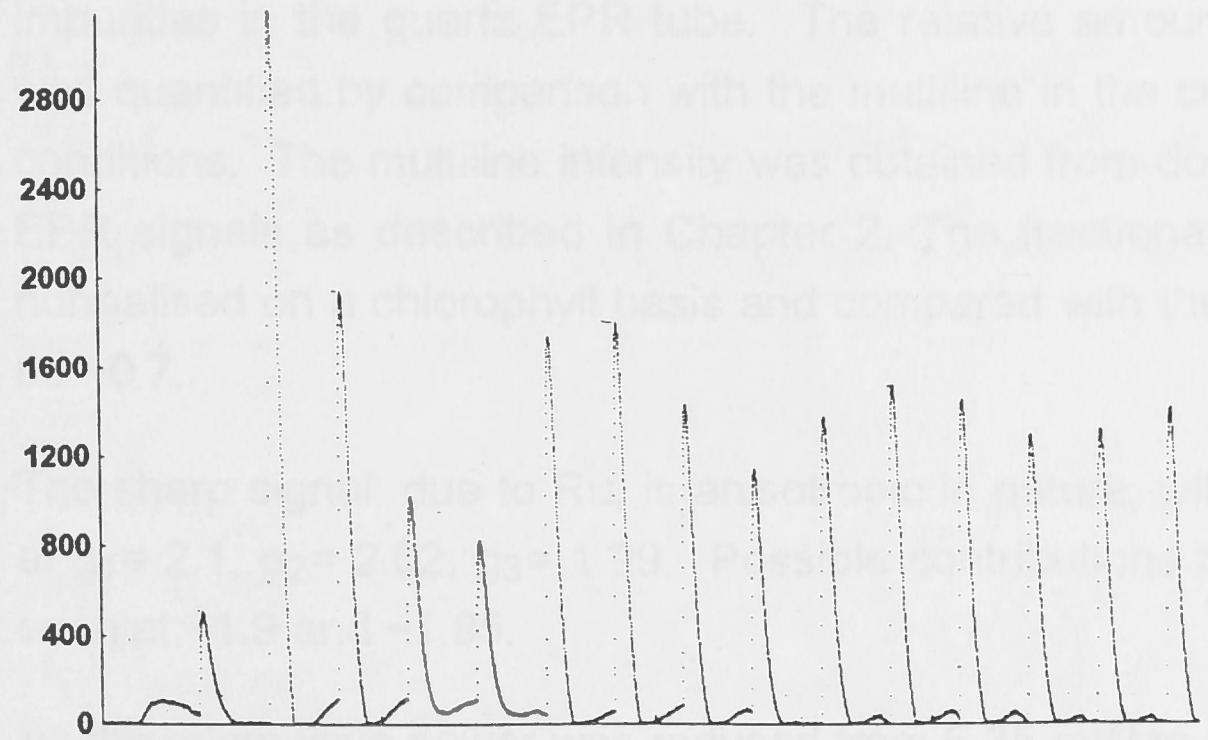

Figure 6.3 Flash-induced O_2 evolution measured in normal leaf and leaf grown on $RuCl_3$.

Ru^{III} showed a normal O_2 oscillation pattern at the same level as the normal leaf, see Figure 6.3.

PSII sample measurements

PSII samples were prepared, using the 40g leaf material remaining, according to the method described in Chapter 2 and Appendix 1. Control PSII samples were also prepared under the same conditions.

EPR

Prior to EPR measurements 200μM EDTA, 100μM PpBQ, 100μM DCMU, and 3% EtOH were added to the sample. The PSII samples were loaded into EPR tubes and allowed to dark adapt at room temperature for 10 minutes.

EPR measurements of the dark adapted material showed a sharp signal, with g-anisotropy, centred around g=2. Illumination at 130K for 3 min with yellow light (intensity 600 W m^{-2}), caused a significant reduction of this signal. Subsequent illumination at 200K for 3 min with yellow light, did not induce any significant change (Figure 6.4). A sample illuminated at 200K without prior illumination at 130K showed some Mn multiline as well as the peaks due to Ru (Figure 6.5). The Ru signal did not diminish under illumination, compared with the dark. This can be seen as there is no significant subtraction artefact in the illuminated-dark difference spectrum which reveals the multiline. The broad signal seen in these spectra we believe to be due to paramagnetic impurities in the quartz EPR tube. The relative amount of multiline present was quantified by comparison with the multiline in the control under the same conditions. The multiline intensity was obtained from double integration of the EPR signals as described in Chapter 2. The fractional amount of multiline, normalised on a chlorophyll basis and compared with the control was found to be ~0.7.

The sharp signal, due to Ru, is anisotropic in nature, with three turning points at g_1= 2.1, g_2= 2.02, g_3= 1.99. Possible contributions from Q_A^- can often be seen at ~1.9 and ~1.85.

As the microwave power was reduced from 6.35 mW to 6.35 μW at 7K regular fine structure appeared on the main peaks, always in the same position. The peak separations are about 15-30 Gauss, see Figure 6.6. There are some additional features downfield of the main peaks. These features are ~75 Gauss apart, and cannot be distinguished from Mn hyperfine. It is however possible that the additional features on the main peaks may be due to Ru hyperfine from ^{99}Ru and ^{101}Ru.

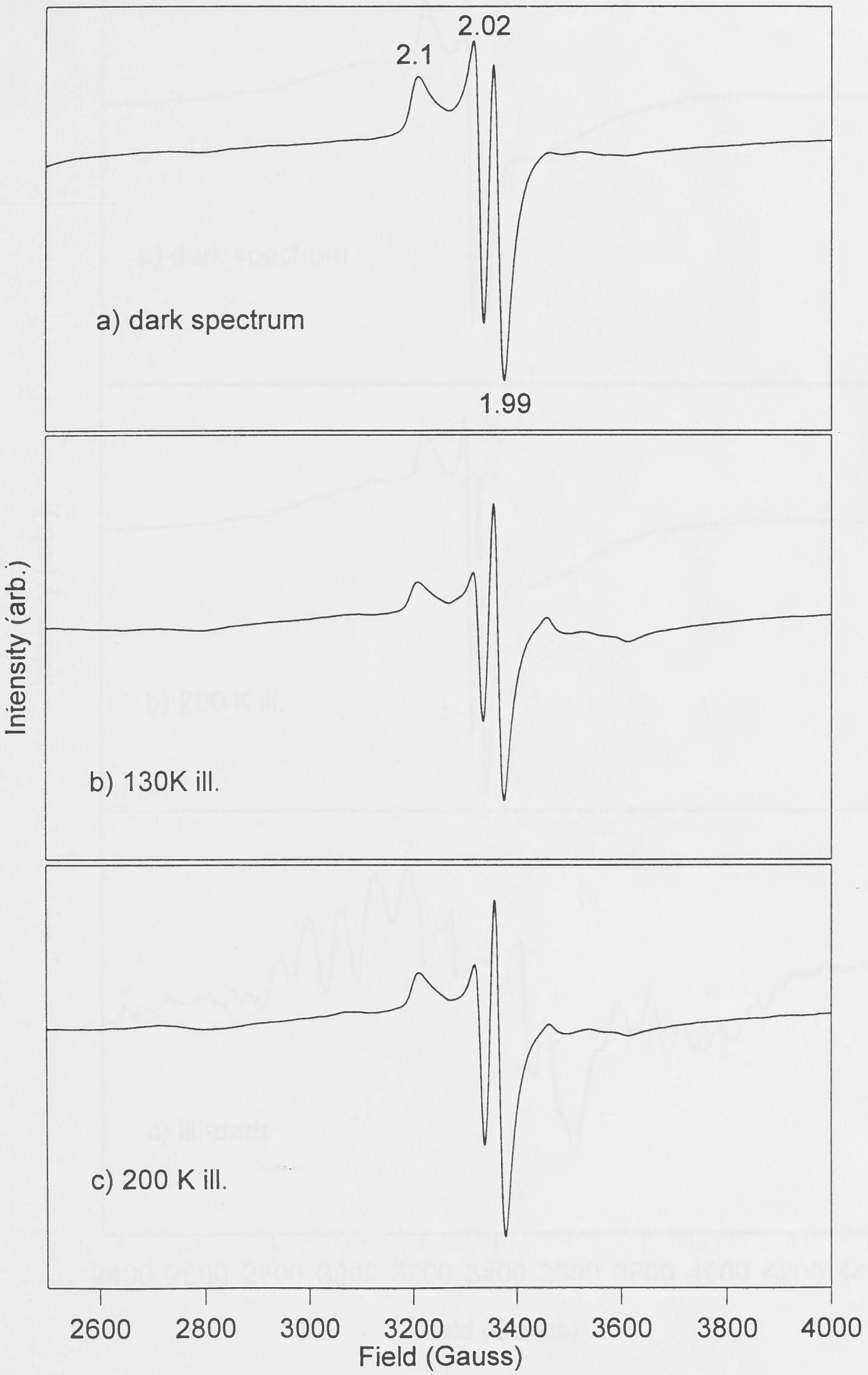

Figure 6.4. EPR of low temperature (130K) illuminated Ru-PSII sample.
(a) Spectrum before illumination, (b) after 130K illumination, 3 min, yellow light (c) after 200K illumination, 3 min, yellow light. The g-value for each turning point is indicated. Sample containing 200 μM EDTA. Spectrometer conditions: Frequency 9.42GHz; modulation amplitude 20 Gauss; microwave power 6.35 mW; modulation frequency 100 kHz; temperature 7K. Two scans were taken for each spectrum.

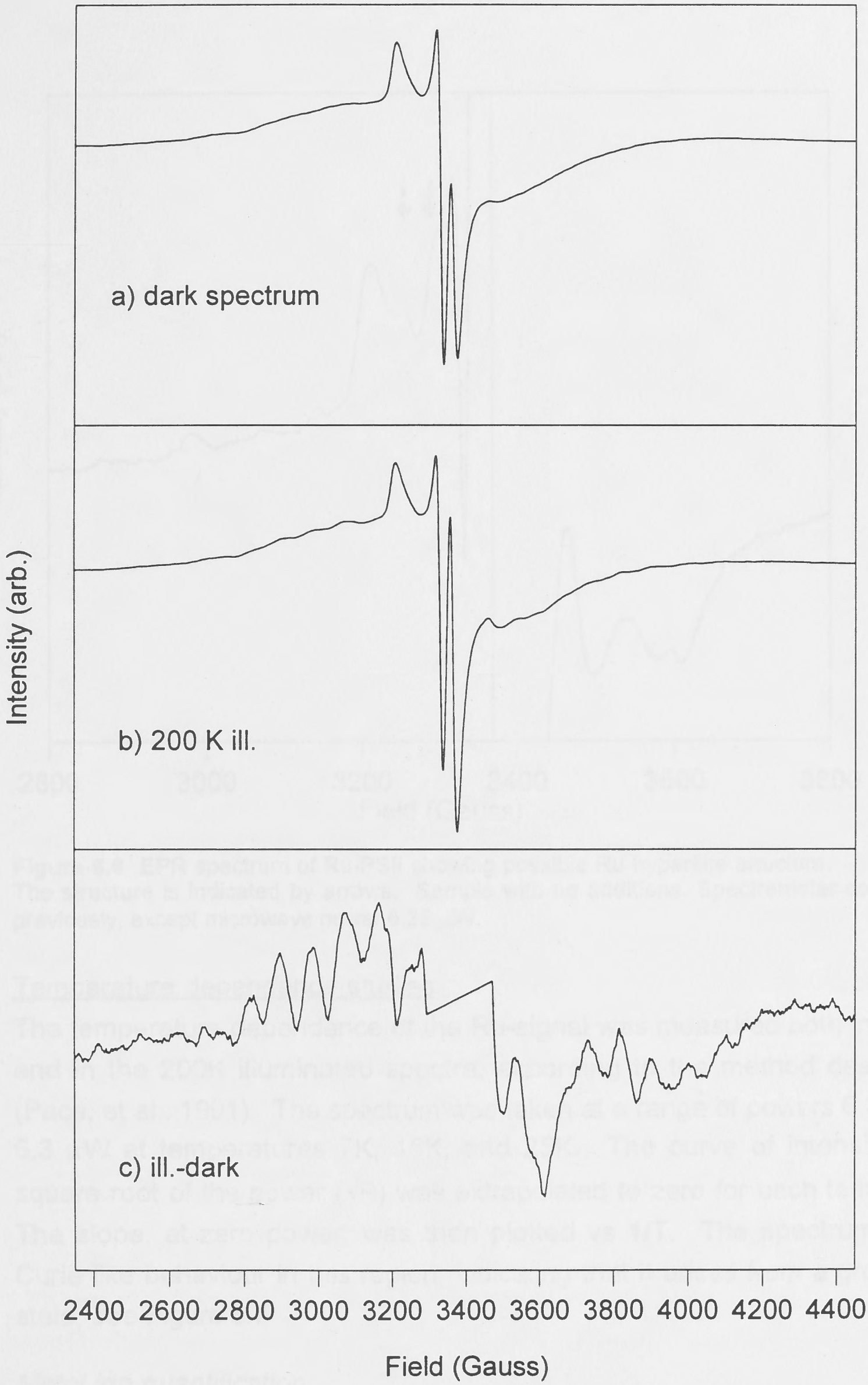

Figure 6.5. EPR of Ru-PSII sample illuminated at 200K, showing multiline signal.
(a) Spectrum before illumination, (b) after 200K illumination with yellow light, 3 min, (c) illuminated minus dark spectrum. Sample containing 200 μM EDTA and 3% MeOH. Spectrometer conditions: Frequency 9.42 GHz;modulation amplitude 20 Gauss; microwave power 6.35 mW; modulation frequency 100 kHz; temperature 7K. Two scans were taken for each spectrum.

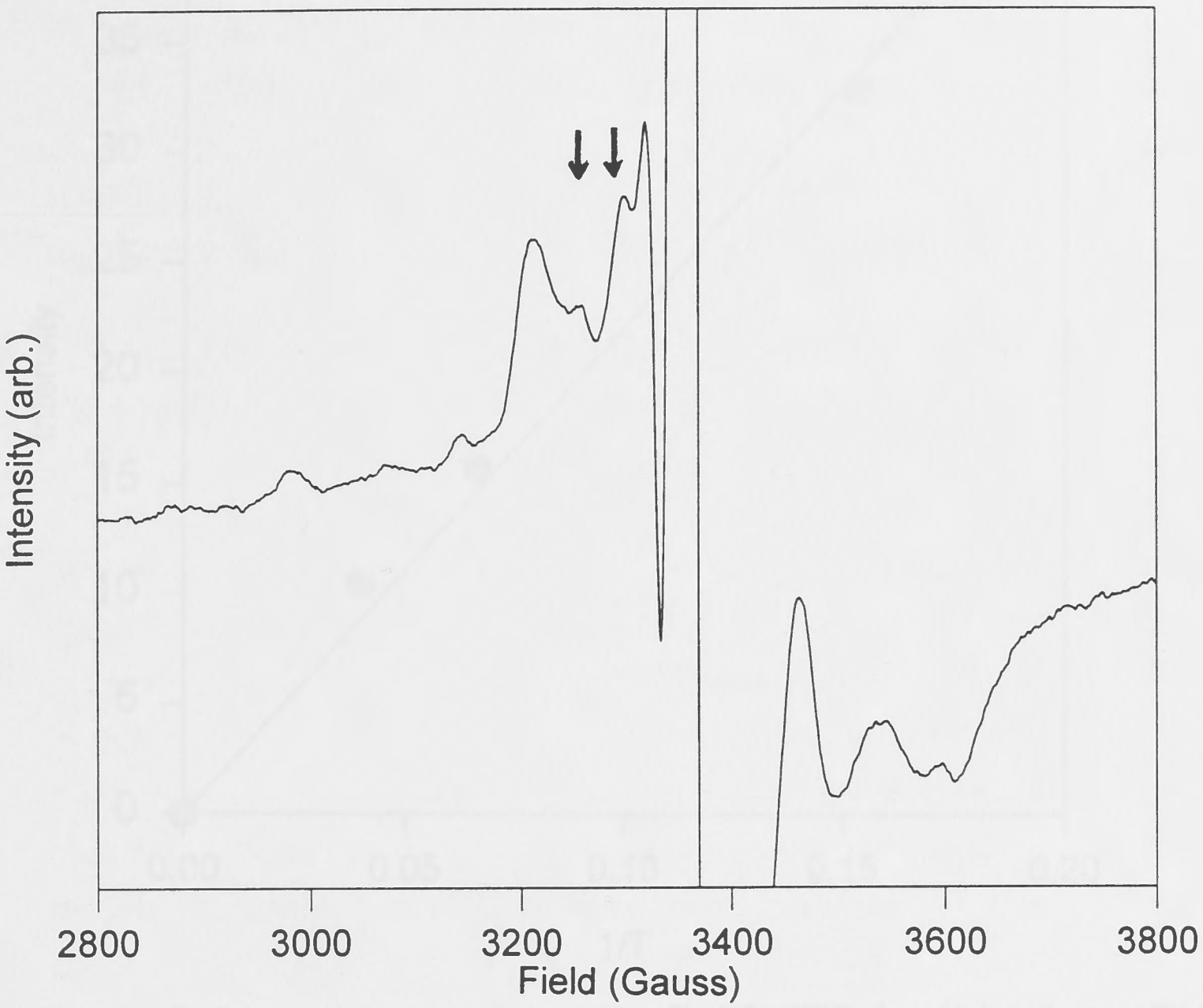

Figure 6.6 EPR spectrum of Ru-PSII showing possible Ru hyperfine structure.
The structure is indicated by arrows. Sample with no additions. Spectrometer conditions as previously, except microwave power 6.35 μW.

Temperature dependence studies

The temperature dependence of the Ru-signal was measured both in the dark and in the 200K illuminated spectra, according to the method described in (Pace, et al., 1991). The spectrum was taken at a range of powers 6.35 mW to 6.3 μW at temperatures 7K, 15K, and 25K. The curve of intensity vs the square root of the power ($\sqrt{P}$) was extrapolated to zero for each temperature. The slope, at zero power, was then plotted vs 1/T. The spectrum exhibits Curie like behaviour in this region, indicating that it arises from a ground spin state, see Figure 6.7

Metal ion quantification

Inductively coupled plasma spectroscopy (ICP) was used to quantify the amount of Mn and Ru ions in the sample. The sample, previously treated with EDTA, was acidified to 300mM HCl and the released Mn^{2+} and Ru^{3+} measured against a standard curve. The procedure showed that ~2.4 Mn ions and 2.1 Ru ions were present per 250 Chl molecules.

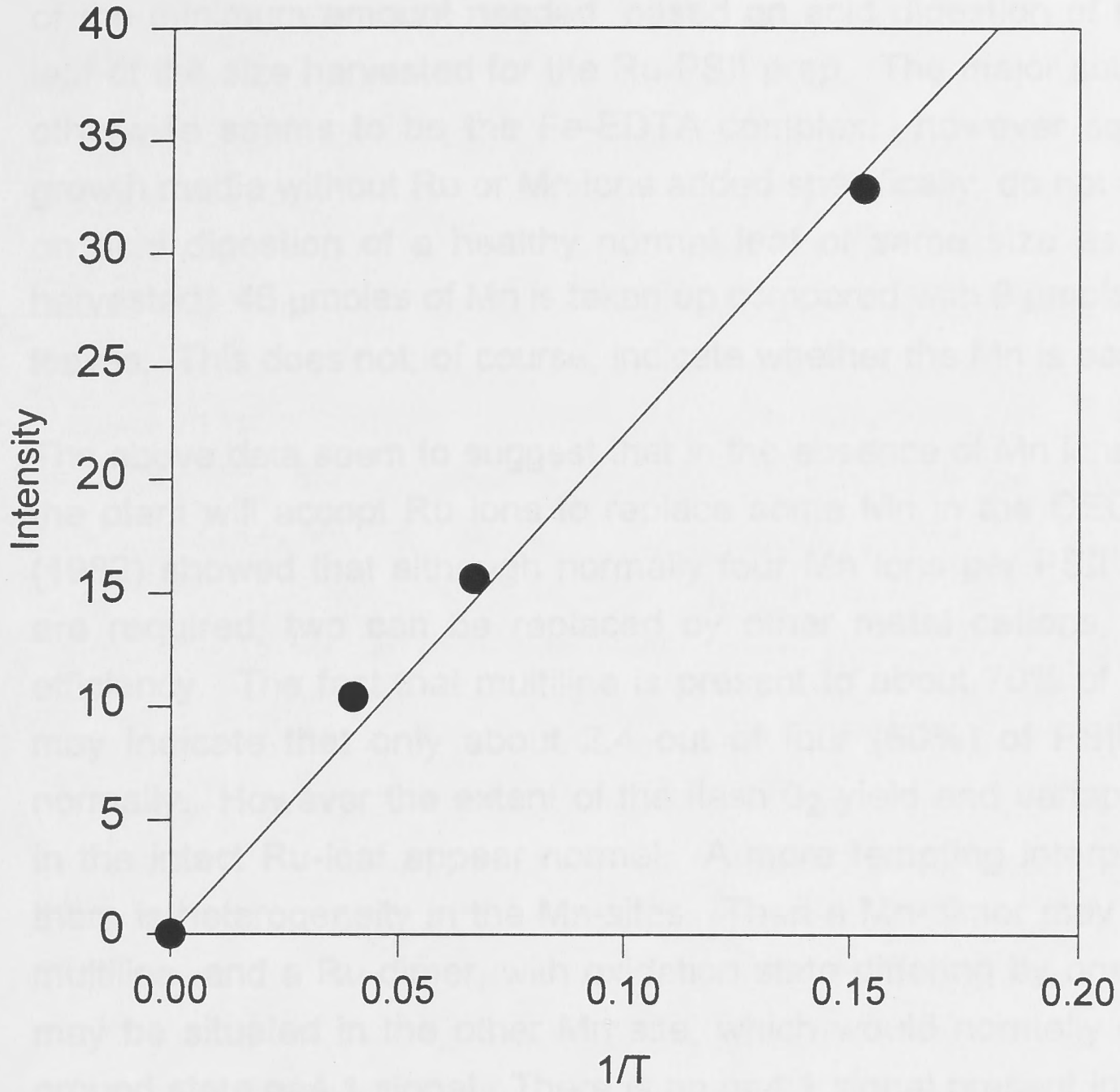

Figure 6.7 Temperature dependence of the Ru-PSII EPR signal intensity over 7K to 25K.

Oxygen evolution

Flash-induced 0_2 oscillation patterns were also measured in the Ru-PSII prep. and compared with that of the control prep (Johannes Messinger). The patterns were again very similar, however, the yield of oxygen from the Ru-PSII samples was about 50% of the control. It must be stated here that owing the small amount of sample available for each experiment, the Ru samples had been frozen and thawed twice before the oxygen activity measurement, so that this measurement may be artificially low.

Discussion

The work reported above is very much work in progress. The experiment was repeated successfully twice, but not again. Factors, such as trying to grow larger amounts in larger volumes and light intensity in the growth chamber, may have affected the results.

From the growth experiments to date, it is clear that some Mn ions must be present for growth to occur. Mn ions are often present as impurities in many components of the growth media, such as $MgCl_2$, $MgSO_4$(trace only), $RuCl_3$ (0.1%), Fe-EDTA complex (0.15%). The seeds themselves supply about 11%

of the minimum amount needed, based on acid digestion of a homogenised leaf of the size harvested for the Ru-PSII prep. The major source of Mn ions otherwise seems to be the Fe-EDTA complex, however seeds planted in growth media without Ru or Mn ions added specifically, do not survive. Based on acid digestion of a healthy normal leaf of same size as the Ru-leaves harvested, 46 μmoles of Mn is taken up compared with 9 μmoles of Mn for Ru-leaves. This does not, of course, indicate whether the Mn is bound or not.

The above data seem to suggest that in the absence of Mn ions in abundance, the plant will accept Ru ions to replace some Mn in the OEC. Klimov *et al* (1982) showed that although normally four Mn ions per PSII reaction centre are required, two can be replaced by other metal cations, but with lower efficiency. The fact that multiline is present to about 70% of normal amount may indicate that only about 2.4 out of four (60%) of PSII is functioning normally. However the extent of the flash O_2 yield and variable fluorescence in the intact Ru-leaf appear normal. A more tempting interpretation, is that there is heterogeneity in the Mn-sites. Then a Mn-dimer may give rise to the multiline, and a Ru-dimer, with oxidation state differing by one (II/III or III/IV), may be situated in the other Mn site, which would normally give rise to the ground state g=4.1 signal. There is no g=4.1 signal present in the EPR of the Ru-PSII prep. (Figure 6.8) at 130K illumination. On the other hand, ethylene glycol, which enhances the ground state g=4.1 signal, had not been added to these samples.

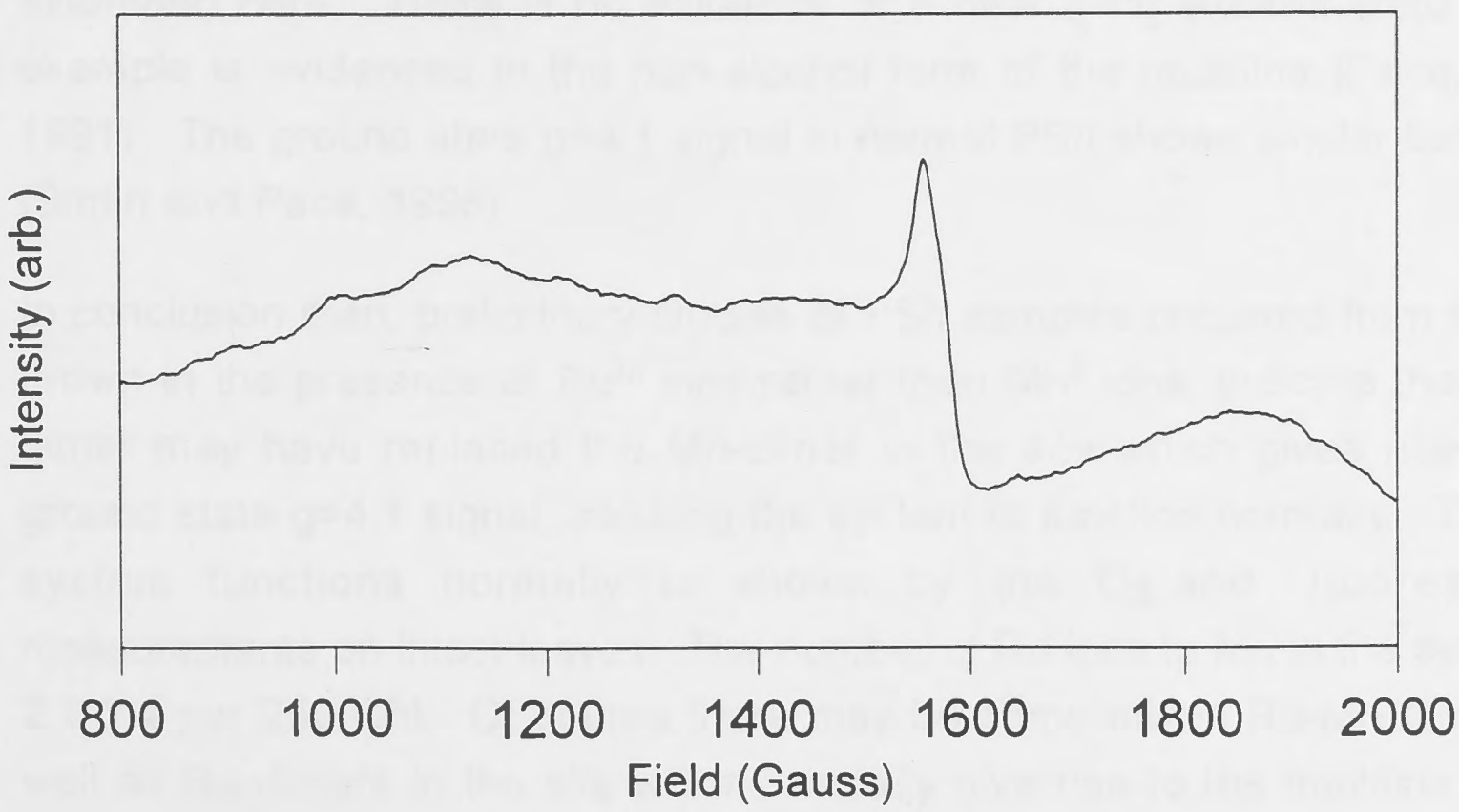

Figure 6.8 Spectrum of the g=4 region at 130K illumination.
Sample containing 200 μM EDTA. Spectrometer conditions: Frequency 9.42 GHz; modulation amplitude 20 Gauss; 6.35 mW microwave power; modulation frequency 100 kHz; temperature 7K. Two scans were taken for each spectrum.

The Ru EPR signal looks much like EPR signals of monomeric Ru^{III} complexes, which are low spin and therefore have one unpaired electron. However, dimeric Ru complexes of oxidation states II/III also exhibit similar signals with the g-anisotropy as seen here (Kasack, et al., 1995; Whittle, et al., 1995). Antiferromagnetic coupling between a Ru^{III} and Ru^{IV} ion would also produce a net S=1/2 state. The signal is therefore also consistent with a dimer interpretation. One electron oxidation, brought about by illumination at 130K, causes most of the signal to disappear. However, illumination at 200K does not affect this putative dimer. Interestingly this is similar behaviour to that of the intact system, where 130K illumination causes the appearance of the g=4.1 ground state signal, and 200K illumination (in the presence of 3% EtOH as in the Ru-PSII sample) causes the appearance of the multiline signal only.

There is very little published data regarding hyperfine interaction for Ru. Hyperfine interaction of order 10 Gauss was observed on an EPR signal assigned to the spin adduct of the radical $\cdot Ru(CO)_2Cp$ to nitrosodurene (Sostero, et al., 1993). The interaction for each isotope was measured to be ~ 5-6 Gauss. The two isotopes, both with I=5/2, have similar values of g_n (-0.249 for ^{99}Ru and -0.279 for ^{101}Ru, (Dean, 1985)), so that one does not expect to resolve the two isotopes over the field range employed here. The magnitude of the hyperfine would be expected to be smaller than that of Mn generally as the ratio g_n (Ru)/g_n (Mn) is ~0.18.

The temperature dependence of the Ru-signal is Curie over the range examined here. There is no evidence of a near lying excited state, as for example is evidenced in the non-alcohol form of the multiline (Pace, et al., 1991). The ground state g=4.1 signal in normal PSII shows similar behaviour (Smith and Pace, 1996).

In conclusion then, preliminary studies of PSII samples prepared from spinach grown in the presence of Ru^{III} ions rather than Mn^{II} ions, indicate that a Ru-dimer may have replaced the Mn-dimer in the site which gives rise to the ground state g=4.1 signal, allowing the system to function normally. That the system functions normally is shown by the O_2 and fluorescence measurements on intact leaves. The number of Ru ions to Mn in the system is 2.1:2.4 per 250 Chl. Of course there may be some mixed Ru-Mn dimers as well as Ru-dimers in the site which normally give rise to the multiline signal. However, the whole leaf measurements speak against approximately half of the centres being inactive due to Ru. The low oxygen evolution for Ru-PSII samples is probably a reflection of the sample having been thawed twice.

One can not rule out that an adjustment to the preparation method is needed for samples grown on Ru ions, in order to achieve maximum activity.

The data presented above is presented as work in progress. The evidence for plants accepting Ru ions in lieu of Mn ions is not conclusive, but promising. It would be a very interesting topic for further study.

7: CONCLUSION

The data presented herein lend strong support for a model of the Mn organisation in the OEC consisting of two magnetically isolated μ-oxo Mn dimers. The EPR signals arising from the S_2 state of PSII can all be simulated assuming that each arises from one or other of these Mn dimers. The multiline EPR signal, has been simulated at three frequencies using a model assuming a di-μ-oxo bridged Mn^{III}-Mn^{IV} dimer, antiferromagnetically coupled, yielding a net S=1/2 state (Chapter 2). Crucial to this model is large hyperfine and quadrupolar anisotropy not seen in distorted octahedral synthetic Mn dimers, but totally consistent with a five-coordinate square planar geometry at each Mn. EXAFS data, eg (Yachandra, *et al*, 1987), have shown that each Mn ion is probably coordinatively unsaturated, but this fact has been generally overlooked in previous attempts to model the multiline centre. Zheng and Dismukes (1996), however, have also concluded, from separate reasoning, that the Mn are ligand deficient.

In Chapter 4, I have shown that the two forms of the g=4.1 signals, identified by Smith and Pace (1996), are distinguishable by their different ZFS parameters. One arises from a ground state S=3/2 state (Smith and Pace, 1996) and can be observed after low temperature (130K) illumination of PSII samples cryoprotected with ethylene glycol. This ground state 4.1 signal has a small net ZFS, consistent with a significant tetragonal distortion or with non-coincidence of the two intrinsic ***D***-tensors. The other is the first excited state of the S=1/2 ground state giving rise to the multiline. It is produced by 200K illumination in samples cryoprotected with sucrose in the absence of alcohol. The excited state 4.1 signal has a large ZFS parameter, consistent with a major contribution from Mn^{III}. Whereas the 4.1 signals are essentially indistinguishable at X-band, they are quite different at Q-band and there is no single parameter set that can fit the two types of signals. The g=4.1 signal reported by Haddy *et al* (1992) appears (from the sample preparation protocol) to be an excited state signal. It also has a large ZFS parameter, but not as large as that reported here. However, it is slightly more rhombic than the g=4.1 signal in our hands and the difference may be a reflection of protonation/deprotonation brought about by different preparation protocols.

Experimental studies, both here (Chapters 3 and 4) and elsewhere, of the orientation dependence of EPR signals arising from the OEC of one dimensionally ordered samples have provided an extensive new data set to test models of the Mn organisation in this centre. The orientation dependence

of the multiline signal reported here, in particular, implies a substantial degree of anisotropy in the ligand environment for this species. Such effects have been generally ignored in previous attempts to model the multiline centre, as noted above. From my present simulation studies we now have available orientations, relative to the membrane plane, of both the ground state hyperfine tensors and first excited state ZFS-tensor of the multiline species, interpreted as a mixed valence dimer. Significantly, this allows an interpretation to be made of the likely molecular orientation of the dimer with the membrane plane.

In a recent EXAFS study on oriented PSII, Dau *et al* (1995) have reported the orientation of the Mn-Mn vectors of the two dimers in the OEC, using ammonia treated samples. They were able to demonstrate that ammonia binds to one of the dimers only, presumably replacing water. With ammonia binding, one dimer experienced a change in the Mn-Mn distance from 2.7Å to ~2.8Å. Because of this effect they were able to differentiate between the orientation of the two Mn-Mn dimers. The ammonia influenced dimer was found to have its Mn-Mn vector oriented 67° to the membrane plane normal, compared with 55° for the other, unaffected Mn-Mn dimer. As the excited state 4.1 signal arises from the dimer which also gives rise to the multiline and is the one that would presumably bind water to it, the orientation data presented here for this signal can be combined with the EXAFS data to arrive at a consistent orientation of the oxygen chemistry related Mn-Mn dimer in the membrane plane, see Figure 7.1.

This orientation is consistent with the ZFS tensor, dominated by the intrinsic ZFS of Mn^{III}, having its x- and y-axis nearly coincident with the μ-oxo bridges. The Mn-O distance for the μ-oxo ligands is about 1.8Å (MacLachlan, *et al*, 1992). This together with the 2.7Å Mn-Mn distance (MacLachlan, *et al*, 1992) would lead to and angle of ~82° between the μ-oxo ligands.

The hyperfine and quadrupole tensors show an orientation of the z-axes at ~35° off the membrane plane, and the x- and y-axes at 45° off the membrane plane. The z-axes of *all* the tensors (zero field, hyperfine and quadrupole) are therefore nearly coincident. The x- and y-axes of the hyperfine tensors will however, be oriented ~30° to the μ-oxo bridges. This on its own may not be so surprising. It is expected that the ***D***-tensor is dominated by the intrinsic ZFS of Mn^{III} as the contribution from Mn^{IV} is typically much smaller ($<1cm^{-1}$ compared with 3-4 cm^{-1}(Al'tshuler and Kozyrev, 1974; Kennedy and Murray,

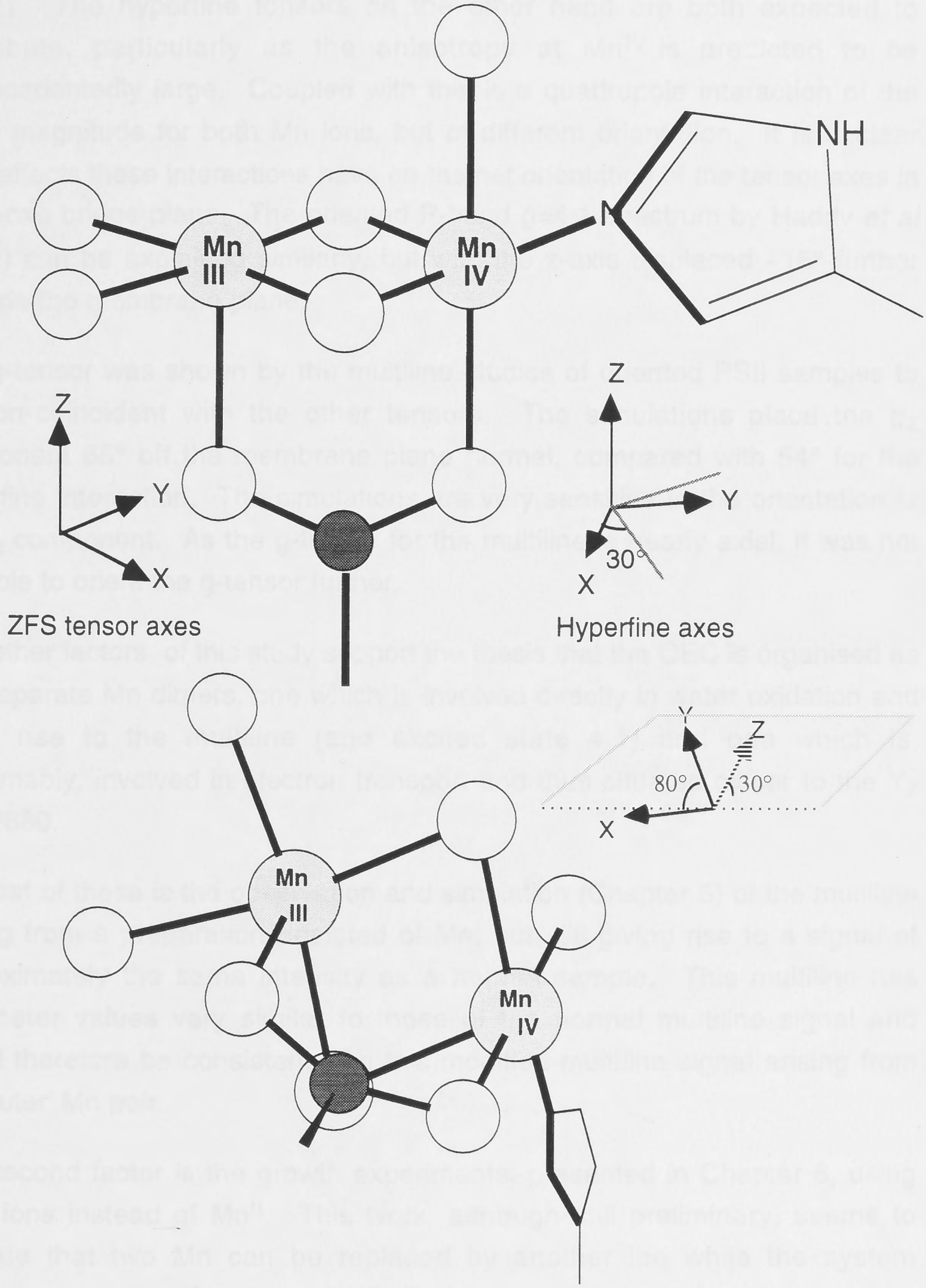

Figure 7.1 My model of the Mn-dimer giving rise to the multiline and excited state g=4.1 signals, together with the orientation of the ZFS-tensor and the Mn-Mn vector in the membrane plane. The orientation of the z-axis of ZFS-tensor 60° from the membrane plane normal (30° from the membrane plane), orients the Mn-Mn vector of the dimer ~25° from the membrane plane (65° from the membrane plane normal) (Dau, *et al.*, 1995). The hyperfine z-axis is nearly coincident with the ZFS z-axis. Thus the orientation studies undertaken here agree well with Dau *et al* and give a consistent picture of the orientation of the Mn-Mn vector of the dimer that, in our view, give rise to the multiline.

1985)). The hyperfine tensors on the other hand are both expected to contribute, particularly as the anisotropy at Mn^{IV} is predicted to be unprecedentedly large. Coupled with this is a quadrupole interaction of the same magnitude for both Mn ions, but of different orientation. It is unclear what effects these interactions have on the net orientation of the tensor axes in the μ-oxo bridge plane. The oriented P-band g=4.1 spectrum by Haddy *et al* (1992) can be explained similarly, but with the z-axis displaced ~15° further towards the membrane plane.

The g-tensor was shown by the multiline studies of oriented PSII samples to be non-coincident with the other tensors. The simulations place the g_z component 65° off the membrane plane normal, compared with 54° for the hyperfine interaction. The simulations are very sensitive to the orientation of the g_z component. As the g-tensor for the multiline is nearly axial, it was not possible to orient the g-tensor further.

Two other factors of this study support the thesis that the OEC is organised as two separate Mn dimers, one which is involved directly in water oxidation and gives rise to the multiline (and excited state 4.1) and one which is, presumably, involved in electron transport and thus situated closer to the Y_z and P680.

The first of these is the observation and simulation (Chapter 5) of the multiline arising from a preparation depleted of Mn, but still giving rise to a signal of approximately the same intensity as a normal sample. This multiline has parameter values very similar to those of the normal multiline signal and would therefore be consistent with this modified multiline signal arising from the 'outer' Mn pair.

The second factor is the growth experiments, presented in Chapter 6, using Ru^{III} ions instead of Mn^{II}. This work, although still preliminary, seems to indicate that two Mn can be replaced by another ion while the system functions normally. Klimov *et al* (1982) observed a similar effect.

Some recent reports also reflect on the concept of two magnetically non-interacting dimers. Riggs-Gelasco *et al* (1996b) find that reducing PSII samples with hydroquinone produces X-ray absorption spectroscopy signals consistent with two Mn^{II} and a single, oxidised di-μ-oxo Mn_2 core. Mei and Yocum (1992) showed that this treatment produced EPR signals consistent with uncoupled Mn^{II}. The effects are reversed by photo activation, indicating the reductant induced changes are not the result of sample decomposition.

The edge shift in the EXAFS data is consistent with hydroquinone reducing half the Mn in the OEC, while the other half retain the di-μ-oxo structure. Reduction with NH_2OH, on the other hand, produced no significant structural change as detected by EXAFS. As indicated by the Riggs-Gelasco *et al*, the data suggests strongly that there are two Mn-dimers with different reactivities and that these dimers do not chemically interact. NH_2OH is a water analogue and would probably therefore first interact with the dimer giving rise to the multiline signal. Hydroquinone, although a larger molecule, is much more hydrophobic and therefore more likely to be able to interact with the pair embedded further into the protein.

One of the conventionally perceived stumbling blocks to the concept of non-interacting dimers in the OEC is the Mn-metal interaction of ~3.3Å detected by EXAFS. In most researchers' hands, this interaction is interpreted as a Mn-Mn interaction. However, MacLachlan *et al* (1992) have reported this distance to be ~3.7Å and, even though Mn, C and Ca scatterers can be used to model the interaction, Ca resulted in the best fit. Two studies (Riggs-Gelasco, *et al.*, 1996a; Latimer, *et al.*, 1995) on this topic have recently been published. Riggs-Gelasco *et al* find there is no evidence for a change at 3.3Å following Ca replacement and that it is impossible to distinguish between Mn and Ca or Sr by curve fitting alone. They do observe a change in the 2.7Å Mn-Mn distance upon exchange of Ca with Sr or Dr. This change is interpreted as a possible change in strength of hydrogen bond of a water molecule bound to Ca. Latimer *et al,* on the other hand, observe an effect in studies using Sr to replace Ca. The change is consistent with Ca occupying a binding site 3.4-3.5Å from one Mn ion. They conclude that the most likely model based on their data is one in which both Mn-Mn and Mn-Ca interactions contribute to the ~3.3Å interaction. However, they do not exclude Mn-Ca being the only interaction at this distance. The difference between the two studies may be a reflection of the amount of Ca extracted and replaced by Sr or other ion. Without analysis of amount of Ca/Sr present per PSII by atomic absorption spectroscopy, for example, it is difficult to draw any conclusion about the differences in the two studies.

The ENDOR data on the centre giving rise to the multiline EPR signal (Randall, *et al.*, 1995) and the poor resulting fit to it using the parameter set presented here, is a problem. However, as shown in Figure 2.8 the absorption signal that the ENDOR experiment relies on may contain contributions from other spin centres. The difference in this absorption signal

compared with the integrated EPR multiline signal is particularly clear in the region near g=2, where the pulsed ENDOR experiment was conducted.

Finally a recent EPR study of PSII samples in the S_2 state, subjected to near-infrared light (Boussac, *et al.*, 1996), showed that the Mn centre underwent an interconversion between the g=4.1 signal and the multiline signal states. Their interpretation is that the absorption of infrared light (at 150K) results in electron transfer from Mn^{III}- Mn^{IV} and that the g=4.1 signal arises from a state which differs from the state giving rise to the multiline signal only in terms of a change in valence distribution. The results could equally be interpreted as absorption of near-infrared light by the pair close to P680, resulting in a photoexcited 'backwards' electron transfer at 150K to the Mn^{III}-Mn^{IV} multiline dimer. This would not normally be seen, as near-infrared light is not of sufficient energy to excite P680 causing electrons to flow in the normal direction. By taking the temperature to 200K the system is allowed to assume its more stable redox distribution.

APPENDIX 1: SAMPLE PREPARATION

Bricker Preparation

Bricker (1985) as modified by Smith (1993).

The preparation as described below is for 50 g of spinach leaves. The spinach was grown in a glass house and harvested on the day of the preparation.

All pellet homogenisations were done at 4°C, in the dark. Gloves were worn during homogenisations to reduce heat transfer to the preparation.

1. The major vein along the back of leaf was removed. The leaves were washed in distilled water, removing insecticides and other chemicals from greenhouse treatment. They were then shredded by hand into a blender and blended with about 100 ml of Buffer 1.
2. The blended solution was placed into filter cone of 'Mira Cloth' and gauze and was allowed to drain through for approximately 2 mins. The filter material was squeezed gently to keep filter solution flowing until the filter parcel was unable to give much return when squeezed.
3. The chloroplast solution was transferred to centrifuge tubes and the solution was centrifuged at 8000 rpm for 10 mins.
4. The supernatant was removed. The pellets were transferred to a homogeniser and homogenised with Buffer 2.
5. The homogenate was balanced in centrifuge tubes and centrifuged at 8000 rpm for 10 minutes.
6. The supernatant was poured off. Buffer 2 was aliquotted for the resuspension and homogenisation in 1 ml steps. After the homogenisation, the material was placed into a graduated cylinder, the volume was measured, and samples taken for the first chlorophyll determination, method according to Porra (1989).
7. The homogenate was left in the dark, in the cold for I hr, to allow the PSII containing regions to stack into grana.
8. After this time, Triton Tx-100 was added to obtain a detergent/ Chlorophyll ratio of 15:1. The detergent was added with Buffer 2 to enable the addition of the detergent without pH changes. It was added while stirring. The detergent dissolves single membrane regions, leaving the grana regions behind.
9. The solution was quickly transferred to an SS34 centrifuge tube, and centrifuged at 18000 rpm for 30 minutes.

10. The supernatant was removed. The pellet was resuspended and homogenised in approx 12 ml of Buffer 3. This homogenisation has to be completed quickly to reduce solubilisation effects due to the Tx-100.
11. The suspension was transferred to a centrifuge tube and centrifuged at 8000 rpm for 1 min, during which time a pellet of essentially starch material was formed. The supernatant was poured into another tube and the tubes were rebalanced. The solution was centrifuged at 17,000 rpm for 30 minutes.
12. The pellet was transferred to a homogenising vessel for the final homogenisation, where a maximal concentration was attempted.
13. After homogenising the solution was placed in a graduated tube (10ml). A chlorophyll determination was undertaken.
14. The PSII solution was aliquotted into 0.3-0.6 ml samples into screw cap cryotubes. The samples were stored in liquid N_2, or used for spreading on mylar sheets immediately.

Buffers

1. BUFFER 1: Blender Buffer
   100 mM Sucrose
   Phosphate Buffer, consisting of
   50 mM KH_2PO_4
   50 mM Na_2HPO_4
   200 mM NaCl

pH set to 7.5 $\pm$ 0.02 on day of prep. On day of prep Bovine Serum Albumin at the rate of 2.0 grams per litre was added. About 125 ml of buffer was needed.

2. BUFFER 2: Wash/Stacking Buffer
   400 mM Sucrose
   15 mM NaCl
   5 mM $MgCl_2$
   50 mM 2-[N-Morpholino]ethanesulfonic acid (MES)
   5 mM Ethylenediaminetetraacetic acid (EDTA)

pH set to 6.0 $\pm$ 0.02 on day of prep. Bovine Serum Albumin at the rate of 2.5 grams per litre was added. About 60 ml of buffer was needed.

3. BUFFER 2 with TRITON: Detergent Step Buffer

400 mM Sucrose

15 mM NaCl

5 mM $MgCl_2$

50 mM MES

5 mM EDTA

150g/l Triton x-100 detergent.

pH set to 6.0 ± 0.02 on day of prep.

4. BUFFER 3: Post Detergent Wash Buffer

50 mM NaCl

5 mM $MgSO_4$

50 mM MES

pH set to 6.0 ± 0.02 on day of prep.

5. BUFFER 4 : Storage Buffer

20 mM MES

10 mM $MgCl_2$

15 mM NaCl

400 mM Sucrose

pH set to 6.0 ± 0.02 on day of prep.

All the buffers were pH adjusted using KOH and H_2SO_4.

APPENDIX 2:
MULTILINE SIMULATION PROGRAM

```
C     PROGRAM TO CALCULATE MULTILINE POWDER PATTERN
C     SPECTRUM
C     Simulations of S=1/2 state with hyperfine projection
C     operators of  2 (MnIII) and-1 (MnIV).
C     Program includes nuclear Zeeman and quadrupole interaction
C     Gaussian line shape
C     Variable parameters are entered via program intrunz.for
C     Program includes minimisation by a simplex routine, Amoeba
C     This program is written by Karin Ahrling
C     Dept Chem. Fac Science, ANU, Australia
C     Language = Fortran, Library Routine, NAG FO2AXF
C     ******************************************************************
      PARAMETER(NDim=13,Mpts=NDim+1,NDat=4000)
      CHARACTER*12 logn,resn

      DIMENSION ExpX(NDat), ExpY(NDat)
      DIMENSION XX(Mpts), Step(Ndim), P(Mpts,NDim),Y(Mpts)
C     ******************************************************************
C     READING THE INPUT PARAMETERS
C     ******************************************************************
C     WL is the isotropic line width
C     FR - the frequency of microwave radiation in Gigahertz
C     A1x,A1y,A1z hyperfine terms for MnIII
C     A2x,A2y,A2z hyperfine terms for MnIV
C     X1p,Y1p,X2p,Y2p, quadrupole tensor components for MnIII & MnIV
C     Gx,Gy,Gx, g-value components
C     N = Maximum number of angles calculated for each phi and theta
C    ******************************************************************
       OPEN(Unit=20,File = 'inputz.dat',action = 'read',
     c          Status='Unknown')
      READ (20,1) WL,A1x,A1y,A1z,X1p,Y1p,A2x,A2y,A2z,X2p,Y2p,Gx,
     c         Gy,Gz,Fr,Sc,N,logn,resn
     1   FORMAT (1x,16(F12.5,/),I6,/,A10,/,A10)

      OPEN(Unit=21,File = 'expx.dat', action = 'read',
     c          Status='Unknown')


      OPEN(Unit=11, FILE = logn ,STATUS = 'Unknown')

      WRITE(11,3) A1x,A1y,A1z,X1p,Y1p,A2x,A2y,A2z,X2p,Y2p,
     c       Gx,Gy,Gz,Fr,Sc, WL,N
     3   FORMAT (1x,'A1x= ',F12.5,2x,'A1y= ',F12.5,2x,'A1z= ',F12.5,/,
     c       'X1p= ',F12.5,2x,'Y1p= ',F12.5,/,
     c       'A2x= ',F12.5,2x,'A2y= ',F12.5,2x,'A2z= ',F12.5,/,
     c       'X2p= ',F12.5,2x,' Y2p= ', F12.5,/,
     c       1x,'Gx= ',F12.5,2x,'Gy= ',F12.5,/,
     c       1x,'Gz= ',f12.5,2x,'Frequency= ',F12.5,/,
```

```
     c        1x,'Sc= ',f12.5,/,
     c         1x,'Linewidth= ',F12.5,2x,'No.angles= ',I6)

C       Read in experimental spectrum
!OCL NOVREC(EXPX,EXPY)
        Do 2 J=1,3984,2
        READ (21,4) ExpX(J), ExpY(J),ExpX(J+1),ExpY(J+1)
   4    FORMAT (1x,F12.3,F15.6,F15.3,F15.6)
   2     Continue

C   Read in variable parameters into simplex array
      XX(1)=A1x
      XX(2)=A1y
      XX(3)=A1z
      XX(4)=X1p
      XX(5)=Y1p
      XX(6)=A2x
      XX(7)=A2y
      XX(8)=A2z
      XX(9)=X2p
      XX(10)=Y2p
      XX(11)=Gx
      XX(12)=Gy
      XX(13)=Gz
      Step(1)=1.0
      Step(2)=1.0
      Step(3)=1.0
      Step(4)=0.5
      Step(5)=0.5
      Step(6)=1.0
      Step(7)=1.0
      Step(8)=1.0
      Step(9)=0.5
      Step(10)=0.50
      Step(11)=0.005
      Step(12)=0.005
      Step(13)=0.005

C       Initialise Simplex

        Do 5 i=1,Mpts
          Do 6 j=1,NDim
                P(i,j)=XX(j)
   6      Continue
   5    Continue

        Do 7 i=1,NDim
         P(i,i)=XX(i) + step(i)
   7    Continue

C   Calculate Matrix Y holding initial Chisq values corresponding to P


      Do 8 i=1,Mpts
```

```
      Do 9 j=1,NDim
       xx(j)=P(i,j)
 9    Continue
      Call Multiline (ExpX,NDat,ExpY,WL,Sc,
 c          Fr,Y(i),XX,Ndim,N)
        Write (11,777) Y(i)
777    FORMAT (1x,f12.5)
 8   Continue


    Call Amoeba2(ExpX,NDat,ExpY,WL,Sc,
 c          Fr,P,Y,Mpts,NDim,N,Chisq,ITER)


    END
C*******************************************************************************
      SUBROUTINE MULTILINE(ExpX,NDat,ExpY,WL,Sc,
   c   Fr,Chisq,XX,NDim,N)

C*******************************************************************************

      PARAMETER(Ib=72,Ic=4400)
      INTEGER ZQ

      DIMENSION AHX(Ic),ALH(Ic),StoreY(Ic)
      DIMENSION CalcY(Ic)
      DIMENSION ExpX(NDat), ExpY(NDat)
      DIMENSION VLW(200)
      DOUBLE PRECISION EV(Ib),EVR(Ib,Ib), EVIM(Ib,Ib)
      DIMENSION EVal(Ib),ER(Ib,Ib),EIM(Ib,Ib)
      DIMENSION XX(NDim)
      REAL NPT, MoveX

      COMPLEX C

      EXTERNAL F02AXF
C*******************************************************************************
C     CREATING A FIELD SPACE DETERMINED BY THE FREQUENCY,
C     THE Giso PARAMETER AND THE CONSTANT 714.48.The constant
C     is given by Planck's constant/Bohr magneton * conversion for
c     Tesla to Gauss,  and Gigahertz to Hertz
C*******************************************************************************
C     Subroutine Eigen - Takes Phi and Theta (in radians), A1iso,A2iso
C     X1a,Y1a,X2a,Y2a,Xp,Yp; calculates the rotation matrices for
C     H=gBHoSz + A1isoSI + SA1anI + A2isoSI + SA2anI + IPI
C     and returns the eigenvalues,real,  and eigenvectors, real and
C     imaginary, for each solid angle given to the subroutine.The
C     matrix fed to the subroutine is Hermitian.
C     ***************************************************************************
      A1x=-2*XX(1)
      A1y=-2*XX(2)
      A1z=-2*XX(3)
      X1p=XX(4)
```

```
      Y1p=XX(5)
      A2x=XX(6)
      A2y=XX(7)
      A2z=XX(8)
      X2p=XX(9)
      Y2p=XX(10)
      Gx=XX(11)
      Gy=XX(12)
      Gz=XX(13)

C The code here allows Ax,Ay and Az to vary - previously Az was derived
C only from Xa and Ya.

      A1iso=(A1x+A1y+A1z)/3.
      X1a=A1x-A1iso
      Y1a=A1y-A1iso
      A2iso=(A2x+A2y+A2z)/3.
      X2a=A2x-A2iso
      Y2a=A2y-A2iso
      giso=(Gx+Gy+Gz)/3.
      Xg=Gx-giso
      Yg=Gy-giso

      Chisq=0.

C       BH0=FIELD POSITION FOR g=2.0032 IN GAUSS
      Pi=3.1415926

      CON = 714.482
      BH0=CON*FR/Giso

      AHXX=FLOAT(IFIX(BH0))-1000.5

      p=0.0
      DO 10 I=1,4400
        StoreY(I)=0.0
        ALH(I)=0.0
        AHX(I)=AHXX+p
        p=p+0.5
   10   CONTINUE


C     ******************************************************************************

C     CALCULATING THE GAUSSIAN PATTERN CHARACTERISING
C     THE PEAK SHAPES. WIDTH OF GAUSSIAN ENVELOPE = 75 GAUSS

C     ******************************************************************************
!OCL SCALAR
      GP=-37.5000
      DO 500 I=1,151
       VLW(I)=10.00*EXP(-1.*(GP/WL)**2)
  490   GP=GP+0.5000
```

```
 500   CONTINUE

C       **********************************************************************
C      CALCULATING THE PEAK POSITIONS CORRESPONDING TO
C      THE SOLID ANGLES (one octant only) OF ORIENTATION
C     FOR THE POWDER PATTERN.
C       **********************************************************************
      Ip=N
      DTH = Pi*90/(Float(Ip)*180)
      Zq=0
      MoveX=0.
      DO 150 JA=1,Ip
       Angth=DTH * real(Ja)
       DPH=DTH/SIN(Angth)
       NPT=(Pi/(2.*DPH))
       IF ((NPT-FLOAT(IFIX(NPT))).LT.0.5000) THEN
        ZQ=IFIX(NPT)
        Else
        ZQ=IFIX(NPT+1)
       ENDIF
       Numc=ZQ+1

       MoveX=(Pi/2.-DPH*FLOAT(ZQ))/2.

!OCL NOVREC(ANGPH)
       DO 140 JB=1,Numc
        Angph=MoveX+DPH*Real(Jb-1)

C       **********************************************************************
 125    CALL EIGEN(ANGTH,ANGPH,A1iso,X1a,Y1a,X1p,Y1p,
     c   A2iso,X2a,Y2a,X2p,Y2p,BH0,Giso,Xg,Yg,EV,M, EVR,I,EVIM,K)
C       **********************************************************************

C      Nested loops for the calculation of intensities, ie
C      transition probabilities (stored in FACINT)
C      and the field positions from the spin-up and spin-down
C      eigenvalues

C       **********************************************************************
C       **********************************************************************

      DO 221 I=1,72
       EVal(I)=REAL(EV(I))
       DO 222 J=1,72
        ER(I,J)=REAL(EVR(I,J))
        EIM(I,J)=REAL(EVIM(I,J))
 222     CONTINUE
 221    CONTINUE

      Num=1
      DO 220 I=1,36
       DO 230  J=1,36
        FPMn=EVal(I+36)-EVal(J)
        BHX= 2.*BH0 - FPMN
```

```
            C=(0.,0.)

            DO 240 K=1,36
              C=C + CONJG(CMPLX(ER(K+36,I),EIM(K+36,I)))*
     c                CMPLX(ER(K,J+36),EIM(K,J+36))
    240        CONTINUE

            FACINT=CABS(C)**2

            IF (FACINT.NE.0) THEN
              YX=((BHX+0.5)-AHXX)/0.5
              IY=IFIX(YX)
               StoreY(IY)=StoreY(IY)+FACINT
            ENDIF
            Num=Num+1
    230       CONTINUE
    220     CONTINUE
    140   CONTINUE
    150  CONTINUE

    C       ***************************************************************************
    C
    C      NESTED LOOPS FOR
    c      SETTING THE POSITIONS OF THE CALCULATED PEAKS INTO THE
    C      READY CALCULATED FIELD POINTS FOR THE X-AXIS.
    C       ***************************************************************************

          DO 116 IY=1,4002
           IF (StoreY(IY).NE.0) THEN
    c      Gaussian pattern width is 150 points, ie 75 Gauss
           IHM=1
           DO 43 NI=(IY-75),(IY+75)
            IF(NI.LT.1) GO TO 627
            IF (NI.GT.4001) GO TO 627
             ALH(NI)=ALH(NI)+VLW(IHM)*StoreY(IY)
     627       IHM = IHM + 1
      43     CONTINUE
           ENDIF
     116   CONTINUE

    C      Take the derivative of the simulated spectrum
          DO 54 J=2,4001
            CalcY(J)=(ALH(J+1)-ALH(J-1))/(AHX(J+1)-AHX(J-1))
     54   CONTINUE

    C      Compare calculated spectra with experimental and calculate the
    C      sum of the squares of the difference at each point
          J=1
          Do 56 I=1,NDat
    C        Finds the same field position to compare
      58    If ((ExpX(I)-Ahx(J)).GT.0.5) Then
            J=J+1
            Go to 58
          Else if ((ExpX(I)-Ahx(J)).LT.0) Then
    C        Skips an experimental point when there are too many
```

```
        Go to 56
       Else if ((ExpX(I)-Ahx(J)).LE.0.5) Then
C          Takes the sum of squares except where exp spectrum=0
        If (ExpY(I).NE.0.00000) then
          Chisq= Chisq+((ABS(A1iso/164.0)+(A2iso/92.))/2)*
     c      ((CalcY(J)-(ExpY(I)/Sc))**2)
         J=J+1
        Endif
        If (ExpY(I).EQ.0.00000) then
         J=J+1
        Endif
       Endif
   56  Continue

      Write (11,59) Chisq
   59  FORMAT (1x, 'Chisq:',F16.3)

       RETURN
         END
C  End Subroutine Multiline
C  ------------------------------------------------------------------
       SUBROUTINE EIGEN(ATHs,APHs,A1isos,X1as,Y1as,
     c  X1ps,Y1ps,A2isos,X2as,Y2as, X2ps,Y2ps, Heff,Gisos,Xgs,
     c  Ygs,EVs,Mr,EVRs,NR1,EVIMs,NI)
C  ------------------------------------------------------------------

       PARAMETER (Ms=72,NRIn=72,NIIn=72,NRO=72,NIO=72)

       DOUBLE PRECISION QUDIM(72,72),QUDRL(72,72)
       DOUBLE PRECISION EVs(Ms), EVRs(NRO,Ms), EVIMs(NIO,Ms)
       DOUBLE PRECISION WK1(Ms),WK2(Ms),WK3(Ms)
       REAL NZ, I2,I1,I1pls,i11pls,I1min,I2pls,i22pls,I2min

C   Mquad (Real and Imaginary) is an internal matrix holding the
C   values of < |Hq| >. EV etc specified earlier.

       DO 800 I=1,72
        DO 801 J=1,72
         QUDRL(I,J)=0.
         QUDIM(I,J)=0.
   801    CONTINUE
   800  CONTINUE


C       Hyperfine terms for Mn3

   802   A1xx = ((COS(APHs)**2)*(COS(ATHs)**2)*X1as)+
     c       ((SIN(APHs)**2)*(COS(ATHs)**2)*Y1as)-
     c       ((SIN(ATHs)**2)*(X1as+Y1as))
         A1yy = ((SIN(APHs)**2)*X1as)+((COS(APHs)**2)*Y1as)
         A1xy = (COS(APHs)*SIN(APHs)*COS(ATHs)*(Y1as-X1as))
        A1xz = SIN(ATHs)*COS(ATHs)*
     c       ((COS(APHs)**2)*X1as+(SIN(APHs)**2)*Y1as+X1as+Y1as)
         A1yz = (SIN(APHs)*COS(APHs)*SIN(ATHs)*(Y1as-X1as))
```

```
      A1zz = ((COS(APHs)**2)*(SIN(ATHs)**2)*X1as)+
     c       ((SIN(APHs)**2)*(SIN(ATHs)**2)*Y1as)-
     c       ((COS(ATHs)**2)*(X1as+Y1as))


C     Hyperfine terms for Mn4

      A2xx = ((COS(APHs)**2)*(COS(ATHs)**2)*X2as)+
     c       ((SIN(APHs)**2)*(COS(ATHs)**2)*Y2as)-
     c       ((SIN(ATHs)**2)*(X2as+Y2as))
      A2yy = ((SIN(APHs)**2)*X2as)+((COS(APHs)**2)*Y2as)
      A2xy = (COS(APHs)*SIN(APHs)*COS(ATHs)*(Y2as-X2as))
      A2xz = SIN(ATHs)*COS(ATHs)*
     c       ((COS(APHs)**2)*X2as+(SIN(APHs)**2)*Y2as+X2as+Y2as)
      A2yz = (SIN(APHs)*COS(APHs)*SIN(ATHs)*(Y2as-X2as))
      A2zz = ((COS(APHs)**2)*(SIN(ATHs)**2)*X2as)+
     c       ((SIN(APHs)**2)*(SIN(ATHs)**2)*Y2as)-
     c       ((COS(ATHs)**2)*(X2as+Y2as))


C     Quadrupolar terms for Mn3

      P1xx =((COS(APHs)**2)*(COS(ATHs)**2)*X1ps)+
     c       ((SIN(APHs)**2)*(COS(ATHs)**2)*Y1ps)-
     c       ((SIN(ATHs)**2)*(X1ps+Y1ps))
      P1yy =((SIN(APHs)**2)*X1ps)+((COS(APHs)**2)*Y1ps)
      P1zz =((COS(APHs)**2)*(SIN(ATHs)**2)*X1ps)+
     c       ((SIN(APHs)**2)*(SIN(ATHs)**2)*Y1ps)-
     c       ((COS(ATHs)**2)*(X1ps+Y1ps))
      P1xz =SIN(ATHs)*COS(ATHs)*((COS(APHs)**2)*
     c       X1ps+(SIN(APHs)**2)*Y1ps+X1ps+Y1ps)
      P1yz =SIN(APHs)*COS(APHs)*SIN(ATHs)*(Y1ps-X1ps)
      P1xy =SIN(APHs)*COS(APHs)*COS(ATHs)*(Y1ps-X1ps)


C     Quadrupolar terms for Mn4

      P2xx =((COS(APHs)**2)*(COS(ATHs)**2)*X2ps)+
     c       ((SIN(APHs)**2)*(COS(ATHs)**2)*Y2ps)-
     c       ((SIN(ATHs)**2)*(X2ps+Y2ps))
      P2yy =((SIN(APHs)**2)*X2ps)+((COS(APHs)**2)*Y2ps)
      P2zz =((COS(APHs)**2)*(SIN(ATHs)**2)*X2ps)+
     c       ((SIN(APHs)**2)*(SIN(ATHs)**2)*Y2ps)-
     c       ((COS(ATHs)**2)*(X2ps+Y2ps))
      P2xz =SIN(ATHs)*COS(ATHs)*((COS(APHs)**2)*
     c       X2ps+(SIN(APHs)**2)*Y2ps+X2ps+Y2ps)
      P2yz =SIN(APHs)*COS(APHs)*SIN(ATHs)*(Y2ps-X2ps)
      P2xy =SIN(APHs)*COS(APHs)*COS(ATHs)*(Y2ps-X2ps)


C     Anisotropic g-value
C     g-value axial, so that Xg=Yg and Zg=-(Xg+Yg)

      Gxz = SIN(ATHs)*COS(ATHs)*
```

```
c      ((COS(APHs)**2)*Xgs+(SIN(APHs)**2)*Ygs+Xgs+Ygs)
       Gyz = (SIN(APHs)*COS(APHs)*SIN(ATHs)*(Ygs-Xgs))
       Gzz = ((COS(APHs)**2)*(SIN(ATHs)**2)*Xgs)+
c        ((SIN(APHs)**2)*(SIN(ATHs)**2)*Ygs)-
c        ((COS(ATHs)**2)*(Xgs+Ygs))

C      To express zeeman terms in field equivalent units, divide
C      throughout by gB  ie gzzBHoSz/gisoB so that:
       Gxz = Gxz/Gisos
       Gyx = Gyz/Gisos
       Gzz = Gzz/Gisos

C      Terms for nuclear zeeman -gnBnHeff/gisoBe(Iz1+Iz2)
       NZ=-0.000751359*Heff/gisos

       Sz=0.5
       Szz=-0.5

C      Elements of Mnquad - Real
C      only lower half of matrix need to be given

C      Diagonal elements
       J=1
       I1=-5./2.
       Do 701 Ji=1,6
        I2=-5./2.
        I1pls=SQRT((5./2.-I1)*(5./2.+I1+1.))
        Do 702 Jl=1,6
        QUDRL(J,J)=I1*A1isos*Sz+I1*A1zz*Sz+
c              I2*A2isos*Sz+I2*A2zz*Sz+
c              Sz*Heff+Gzz*Sz*Heff+NZ*(I1+I2)+
c              P1zz*(3*I1*I1-2.5*(3.5))/2.+
c              P2zz*(3*I2*I2-2.5*(3.5))/2.

        QUDRL(J+36,J+36)=I1*A1isos*Szz+I1*A1zz*Szz+
c              I2*A2isos*Szz+I2*A2zz*Szz+
c              Szz*Heff+Gzz*Szz*Heff+NZ*(I1+I2)+
c              P1zz*(3*I1*I1-2.5*(3.5))/2.+
c              P2zz*(3*I2*I2-2.5*(3.5))/2.
C      The imaginary portion of the matrix does not have any nonzero
C      elements along the diagonal


       QUDRL(J+36,J)=QUDRL(J+36,J)+ Gxz*Heff/2.+A1xz*I1/2.
c              +A2xz*I2/2.
       QUDIM(J+36,J)=QUDIM(J+36,J)+ Gyz*Heff/2.+A1yz*I1/2.
c              +A2yz*I2/2.

       j=j+1
       I2=I2+1.
 702    Continue
       I1=I1+1.
 701    Continue
```

```
      J=2
      m=38
       Do 710 Ji=1,6

       i2=-5./2.
        Do 705 Jl=1,6
        l2pls=SQRT((5./2.-l2)*(5./2.+l2+1.))
        If (m.le.72) THEN
        QUDRL(J,J-1)=QUDRL(J,J-1)+Sz*A2xz*l2pls/2.+
     c              P2xz*(l2pls*l2+(l2+1.)*l2pls)
        QUDIM(J,J-1)=QUDIM(J,J-1)-Sz*A2yz*l2pls/2.-
     c              P2yz*(l2pls*l2+(l2+1.)*l2pls)
        QUDRL(m,m-1)=QUDRL(m,m-1)+Szz*A2xz*l2pls/2.+
     c              P2xz*(l2pls*l2+(l2+1.)*l2pls)
        QUDIM(m,m-1)=QUDIM(m,m-1)-Szz*A2yz*l2pls/2.-
     c              P2yz*(l2pls*l2+(l2+1.)*l2pls)
        QUDRL(m,J-1)=QUDRL(m,J-1)
     c               +i2pls*(a2xx+A2yy)/4.+A2isos*l2pls/2.

            l2=l2+1.
            J=J+1
     C        If (m.EQ.72) go to 703
            m=m+1
            ENDIF
      705     Continue
      710    Continue


      703    J=3
           m=39
           Do 711 Ji=1,6

           l2=-5./2.
           Do 707 Jl=1,6
           l2pls=SQRT((5./2.-l2)*(5./2.+l2+1.))
           if (i2.EQ.2.5) then
           i22pls=0.
           else
           l22pls=SQRT((5./2.-(l2+1.))*(5./2.+(l2+1.)+1.))
           Endif
           If (m.LE.72) then
            QUDRL(J,J-2)=QUDRL(J,J-2)+i22pls*i2pls*(P2xx-P2yy)/4.
            QUDIM(J,J-2)=QUDIM(J,J-2)-l22pls*l2pls*P2xy/2.
            QUDRL(m,m-2)=QUDRL(m,m-2)+i22pls*i2pls*(P2xx-P2yy)/4.
            QUDIM(m,m-2)=QUDIM(m,m-2)-l22pls*l2pls*P2xy/2.

           l2=l2+1.
           J=J+1
           m=m+1
           endif
      707    Continue

      711    COntinue
```

```
704   J=7
      m=43
      i1=-5./2.
      Do 713 n=1,6
      I1pls=SQRT((5./2.-I1)*(5./2.+I1+1.))
      Do 708 Ji=1,6
      If (m.le.72) then
      QUDRL(J,J-6)=QUDRL(J,J-6)+Sz*A1xz*I1pls/2.+
     c            P1xz*(I1pls*I1+(I1+1.)*I1pls)
      QUDIM(J,J-6)=QUDIM(J,J-6)-Sz*A1yz*I1pls/2.-
     c            P1yz*(I1pls*I1+(I1+1.)*I1pls)
      QUDRL(m,m-6)=QUDRL(m,m-6)+Szz*A1xz*I1pls/2.+
     c            P1xz*(I1pls*I1+(I1+1.)*I1pls)
      QUDIM(m,m-6)=QUDIM(m,m-6)-Szz*A1yz*I1pls/2.-
     c            P1yz*(I1pls*I1+(I1+1.)*I1pls)
      QUDRL(m,J-6)=QUDRL(M,J-6)+I1pls*(A1xx+A1yy)/4.+
     c            A1isos*I1pls/2.

       J=J+1
       m=m+1
      endif
708   Continue
      i1=I1+1.
713   Continue

      j=1
      i1=-3./2.
      DO 730 n=1,6
      Do 731 ji=1,6
       if (j.le.30) then
       i1min=SQRT((5./2.+i1)*(5./2.-I1+1.))
      QUDRL(J+36,J+6)=QUDRL(J+36,J+6)+I1min*(A1xx-A1yy)/4.
      QUDIM(J+36,J+6)=QUDIM(J+36,J+6)+I1min*A1xy/2.

      j=j+1
      endif
731   Continue
      i1=i1+1
730   Continue
```

```
706   j=1
      DO 714 n=1,6
       i2=-3./2.
      Do 709 ji=1,6
       I2min=SQRT((5./2.+I2)*(5./2.-I2+1.))
       if (j.le.35) then
      QUDRL(J+36,J+1)=QUDRL(J+36,J+1)+I2min*(A2xx-A2yy)/4.
      QUDIM(J+36,J+1)=QUDIM(J+36,J+1)+I2min*A2xy/2.
       i2=I2+1.
       J=J+1
      endif
709   Continue
```

```
      i2=-5./2.
714   Continue


718  J=13
     m=49
     i1=-5./2.
     DO 715 n=1,6
      I1pls=SQRT((5./2.-I1)*(5./2.+I1+1.))
      if (i1.EQ.2.5) then
      i11pls=0.
      else
      I11pls=SQRT((5./2.-(I1+1.))*(5./2.+(I1+1.)+1.))
      endif
     Do 712 Ji=1,6
      if (m.le.72) then
       QUDRL(J,J-12)=QUDRL(J,J-12)+i11pls*i1pls*(P1xx-P1yy)/4.
       QUDIM(J,J-12)=QUDIM(J,J-12)-I11pls*I1pls*P1xy/2.
       QUDRL(m,m-12)=QUDRL(m,m-12)+i11pls*i1pls*(P1xx-P1yy)/4.
       QUDIM(m,m-12)=QUDIM(m,m-12)-I11pls*I1pls*P1xy/2.

      j=J+1
      m=m+1
      endif
 712    Continue
     i1=i1+1.
 715  Continue

C   Text for F02AXF External Subroutine, returning eigenvalues
C   and eigenvectors for Sz=0.5(up) and Sz=-0.5(down)
C   ------------------------------------------------------------------------

 804   IFAIL=0
       CALL F02AXF(QUDRL,NRIn,QUDIM,NIIn,Ms,EVs,EVRs,NRO,
   c             EVIMs,NIO,WK1,WK2,WK3,IFAIL)
       IF(IFAIL.NE.0)  PRINT 805, IFAIL
 805   FORMAT (1x,'IFAIL= ',I4)

       Mr=Ms
       NR1=NRO
       NI=NIO
       RETURN
       END

C    End Subroutine Eigen



C*********************************************************************
C  Subroutine AMOEBA, From "Numerical Recipes", modified to
C  be used to minimise 'multiline'.
C*********************************************************************
```

```
      SUBROUTINE AMOEBA2(ExpX,NDat,ExpY,WL,Sc,
     c      Fr,P,Y,Mpts,NDIM,N,Chilow,ITER)
C*************************************************************
c  Output P and Y are the new points all within FTOL of a minimum
C  function value.  Presumably Y(ILO) is that minimum value.

      PARAMETER
(NMAX=20,ALPHA=1.0,BETA=0.5,GAMMA=2.0,ITMAX=500)
      DIMENSION
P(Mpts,Ndim),Y(Mpts),PR(NMAX),PRR(NMAX),PBAR(NMAX)
      DIMENSION ExpX(Ndat), ExpY(Ndat)
      FTOL=1E-3
      ITER=0
      itcount=20
C  Check which point is the highest, next highest, and lowest
C by looping over the points in the simplex
 111    ILO=1
      IF(Y(1).GT.Y(2))THEN
       IHI=1
       INHI=2
      ELSE
       IHI=2
       INHI=1
      ENDIF
      DO 11 I=1,MPTS
       IF(Y(I).LT.Y(ILO)) ILO=I
       IF(Y(I).GT.Y(IHI))THEN
        INHI=IHI
        IHI=I
       ELSE IF(Y(I).GT.Y(INHI))THEN
        IF(I.NE.IHI) INHI=I
       ENDIF
  11   CONTINUE
c  Compute the fractional range and return if satisfactory
      RTOL=2.*ABS(Y(IHI)-Y(ILO))/(ABS(Y(IHI))+ABS(Y(ILO)))
      IF(RTOL.LE.FTOL) Then
       Chilow=Y(ILO)
      Write (11,710) RTOL,Chilow,ILO,Y(IHI),IHI
 710    Format (1x,'Rtol lt Ftol (Rtol,Chilow):',
  c        F12.5,2x,f16.3,2x,i4,2x,F16.3,2x,i4)
       Write (11,29) Chilow,ILO,IHI,Y(IHI),
  c        (P(ILO,J),P(IHI,J),J=1,NDim)
 29     FORMAT (1x,' Chilow:',
  c        f16.3, 2x,i4,2x,i4,f16.3,/,10(f12.5,2x,f12.5,/))
       RETURN
      ENDIF
       Write (11,704) ITER
 704     Format (1x,'Iterations',I6)
      IF(ITER.GE.ITMAX) Then
       Chilow=Y(ILO)
       Write (11,26) Chilow,ILO,IHI,Y(IHI),
  c        (P(ILO,J),P(IHI,J),J=1,NDim)
 26     FORMAT (1x,'Amoeba exceeding maximum iterations., Chilow:',
```

```
     c          f16.3, 2x,i4,2x,i4,f16.3,/,10(f12.5,2x,f12.5,/))
          RETURN
         ENDIF
         If (iter.GE.itcount) then
           Write (11,27) itcount, (P(ILO,J),J=1,NDim)
   27     FORMAT (1x,i4,/,10(f12.5,/))
          Itcount=itcount+20
         endif

         DO 12 J=1,NDIM
          PBAR(J)=0.
   12    CONTINUE
C  begin a new iteration
         DO 14 I=1,MPTS
         IF(I.NE.IHI)THEN
           DO 13 J=1,NDIM
            PBAR(J)=PBAR(J)+P(I,J)
   13      CONTINUE
         ENDIF
   14    CONTINUE
C Extrapolate by a factor alpha through the face ie reflect simplex
C from the high point
!OCL NOVREC
         DO 15 J=1,NDIM
          PBAR(J)=PBAR(J)/NDIM
          PR(J)=(1.+ALPHA)*PBAR(J)-ALPHA*P(IHI,J)
   15    CONTINUE
C  Calculate Chisq at the reflected point.
         Call Multiline (ExpX,NDat,ExpY,WL,Sc,
     c       Fr,YPR,PR,NDim,N)
         Iter=Iter+1
C  If better result, extrapolate by factor gamma
         IF(YPR.LE.Y(ILO))THEN
!OCL NOVREC
          DO 16 J=1,NDIM
           PRR(J)=GAMMA*PR(J)+(1.-GAMMA)*PBAR(J)
   16      CONTINUE
          Call Multiline (ExpX,NDat,ExpY,WL,Sc,
     c       Fr,YPRR,PRR,Ndim,N)
          Iter=Iter+1
          IF(YPRR.LT.Y(ILO))THEN
C  If successful replace previous highpoint
!OCL NOVREC
            DO 17 J=1,NDIM
            P(IHI,J)=PRR(J)
   17       CONTINUE
           Y(IHI)=YPRR
C  If not, use previous (alhpa) extrapolated point
          ELSE
!OCL NOVREC
            DO 18 J=1,NDIM
            P(IHI,J)=PR(J)
   18       CONTINUE
           Y(IHI)=YPR
```

```
        ENDIF
C The reflected point is worse than the second highest,but
C  if it's better than the highest, replace highest point
       ELSE IF(YPR.GE.Y(INHI))THEN
        IF(YPR.LT.Y(IHI))THEN
          DO 19 J=1,NDIM
           P(IHI,J)=PR(J)
 19        CONTINUE
          Y(IHI)=YPR
        ENDIF
C  Look for an immediate lower point by contracting simplex along one
C  dimension.
        DO 21 J=1,NDIM
          PRR(J)=BETA*P(IHI,J)+(1.-BETA)*PBAR(J)
 21       CONTINUE
         Call Multiline (ExpX,NDat,ExpY,WL,Sc,
  c          Fr,YPRR,PRR,Ndim,N)
        Iter=Iter+1
C  If contraction gives improvement, accept point
        IF(YPRR.LT.Y(IHI))THEN
!OCL NOVREC
          DO 22 J=1,NDIM
           P(IHI,J)=PRR(J)
 22        CONTINUE
          Y(IHI)=YPRR
C  If nothing else work contract around lowest point
        ELSE
          DO 24 I=1,MPTS
           IF(I.NE.ILO)THEN
             DO 23 J=1,NDIM
              PR(J)=0.5*(P(I,J)+P(ILO,J))
             P(I,J)=PR(J)
 23           CONTINUE
            Call Multiline (ExpX,NDat,ExpY,WL,Sc,
  c            Fr,Y(I),PR,Ndim,N)
           ENDIF
 24        CONTINUE
          Iter=Iter+NDim
        ENDIF
C  If original reflection gives midling point, replace old high
C  point and continue
       ELSE
!OCL NOVREC
          DO 25 J=1,NDIM
           P(IHI,J)=PR(J)
 25        CONTINUE
          Y(IHI)=YPR
        ENDIF
        GO TO 111
        END
```

APPENDIX 3:
SIMULATION PROGRAM FOR MULTILINE EPR SPECTRA OF ORIENTED PSII PARTICLES

```
C     ************************************************************************
C     THIS PROGRAM CALCULATES TWO DIMENSIONAL
C     POWDER PATTERN FOR ORIENTED SAMPLES

C     Simulations of S=1/2 state with hyperfine projection
C     operators of  2 (MnIII) and-1 (MnIV).
C     Program includes nuclear Zeeman and quadrupole interaction
C     Gaussian line shape
C     Variable parameters are entered via program int2o.for
C     This program is written by Karin Ahrling
C     Dept Chem. Fac Science, ANU, Australia
C     Language = Fortran, Library Routine, NAG F02AXF

C     ************************************************************************
      PARAMETER(Ia=25,Ib=72,Ic=4400,Id=1400)

      DIMENSION AHX(Ic),ALH(Ic),StoreY(Ic)
      DIMENSION VLW(200)
      DOUBLE PRECISION EV(72),EVR(72,72), EVIM(72,72)
      DIMENSION EVal(72),ER(72,72),EIM(72,72)

      REAL NPT, MoveX
      INTEGER ZQ
      COMPLEX C

      EXTERNAL F02AXF
C     ************************************************************************
C     Subroutine Eigen - Takes Phi and Theta (in radians), A1iso,A2iso
C     X1a,Y1a,X2a,Y2a,Xp,Yp; calculates the rotation matrices for
C     H=gBHoSz + A1isoSI + SA1anI + A2isoSI + SA2anI + IPI
C     and returns the eigenvalues,real,  and eigenvectors, real and
C     imaginary, for each solid angle given to the subroutine.The
C     matrix fed to the subroutine is Hermitian.
C     ************************************************************************

      Pi=3.1415926

C     INITIALISING THE ARRAYS

      DO 690 LWV=1,151
      VLW(LWV)=0.000
 690  CONTINUE

C     ************************************************************************
C     WL is the isotropic line width
C     FR - the frequency of microwave radiation in Gigahertz
C     A1x,A1y,A1z hyperfine terms for MnIII
C     A2x,A2y,A2z hyperfine terms for MnIV
```

```
C       X1p,Y1p,X2p,Y2p, quadrupole tensor components for MnIII & MnIV
C       Gx,Gy,Gx, g-value components
C       N = Maximum number of angles calculated for each phi and theta
C       ***************************************************************************

      READ (24,1) WL,A1x,A1y,A1z,X1p,Y1p,A2x,A2y,A2z,X2p,Y2p,
     c          Gx,Gy,Gz,Fr,N , AngAL,AngB
    1 FORMAT (1x,15(F12.5,/),I6,/,2(F12.5,/))

      OPEN(6, FILE = 'mq3in20.log',STATUS = 'UNKNOWN')

      WRITE(6,3) A1x,A1y,A1z,X1p,Y1p,A2x,A2y,A2z,X2p,Y2p,Gx,Gy,
     c          Gz,Fr, WL,N, Angal,AngB
    3 FORMAT (1x,'A1x= ',F12.5,2x,'A1y= ',F12.5,2x,'A1z= ',F12.5,/,
     c         'X1p= ',F12.5,2x,' Y1p= ', F12.5,/,
     c         'A2x= ',F12.5,2x,'A2y= ',F12.5,2x,'A2z= ',F12.5,/,
     c         'X2p= ',F12.5,2x,' Y2p= ', F12.5,/,
     c         1x,'Gx= ',F12.5,2x,'Gy= ',F12.5,/,
     c         1x,'Gz = ',f12.5,2x, 'Frequency= ',F12.5,/,
     c         1x,'Linewidth= ',F12.5,2x,'No.angles= ',I6,/,
     c         1x,'Alpha= ',F12.5,2x,'Beta= ',F12.5)
C       ***************************************************************************
C
C       CREATING A FIELD SPACE DETERMINED BY THE FREQUENCY,
C       THE Giso PARAMETER AND THE CONSTANT 714.48.The constant
C       is given by Planck's constant/Bohr magneton * conversion for
C       Tesla to Gauss,  and Gigahertz to Hertz
C       ***************************************************************************
C       BH0=FIELD POSITION FOR g=2.0032 IN GAUSS

      A1iso=(A1x+A1y+A1z)/3.
       X1a=A1x-A1iso
       Y1a=A1y-A1iso
      A2iso=(A2x+A2y+A2z)/3.
       X2a=A2x-A2iso
       Y2a=A2y-A2iso
      Giso=(Gx+Gy+Gz)/3.
       Xg=Gx-Giso
       Yg=Gy-Giso

       A1iso=-2*A1iso
       X1a=-2*X1a
       Y1a=-2*Y1a
       gave=(Gx+Gy)/2.

       CON = 714.482
  710  BH0=CON*FR/Giso
       BH02=CON*FR/Gave

       AHXX=FLOAT(IFIX(BH0))-1000
       p=0.0
       DO 10 I=1,4400
        ALH(I)=0.0
        AHX(I)=AHXX+p
        p=p+0.5
```

```
  10   CONTINUE

C       ************************************************************************
C       Loops here to calculate the three orientations for the
C       one dimensionally oriented EPR spectra, 0,45,90 dgr.
C       ************************************************************************

      N=40
      Angth=0.
      DTH = Pi*90./(Float(N)*180.)
      Do 715 I3=1,3
       n=40
C       ************************************************************************
C       CALCULATING THE GAUSSIAN PATTERN CHARACTERISING
C       THE PEAK SHAPES. WIDTH OF GAUSSIAN ENVELOPE = 75 GAUSS
C       ************************************************************************
      GP=-37.5000
      DO 500 I=1,151
        VLW(I)=10.00*EXP(-1.*(GP/WL)**2)
  490    GP=GP+0.5000
  500   CONTINUE
C       ************************************************************************
C       CALCULATING THE PEAK POSITIONS CORRESPONDING TO
C       THE SOLID ANGLES OF ORIENTATION
C       FOR THE POWDER PATTERN.
C       ************************************************************************

      Alph = Pi * AngAl /180.
      Bet  = Pi * AngB/180.

C Calculate how many increments needed to cover half of X dgr
C       10 dgr=0.1745,5=0.0873,15 dgr = 0.261799, 20dgr=0.3491
      Cone = 0.261799/DTH
      If (Cone-FLOAT(IFIX(Cone)).LT.0.500) THEN
      JAn=IFIX(Cone)
      ELSE
      JAn=IFIX(Cone)+1
      ENDIF

      Numb=0
      ZQ=0.
      ZA=-1.*(FLOAT(n/2))

      IF (Angth.EQ.90) Then
      n=n/2
      ENDIF

      IF (Angth.EQ.0.) THEN
      ZA=0.
      n=n/2
      ENDIF

      Angth2= Angth * Pi/180.
```

```
      DO 150 JA=1,n
       theta=Angth2 + DTH * ZA
       IF (Theta.LE.0.000) THEN
       DPH = 1.
       GO TO 888
       ENDIF

       DPH=DTH/SIN(Theta)
C        this calculates the spectrum over 4 octants
 888   NPT=2*Pi/DPH
       IF ((NPT-FLOAT(IFIX(NPT))).LT.0.5000) THEN
        ZQ=IFIX(NPT)
        Else
        ZQ=IFIX(NPT+1)
       ENDIF

       Numc=ZQ+1
       MoveX=(2*Pi-DPH *FLOAT(ZQ))/2.
      ZQA=0

       DO 140 JB=1,Numc
        Phi=MoveX+DPH*ZQA
       ZQA=ZQA+1.
        NUMB = Numb + 1


C       ***************************************************************************
 125    CALL EIGEN(ALPH,BET,Theta,Phi,N,Na,A1iso,X1a,Y1a,
     c     X1p,Y1p,A2iso,X2a,Y2a,X2p,Y2p,BH0,Giso,Xg,Yg,
     c     EV,M, EVR,I,EVIM,K)
C       ***************************************************************************
C     Nested loops for the calculation of intensities, ie
C     transition probabilities (stored in FACINT)
C     and the field positions from the spin-up and spin-down
C     eigenvalues
C       ***************************************************************************

      DO 221 I=1,72
       EVal(I)=REAL(EV(I))
       DO 222 J=1,72
        ER(I,J)=REAL(EVR(I,J))
        EIM(I,J)=REAL(EVIM(I,J))
222      CONTINUE
221     CONTINUE

      Num=1
      Iv=37
      DO 220 I=1,36
       Jv=37
       DO 230  J=1,36
        FPMn=EVal(Iv)-EVal(J)
        BHX= 2.*BH0 - FPMN
```

```
            C=(0.,0.)
            Nv=37
            DO 240 K=1,36
              C=C + CONJG(CMPLX(ER(Nv,I),EIM(Nv,I)))*
     c              CMPLX(ER(K,Jv),EIM(K,Jv))
             Nv=Nv+1
  240         CONTINUE
            FACINT=CABS(C)**2

            IF (FACINT.NE.0) THEN
              YX=((BHX+0.5)-AHXX)/0.5
             IY=IFIX(YX)
              FACINT2=FACINT*EXP(-1.*((Za/FLOAT(Jan))**2)/2)
              StoreY(IY)=StoreY(IY)+FACINT
            ENDIF

            Num=Num+1
            Jv=Jv+1
  230       CONTINUE
           Iv=Iv+1
  220      CONTINUE
  140     CONTINUE
  610     ZA = ZA+1.0
  150   CONTINUE

C       ************************************************************************
C       NESTED LOOPS FOR
C       SETTING THE POSITIONS OF THE CALCULATED PEAKS INTO THE
C       READY CALCULATED FIELD POINTS FOR THE X-AXIS.
C       ************************************************************************

            DO 116 IY=1,4002
              IF (StoreY(IY).NE.0) THEN
C           Gaussian pattern width is 150 points, ie 75 Gauss
              IHL=IY-75
              IHU=IY+75
              IHM=1

            DO 43 NI=IHL,IHU

             IF(IHL.LT.1) GO TO 627

             IF (IHU.GT.4400) GO TO 627
              ALH(NI)=ALH(NI)+VLW(IHM)*StoreY(IY)
  627           IHM = IHM + 1
   43         CONTINUE
             ENDIF
  116        CONTINUE

        If (Angth.Eq.0.) then
         OPEN(Unit=31, FILE = 'x0.dat' , STATUS = 'Unknown')
  560    DO 55 JI=1,4000,2
         WRITE(31,60) AHX(JI),ALH(JI),AHX(JI+1),ALH(JI+1)
   60     FORMAT (1X,F10.3,3X,F14.3,3X,F10.3,3X,F14.3)
```

```
 55   CONTINUE
      Endif

      If (Angth.Eq.45.) then
       OPEN(Unit=31, FILE = 'x45.dat' , STATUS = 'Unknown')
      DO 755 JI=1,4000,2
        WRITE(31,760) AHX(JI),ALH(JI),AHX(JI+1),ALH(JI+1)
760     FORMAT (1X,F10.3,3X,F14.3,3X,F10.3,3X,F14.3)
755   CONTINUE
      Endif

      If (Angth.Eq.90.) then
       OPEN(Unit=31, FILE = 'x90.dat', STATUS = 'Unknown')
      DO 756 JI=1,4000,2
        WRITE(31,761) AHX(JI),ALH(JI),AHX(JI+1),ALH(JI+1)
761     FORMAT (1X,F10.3,3X,F14.3,3X,F10.3,3X,F14.3)
756   CONTINUE
      Endif

      write (6,*) numb,numc
      Angth=Angth+45.
 715  Continue

      STOP
      END
C     ------------------------------------------------------------------
      SUBROUTINE EIGEN(ALPHs,BETs,ATHs,APHs,Ns,Nas,A1isos,X1as,
     c  Y1as,X1ps,Y1ps,A2isos,X2as,Y2as, X2ps,Y2ps,
     c  Heff,Gisos,Xgs,Ygs,EVs,Mr,EVRs,NR1,EVIMs,NI)
C     ------------------------------------------------------------------

      PARAMETER (Ms=72,NRIn=72,NIIn=72,NRO=72,NIO=72)

      DOUBLE PRECISION QUDIM(72,72),QUDRL(72,72)
      DOUBLE PRECISION EVs(Ms), EVRs(NRO,Ms), EVIMs(NIO,Ms)
      DOUBLE PRECISION WK1(Ms),WK2(Ms),WK3(Ms)
      REAL NZ

C     Mquad (Real and Imaginary) is an internal matrix holding the
C     values of < |Hq| >. EV etc specified earlier.

       DO 800 I=1,72
        DO 801 J=1,72
         QUDRL(I,J)=0.
         QUDIM(I,J)=0.
 801     CONTINUE
 800   CONTINUE

C      ROTATING ALPHA & BETA, IE MOLECULAR FRAME TO MEMBRANE
C      Hyperfine terms for Mn3

 802   A1mxx = ((COS(ALPHs)**2)*(COS(BETs)**2)*X1as)+
     c      ((SIN(ALPHs)**2)*(COS(BETs)**2)*Y1as)-
     c      ((SIN(BETs)**2)*(X1as+Y1as))
```

```
      A1myy = ((SIN(ALPHs)**2)*X1as)+((COS(ALPHs)**2)*Y1as)
      A1mxy = (COS(ALPHs)*SIN(ALPHs)*COS(BETs)*(Y1as-X1as))
     A1mxz = SIN(BETs)*COS(BETs)*
     c       ((COS(ALPHs)**2)*X1as+(SIN(ALPHs)**2)*Y1as+X1as+Y1as)
      A1myz = (SIN(ALPHs)*COS(ALPHs)*SIN(BETs)*(Y1as-X1as))
      A1mzz = ((COS(ALPHs)**2)*(SIN(BETs)**2)*X1as)+
     c        ((SIN(ALPHs)**2)*(SIN(BETs)**2)*Y1as)-
     c        ((COS(BETs)**2)*(X1as+Y1as))

C     Hyperfine terms for Mn4

      A2mxx = ((COS(ALPHs)**2)*(COS(BETs)**2)*X2as)+
     c        ((SIN(ALPHs)**2)*(COS(BETs)**2)*Y2as)-
     c        ((SIN(BETs)**2)*(X2as+Y2as))
      A2myy = ((SIN(ALPHs)**2)*X2as)+((COS(ALPHs)**2)*Y2as)
      A2mxy = (COS(ALPHs)*SIN(ALPHs)*COS(BETs)*(Y2as-X2as))
     A2mxz = SIN(BETs)*COS(BETs)*
     c       ((COS(ALPHs)**2)*X2as+(SIN(ALPHs)**2)*Y2as+X2as+Y2as)
      A2myz = (SIN(ALPHs)*COS(ALPHs)*SIN(BETs)*(Y2as-X2as))
      A2mzz = ((COS(ALPHs)**2)*(SIN(BETs)**2)*X2as)+
     c        ((SIN(ALPHs)**2)*(SIN(BETs)**2)*Y2as)-
     c        ((COS(BETs)**2)*(X2as+Y2as))

C     Quadrupolar terms for Mn3

      P1mxx =((COS(ALPHs)**2)*(COS(BETs)**2)*X1ps)+
     c        ((SIN(ALPHs)**2)*(COS(BETs)**2)*Y1ps)-
     c        ((SIN(BETs)**2)*(X1ps+Y1ps))
      P1myy =((SIN(ALPHs)**2)*X1ps)+((COS(ALPHs)**2)*Y1ps)
      P1mzz =((COS(ALPHs)**2)*(SIN(BETs)**2)*X1ps)+
     c        ((SIN(ALPHs)**2)*(SIN(BETs)**2)*Y1ps)-
     c        ((COS(BETs)**2)*(X1ps+Y1ps))
      P1mxz =SIN(BETs)*COS(BETs)*((COS(ALPHs)**2)*
     c        X1ps+(SIN(ALPHs)**2)*Y1ps+X1ps+Y1ps)
      P1myz =SIN(ALPHs)*COS(ALPHs)*SIN(BETs)*(Y1ps-X1ps)
      P1mxy =SIN(ALPHs)*COS(ALPHs)*COS(BETs)*(Y1ps-X1ps)

C     Quadrupolar terms for Mn4

      P2mxx =((COS(ALPHs)**2)*(COS(BETs)**2)*X2ps)+
     c        ((SIN(ALPHs)**2)*(COS(BETs)**2)*Y2ps)-
     c        ((SIN(BETs)**2)*(X2ps+Y2ps))
      P2myy =((SIN(ALPHs)**2)*X2ps)+((COS(ALPHs)**2)*Y2ps)
      P2mzz =((COS(ALPHs)**2)*(SIN(BETs)**2)*X2ps)+
     c        ((SIN(ALPHs)**2)*(SIN(BETs)**2)*Y2ps)-
     c        ((COS(BETs)**2)*(X2ps+Y2ps))
      P2mxz =SIN(BETs)*COS(BETs)*((COS(ALPHs)**2)*
     c        X2ps+(SIN(ALPHs)**2)*Y2ps+X2ps+Y2ps)
      P2myz =SIN(ALPHs)*COS(ALPHs)*SIN(BETs)*(Y2ps-X2ps)
      P2mxy =SIN(ALPHs)*COS(ALPHs)*COS(BETs)*(Y2ps-X2ps)

C     G-tensor
```

```
      Gmxx = ((COS(ALPHs)**2)*(COS(BETs)**2)*Xgs)+
     c       ((SIN(ALPHs)**2)*(COS(BETs)**2)*Ygs)-
     c       ((SIN(BETs)**2)*(Xgs+Ygs))
      Gmyy = ((SIN(ALPHs)**2)*Xgs)+((COS(ALPHs)**2)*Ygs)
      Gmxy = (COS(ALPHs)*SIN(ALPHs)*COS(BETs)*(Ygs-Xgs))
      Gmxz = SIN(BETs)*COS(BETs)*
     c       ((COS(ALPHs)**2)*Xgs+(SIN(ALPHs)**2)*Ygs+Xgs+Ygs)
      Gmyz = (SIN(ALPHs)*COS(ALPHs)*SIN(BETs)*(Ygs-Xgs))
      Gmzz = ((COS(ALPHs)**2)*(SIN(BETs)**2)*Xgs)+
     c       ((SIN(ALPHs)**2)*(SIN(BETs)**2)*Ygs)-
     c       ((COS(BETs)**2)*(Xgs+Ygs))

C     ROTATING MEMBRANE TO APPLIED FIELD FRAME

      A1xx = ((COS(APHs)**2)*(COS(ATHs)**2)*A1mxx)+
     c       ((SIN(APHs)**2)*(COS(ATHs)**2)*A1myy)+
     c       (SIN(ATHs)**2*A1mzz)+
     c       (2*COS(APHs)*SIN(APHs)*(COS(ATHs)**2)*A1mxy)
     c       - (2*COS(ATHs)*SIN(ATHs)*(SIN(APHs)*A1myz
     c       +COS(APHs)*A1mxz))
      A1yy = ((SIN(APHs)**2)*A1mxx)+((COS(APHs)**2)*A1myy)
     c       -(2*COS(APHs)*SIN(APHs)*A1mxy)
      A1xy = (COS(APHs)*SIN(APHs)*COS(ATHs)*(A1myy-A1mxx))
     c       + ((COS(APHs)**2)-(SIN(APHs)**2))*COS(ATHs)*A1mxy +
     c       (SIN(ATHs)*(SIN(APHs)*A1mxz - COS(APHs)*A1myz))
      A1xz = SIN(ATHs)*COS(ATHs)*
     c       ((COS(APHs)**2)*A1mxx+(SIN(APHs)**2)*A1myy - A1mzz) +
     c       2*COS(APHs)*SIN(APHs)*COS(ATHs)*SIN(ATHs)*A1mxy +
     c       ((Cos(ATHs)**2) - (SIN(ATHs)**2))*
     c       (COS(APHs)*A1mxz + SIN(APHs)*A1myz)
      A1yz = (SIN(APHs)*COS(APHs)*SIN(ATHs)*(A1myy-A1mxx)) +
     c       ((COS(APHs)**2) - (SIN(APHs)**2))*SIN(ATHs)*A1mxy +
     c       (COS(ATHs)*(COS(APHs)*A1myz - SIN(APHs)*A1mxz))
      A1zz = ((COS(APHs)**2)*(SIN(ATHs)**2)*A1mxx)+
     c       ((SIN(APHs)**2)*(SIN(ATHs)**2)*A1myy)+
     c       ((COS(ATHs)**2)*A1mzz)+
     c       (2* COS(APHs)*SIN(APHs)*(SIN(ATHs)**2)*A1mxy) +
     c       (2*COS(ATHs)*SIN(ATHs)*(SIN(APHs)*A1myz +
     c       COS(APHs)*A1mxz))

      P1xx = ((COS(APHs)**2)*(COS(ATHs)**2)*P1mxx)+
     c       ((SIN(APHs)**2)*(COS(ATHs)**2)*P1myy)+
     c       (SIN(ATHs)**2*P1mzz)+
     c       (2*COS(APHs)*SIN(APHs)*(COS(ATHs)**2)*P1mxy)
     c       - (2*COS(ATHs)*SIN(ATHs)*(SIN(APHs)*P1myz
     c       +COS(APHs)*P1mxz))
      P1yy = ((SIN(APHs)**2)*P1mxx)+((COS(AP Hs)**2)*P1myy)
     c       -(2*COS(APHs)*SIN(APHs)*P1mxy)
      P1xy = (COS(APHs)*SIN(APHs)*COS(ATHs)*(P1myy-P1mxx))
     c       + ((COS(APHs)**2)-(SIN(APHs)**2))*COS(ATHs)*P1mxy +
     c       (SIN(ATHs)*(SIN(APHs)*P1mxz - COS(APHs)*P1myz))
      P1xz = SIN(ATHs)*COS(ATHs)*
     c       ((COS(APHs)**2)*P1mxx+(SIN(APHs)**2)*P1myy - P1mzz) +
     c       2*COS(APHs)*SIN(APHs)*COS(ATHs)*SIN(ATHs)*P1mxy +
```

```
c       ((COS(ATHs)**2) - (SIN(ATHs)**2))*
c       (COS(APHs)*P1mxz + SIN(APHs)*P1myz)
      P1yz = (SIN(APHs)*COS(APHs)*SIN(ATHs)*(P1myy-P1mxx)) +
c       ((COS(APHs)**2) - (SIN(APHs)**2))*SIN(ATHs)*P1mxy +
c       (COS(ATHs)*(COS(APHs)*P1myz - SIN(APHs)*P1mxz))
      P1zz = ((COS(APHs)**2)*(SIN(ATHs)**2)*P1mxx)+
c       ((SIN(APHs)**2)*(SIN(ATHs)**2)*P1myy)+
c       ((COS(ATHs)**2)*P1mzz)+
c       (2* COS(APHs)*SIN(APHs)*(SIN(ATHs)**2)*P1mxy) +
c       (2*COS(ATHs)*SIN(ATHs)*(SIN(APHs)*P1myz +
c       COS(APHs)*P1mxz))

      A2xx = ((COS(APHs)**2)*(COS(ATHs)**2)* A2mxx)+
c       ((SIN(APHs)**2)*(COS(ATHs)**2)*  A2myy)+
c       (SIN(ATHs)**2*  A2mzz)+
c       (2*COS(APHs)*SIN(APHs)*(COS(ATHs)**2)*A2mxy)
c       - (2*COS(ATHs)*SIN(ATHs)*(SIN(APHs)*A2myz
c       +COS(APHs)*A2mxz))
      A2yy = ((SIN(APHs)**2)*A2mxx)+((COS(APHs)**2)*A2myy)
c       -(2*COS(APHs)*SIN(APHs)*A2mxy)
      A2xy = (COS(APHs)*SIN(APHs)*COS(ATHs)*(A2myy-A2mxx))
c       + ((COS(APHs)**2)-(SIN(APHs)**2))*COS(ATHs)*A2mxy +
c       (SIN(ATHs)*(SIN(APHs)*A2mxz - COS(APHs)*A2myz))
      A2xz = SIN(ATHs)*COS(ATHs)*
c       ((COS(APHs)**2)*A2mxx+(SIN(APHs)**2)*A2myy - A2mzz) +
c       2*COS(APHs)*SIN(APHs)*COS(ATHs)*SIN(ATHs)*A2mxy +
c       ((COS(ATHs)**2) - (SIN(ATHs)**2))*
c       (COS(APHs)*A2mxz + SIN(APHs)*A2myz)
      A2yz = (SIN(APHs)*COS(APHs)*SIN(ATHs)*(A2myy-A2mxx)) +
c       ((COS(APHs)**2) - (SIN(APHs)**2))*SIN(ATHs)*A2mxy +
c       (COS(ATHs)*(COS(APHs)*A2myz - SIN(APHs)*A2mxz))
      A2zz = ((COS(APHs)**2)*(SIN(ATHs)**2)*A2mxx)+
c       ((SIN(APHs)**2)*(SIN(ATHs)**2)*A2myy)+
c       ((COS(ATHs)**2)*A2mzz)+
c       (2* COS(APHs)*SIN(APHs)*(SIN(ATHs)**2)*A2mxy) +
c       (2*COS(ATHs)*SIN(ATHs)*(SIN(APHs)*A2myz +
c       COS(APHs)*A2mxz))

      P2xx = ((COS(APHs)**2)*(COS(ATHs)**2)*P2mxx)+
c       ((SIN(APHs)**2)*(COS(ATHs)**2)*P2myy)+
c       (SIN(ATHs)**2*P2mzz)+
c       (2*COS(APHs)*SIN(APHs)*(COS(ATHs)**2)*P2mxy)
c       - (2*COS(ATHs)*SIN(ATHs)*(SIN(APHs)*P2myz
c       +COS(APHs)*P2mxz))
      P2yy = ((SIN(APHs)**2)*P2mxx)+((COS(APHs)**2)*P2myy)
c       -(2*COS(APHs)*SIN(APHs)*P2mxy)
      P2xy = (COS(APHs)*SIN(APHs)*COS(ATHs)*(P2myy-P2mxx))
c       + ((COS(APHs)**2)-(SIN(APHs)**2))*COS(ATHs)*P2mxy +
c       (SIN(ATHs)*(SIN(APHs)*P2mxz - COS(APHs)*P2myz))
      P2xz = SIN(ATHs)*COS(ATHs)*
c       ((COS(APHs)**2)*P2mxx+(SIN(APHs)**2)*P2myy - P2mzz) +
c       2*COS(APHs)*SIN(APHs)*COS(ATHs)*SIN(ATHs)*P2mxy +
c       ((COS(ATHs)**2) - (SIN(ATHs)**2))*
c       (COS(APHs)*P2mxz + SIN(APHs)*P2myz)
```

```
      P2yz = (SIN(APHs)*COS(APHs)*SIN(ATHs)*(P2myy-P2mxx)) +
     c       ((COS(APHs)**2) - (SIN(APHs)**2))*SIN(ATHs)*P2mxy +
     c       (COS(ATHs)*(COS(APHs)*P2myz - SIN(APHs)*P2mxz))
      P2zz = ((COS(APHs)**2)*(SIN(ATHs)**2)*P2mxx)+
     c       ((SIN(APHs)**2)*(SIN(ATHs)**2)*P2myy)+
     c       ((COS(ATHs)**2)*P2mzz)+
     c       (2* COS(APHs)*SIN(APHs)*(SIN(ATHs)**2)*P2mxy) +
     c       (2*COS(ATHs)*SIN(ATHs)*(SIN(APHs)*P2myz +
     c        COS(APHs)*P2mxz))

      Gxz = SIN(ATHs)*COS(ATHs)*
     c       ((COS(APHs)**2)*Gmxx+(SIN(APHs)**2)*Gmyy - Gmzz) +
     c       2*COS(APHs)*SIN(APHs)*COS(ATHs)*SIN(ATHs)*Gmxy +
     c       ((COS(ATHs)**2) - (SIN(ATHs)**2))*
     c       (COS(APHs)*Gmxz + SIN(APHs)*Gmyz)
      Gyz = (SIN(APHs)*COS(APHs)*SIN(ATHs)*(Gmyy-Gmxx)) +
     c       ((COS(APHs)**2) - (SIN(APHs)**2))*SIN(ATHs)*Gmxy +
     c       (COS(ATHs)*(COS(APHs)*Gmyz - SIN(APHs)*Gmxz))
      Gzz = ((COS(APHs)**2)*(SIN(ATHs)**2)*Gmxx)+
     c       ((SIN(APHs)**2)*(SIN(ATHs)**2)*Gmyy)+
     c       ((COS(ATHs)**2)*Gmzz)+
     c       (2* COS(APHs)*SIN(APHs)*(SIN(ATHs)**2)*Gmxy) +
     c       (2*COS(ATHs)*SIN(ATHs)*(SIN(APHs)*Gmyz +
     c        COS(APHs)*Gmxz))

C      To express zeeman terms in field equivalent units, divide
C      throughout by gB  ie gzzBHoSz/gisoB so that:
       Gxz = Gxz/Gisos
       Gyz = Gyz/Gisos
       Gzz = Gzz/Gisos
C      Terms for nuclear zeeman -gnBnHeff/gisoBe(Iz1+Iz2)
       NZ=-0.000751359*Heff/gisos

       ROOT2=SQRT(2.)
       ROOT5=SQRT(5.)
       ROOT10=SQRT(10.)

       Sz=0.5
       Szz=-0.5

C      Diagonal elements
       J=1
       I1=-5./2.
       Do 701 Ji=1,6
       I2=-5./2.
       I1pls=SQRT((5./2.-I1)*(5./2.+I1+1.))
       Do 702 Jl=1,6
       QUDRL(J,J)=I1*A1isos*Sz+I1*A1zz*Sz+
     c            I2*A2isos*Sz+I2*A2zz*Sz+
     c            Sz*Heff+Gzz*Sz*Heff+NZ*(I1+I2)+
     c            P1zz*(3*I1*I1-2.5*(3.5))/2.+
     c            P2zz*(3*I2*I2-2.5*(3.5))/2.

       QUDRL(J+36,J+36)=I1*A1isos*Szz+I1*A1zz*Szz+
```

```
c               I2*A2isos*Szz+I2*A2zz*Szz+
c               Szz*Heff+Gzz*Szz*Heff+NZ*(I1+I2)+
c               P1zz*(3*I1*I1-2.5*(3.5))/2.+
c               P2zz*(3*I2*I2-2.5*(3.5))/2.
      QUDRL(J+36,J)=QUDRL(J+36,J)+ Gxz*Heff/2.+A1xz*I1/2.
c               +A2xz*I2/2.
      QUDIM(J+36,J)=QUDIM(J+36,J)+ Gyz*Heff/2.+A1yz*I1/2.
c               +A2yz*I2/2.

      j=j+1
      I2=I2+1.
702     Continue
      I1=I1+1.
701     Continue

     J=2
     m=38
      Do 710 Ji=1,6

     i2=-5./2.
      Do 705 Jl=1,6
      I2pls=SQRT((5./2.-I2)*(5./2.+I2+1.))
      If (m.le.72) THEN
      QUDRL(J,J-1)=QUDRL(J,J-1)+Sz*A2xz*I2pls/2.+
c               P2xz*(I2pls*I2+(I2+1.)*I2pls)
      QUDIM(J,J-1)=QUDIM(J,J-1)-Sz*A2yz*I2pls/2.-
c               P2yz*(I2pls*I2+(I2+1.)*I2pls)
      QUDRL(m,m-1)=QUDRL(m,m-1)+Szz*A2xz*I2pls/2.+
c               P2xz*(I2pls*I2+(I2+1.)*I2pls)
      QUDIM(m,m-1)=QUDIM(m,m-1)-Szz*A2yz*I2pls/2.-
c               P2yz*(I2pls*I2+(I2+1.)*I2pls)
      QUDRL(m,J-1)=QUDRL(m,J-1)
c                +i2pls*(a2xx+A2yy)/4.+A2isos*I2pls/2.
      I2=I2+1.
      J=J+1
C       If (m.EQ.72) go to 703
      m=m+1
      ENDIF
705     Continue
710     Continue


703    J=3
      m=39
      Do 711 Ji=1,6

      I2=-5./2.
      Do 707 Jl=1,6
      I2pls=SQRT((5./2.-I2)*(5./2.+I2+1.))
      if (i2.EQ.2.5) then
      i22pls=0.
      else
      I22pls=SQRT((5./2.-(I2+1.))*(5./2.+(I2+1.)+1.))
      Endif
```

```
      If (m.LE.72) then
       QUDRL(J,J-2)=QUDRL(J,J-2)+i22pls*i2pls*(P2xx-P2yy)/4.
       QUDIM(J,J-2)=QUDIM(J,J-2)-I22pls*I2pls*P2xy/2.
       QUDRL(m,m-2)=QUDRL(m,m-2)+i22pls*i2pls*(P2xx-P2yy)/4.
       QUDIM(m,m-2)=QUDIM(m,m-2)-I22pls*I2pls*P2xy/2.

      I2=I2+1.
      J=J+1
c       if (m.EQ.72) go to 704
      m=m+1
      endif
 707   Continue

 711   COntinue

 704   J=7
      m=43
      i1=-5./2.
      Do 713 n=1,6
      I1pls=SQRT((5./2.-I1)*(5./2.+I1+1.))
      Do 708 Ji=1,6
      If (m.le.72) then
      QUDRL(J,J-6)=QUDRL(J,J-6)+Sz*A1xz*I1pls/2.+
     c          P1xz*(I1pls*I1+(I1+1.)*I1pls)
      QUDIM(J,J-6)=QUDIM(J,J-6)-Sz*A1yz*I1pls/2.-
     c          P1yz*(I1pls*I1+(I1+1.)*I1pls)
      QUDRL(m,m-6)=QUDRL(m,m-6)+Szz*A1xz*I1pls/2.+
     c          P1xz*(I1pls*I1+(I1+1.)*I1pls)
      QUDIM(m,m-6)=QUDIM(m,m-6)-Szz*A1yz*I1pls/2.-
     c          P1yz*(I1pls*I1+(I1+1.)*I1pls)
      QUDRL(m,J-6)=QUDRL(M,J-6)+I1pls*(A1xx+A1yy)/4.+
     c          A1isos*I1pls/2.

       J=J+1
       m=m+1
      endif
708   Continue
      i1=I1+1.
713   Continue
      j=1
      i1=-3./2.
      DO 730 n=1,6
      Do 731 ji=1,6
       if (j.le.30) then
       i1min=SQRT((5./2.+i1)*(5./2.-I1+1.))
      QUDRL(J+36,J+6)=QUDRL(J+36,J+6)+I1min*(A1xx-A1yy)/4.
      QUDIM(J+36,J+6)=QUDIM(J+36,J+6)+I1min*A1xy/2.
      j=j+1
      endif
731   Continue
      i1=i1+1
730   Continue

706   j=1
```

```
      DO 714 n=1,6
       i2=-3./2.
      Do 709 ji=1,6
       I2min=SQRT((5./2.+I2)*(5./2.-I2+1.))
       if (j.le.35) then
      QUDRL(J+36,J+1)=QUDRL(J+36,J+1)+I2min*(A2xx-A2yy)/4.
      QUDIM(J+36,J+1)=QUDIM(J+36,J+1)+I2min*A2xy/2.
       i2=I2+1.
       J=J+1
      endif
709   Continue
     i2=-5./2.
714   Continue

718  J=13
    m=49
    i1=-5./2.
    DO 715 n=1,6
     I1pls=SQRT((5./2.-I1)*(5./2.+I1+1.))
     if (i1.EQ.2.5) then
     i11pls=0.
     else
     I11pls=SQRT((5./2.-(I1+1.))*(5./2.+(I1+1.)+1.))
     endif
    Do 712 Ji=1,6
     if (m.le.72) then
      QUDRL(J,J-12)=QUDRL(J,J-12)+i11pls*i1pls*(P1xx-P1yy)/4.
      QUDIM(J,J-12)=QUDIM(J,J-12)-I11pls*I1pls*P1xy/2.
      QUDRL(m,m-12)=QUDRL(m,m-12)+i11pls*i1pls*(P1xx-P1yy)/4.
      QUDIM(m,m-12)=QUDIM(m,m-12)-I11pls*I1pls*P1xy/2.
     j=J+1
     m=m+1
     endif
712    Continue
    i1=i1+1.
715  Continue


C   Text for F02AXF External Subroutine, returning eigenvalues
C   and eigenvectors for Sz=0.5(up) and Sz=-0.5(down)
C   ------------------------------------------------------------------
 804   IFAIL=0
       CALL F02AXF(QUDRL,NRIn,QUDIM,NIIn,Ms,EVs,EVRs,NRO,
    c            EVIMs,NIO,WK1,WK2,WK3,IFAIL)
       IF(IFAIL.NE.0)  PRINT 805, IFAIL
 805   FORMAT (1x,'IFAIL= ',I4)

       Mr=Ms
       NR1=NRO
       NI=NIO
       RETURN
       END

C   End Subroutine Eigen
```

APPENDIX 4:
g=4.1 SIMULATION PROGRAM

```
C     ************************************************************************
C     Program to calculate S=3/2 excited state 4.1 signal.
C     The program includes hyperfine interactions explicitly,
C     with A1 interactions by first order perturbation,
C     A2 interactions, including quadrupole int. by
C     matrix perturbation.
C     The program calculates powder pattern spectra with
C     Gaussian line shape approximation.
C     Variables entered via program int4.for
C     This program is written by Karin Ahrling
C     Dept Chem. Fac Science, ANU, Australia
C     Language = Fortran, Library Routine, NAG FO2AXF
C     ************************************************************************
      PARAMETER (Ia=151,Ib=6,Ic=216,Id=6)
      INTEGER ZQ
      REAL NPT,MoveX, p1,p2

      COMPLEX C4,C5,C7,C8,C9,C10,Cm
      COMPLEX C41,C51,C71,C81,C91,C101
      COMPLEX Sx,Sy,S_x,S_y
      COMPLEX Sx1,Sy1,S_x1,S_y1

      Character*12 logn,resn

      DIMENSION AHX(4500),ALH(4500)
      DIMENSION StoreY(4500)
      DIMENSION DeltE(Ic)
      DIMENSION VLW(301)
      DIMENSION EV(4),EVR(4,4),EVIM(4,4)
      DIMENSION Buffer1(Ib), Buffer2(Ib)
      DIMENSION  EVRh1(Id,Id), EVImh1(Id,Id)
      DIMENSION  EVRh2(Id,Id), EVImh2(Id,Id)

      EXTERNAL F02AXF

C     ************************************************************************
C     Subroutine Eigen - Takes Phi and Theta (in rads),A1iso,A2iso
C     X1a,Y1a,X2a,Y2a,Xp,Yp; calculates the rotation matrices for
C     H=gBHoSz + SDS
C     and returns the eigenvalues,real,  and eigenvectors, real and
C     imaginary, for each solid angle given to the subroutine.The
C     matrix fed to the subroutine is Hermitian.
C     ************************************************************************
C     READING THE INPUT PARAMETERS
C     ************************************************************************
C     WL is the isotropic line width
C     FR - the frequency of microwave radiation in Gigahertz
C     Xd,Yd are the zero field splitting parameters for the dimer
C     A1x,A1y,A1z hyperfine terms for MnIII
C     A2x,A2y,A2z hyperfine terms for MnIV
```

```
C       X1p,Y1p,X2p,Y2p, quadrupole tensor components for MnIII & MnIV
C       Gx,Gy,Gx, g-value components
C       N = Maximum number of angles calculated for each phi and theta
C       H0 = is the starting field position for calculations
C       ***************************************************************************
      OPEN(Unit=9, FILE ='input4.dat' ,STATUS = 'Unknown')
      READ (9,1) WL,Xd,Yd,A1x,A1y,A1z,A2x,A2y,A2z,
     c           X2p,Y2p,H0,Gx,Gy,Gz,Fr,N,logn,resn
    1 FORMAT (1x,16(F12.5,/),I6,/,A10,/,A10,/)

      OPEN(Unit=11, FILE = logn ,STATUS = 'Unknown')
      OPEN(Unit=31, FILE = resn , STATUS = 'Unknown')

      A1iso=(A1x+A1y+a1z)/3.
      X1a=A1x-A1iso
      Y1a=A1y-A1iso

      A2iso=(A2x+A2y+a2z)/3.
      X2a=A2x-A2iso
      Y2a=A2y-A2iso

      giso=(Gx+Gy+Gz)/3.
      Xg=Gx-giso
      Yg=Gy-giso

     p1=0.5
     p2=0.5

      A1iso=A1iso*p1
      X1a=X1a*P1
      Y1a=Y1a*p1
      A2iso=A2iso*p2
      X2a=X2a*p2
      Y2a=Y2a*p2

      WRITE (11,3) Xd,Yd,A1iso,X1a,Y1a,A2iso,X2a,Y2a,
     c           X2p,Y2p,H0,giso,Xg,Yg,Fr, WL,N
    3 FORMAT (1x,'Xd= ',F12.5,2x,'Yd= ',F12.5,/,
     c       1x,'A1iso= ',F12.5,2x,/,
     c       1x,'X1a= ',F12.5,2x,'Y1a= ',F12.5,/,
     c       1x,'A2iso= ',F12.5,2x,/,
     c       1x,'X2a= ',F12.5,2x,'Y2a= ',F12.5,/,
     c       1x,'X2p= ',F12.5,2x,'Y2p= ',F12.5,/,
     c      1x,'H0= ',F12.5,/,
     c       1x,'giso= ',F12.5,2x,'Xg= ',F12.5,2x,/,
     c       1x,'Yg= ',F12.5,2x, 'Frequency= ',F12.5,/,
     c       1x,'Linewidth= ',F12.5,2x,'No.angles= ',I6)
C*************************************************************************  **
C
C      CREATING A FIELD SPACE DETERMINED BY THE FREQUENCY,
C      THE Giso PARAMETER AND THE CONSTANT 714.48.The constant
C      is given by Planck's constant/Bohr magneton * conversion for
C      Tesla to Gauss,  and Gigahertz to Hertz
C*************************************************************************
C
C       BH0=FIELD POSITION FOR g=2.0032 IN GAUSS
```

```
      Pi=3.1415926

      CON = 714.482
710   BH0=CON*FR/Giso
      MaxH = H0 + 4000
      StoreH=H0
      STOPP =H0

      AHXX=H0
      p=0.0
       DO 10 I=1,4000
        ALH(I)=0.0
        StoreY(I)=0.0
        AHX(I)=AHXX+p
        p=p+1.0
 10    CONTINUE

C       ***************************************************************************
C       CALCULATING THE GAUSSIAN PATTERN CHARACTERISING
C       THE PEAK SHAPES. WIDTH OF GAUSSIAN ENVELOPE = 300 GAUSS
C       ***************************************************************************
      GP=-150.000
      DO 500 I=1,301
       VLW(I)=10.00*EXP(-1.*(GP/WL)**2)
 490    GP=GP+1.000
 500   CONTINUE

C       ***************************************************************************
C       CALCULATING THE PEAK POSITIONS CORRESPONDING TO
C       THE SOLID ANGLES (one octant only) OF ORIENTATION
C       FOR THE POWDER PATTERN.
C       ***************************************************************************

      DTH = Pi*90/(Float(N)*180)
      Numb=0
      ZQ=0
      MoveX=0.
      ZA=1.0
      DO 150 JA=1,N
       th=DTH * ZA
       DPH=DTH/SIN(th)
       NPT=(Pi/(2.*DPH))
        ZQ=IFIX(NPT)
       Numc=ZQ+1

       MoveX=(Pi/2.-DPH*FLOAT(ZQ))/2.
       ZQA=0.
       DO 140 JB=1,Numc
        H0 = StoreH
        Stopp=StoreH
        ph=MoveX+DPH*ZQA
        ZQA=ZQA+1.
```

```
C     ***************************************************************************
C     Nested loops for the calculation of intensities, ie
C     transition probabilities (stored in FACINT)
C     and the field positions from the spin-up and spin-down
C     eigenvalues
C     Subroutine EIGEN calculates eigenvalues and eigenvectors for
C     main transitions (Zeeman + Zero field)
C     ***************************************************************************

      deltaH = 100.
125     IF (H0.LE.MaxH) THEN
        CALL EIGEN(TH,Ja,PH,Jb,N,Na,Xd,Yd,
 c       H0,Giso,Xg,Yg,EV,M, EVR,In,EVIM,K)

        Jn=1
        DO 225 I=1,4
          DO 230  J=I+1,4
C       Calculate DeltE=BHO for one field
            IF (Jn.EQ.1.Or.Jn.Eq.6) THEN
             Buffer1(Jn)= EV(J)-EV(I)-BH0
            ENDIF
            Jn=Jn+1
230         CONTINUE
225       CONTINUE

        H0=H0 + deltaH
        CALL EIGEN(TH,Ja,PH,Jb,N,Na,Xd,Yd,
 c       H0,Giso,Xg,Yg,EV,M, EVR,In,EVIM,K)

       Jn=1
       DO 232 I=1,4
         DO 233 J=I+1,4
          IF (Jn.EQ.1.Or.Jn.Eq.6) THEN
C       Calculate DeltE=BHO for another
           Buffer2(Jn) = EV(J) - EV(I) -BH0
          ENDIF
          Jn=Jn+1
233       CONTINUE
232     CONTINUE


DO 236 Jn=1,6
 IF (Jn.EQ.1) then
  I=1
  J=2
 ELSE IF (Jn.EQ.2) then
 I=1
  J=3
 ELSE IF (Jn.EQ.3) then
  I=1
  J=4
 ELSE IF (Jn.EQ.4) then
  I=2
  J=3
```

```
            ELSE IF (Jn.EQ.5) then
             I=2
             J=4
             ELSE IF (Jn.Eq.6) then
             I=3
             J=4
            ENDIF

C       Compare the two to see if a transition has occurred
 220         IF (Buffer1(Jn).LT.0.and.Buffer2(Jn).GT.0) then
            GO TO 231
            ELSE IF  (Buffer1(Jn).GT.0.and.Buffer2(Jn).LT.0) then
            GO TO 231
C      Transition has occurred
 231          IF (deltaH.EQ.1) then
             GO TO 235
            ELSE
             STOPP = H0
              H0=H0-deltaH
            ENDIF
           ENDIF

           IF(H0.LT.STOPP) then
            deltaH=1.
            H0=H0+deltaH
            CALL EIGEN(TH,Ja,PH,Jb,N,Na,Xd,Yd,
     c        H0,Giso,Xg,Yg,EV,M, EVR,In,EVIM,K)
            Buffer2(Jn)=EV(J)-EV(I)-BH0
            GO TO 220
           ELSE IF(H0.EQ.STOPP) Then
            deltaH=100.
            GO TO 236
           ELSE
            GO TO 236
           ENDIF

C Fieldposition where transition occurs, has been found

C  Intensity calculations given by in x,y direction
C  |<u|H1.g.S|d>|**2

 235       Gxx=Giso+0.5*((COS(th)**2)*((COS(ph)**2)*Xg+
     c       (SIN(ph)**2)*Yg))+ 0.5*((SIN(ph)**2)*Xg+
     c       (COS(ph)**2)*Yg)+ 2*0.31831*COS(ph)*
     c       SIN(ph)*COS(th)*(Yg-Xg)-0.5*(SIN(th)**2)*(Xg+Yg)
           Gyy=Giso+0.5*((COS(th)**2)*((COS(ph)**2)*Xg+(SIN(ph)**2)
     c       *Yg))+ 0.5*((SIN(ph)**2)*Xg+(COS(ph)**2)*Yg)+
     c       2*0.31831*COS(ph)*SIN(ph)*COS(th)*(Yg-Xg)-
     c       0.5*(SIN(th)**2)*(Xg+Yg)
           Gxy=0.31831*((SIN(ph)**2)*Xg+(COS(ph)**2)*Yg+
     c       (SIN(th)**2)*(Xg+Yg)-(COS(th)**2)*
     c       ((COS(ph)**2)*Xg+(SIN(ph)**2)*Yg))
           Gxz=0.6366*(COS(th)*SIN(th)*(Xg+Yg+(COS(ph)**2)*Xg+
     c       (SIN(ph)**2)*Yg)+COS(ph)*SIN(ph)*SIN(th)*(Yg-Xg))
```

```
            Gyz=0.6366*(COS(th)*SIN(th)*(-Xg-Yg-(COS(ph)**2)*Xg-
     c        (SIN(ph)**2)*Yg)+COS(ph)*SIN(ph)*SIN(th)*(Yg-Xg))

            C51=(0.,0.)
            C41=(0.,0.)
            C71=(0.,0.)
            C81=(0.,0.)
            C91=(0.,0.)
            C101=(0.,0.)
            Cm=(0.,-1.)

C Terms <u|Sz|d> & <d|Sz|u> j=up, i=down
            DO 649 K=1,4
              C71=C71 +(CONJG(CMPLX(EVR(K,j),EVIM(K,j)))*
     c              CMPLX(EVR(K,i),EVIM(K,i)))
              C81=C81 +(CONJG(CMPLX(EVR(K,i),EVIM(K,i)))*
     c              CMPLX(EVR(K,j),EVIM(K,j)))
 649         CONTINUE

C   Terms for S+ and S-, I=lower,J=upper
            NV=2
            DO 647 K=1,3

C       <J|S+|L>
              C41=C41 + (CONJG(CMPLX(EVR(Nv,j),EVIM(Nv,j)))*
     c              CMPLX(EVR(K,i),EVIM(K,i)))
C       <j|S-|L>
              C51=C51 + (CONJG(CMPLX(EVR(K,j),EVIM(K,j)))*
     c              CMPLX(EVR(Nv,i),EVIM(Nv,i)))
C       <I|S+|J>
              C91=C91 + (CMPLX(EVR(K,j),EVIM(K,j))*
     c              CONJG(CMPLX(EVR(Nv,i),EVIM(Nv,i))))
C       <L|S-|J>
              C101=C101 + (CMPLX(EVR(Nv,j),EVIM(Nv,j))*
     c              CONJG(CMPLX(EVR(K,i),EVIM(K,i))))
            Nv=Nv+1
 647         CONTINUE

            Sx1=C41+C51/2.
            Sy1=C41-C51/2.
            S_x1=C91+C101/2.
            S_y1=C91-C101/2.

C       Calculate intensity of each main transition
              FACINT1= Gxx**2*CABS(Sx1)**2+Gxy**2*CABS(Sy1)**2
     c          +Gxz**2*CABS(C71)**2+Gxy**2*CABS(Sx1)**2
     c          +Gyy**2*CABS(Sy1)**2+Gyz**2*CABS(C71)**2
     c         +2*Gxx*Gxy*(CABS(Sx1)**2)
     c         -Gxx*Gyy*(S_x1*Cm*Sy1+Sx1*Cm*S_y1)
     c         -(Gxy**2)*(Cm*S_y1*Sx1+Cm*Sy1*S_x1)
     c        +2*Gxy*Gyy*(CABS(Sy1)**2)
     c         +Gxz*Gxy*((C81)*(Sx1)+(C71)*(S_x1))
     c         -Gxz*Gyy*(Cm*C81*Sy1+Cm*C71*S_y1)
```

```
c              +2*Gxz*Gyz*(CABS(C71)**2)
c              +Gxx*Gyz*((S_x1)*(C71)+(Sx1)*(C81))
c              -Gxy*Gyz*(Cm*S_y1*C71+Cm*Sy1*C81)

C*****************************************************************************
C       Calculate hyperfine transitions on each main transition.

      CALL EIGEN2 (Ja,Jb,I,J,H0,A1iso,X1a,Y1a,A2iso,X2a,Y2a,X2p,
   c  Y2p,giso,BH0,Th,Ph,Ev,EVR,EVIM,DeltE,
   c   EVRh1,EVIMh1,EVRh2,EVIMh2)
C*****************************************************************************
          Jf=1
          Do 530 L=1,6
           Do 531 M=1,6
            Do 532 N=1,6
            C5=(0.,0.)
            C4=(0.,0.)
            C7=(0.,0.)
            C8=(0.,0.)
            C9=(0.,0.)
            C10=(0.,0.)
            Cm=(0.,-1.)

C Terms <u|Sz|d> & <d|Sz|u> j=up, i=down
            DO 249 K=1,6
              C7=C7 +(CONJG(CMPLX(EVRh2(K,M),EVIMh2(K,M)))*
   c                CMPLX(EVRh1(K,N),EVIMh1(K,N)))
              C8=C8 +(CONJG(CMPLX(EVRh1(K,N),EVIMh1(K,N)))*
   c                CMPLX(EVRh2(K,M),EVIMh2(K,M)))
 249          CONTINUE

C   Terms for S+ and S-, I=lower,J=upper
            Nv=2
            DO 247 K=1,5

C      <J|S+|L>
              C4=C4 + (CONJG(CMPLX(EVRh2(Nv,M),EVIMh2(Nv,M)))*
   c                CMPLX(EVRh1(K,N),EVIMh1(K,N)))
C       <j|S-|L>
              C5=C5 + (CONJG(CMPLX(EVRh2(K,M),EVIMh2(K,M)))*
   c                CMPLX(EVRh1(Nv,N),EVIMh1(Nv,N)))
C      <I|S+|J>
              C9=C9 + (CMPLX(EVRh2(K,M),EVIMh2(K,M))*
   c                CONJG(CMPLX(EVRh1(Nv,N),EVIMh1(Nv,N))))
C     <L|S-|J>
              C10=C10 + (CMPLX(EVRh2(Nv,M),EVIMh2(Nv,M))*
   c                CONJG(CMPLX(EVRh1(K,N),EVIMh1(K,N))))
             Nv=Nv+1
 247          CONTINUE

              Sx=C4+C5/2.
              Sy=C4-C5/2.
```

```
            S_x=C9+C10/2.
            S_y=C9-C10/2.

C       Modify each main transition with hyperfine contribution
            FACINT=FACINT1+(Gxx**2*CABS(Sx)**2
     c             +Gxy**2*CABS(Sy)**2+Gxz**2*CABS(C7)**2
     c             +Gxy**2*CABS(Sx)**2+Gyy**2*CABS(Sy)**2
     c             +Gyz**2*CABS(C7)**2
     c             +2*Gxx*Gxy*(CABS(Sx)**2)
     c             -Gxx*Gyy*(S_x*Cm*Sy+Sx*Cm*S_y)
     c             -(Gxy**2)*(Cm*S_y*Sx+Cm*Sy*S_x)
     c             +2*Gxy*Gyy*(CABS(Sy)**2)
     c             +Gxz*Gxy*((C8)*(Sx)+(C7)*(S_x))
     c             -Gxz*Gyy*(Cm*C8*Sy+Cm*C7*S_y)
     c             +2*Gxz*Gyz*(CABS(C7)**2)
     c             +Gxx*Gyz*((S_x)*(C7)+(Sx)*(C8))
     c             -Gxy*Gyz*(Cm*S_y*C7+Cm*Sy*C8)))

C       Modify fieldpos. for transition with hyperfine
C       contribution
          If (Facint.NE.0.) then
            Fieldpos=H0+DeltE(Jf)

             YX=((Fieldpos+0.5)-AHXX)/1.0
            IY=IFIX(YX)
            If (IY.GT.0) then
              StoreY(IY)=StoreY(IY)+Facint
            Endif
           ENDIF

            Jf=Jf+1
 532          Continue
 531         Continue
 530        Continue
           H0=Stopp
           DeltaH=100.

 236        CONTINUE
          GO TO 125
         ENDIF
 140    CONTINUE
 610    ZA = ZA+1.0
 150   CONTINUE
C       ************************************************************************
C      NESTED LOOPS FOR
C      SETTING THE POSITIONS OF THE CALCULATED PEAKS INTO THE
C      READY CALCULATED FIELD POINTS FOR THE X-AXIS.
C       ************************************************************************
       DO 116 IY=0,4000
        If (StoreY(IY).NE.0.)  Then
c      Gaussian pattern width is 151 Gauss
          IHL=IY-150
          IHU=IY+150
```

```
          IHM=1

          DO 43 NI=IHL,IHU
           IF(NI.LT.1) GO TO 627
           IF (NI.GT.4000) GO TO 627
            ALH(NI)=ALH(NI)+VLW(IHM)*StoreY(IY)
627           IHM = IHM + 1
 43         CONTINUE
           ENDIF
116         CONTINUE

560    DO 55 JI=1,4000,2
       WRITE(31,60) AHX(JI),ALH(JI),AHX(JI+1),ALH(JI+1)
 60     FORMAT (1X,F10.3,3X,F14.3,3X,F10.3,3X,F14.3)
 55    CONTINUE

       STOP
         END
C      ------------------------------------------------------------------
       SUBROUTINE EIGEN(ATHs,Ks,APHs,L,Ns,Nas,Xds,Yds,
     c  Heff,Gisos,Xgs,Ygs,
     c  EVal,Mr,ER,NR1,EIM,NI)
C      ------------------------------------------------------------------

       PARAMETER (Ms=4,NRIn=4,NIIn=4,NRO=4,NIO=4)

       DOUBLE PRECISION MnfnRI(4,4),MnfnIm(4,4)
       DOUBLE PRECISION EVs(Ms), EVRs(NRO,Ms), EVIMs(NIO,Ms)
       DOUBLE PRECISION WK1(Ms),WK2(Ms),WK3(Ms)
       REAL EVal(Ms), ER(NRO,Ms), EIM(NIO,Ms)

C    Mquad (Real and Imaginary) is an internal matrix holding the
C    values of < |Hq| >. EV etc specified earlier.

       DO 800 I=1,4
        DO 801 J=1,4
         MnfnRI(I,J)=0.
         MnfnIm(I,J)=0.
 801     CONTINUE
 800    CONTINUE

C      Hyperfine terms for Mn3

 802    Dxx = ((COS(APHs)**2)*(COS(ATHs)**2)*Xds)+
     c       ((SIN(APHs)**2)*(COS(ATHs)**2)*Yds)-
     c       ((SIN(ATHs)**2)*(Xds+Yds))
        Dyy = ((SIN(APHs)**2)*Xds)+((COS(APHs)**2)*Yds)
        Dxy = (COS(APHs)*SIN(APHs)*COS(ATHs)*(Yds-Xds))
       Dxz = SIN(ATHs)*COS(ATHs)*
     c      ((COS(APHs)**2)*Xds+(SIN(APHs)**2)*Yds+Xds+Yds)
        Dyz = (SIN(APHs)*COS(APHs)*SIN(ATHs)*(Yds-Xds))
        Dzz = ((COS(APHs)**2)*(SIN(ATHs)**2)*Xds)+
     c       ((SIN(APHs)**2)*(SIN(ATHs)**2)*Yds)-
     c       ((COS(ATHs)**2)*(Xds+Yds))
```

```
C       Anisotropic g-value, traceless
C       g-value: Zg=-(Xg+Yg)

      Gxz = SIN(ATHs)*COS(ATHs)*
     c      ((COS(APHs)**2)*Xgs+(SIN(APHs)**2)*Ygs+Xgs+Ygs)
        Gyz = (SIN(APHs)*COS(APHs)*SIN(ATHs)*(Ygs-Xgs))
        Gzz = ((COS(APHs)**2)*(SIN(ATHs)**2)*Xgs)+
     c       ((SIN(APHs)**2)*(SIN(ATHs)**2)*Ygs)-
     c       ((COS(ATHs)**2)*(Xgs+Ygs))

C       To express zeeman terms in field equivalent units, divide
C       throughout by gB  ie gzzBHoSz/gisoB so that:
        Gxz = Gxz/Gisos
        Gyz = Gyz/Gisos
        Gzz = Gzz/Gisos

        ROOT3=SQRT(3.)

C       Elements of Mnfine - Real
C       only lower half of matrix need to be given

        MnfnRl(1,1) = -3.*(Heff+gzz*Heff-Dzz)/2.
        MnfnRl(2,1) = ROOT3*(gxz*Heff/2.-Dxz)
        MnfnRl(3,1) = ROOT3*(Dxx-Dyy)/2.
        MnfnRl(2,2) = -(Heff+gzz*Heff+3*Dzz)/2.
        MnfnRl(3,2) = gxz*Heff
        MnfnRl(4,2) = ROOT3*(Dxx-Dyy)/2.
        MnfnRl(3,3) = (Heff+gzz*Heff-3*Dzz)/2.
        MnfnRl(4,3) = ROOT3*(gxz*Heff/2.+Dxz)
        MnfnRl(4,4) = 3.*(Heff+gzz*Heff+Dzz)/2.

C       Elements of Mnfine - imaginary
C       only lower half of matrix need to be given

        MnfnIm(2,1) = -ROOT3*(gyz*Heff/2.-Dyz)
        MnfnIm(3,1) = -ROOT3*Dxy
        MnfnIm(3,2) = -gyz*Heff
        MnfnIm(4,2) = -ROOT3*Dxy
        MnfnIm(4,3) = -ROOT3*(gyz*Heff/2.+Dyz)

C   Text for F02AXF External Subroutine, returning eigenvalues
C   and eigenvectors for Sz=0.5(up) and Sz=-0.5(down)
C   ------------------------------------------------------------

 804   IFAIL=0
       CALL F02AXF(MnfnRl,NRIn,MnfnIm,NIIn,Ms,EVs,EVRs,NRO,
     c             EVIMs,NIO,WK1,WK2,WK3,IFAIL)
       IF(IFAIL.NE.0)  WRITE (11,805) IFAIL
 805   FORMAT (1x,'IFAILeigen= ',I4)

          DO 221 I=1,4
           EVal(I)=REAL(EVs(I))
           DO 222 J=1,4
```

```
            ER(I,J)=REAL(EVRs(I,J))
            EIM(I,J)=REAL(EVIMs(I,J))
  222        CONTINUE
  221       CONTINUE

        Mr=Ms
        NR1=NRO
        NI=NIO
        RETURN
        END

C   End Subroutine Eigen

C  ---------------------------------------------------------------------

      SUBROUTINE EIGEN2 (Ja2,Jb2,I2,J2,H02,A1iso2,X1a2,Y1a2,A2iso2,
     c              X2a2,Y2a2,X2p2,Y2p2,giso2,BH02,Th2,Ph2,
     c              Ev2,EVR2,EVIM2,DeltE2,EvRh1,EVIMh1,EVRh2,EVIMh2)
C  ---------------------------------------------------------------------

      Parameter (Ib=6,Ic=216,Id=6)

      REAL I1z,I2z

      COMPLEX Cm,Cd,Cu,Cdu
      COMPLEX Matrix1(Id,Id), Matrix2(Id,Id)

      DIMENSION Ev2(4),EVR2(4,4),EVIM2(4,4),DeltE2(Ic)
      DIMENSION EVh1(Id),EVRh1(Id,Id),EVIMh1(Id,Id)
      DIMENSION EVh2(Id),EVRh2(Id,Id),EVIMh2(Id,Id)
      DOUBLE PRECISION EVhd1(Id),EVRhd1(Id,Id),EVIMhd1(Id,Id)
      DOUBLE PRECISION EVhd2(Id),EVRhd2(Id,Id),EVIMhd2(Id,Id)
      DOUBLE PRECISION WK1(Id),WK2(Id),WK3(Id)
      DOUBLE PRECISION HypRI1(Id,Id),HypIm1(Id,Id)
      DOUBLE PRECISION HypRI2(Id,Id),HypIm2(Id,Id)

C calculating the Anistropic hyperfine interaction as a perturbation to H0
C      <u|sz|u>-<d|Sz|d>[const* A1zz*I1z+const*A2zz*I2z]
C      <n|Sz|n> given by:

          A1zz = (A1iso2+((COS(PH2)**2)*(SIN(TH2)**2)*X1a2)+
     c       ((SIN(PH2)**2)*(SIN(TH2)**2)*Y1a2)-
     c       ((COS(TH2)**2)*(X1a2+Y1a2)))
          A2zz =((COS(PH2)**2)*(SIN(TH2)**2)*X2a2)+
     c       ((SIN(PH2)**2)*(SIN(TH2)**2)*Y2a2)-
     c       ((COS(TH2)**2)*(X2a2+Y2a2))
          A2xz = SIN(TH2)*COS(TH2)*
     c       ((COS(PH2)**2)*X2a2+(SIN(PH2)**2)*Y2a2+X2a2+Y2a2)
          A2yz = (SIN(PH2)*COS(PH2)*SIN(TH2)*(Y2a2-X2a2))

          P2zz =((COS(PH2)**2)*(SIN(TH2)**2)*X2p2)+
     c       ((SIN(PH2)**2)*(SIN(TH2)**2)*Y2p2)-
     c       ((COS(TH2)**2)*(X2p2+Y2p2))
          P2xx = ((COS(PH2)**2)*(COS(TH2)**2)*X2p2)+
```

```
c        ((SIN(PH2)**2)*(COS(TH2)**2)*Y2p2)-
c        ((SIN(TH2)**2)*(X2p2+Y2p2))
         P2yy = ((SIN(PH2)**2)*X2p2)+((COS(PH2)**2)*Y2p2)
         P2xy = (COS(PH2)*SIN(PH2)*COS(TH2)*(Y2p2-X2p2))
         P2xz = SIN(TH2)*COS(TH2)*
c        ((COS(PH2)**2)*X2p2+(SIN(PH2)**2)*Y2p2+X2p2+Y2p2)
         P2yz = (SIN(PH2)*COS(PH2)*SIN(TH2)*(Y2p2-X2p2))


C Changing the reduced hyperfine values normally A/giso*beta, to be
C divided by the effective g-value at that field for an effective s=1/2
C perturbation

         Cu=(0.,0.)
         Cd=(0.,0.)
         Cdu=(0.,0.)
C  Terms <u|Sz|u>=Cu and <d|Sz|d>=Cd for A1,A2 perturbation s=3/2
         S=-3./2.
         Do 223 N=1,4
           Cu=Cu +(S* CONJG(CMPLX(EVR2(N,J2),EVIM2(N,J2)))*
c                 CMPLX(EVR2(N,J2),EVIM2(N,J2)))
           Cd=Cd +(S* CONJG(CMPLX(EVR2(N,I2),EVIM2(N,I2)))*
c                 CMPLX(EVR2(N,I2),EVIM2(N,I2)))


          S=S+1.
 223       CONTINUE

C   Terms  S-, I=lower,J=upper
          Nv=2
          DO 248 K=1,3
            If (K.eq.2) then
             S=2.
            Else
             S=SQRT(3.)
            Endif
C            <I|S-|J>
             Cdu=Cdu + S*(CONJG(CMPLX(EVR2(K,I2),EVIM2(K,I2)))*
c                   CMPLX(EVR2(Nv,J2),EVIM2(Nv,J2)))

           Nv=Nv+1
 248       CONTINUE

          Cm=(0.,1.)

C Matrix elements for hyperfine envelope for MnIV
C  Perturbation on Main transitions (Zeeman+Zerofield)
C only lower half need be given
          Root5=Sqrt(5.)
          Root2=Sqrt(2.)
          Root10=Sqrt(10.)

          Do 520 n=1,Id
           Do 521 m=1,Id
```

```
            Matrix1(n,m)=(0.,0)
            Matrix2(n,m)=(0.,0)
521          Continue
520         Continue

          I2z=-5./2.
          DO 502 n=1,Id
            Matrix1(n,n)=Cu*A2iso2*I2z+Cu*A2zz*I2z+
     c        P2zz*(3*(I2z**2)-35/4)/2.
            Matrix2(n,n)=Cd*A2iso2*I2z+Cd*A2zz*I2z+
     c        P2zz*(3*(I2z**2)-35/4)/2.
          I2z=I2z+1
502         CONTINUE

          Matrix1(2,1)=Root5*(Cu*(A2xz-Cm*A2yz)/2.
     c              -2*(P2xz-Cm*P2yz))
          Matrix1(3,2)=Root2*(Cu*(A2xz-Cm*A2yz)
     c              -2*(P2xz-Cm*P2yz))
          Matrix1(4,3)=3.*(Cu*(A2xz-Cm*A2yz)/2.)
          Matrix1(5,4)=Root2*(Cu*(A2xz-Cm*A2yz)
     c              +2*(P2xz-Cm*P2yz))
          Matrix1(6,5)=Root5*(Cu*(A2xz-Cm*A2yz)/2.
     c              +2*(P2xz-Cm*P2yz))

          Matrix2(2,1)=Root5*(Cd*(A2xz-Cm*A2yz)/2.
     c              -2*(P2xz-Cm*P2yz))
          Matrix2(3,2)=Root2*(Cd*(A2xz-Cm*A2yz)
     c              -2*(P2xz-Cm*P2yz))
          Matrix2(4,3)=3.*(Cd*(A2xz-Cm*A2yz)/2.)
          Matrix2(5,4)=Root2*(Cd*(A2xz-Cm*A2yz)
     c              +2*(P2xz-Cm*P2yz))
          Matrix2(6,5)=Root5*(Cd*(A2xz-Cm*A2yz)/2.
     c              +2*(P2xz-Cm*P2yz))

          Matrix1(3,1)=Root10*((P2xx-P2yy)/2.-Cm*P2xy)
          Matrix1(4,2)=3*Root2*((P2xx-P2yy)/2.-Cm*P2xy)
          Matrix1(5,3)=3*Root2*((P2xx-P2yy)/2.-Cm*P2xy)
          Matrix1(6,4)=Root10*((P2xx-P2yy)/2.-Cm*P2xy)

          Matrix2(3,1)=Root10*((P2xx-P2yy)/2.-Cm*P2xy)
          Matrix2(4,2)=3*Root2*((P2xx-P2yy)/2.-Cm*P2xy)
          Matrix2(5,3)=3*Root2*((P2xx-P2yy)/2.-Cm*P2xy)
          Matrix2(6,4)=Root10*((P2xx-P2yy)/2.-Cm*P2xy)

          Do 522 n=1,Id
           Do 523 m=1,Id
             HypRI1(n,m)=REAL(Matrix1(n,m))
             HypIm1(n,m)=AIMAG(Matrix1(n,m))
             HypRI2(n,m)=REAL(Matrix2(n,m))
             HypIm2(n,m)=AIMAG(Matrix2(n,m))
523           Continue
            HypIm1(n,n)=0.
            HypIm2(n,n)=0.
522         Continue
```

```
C   Text for F02AXF External Subroutine, returning eigenvalues
C   NB if Hyperfine interaction is negative, EVH1 represents upper
C   energy levels and EVH2 represents lower, this is reversed if hyperfine
C   is positive.  Here hyperfine is negative.
C
      ------------------------------------------------------------------
            NRIn=Id
            NIIn=Id
            Ms=Id
            NRO=Id
            NIO=Id

 504          IFAIL=0
             CALL F02AXF(HypRI1,NRIn,HypIm1,NIIn,Ms,EVhd1,EVRhd1,NRO,
     c            EVIMhd1,NIO,WK1,WK2,WK3,IFAIL)
             IF(IFAIL.NE.0)  PRINT 505, IFAIL
 505          FORMAT (1x,'IFAIL= ',I4)

c Change from DP to SP real

             DO 511 n=1,Ms
              EVh1(n)=REAL(EVhd1(n))
              DO 512 m=1,Ms
               EVRh1(n,m)=REAL(EVRhd1(n,m))
               EVIMh1(n,m)=REAL(EVIMhd1(n,m))
 512           CONTINUE
 511          CONTINUE

 604          IFAIL=0
             CALL F02AXF(HypRI2,NRIn,HypIm2,NIIn,Ms,EVhd2,EVRhd2,NRO,
     c            EVIMhd2,NIO,WK1,WK2,WK3,IFAIL)
             IF(IFAIL.NE.0)  PRINT 605, IFAIL
 605          FORMAT (1x,'IFAIL= ',I4)

C Change from DP to SP real

             DO 611 n=1,Ms
              EVh2(n)=REAL(EVhd2(n))
              DO 612 m=1,Ms
               EVRh2(n,m)=REAL(EVRhd2(n,m))
               EVIMh2(n,m)=REAL(EVIMhd2(n,m))
 612           CONTINUE
 611          CONTINUE

C The intensities of
Cthe field positions will be modified by the new eigenvectors
C Calculation of intensities

C Energy due to hyperfine DeltE(Jf), scaled depending on effective
C g-value

              geff2=giso2*BH02/H02
             Jf=1
```

```
      I1z=-5./2.
      DO 239 L=1,6
        DO 237 M=1,6
          DO 238 N=1,6
            DeltE2(Jf)=((Cu-Cd)*(A1zz*I1z)+EVh1(M)-EVh2(N))*
     c            giso2/geff2

            Jf=Jf+1
238           CONTINUE
237         CONTINUE
        I1z=I1z+1
239       CONTINUE


      RETURN
      END
```

C end of subroutine Eigen2

APPENDIX 5:
WATER CULTURE SOLUTION FOR SPINACH

(Walker, 1987)

Stock solution	volume (ml) in 10L
2M KNO_3	30
2M $MgCl_3$	20
2M $Ca(NO_3)_2$	20
1M $MgSO_4$	20
1M $K_2H_2PO_4$	10
Fe-EDTA	10
Trace elements	10

Trace minerals for nutrient solution with ruthenium replacing manganese.

Trace elements (100ml)	~mM	g
H_3BO_3	46	0.286
$RuCl_3.3H_2O$	9	0.241
$ZnSO_4.7H_2O$	0.77	0.022
$CuSO_4.5H_2O$	0.3	0.0073
$NaMoO_4.2H_2O$	0.12	0.0029

Fe-EDTA solution: 33.39 g di-Na-EDTA in 880 ml H_2O
24.90 g $FeSO_4$ in 200 ml H_2O

Add 10 g KOH pellets and aerate overnight to form stable complex (pH ~5.5).

Solutions were made up with Milli-Q water. A fungicide was used as requried.

REFERENCES

Abragam, A. and Bleaney, B. 1986. Electron paramagnetic resonance of transition ions. Dover Publications Inc. Mineola, N.Y.910 pp.

Åhrling, K. A. and Pace, R. J. 1995. Simulation of the S_2 state multiline electron paramagnetic resonance signal of photosystem II: A multifrequency approach. *Biophys. J.***68**:2081-2090.

Al'tshuler, S. A. and Kozyrev, B. M. 1974. Electron paramagnetic resonance in compounds of transition elements. 2nd rev. ed. John Wiley & Sons. New York.

Andreasson, L.-E. 1989. Is nitrogen liganded to manganese in the photosynthetic oxygen-evolving system? EPR studies after isotropic replacement with ^{15}N. *Biochim. Biophys. Acta.***973**:465-467.

Astashkin, A. V., Kodera, Y. and Kawamori, A. 1994. Pulsed EPR study of manganese g=4.1 signal in plant photosystem II.*J. Mag. Res.***Series B 105**:113-119.

Baldas, J., Boas, J. F., Bonnyman, J. and Williams, G. A. 1984a. An electron spin resonance study of Bis(tetraphenylarsonium)pentakis(isothiocyanato) nitrosyltechnetate(II): A six-co-ordinate low-spin $4d^5$ technetium(II) complex. *J. Chem. Soc. Dalton Trans.*827-831.

Baldas, J., Boas, J. F., Bonnyman, J. and Williams, G. A. 1984b. Studies of technetium complexes. Part 6. The preparation, characterisation, and electron spin resonance spectra of salts of tetrachloro- and tetrabromo-nitridotechnetate(VI): Crystal structure of tetraphenylarsonium tetrachloro-nitridotechnetate(VI). *J. Chem. Soc. Dalton Trans.*2395-2400.

Baldwin, M. J., Gelasco, A. and Pecoraro, V. L. 1993. The effect of protonation on $[Mn(IV)(\mu\text{–}O)]_2$ complexes. *Photosyn. Res.***38**:303-308.

Baldwin, M. J., Stemmler, T. L., Riggs-Gelasco, P. J., Kirk, M. L., Penner-Hahn, J. E. and Pecoraro, V. L. 1994. Structural and magnetic effects of successive protonations of oxo bridges in high-valent manganese dimers. *J. Am. Chem. Soc.***116**:11349-11356.

Bashkin, J. S., Chang, H.R., Streib, W. E., Huffman, J. C., Hendrickson, D. N. and Christou, G. 1987. Modelling the photosynthetic water oxidation center: Preparation and physical properties of a tetranuclear oxide bridged Mn complex corresponding to the native S_2 state. *J. Am. Chem. Soc.***109**:6502-6504.

Beck, W. F., de Paula, J. C. and Brudvig, G. W. 1985. Active and resting states of the O_2-evolving complex of photosystem II. *Biochem.***24**:3035-3043.

Belford, R. L., Huang, D. T. and So, H. 1972. Quadrupole moment of vanadium-51: Forbidden lines in EPR of oxovanadium(IV). *Chem. Phys. Letts.***14**:592-594.

Bencini, A. and Gatteschi, D. 1990. Electron Paramagnetic Resonance of Exchange Coupled Systems.1st ed. Springer-Verlag. Berlin.300pp.

Bersohn, M. and Baird, J. C. 1966. An Introduction to Electron Paramagnetic Resonance. W.A. Benjamin Inc. New York.

Berthold, D. A., Babcock, G. T. and Yocum, C. F. 1981. A highly resolved, oxygen-evolving photosystem II preparation from spinach thylakoid membranes. EPR and electron-transport properties. *FEBS Letts.***134**:231-234.

Berthomieu, C. and Boussac, A. 1995. Histidine oxidation in the S_2 to S_3 transition probed by FTIR difference spectroscopy in the Ca^{2+} depleted photosystem II: Comparison with histidine radicals generated by UV irradiation. *Biochem.***34**:1541-1548.

Bertrand, P., Guigliarelli, B. and More, C. 1991. The mixed-valence [Fe(III),FE(II)] binuclear centers of biological molecules viewed through EPR spectroscopy. *New J. Chem.***15**:445-454.

Bonvoisin, J., Blondin, G., Girerd, J. and Zimmerman, J. 1992. Theoretical study of the multiline EPR signal from the S_2 state of the oxygen evolving complex of photosystem II. *Biophys. J.***61**:1076-1086.

Boussac, A., Girerd, J.-J. and Rutherford, A. W. 1996. Conversion of the spin state of the manganese complex in photosystem II induced by near-infrared light. *Biochem.***35**:6984-6989.

Bricker, T. M., Pakrasi, H. B. and Sherman, L. A. 1985. Characterization of a spinach photosystem II core preparation isolated by a simplified method. *Arch. Biochem. Biophys.* **237**:170-176.

Britt, R. D., Lorigan, G. A., Sauer, K., Klein, M. P. and Zimmerman, J. 1992. The g=2 multiline EPR signal of the S_2 state of the photosynthetic oxygen-evolving complex originates from a ground spin state. *Biochim. Biophys. Acta.***1040**:95-101.

Britt, R. D., Zimmermann, J.-L., Sauer, K. and Klein, M. P. 1989. Ammonia binds to the catalytic Mn of the oxygen-evolving complex of photosystem II: Evidence by electron spin-echo envelope modulation spectroscopy. *J. Am. Chem. Soc.***111**:3522-3532.

Brudvig, G. W. 1989. EPR spectroscopy of manganese enzymes. *In:* Advanced EPR. Applications in biology and biochemistry. A. J. Hoff ed. Elsevier. Amsterdam. 839-863.

Carrington, A. and McLachlan,1967. A. D. Introduction to Magnetic Resonance - with applications to chemistry and chemical physics.Harper & Row. London.266pp

Chitnis, P. R. 1996. Photosystem 1.*Plant. Physiol.***111**:661-669.

Christou, G. 1989. Manganese carboxylate chemistry and its biological relevance. *Acc. Chem. Res.* **22**:328-335.

Comte, P., Nazeeruddin, M. K., Rotzinger, F. P., Frank, A. J. and Grätzel, M. 1989. Artificial analogues of the oxygen-evolving complex in photosynthesis: The oxo-bridged ruthenium dimer $L_2(H_2O)Ru^{III}$-O-$Ru^{III}(H_2O)L_2$. *J. Molec. Cat.* **52**: 63-84.

Cotton, F. A. and Wilkinson, G. 1966. Advanced Inorganic Chemistry.2nd edition. Interscience Publishers. New York.

Dau, H., Andrews, J. C., Roelofs, T. A., Latimer, M. J., Liang, W., Yachandra, V. K., Sauer, K. and Klein, M. P. 1995. Structural consequences of ammonia binding to the manganese center of the photosynthetic oxygen-evolving comples: An X-ray absorption spectroscopy study of isotropic and oriented photosystem II particles. *Biochem.***34**:5274-5287.

de Paula, J. C., Beck, W. F. and Brudvig, G. W. 1986. Magnetic properties of manganese in the photosynthetic O_2-evolving complex. 2. Evidence for a manganese tetramer.*J. Am. Chem. Soc.***18**:4002-4009.

Dean, J. A. 1985. Lange's Handbook of Chemistry.13th Ed. McGraw-Hill Book Co. New York.

Debus, R. J., Barry, B. A., Babcock, G. T. and McIntosh, L. 1988. Site-directed mutagenesis identifies a tyrosine radical involved in the photosynthetic oxygen-evolving system. *Proc. Natl. Acad. Sci. USA* **85**:427-430.

Debus, R. J. 1992. The manganese and calcium ions of photosynthetic oxygen evolution.*Biochim. Biophys. Acta.***1102**:269-352.

Debus, R. J., Barry, B. A., Sithole, I., Babcock, G. T. and McIntosh, L. 1988. Directed mutagenesis indicates that the donor to P^+_{680} in photosystem II is tyrosine-161 of the D1 polypeptide.*Biochem.***27**:9071-9074.

Dedieu, A., Rohmer, M.-M., Veillard, H. and Veillard, A. 1979. Electronic and structural aspects of dioxygen complexes of metalloporphyrins. An *ab initio* study. *Nov. J. Chimie.***3**:653-667.

Deisenhofer, J., Epp, O., Miki, K., Huber, R. and Michel, H. 1985. Structure of the protein subunits in the photosynthetic reaction centre of *Rhodopseudomonas viridis* at 3Å resolution.*Nature.***318**:618-624.

DeRose, V. J., Mukerji, I., Latimer, M. J., Yachandra, V. K., Sauer, K. and Klein, M. P. 1994. Comparison of the manganese oxygen-evolving complex in photosystem II of Spinach and *Synechococcus* sp. with multinuclear manganese model compounds by X-ray absorption spectroscopy.*J. Am. Chem. Soc.***116**:5239-5249.

DeRose, V. J., Yachandra, V. K., McDermott, A. E., Britt, R. D., Sauer, K. and Klein, M. P. 1991. Nitrogen ligation to manganese in the photosynthetic oxygen-evolving complex: Continuous wave and pulsed EPR studies of photosystem II particles containing ^{14}N or ^{15}N.*Biochem.* **30**:1335-1341.

Dexheimer, S. L. and Klein, M. P. 1992. Detection of a paramagnetic intermediate in the photosynthetic oxygen-evolving complex. *J. Am. Chem. Soc.***114**:2821-2826.

Dexheimer, S. L., Sauer, K. and Klein, M. P. 1990. Parallel polarisation EPR studies of the oxygen-evolving complex of photosystem II. *In:* Current Research in Photosynthesis. M. Baltscheffsky. Kluwer Academic Publishers.Dordrecht. **1**:761-764.

Diner, B. A., Nixon, P. J. and Farchaus, J. W. 1991. Site-directed mutagenesis of photosynthetic reaction centres. *Curr. Op. Struct. Biol.***1**:546-554.

Diner, B. A., Nixon, P. J., Metz, J. G., Rogner, M. and Chisholm, D. 1990. Photosystem II electron donor and acceptor-side function probed by site-directed mutants. *Biophys J.***57**:405a.

Dismukes, G. C. and Siderer, Y. 1981. Intermediates of a polynuclear manganese center involved in photosynthetic oxidation of water.*Proc. Natl. Acad. Sci. USA.***78**:274-278.

Doppelt, P. and Meyer, T. J. 1987. Synthesis and redox properties of the unsymmetrical, oxo-bridged complex $[(bpy)_2(py)Ru^{III}ORu^{III}(H_2O)(bpy)_2]^{4+}$. *Inorg. Chem.***26**:2027-2034.

Ferrante, R. F., Wilkerson, J. L., Graham, W. R. M. and Weltner, W. J. 1977. ESR spectra of the MnO, MnO_2, MnO_3, MnO_4 molecules at 4° K.*J. Chem. Phys.***67**:5904-5913.

Fiege, R., Zweygart, W., Irrgang, K.-D., Adir, N., Geiken, B., Renger, G. and Lubitz, W. 1995. EPR/ENDOR studies of the water oxidizing complex in photosystem II. *In:* Photosynthesis: From light to biosphere. P. Mathis ed. Kluwer Academic Publishers. Dordrecht. **II**:369-372.

Fortman, J. J. and Hayes, R. G. 1965. Electron paramagnetic resonance studies of $Mn(CN)_5NO^{2-}$ and $Cr(CN)_5NO^{3-}$ in dilute single crystals. *J. Chem. Phys.***43**:15-22.

George, G. N., Prince, R. C. and Cramer, S. P. 1989. The manganese site of the photosynthetic water-splitting enzyme.*Science.***243**:789-791.

Goodin, D. B., Yachandra, V. K., Britt, R. D., Sauer, K. and Klein, M. P. 1984. The state of manganese in the photosynthetic apparatus. 3. Light-induced changes in X-ray absorption (K-edge) energies of manganese in photosynthetic membranes.*Biochim. Biophys. Acta.***767**:209-216.

Haddy, A., Aasa, R. and Andreasson, L.-E. 1989. S-Band EPR studies of the S_2-state multiline signal from the photosynthetic oxygen-evolving complex.*Biochemistry.***28**:6954-6959.

Haddy, A., Dunham, W. R., Sands, R. H. and Aasa, R. 1992. Multifrequency EPR investigation into the origin of the S_2-state signal at g=4 of the O_2-evolving complex.*Biochim. Biophys. Acta.***1099**:25-34.

Haddy, A., Waldo, G. S., Sands, R. H. and Penner-Hahn, J. E. 1994. Simulation of multifrequency EPR spectra from Mn(III)/Mn(IV) catalase of *Lactobacillus plantarum* using a new approach based on perturbation theory.*Inorg. Chem.***33**:2677-2682.

Hagen, K. S., Westmoreland, T. D., Scott, M. J. and Armstrong, W. H. 1989. Structural and electronic consequences of protonation in $\{Mn_4O_6\}^{4+}$ cores: pH dependent properties of oxo-bridged manganese complexes.*J. Am. Chem. Soc.***111**:1907-1909.

Hansson, Ö., Aasa, R. and Vänngård, T. 1987. The origin of the multiline and g=4.1 electron paramagnetic resonance signals from the oxygen-evolving system of photosystem II.*Biophys. J.***51**:825-832.

Hansson, Ö. and Andreasson, L. 1982. EPR-detectable, magnetically interacting manganese ions in the photosynthetic oxygen-evolving system after continuous illumination.*Biochim. Biophys. Acta.***679**:261-268.

Hansson, Ö., Andreasson, L.-E. and Vänngård, T. 1986. Oxygen from water is coordinated to manganese in the S_2 state of photosystem II.*FEBS Lett.***195**:151-154.

Hansson, Ö., Andreasson, L.-E. and Vänngård, T. 1984. Studies on the multiline EPR signal associated with state S2 of the oxygen-evolving system. *In:* Advances in Photosynthesis Research. C. Sybesma ed. Martinus Nijoff/ Dr W. Junk eds. The Hague. **1**:1.3.307-1.3.310.

Hansson, Ö. and Wydrzynski, T. 1990. Current perceptions of photosystem II.*Photosyn. Res.***23**:131-162.

Huheey, J. E., Keiter, E. A. and Keiter, R. L. 1993. Inorganic Chemistry. 4th Edition. Harper Collins.

Irrgang, K. D., Boekema, E. J., Vater, J. and Renger, G. 1988. Structural determination of the photosystem II core complex from spinach. *Eur. J. Biochem.***178**:209-217.

Jursinic, P. and Govindjee. 1977. Temperature dependence of delayed light emission in the 6 to 340 microsecond range after a single flash in chloroplasts. *Photochem. Photobiol.***26**:617-628.

Kasack, V., Kaim, W., Binder, H., Jordanov, J. and Roth, E. 1995. When is an odd-electron dinuclear complex a mixed-valent species? Tuning of ligand-to-metal spin shifts in diruthenium(III,II) complexes of noninnocent bridging ligands OC(R)NNC(R)O. *Inorg. Chem.***34**:1924-1933.

Kennedy, B. J. and Murray, K. S. 1985. Magnetic properties and zero-field splitting in high-spin Mn(III) complexes. 1. Mononuclear and polynuclear schiff-base chelates.*Inorg. Chem.***24**:1552-1557.

Kessissoglou, D. P., Kirk, M. L., Bender, C. A., Lah, M. S. and Pecoraro, V. L. 1989. A bent mixed-valence manganese (III/II/III) complex: A new class of trinuclear, acetate bridged Schiff's base compounds exhibiting a g=2 multiline ESR signal.*J. Chem. Soc., Chem. Commun.*84-86.

Kim, D. H., Britt, R. D., Klein, M. P. and Sauer, K. 1990. The g=4.1 EPR signal of the S_2 of the photosynthetic oxygen-evolving complex arises from a multinuclear Mn cluster. *J. Am. Chem. Soc.***112**:9389-9391.

Kim, D. H., Britt, R. D., Klein, M. P. and Sauer, K. 1992. The manganese site of the photosynthetic oxygen-evolving complex probed by EPR spectroscopy of oriented photosystem II membranes: The g=4 and g=2 multiline signals. *Biochem.***31**:541-547.

Klimov, V. V., Allakhverdiev, S. I., Demeter, S. and Krasnovskii, A. 1979. (In Russian) *Doklady Akad. Nauk SSR.***249**:227-230.

Klimov, V. V., Allakhverdiev, S. I., Shuvalov, V. A. and Kransovsky, A. A. 1982. Effects of extraction and re-addition of manganese on light reactions of photosystem II preparations. *FEBS Letts.***148**:307-312.

Kok, B., Forbush, B. and McGloin, M. 1970. Cooperation of charges in photosynthetic O_2 evolution - 1: A linear four step mechanism.*Photochem. Photobiol.***11**:457-475.

Kusunoki, M. 1992. A new paramagnetic hyperfine structure effect in manganese tetramers. The origin of the 'multiline' EPR signals from an S_2 state of a photosynthetic water-splitting enzyme.*Chem. Phys. Letts.***197**:108-116.

Kusunoki, M., Ono, T., Suzuki, M., Noguchi, T., Uehara, A., Matsushita, T., Oyanagi, H. and and Inoue, Y. 1992. Mn K-edge XAFS studies on the valence states of Mn ions as catalyst for water oxidation in photosynthesis. *In:* Research in Photosynthesis. N. Murata. Kluwer Academic Publishers. **II**:293-296.

Lack, G. M. and Gibson, J. F. 1978. EPR in the ($ReNCl_4^-$)ion. *J. Molec. Struct.***46**:299-306.

Landolt-Börnstein. 1988. Numerical Data and Functional Relationships in Science and Technology.K. H. Hellwege and A. M. Hellwege eds.Springer-Verlag. Berlin.**Vol 20a**

Larson, E. J. and Pecoraro, V. L. 1992. Introduction to Manganese Enzymes. *In*: Manganese Redox Enzymes. V. L. Pecoraro. VCH. New York. 1-28.

Latimer, M. J., DeRose, V. J., Mukerji, I., Yachandra, V. K., Sauer, K. and Klein, M. P. 1995. Evidence for the proximity of calcium to the manganese cluster of photosystem II: Determination by X-ray absorption spectroscopy. *Biochem.***34**:10898-10909.

Liang, W., Latimer, M. J., Dau, H., Roelofs, T. A., Yachandra, V. K., Sauer, K. and Klein, M. P. 1994. Correlation between structure and magnetic spin state of the manganese cluster in the oxygen-evolving complex of photosystem II in the S_2 state: Determination by X-ray absorption spectroscopy. *Biochem.* **33**:4923-4932.

MacLachlan, D. J., Hallahan, B. J., Ruffle, S. V., Nugent, J. H. A., Evans, M. C. W., Strange, R. W. and Hasnain, S. S. 1992. An EXAFS study of the manganese O_2-evolving complex in purified photosystem II membrane fractions.*Biochem. J.***285**:569-576.

McCusker, J. K., Jang, H. G., Wang, S., Christou, G. and Hendrickson, D. N. 1992. Ground-state variability in μ_3–oxide trinuclear mixed-valence manganese complexes: Spin frustration. *Inorg. Chem.***31**:1874-1880.

McGarvey, B. R. 1966. Electron spin resonance of transition-metal complexes. *In:* Transition Metal Chemistry. R. L. Carlin ed. Eward Arnold (Publishers) Ltd. London. **3**:89-201.

Mei, R. and Yocum, C.F. 1992. Comparative properties of hydroquinone and hydroxylamine reduction of the Ca^{2+}-stabilised O_2-evolving complex of photosystem II: Reductant-dependent Mn^{2+} formation and activity inhibition. *Biochem.* **31**: 8449-8454.

Messinger, J. and Renger, G. 1990. The reactivity of hydrazine with photosystem II strongly depends on the redox state of the water oxidizing system. *FEBS Letts.***277**:141-146.

Mukerji, I., Andrews, J. C., DeRose, V. J., Latimer, M. J., Yachandra, V. K., Sauer, K. and Klein, M. P. 1994. Orientation of the oxygen-evolving manganese complex in a photosystem II membrane preparation: An X-ray absorption spectroscopy study.*Biochem.***33**:9712-9721.

Nixon, P. J. and Diner, B. A. 1992. Aspartate 170 of the photosystem II reaction center polypeptide D1 is involved in the assembly of the oxygen-evolving manganese cluster.*Biochem.* **31**:942-948.

Nixon, P. J. and Diner, B. A. 1994. Analysis of water-oxidation mutants constructed in the cyanobacterium *Synechocystis* sp PCC 6803. *Biochem. Soc. Trans.* **22**:338-343.

Orton, J. W. 1968. Electron Paramagnetic Resonance.1st ed. Iliffe Books Ltd. London.235pp.

Pace, R. J., Smith, P., Bramley, R. and Stehlik, D. 1991. EPR saturation and temperature dependence studies on signals from the oxygen-evolving centre of photosystem II.*Biochim. Biophys. Acta*.**1058**:161-170.

Penner-Hahn, J. E., Fronko, R. M., Pecoraro, V. L., Yocum, C. F., Betts, S. D. and Bowlby, N. R. 1990. Structural characterization of the manganese sites in the photosynthetic oxygen-evolving complex using X-ray absorption spectroscopy.*J. Am. Chem. Soc.***112**:2549-2557.

Pilbrow, J. R. 1990. Transition ion electron paramagnetic resonance.Oxford Science Publications. Oxford.717 pp.

Porra, R. J., Thompson, W. A. and Kriedermann, P. E. 1989. Determination of accurate extinction coefficients and simultaneous equations for assaying chlorophylls *a* and *b* extracted with four different solvents: Verification of the concentration of chlorophyll standards by atomic absorption spectroscopy. *Biochim. Biophys. Acta*.**975**:384-394.

Press, W. H., Teukolsky, S. A., Vetterling, W. T. and Flannery, B. P. 1986. Numerical recipes in fortran: The art of sciencific computing. 1st ed. Cambridge University Press. p 404.

Randall, D. W., Sturgeon, B. E., Ball, J. A., Lorigan, G. A., Chan, M. K., Klein, M. P., Armstrong, W. H. and Britt, R. D. 1995. Mn ESE-ENDOR of a mixed valence Mn(III)Mn(IV) complex: Comparison with the Mn cluster of the photosynthetic oxygen evolving complex. *J. Am. Chem. Soc.***117**:11780-11789.

Razeghifard, M. R., Klughammer, C. and Pace, R. J. 1996. EPR kinetic studies of the S-states in spinach thylokoids.*Biochem.* **In press**.

Reijerse, E. J., Van Aerle, N. A. J. M., Keijzers, C. P., Bottcher, R., Kirmse, R. and Stach, J. 1986. Comparison of ESEEM, ESE-ENDOR and CW-ENDOR on ^{14}N in a powder.*J. Mag.Res.***67**:114-124.

Riggs-Gelasco, P. J., Mei, R., Ghanotakis, D. F., Yokum, C. F. and Penner-Hahn, J. E. 1996a. X-ray absorption spectroscopy of calcium-substituted derivatives of the oxygen evolving complex of photosystem II. *J. Am. Chem. Soc.***118**:2400-2410.

Riggs-Gelasco, P. J., Mei, R., Yocum, C. F. and Penner-Hahn, J. E. 1996b. Reduced derivatives of the Mn cluster in the oxygen evolving complex of photosystem II: An EXAFS study.*J. Am. Chem. Soc.***118**:2387-2399.

Rose, M. E. 1957. Elementary Theory of Angular Momentum. John Wiley and Sons, Inc. New York.

Rutherford, A. W. 1985. Orientation of EPR signals arising from components in photosystem II membranes.*Biochim. Biophys. Acta.***807**:189-201.

Sands, R. H. and Dunham, W. R. 1975. Spectroscopic studies of two-iron ferredoxins. *Q. Rev. Biophys.***7**:443.

Sarneski, J. E., Thorp, H. H., Brudvig, G. W., Crabtree, R. H. and Schulte, G. K. 1990. Assembly of high-valent oxomanganese clusters in aqueous solution. Redox equilibrium of water stable $Mn_3O_4^{4+}$ and $Mn_2O_2^{3+}$ complexes. *J. Am. Chem. Soc.***112**:7255-7260.

Schreiber, U., Hormann, H., Neubauer, C. and Klughammer, C. 1995. Assessment of photosystem II photochemical quantium yield by chlorophyll fluorescence quenching analysis. *Austr. J. Plant Physiol.***22**:209-220.

Schreiber, U., Schliwa, U. and Bilger, W. 1986. Continuous recording of photochemical and non-photochemical chlorphyll fluorescence quenching with a new type of modulation fluorometer. *Photosyn. Res.***10**:51-62.

Seibert, M. 1995. Reflections on the nature and function of the photosystem II reaction centre. *Austr. J. Plant Physiol.***22**:161-166.

Semin, G. K., Babushkina, T. A. and Yakobson, G. G. 1975. Nuclear Quadrupole Resonance in Chemistry. Pick. A.J. ed. Barouch A. trans. John Wiley and Sons. New York.

Slichter, C. P. 1990. Principles of Magnetic Resonance.3rd Ed. Springer-Verlag. Berlin.650pp.

Smith, P. J., Åhrling, K. A. and Pace, R. J. 1993. Nature of the S_2 state electron paramagnetic resonance signals from the oxygen evolving complex of photosystem II: Q-band and oriented X-band studies. *J. Chem. Soc. Faraday Trans.***89**:2863-2868.

Smith, P. J. and Pace, R. J. 1996. Evidence for two forms of the g=4.1 signal in the S_2 of photosystem II. Two magnetically isolated manganese dimers? *Biochim. Biophys. Acta.***1275**:213-220.

Sostero, S., Rehorek, D., Polo, E. and Traverso, O. 1993. Spin trapping and some reactions of ruthenium-centred radicals.*Inorg. Chim. Acta.***209**:171-176.

Stewart, C. P. and Porte, A. L. 1972. Electron paramagnetic resonance spectra of some oxovanadium(IV) chelates.*J. Chem. Soc., Dalton Trans.*1661-1666.

Svensson, B., Vass, I., Cedergren, E. and Styring, S. 1990. Structure of donor site components in photosystem II predicted by computer modelling. *EMBO J.* **9**:2051-2059.

Tamura, N., Inoue, H. and Inoue, Y. 1990. Inactivation of the water-oxidizing complex by exogenous reductants in PSII membranes depleted of extrinsic proteins. *Plant Cell Physiol.***31**:469-477.

Vänngård, T., Hansson, Ö. and Haddy, A. 1992. EPR studies of manganese in photosystem II. *In:* Manganese Redox Enzymes. V. L. Pecoraro. VCH. New York. 105-118.

Vincent, J. B., Tsai, H.-L., Blackman, A. G., Wang, S., Boyd, P. D. W., Folting, K., Huffman, J. C., Lobkovsky, E. B., Hendrickson, D. N. and Christou, G. 1993. Models of the manganese catalase enzymes. Dinuclear manganese(III) complexes with the $[Mn_2(\mu\text{-}O)(\mu\text{-}O_2\ CR)_2]^{2+}$ core and terminal monodentate ligands. *J. Am. Chem. Soc.***115**:12353-12361.

Völker, M., Ono, T., Inoue, Y. and Renger, G. 1985. Effect of trypsin on PSII particles. Correlation between Hill-activity, Mn-abundance and peptide pattern. *Biochim. Biophys. Acta.***806**:25-34.

Walker, D. 1987. The use of the oxygen electrode and fluorescence probes in simple measurement of photosynthesis. Oxygraphics Ltd, UK

Whittle, B., Everest, N. S., Howard, C. and Ward, M. D. 1995. Synthesis and electrochemical and spectroscopic properties of a series of binuclear and trinuclear ruthenium and palladium complexes based on a new bridging ligand. *Inorg. Chem.***34**:2025-2032.

Yachandra, V. K., DeRose, V. J., Latimer, M. J., Mukerji, I., Sauer, K. and Klein, M. P. 1993. Where plants make oxygen: A structural model for the photosynthetic oxygen-evolving manganese cluster.*Science.***260**:675-679.

Yachandra, V. K., Guiles, R. D., McDermott, A., Britt, R. D., Dexheimer, S. L., Sauer, K. and Klein, M. P. 1986a. The state of manganese in the photosynthetic apparatus. 4. Structure of the manganese complex in photosystem II studied using EXAFS spectroscopy. The S_1 state of O_2-evolving photosystem II complex from spinach. *Biochim. Biophys. Acta.***850**:324-332.

Yachandra, V. K., Guiles, R. D., McDermott, A. E., Cole, J. L., Britt, R. D., Dexheimer, S. L., Sauer, K. and Klein, M. P. 1987. Comparison of the structure of the manganese complex in the S_1 and S_2 states of the photosynthetic O_2-evolving complex: An X-ray absorption spectroscopy study. *Biochem.* **26**:5974-5981.

Yachandra, V. K., Guiles, R. D., Sauer, K. and Klein, M. P. 1986b. The state of manganese in the photosynthetic apparatus. 5. The Chloride effect in photosynthetic oxygen evolution. *Biochim. Biophys. Acta.***850**:333-342.

Yamaguchi, K. and Sawyer, D. T. 1985. Redox chemistry for the mononuclear Tris(picolinato)-, Tris(acetylacetonato)-, and Tris(8-quinolinato)manganese(III) complexes: Reaction mimics for the water-oxidation cofactor in photosystem II.*Inorg. Chem.***24**:971-976.

Yocum, C. F., Yerkes, C. T., Blankenship, R. E., Sharp, R. R. and Babcock, G. T. 1981. Stoichiometry, inhibitor sensitivity, and organisation of manganese associated with photsynthetic oxygen evolution. *Proc. Natl. Acad. Sci. USA.***78**:7507-7511.

Zheng, M. and Dismukes, G. C. 1992. Photosynthetic water oxidation: What have we learned from the multiline EPR signals? *In:* Research in Photosynthesis. N. Murata ed. Kluwer Academic Publishers. Dordrecht. **II**:305-308.

Zheng, M. and Dismukes, G. C. 1996. Orbital configuration of the valence electrons, ligand field symmetry and manganese oxidation states of the photosynthetic water oxidizing complex: Analysis of the S_2 state multiline EPR signals. *Inorg. Chem.***35**:3307-3319.

Zheng, M., Khangulov, S. V., Dismukes, G. C. and Barynin, V. V. 1994. Electronic structure of dimanganese(II,III) and dimanganese(III,IV) complexes and dimanganese catalase enzyme: A general EPR spectral simulation approach. *Inorg. Chem.***33**:382-387.